INVESTIGATION OF ONTOGENY, HOMOLOGY AND HETEROCHRONY IN THE SILURIFORM SKELETON

A Dissertation

by

KOLE MATTHEW KUBICEK

Submitted to the Office of Graduate and Professional Studies of
Texas A&M University
in partial fulfillment of the requirements for the degree of

DOCTOR OF PHILOSOPHY

Chair of Committee,	Kevin W. Conway
Committee Members,	Kirk O. Winemiller
	Gary Voelker
	Christopher D. Marshall
Head of Department,	Kirk O. Winemiller

December 2020

Major Subject: Wildlife and Fisheries Sciences

ABSTRACT

Catfishes (Otophysi: Siluriformes) is a remarkably diverse assemblage (~4000 spp) that is distributed across the globe in fresh and marine waters. Catfishes are united by several modifications of the skeleton, including the extreme modification of certain elements (e.g., the pectoral-fin spine) and the presence of several bones that are currently presumed to be the result of fusion (e.g., the parieto-supraoccipital). In light of this, there have been a vast number of anatomical investigations of the adult skeleton in catfishes; however, comprehensive information on early development of the skeleton remains scarce. This dissertation reports detailed information on the development of the skeleton in catfishes to address issues of homology, provide ontogenetic information on a systematically important character complex, and assess the role that heterochrony may have played in the evolution of the skeleton.

I provide a detailed description of skeletal development for two species of North American catfish, *Ictalurus punctatus* and *Noturus gyrinus*. Development of the skeleton was complete by 22.4 mm SL in *I. punctatus* and 14.1 mm SL in *N. gyrinus*, excluding the dorsal- and anal-fin distal radials in the latter. No major differences were identified between the ossification sequences compiled for each species. No signs of ontogenetic fusion were observed in previously purported compound elements. I also examined the development of the pectoral-fin spine across the order to determine if it develops from a single ontogenetic pathway and standardize terminology of the spine ornamentation for use in systematic studies. The earliest stages of pectoral-fin spine development were

highly conserved across the order and most of the morphological diversity of the structure can be attributed to the presence/absence of five traits (distal rami, anterior/posterior serrae, denticuli, and odontodes). Finally, I compare the ossification sequences of four catfishes and 3 non-siluriform otophysans in order to determine what heterochronic shifts (changes in the relative timing of developmental events), if any, are characteristic of catfishes. Eight different bones were found to be shifted in their appearance within the ossification sequence of catfishes, including the morphologically diverse and functionally important pectoral-fin spine.

DEDICATION

This Dissertation research is dedicated to my family, Bennie, Evelyn, W.C., Rosemary, Gary, Lydia, Lacey, Myles, Hayden, Greyson, Luke, Easton and Layton, for their love and support. I also dedicate this work to Amanda, Iggy and Dooley who have always been there, through the best and worst of times, and without which this work would not be possible.

ACKNOWLEDGEMENTS

I would like to thank my advisor, Dr. Kevin Conway, for all of the years of guidance and support as well as introducing me to the fascinating world of fish morphology and diversity. I could not have asked for better mentor to help guide me throughout my graduate and early scientific career. I would also like to thank Dr. Kirk Winemiller, Dr. Gary Voelker, Dr. Christopher Marshall, and Dr. Ralf Britz for their helpful advice and comments which have greatly improved the contents of this dissertation. Special thanks to Dr. Ralf Britz for welcoming me as a collaborator and sharing his profound knowledge of fish anatomy and development.

I would also like to thank all of the curators, collection managers, and natural history collections (Dr. Barbara Brown [AMNH], Dr. Mark Sabaj [ANSP], Oliver Crimmen [BMNH], Dave Catania [CAS], Dr. Casey Dillman [CUMV], Dr. Caleb McMahan [FMNH], Andy Bentley [KU], Rick Feeney [LACM], Dr. Murilo Pastana and Dr. Veronica Slobodian [MZUSP], Heather Prestridge [TCWC], Doug Nelson [UMMZ], and Dr. Jeff Williams [USNM]) for the loan of specimens and/or assistance with specimen curation, without which this research would not have been possible. I also thank Dr. Delbert Gatlin and Bryan Ray for the providing access to eggs of *Ictalurus punctatus* and Ryan O'Hanlon and Chris Mynatt for helping with the collection of *Noturus gyrinus*. Discussions and comments that improved the overall quality of this work were also provided by Dr. John Lundberg, Dr. Gloria Arratia, Dr. Jackie Webb, Dr. Eric Hilton and Dr. Dave Johnson.

I would like to thank the numerous lab mates that I have over the years (Nick Bertrand, Eric Tsakiris, Daemin Kim, Illiana Mock and Cragen King) for their support and advice. I would also like to thank my family for all of their love and support that they have provided as well as my fiancée Amanda for always being there and encouraging me to look forward.

CONTRIBUTORS AND FUNDING SOURCES

Contributors

This dissertation was supervised by a dissertation committee consisting of Dr. Kevin W. Conway (advisor), Dr. Kirk O. Winemiller, and Dr. Gary Voelker of the Department of Wildlife and Fisheries Sciences, Dr. Christopher D. Marshall of the Department of Marine Biology at Texas A&M Galveston, and Dr. Ralf Britz (special appointment) of the Senckenberg Natural History Collections in Dresden, Germany.

All other work conducted for the dissertation was completed by the student independently.

Funding Sources

This research was funded by Texas A&M Agrilife Research under Grant Number TEX09452.

This work was also made possible in part by the Tom Slick Graduate Research Fellowship from the College of Agriculture and Life Sciences at Texas A&M University.

TABLE OF CONTENTS

Page

LIST OF FIGURES

Page

LIST OF TABLES

Page

CHAPTER I

INTRODUCTION

The series Otophysi is the dominant group of freshwater fishes on the planet today and represents ~11,200 species, almost a third of all known fishes, divided across four orders: Cypriniformes (carps and relatives; 4,676 spp.), Characiformes (tetras and relatives; 2,296 spp.), Gymnotiformes (South American knifefishes; 260 spp.) and the Siluriformes (catfishes; 3,993 spp.) (Fricke, Eschmeyer & Fong, 2020). The Otophysi have been identified as one of nine exceptional vertebrate radiations (Alfaro et al., 2009) and their evolutionary success may be largely attributed to the presence of the Weberian apparatus, an elaborate sound reception system linking the anterior chamber of the swimbladder to the inner ear via a series of highly mobile bones, the Weberian ossicles, representing modified elements of the first four vertebrae. Unsurprisingly, there have been numerous investigations of the Otophysan skeleton (Fink & Fink, 1981, 1996), including several studies which provide developmental information of otophysan fishes. However, most of these studies have been restricted to only particular regions of the skeleton (e.g., the Weberian apparatus; Grande & de Pinna, 2004; Hoffman & Britz, 2006; Britz and Hoffman, 2006). As a result, it has not been possible to compare broadly the development of the skeleton between major groups of otophysan fishes. One group, the Siluriformes, has proven particularly problematic due to the difficulty in determining the homology of multiple skeletal elements, which are highly modified when compared

to presumed homologous elements in other groups of otophysans (Lundberg, 1975; Arratia & Gayet, 1995; Arratia, 2003a,b).

The order Siluriformes (catfishes) are a highly diverse group of otophysan fishes, comprising ~4000 species distributed across three suborders (Siluroidei, Loricarioidei, and Diplomystoidei) and 43 families (Nelson, Grande & Wilson, 2016; Fricke, Eschmeyer & Fong, 2020) that are distributed in freshwaters across the globe and have invaded marine coastal waters on two separate occasions (Nelson, Grande, & Wilson, 2016). Members of this group are found in both pelagic (Reynolds, 1971; Kaatz, Stewart, Rice, & Lobel, 2010) and benthic environments (Paxton, 1997; Mistri, Kumari, Mittal, & Mittal, 2018), with some species capable of traversing across land to find more suitable habitat (e.g., *Clarias gariepinnus*, Johnels, 1957). Catfishes also exhibit a wide diversity of life history and reproductive strategies, ranging from broadcast spawners with little or no parental care to nest guarders and mouthbrooders in which males protect developing embryos (Mayden, Burr, & Dewey, 1980; Barbieri, dos Santos, & Andreata, 1992; Maehata, 2007). Given this ecological diversity, it is no surprise that siluriforms also exhibit a remarkable amount of morphological variation in body shape and size, with maximum lengths ranging from larger than 3 m in *Silurus glanis* to less than 20 mm (e.g., Friel & Lundberg, 1996; de Pinna & Winemiller, 2000; Schaefer, Provenzano, Pinna, & Baskin, 2005; Copp et al., 2009).

In light of this diversity, it is no surprise that siluriform relationships have been well studied; however, the interfamilial relationships of siluriforms remain unresolved due to conflicting morphological (de Pinna, 1993) and molecular (Sullivan, Lundberg, &

Hardman, 2006; Kappas et al., 2016) hypotheses as well as a general lack of resolution at deeper nodes within the Siluroidei (the suborder which contains the majority of siluriform taxa). Despite this, siluriforms are one of the morphologically best-defined groups of bony fishes with several synapomorphies supporting their monophyly (Fink & Fink, 1981). In many cases, these synapomorphies are derived characteristics of the skeleton including the extreme modification of certain elements (e.g., the pectoral-fin spine and supporting skeleton) and the presence of several ossifications that have been proposed to be the result of ontogenetic (developmental) fusion of bones that are typically separate in other teleosts (e.g., the parieto-supraoccipital; Bamford, 1948; Arratia and Gayet, 1995). As a result, there have been numerous studies on the adult skeleton of catfishes (Alexander, 1966; Rao, & Lakshmi 1984; Brown & Ferraris, 1987; Diogo, Oliveira, & Chardon, 2001; Arratia, 2003a,b; Huysentruyt & Adriaens, 2005; Rodiles-Hernández, Hendrickson, Lundberg, & Humphries, 2005; Egge, 2007; Vigliotta, 2008; Britz, Kakkassery, & Raghavan, 2014 Carvalho, & Reis, 2020); however, far fewer studies have focused on the earliest developmental stages (Kindred, 1919; Reed, 1924; Bamford, 1948; Grande & Shardo, 2002; Geerinckx, Brunain, & Adriaens, 2007; Huysentruyt, Geerinckx, Brunain, & Adriaens, 2011; Kubicek, Britz, & Conway, 2019). This is surprising given that developmental studies have been shown to be of outstanding value in resolving the homology of controversial elements in bony fishes (e.g., Britz & Hoffman, 2006; Hilton & Johnson, 2007; Britz & Johnson, 2012) and can reveal novel morphological information for phylogenetic studies (e.g., Johnson, 1983; Johnson & Washington, 1987; Kubicek & Conway, 2016). In addition, studies of development can

be used to identify changes in developmental timing (i.e., heterochrony; Mabee & Trendler, 1996; Mattox, Britz & Toledo-Piza, 2016) that may have played an important role in generating the tremendous morphological diversity that exists among and between the different groups of bony fishes.

To further our knowledge of the siluriform skeleton as well as that of bony fishes more generally, this dissertation reports detailed information on the development of the skeleton in catfishes in order to address issues of homology, provide ontogenetic information on a systematically important character complex, and assess the role that heterochrony may have played in the evolution of the catfish skeleton. In the first of three studies (Chapter II), I describe in detail for the first time the development of the entire skeleton in two species of ictalurid catfishes, *Ictalurus punctatus* and *Noturus gyrinus*. I compile a sequence of ossification for both species, documenting the progression of development, and provide a high-quality photographic atlas for *I. punctatus*. In addition, I discuss the homology of several bones which have previously been proposed to be compound elements resulting from developmental fusion in light of novel developmental information obtained for the two species.

Chapter III focuses on the development of the morphologically diverse pectoral-fin spine of catfishes. Despite being an important character complex for systematic studies, the inconsistent application of terminology has undermined the usefulness of pectoral-fin spine for both phylogenetic and taxonomic studies. Additionally, most studies of catfish pectoral-fin spine morphology have focused largely on adult anatomy, with only a small portion providing ontogenetic information (Peyer, 1922; Reed, 1924;

Grande & Shardo, 2002; Arratia, 2003b; Vanscoy et al., 2015). I describe the ontogeny of the pectoral-fin spine in six species of catfishes, representing both siluroid and loricarioid catfishes, in order to determine if this morphologically diverse character complex results from a similar ontogenetic pathway in each of these two groups. I address issues of homology associated with components of the spurious ray, the developing portion of the pectoral-fin spine (Reed, 1924; Arratia, 2003b) as well as standardize the terminology of the pectoral-fin spine morphology based on homology. I also identify differences that exist in the early formation of the pectoral-fin spine across catfishes by examining the ontogenetic series of six species as well as the developing portion of the pectoral-fin spine in juvenile and adult specimens of species representing 41 of the currently recognized 43 families of siluriforms obtained from museum collections.

Chapter IV focuses on sequence heterochrony and the evolution of the catfish skeleton. Studies of sequence heterochrony have been applied to a wide variety of tetrapods, including amphibians (Weisbecker & Mitgutsch, 2010; Harrington, Harrison, & Sheil, 2013), squamates (Hugi, Hutchinson, Koyabu, & Sánchez-Villagra, 2012; Ziermann, Mitgutsch, & Olsson, 2014; Werneburg, & Sánchez-Villagra, 2015), turtles (Werneburg, Hugi, Müller, & Sánchez-Villagra, 2009; Sánchez-Villagra et al., 2009), crocodylians (Larsson, 1998), birds (Maxwell, Harrison, & Larsson, 2010; Carril, & Tambussi, 2017), and mammals (Nunn and Smith, 1998; Sánchez-Villagra et al., 2008; Weisbecker, V., Goswami, A., Wroe, S., & Sánchez-Villagra, 2008; Hautier et al., 2011, 2013). These studies have shown that relative changes in the timing of skeletogenesis is

widespread and in some cases is associated with major changes in morphology, life history, and function (Goswami, Weisbecker, & Sánchez-Villagra, 2009; Sears, 2009; Keyte & Smith, 2010). Despite having a more complex skeleton, containing a higher number of elements and exhibiting a wider degree of morphological diversity, studies of sequence heterochrony in fishes are rare (Mabee and Trendler, 1966; Ito, Matsumoto, & Hirata, 2019). To assess the role of sequence heterochrony in the skeleton of catfishes, I generate ossification sequences for one cypriniform, *Danio rerio*, and two loricarioid catfishes, *Corydoras panda* and *Ancistrus* sp. These ossification sequences, along with those currently available for other otophysans (*Enteromius holotaenia*, Conway, Kubicek, & Britz, 2017; *Salminus brasiliensis*, Mattox, Britz, & Toledo-Piza, 2014; *Ictalurus punctatus* and *Noturus gyrinus*, Chapter II), are used to conduct sequence heterochrony analyses for the entire skeleton as well as multiple hierarchical subcomponents of the skeleton. I identify which, if any, heterochronic shifts characterize catfishes and also determine if any of the key synapomorphies of siluriforms, such as the morphologically diverse pectoral-fin spine, exhibit heterochronic shifts compared to non-siluriform otophysans.

CHAPTER II

DEVELOPMENTAL OSTEOLOGY OF *ICTALURUS PUNCTATUS* AND *NOTURUS GYRINUS* (TELEOSTEI: SILURIFORMES)

Introduction

The order Siluriformes (catfishes) are a highly diverse (~4000 species, Fricke, Eschmeyer & Fong, 2020) group of otophysan fishes that are distributed in freshwaters across the globe and have invaded marine coastal waters on two separate occasions (Nelson, Grande, & Wilson, 2016). Members of this group are found in both pelagic (Reynolds, 1971; Kaatz, Stewart, Rice, & Lobel, 2010) and benthic environments (Paxton, 1997; Mistri, Kumari, Mittal, & Mittal, 2018), with some species capable of traversing across land to find more suitable habitat (e.g., *Clarias gariepinnus*, Johnels, 1957). Catfishes also exhibit a wide diversity of life history and reproductive strategies, ranging from broadcast spawners with little or no parental care to nest guarders and mouthbrooders in which males protect developing embryos (Mayden, Burr, & Dewey, 1980; Barbieri, dos Santos, & Andreata, 1992; Maehata, 2007). Given this ecological diversity, it is no surprise that siluriforms also exhibit a remarkable amount of morphological variation in body shape (ranging from anguilliform [e.g., Clariidae; Jansen, Devaere, Weekers, & Adriaens, 2006] to markedly dorsoventrally flattened [e.g., Aspredinidae, Chacidae; Brown & Ferraris, 1988; Carvalho, & Reis, 2020] to thin and elongated [e.g., *Farlowella*; Ballen, Pastana, & Peixoto, 2016] to shortened and stout bodied [*Corydoras*; Tencatt & Ohara, 2016]) and size (ranging from greater than 3

meters in *Siluris glanis* to less than 20 mm in some Neotropical catfishes [e.g., Friel & Lundberg, 1996; de Pinna & Winemiller, 2000; Copp et al., 2009]). Despite this remarkable morphological variation, Siluriformes are well characterized as a monophyletic group by several derived skeletal characters (synapomorphies), including the secondary absence of several ossifications (e.g., subopercle, intercalar) and the extreme modification of others (e.g., pectoral-fin spine, maxilla, metapterygoid) (Fink & Fink, 1981). Catfishes also possess several ossifications that have been proposed to be the result of ontogenetic (developmental) fusion of two bones that are separate in other teleosts. For example, the dermal paired parietals and the chondral median supraoccipital are thought to fuse during development to form a single bone in the adult, referred to as the parieto-supraoccipital. Although some evidence has been presented in favor of this hypothesis (Bamford, 1948, Arratia, Chang, Menu-Marque & Rojas, 1978; Arratia & Menu-Marque, 1981; Arratia & Gayet, 1995), it has been formulated based on the observation of only a small number of individuals representing a limited number of species; a miniscule fraction of the diversity represented within siluriforms. This is also the case for several other skeletal elements that are hypothesized to represent compound elements, including the posttemporo-supracleithrum (Fink & Fink, 1981), the scapulocoracoid (Stark, 1930; Arratia, 2003b), urohyal (Arratia & Schultze, 1990; Geerinckx, Brunain, & Adriaens, 2011), and lacrimal (de Pinna, Reis, & Britski, 2020). Although the suspected compound nature of these elements appears to be generally accepted among the majority of researchers working with the catfish skeleton (e.g., Diogo, Oliveira, & Chardon, 2001; Geerinckx, Brunain, & Adriaens, 2007; Birindelli,

Sousa, & Pérez, 2008; Calegari, Vari & Reis, 2019), the homology of these "compound" bones has yet to be adequately addressed and several independent research groups have adopted different terms for these elements (e.g., de Pinna, Ferraris & Vari, 2007; Lundberg, Hendrickson, Luckenbill & Mariangeles, 2017; Slobodian and Pastana, 2018), perhaps due to uncertainty regarding homology or because of difference of opinion.

The highly modified skeleton of catfishes has been the subject of numerous detailed osteological investigations (e.g., Alexander, 1966; Rao, & Lakshmi 1984; Brown & Ferraris, 1987; Diogo, Oliveira, & Chardon, 2001; Arratia, 2003a,b; Huysentruyt & Adriaens, 2005; Rodiles-Hernández, Hendrickson, Lundberg, & Humphries, 2005; Egge, 2007; Vigliotta, 2008; Britz, Kakkassery, & Raghavan, 2014 Carvalho, & Reis, 2020); however, the majority of these studies have focused on adult individuals with relatively fewer examining the earliest stages of skeletal development (see below). This is surprising given that one potential way to resolve homology of controversial elements (including the suspected compound ossifications of catfishes) is to follow the ontogenetic trajectory of the elements in question. Typically, elements which are highly modified in adults are conserved in their earliest developmental stages and can be compared to similar developmental stages of other taxa in order to determine their homology (e.g., Britz & Hoffman, 2006; Hilton & Johnson, 2007; Britz & Johnson, 2012). In addition to furthering our knowledge of the adult skeleton, studies of development can also reveal novel morphological information for phylogenetic studies (e.g., Johnson, 1983; Johnson & Washington, 1987; Kubicek & Conway, 2016) as well

as identify changes in developmental timing (i.e, heterochrony; Mabee & Trendler, 1996; Mattox, Britz & Toledo-Piza, 2016) that may have played an important role in generating the tremendous morphological diversity that exists among and between the different groups of bony fishes. Though available, studies that have investigated skeletal ontogeny in members of the Siluriformes have focused only on specific regions of the skeleton, such as the cranium (Kindred, 1919; Bamford, 1948; Geerinckx, Brunain, & Adriaens, 2007; Huysentruyt, Geerinckx, Brunain, & Adriaens, 2011), postcranium (Grande & Shardo, 2002), pectoral-fin spine (Reed, 1924; Kubicek, Conway & Britz, 2019), or the Weberian apparatus (Coburn & Grubach, 1998). To date, no single study has investigated development of the entire skeleton for a single species of catfish.

To further our understanding of catfish skeleton, as well that of bony fishes more generally, I investigate skeletal development in the ictalurid catfishes, *Ictalurus punctatus* and *Noturus gyrinus*. I compile a sequence of ossification for both species, documenting the progression of skeletal development (from the earliest stages of ossification through to later stages), and provide a high-quality photographic atlas illustrating select aspects of skeletal ontogeny for *I. punctatus*. Additionally, the homology of the five bones that have been proposed to represent compound elements in ictalurid catfishes (parieto-supraoccipital, posttemporo-supracleithrum, scapulocoracoid, urohyal, and lacrimal) are discussed in light of development. Finally, a comparison is made between the ossification sequences produced herein for ictalurid catfishes and those available for other members of the Otophysi.

Materials and Methods

Eggs of *Ictalurus punctatus* were obtained from the Texas A&M Aquatic Research and Teaching Facility. Eggs were incubated until hatching, at which point embryos were moved to 20 L aquaria where they were raised until sampling. Eggs were treated with Paraguard (Seachem Laboratories, Madison, GA) to prevent fungus. Larvae were sampled daily from 5 days pre-hatch up to 30 days post-hatch (dph) and every third day from 30 dph up to 60 dph. Sampled individuals were euthanized with an overdose of tricaine methanosulfate (MS222) and subsequently fixed in a solution of 10% buffered paraformaldehyde for 24 hr. After fixation, individuals were transferred to a 70% EtOH solution for permanent storage. Adult individuals (N = 8) of *Noturus gyrinus* were collected locally from the Little Brazos River (Brazos Co., TX) and brought back to the lab where they were sexed and divided (1–2 females per male) between 40 L aquaria (pH 7.5–8.0; temperature 26°C ± 1°C). Specimens were fed on a diet of decapsulated brine shrimp eggs, crushed blackworm pellets, and chopped blackworms and maintained for captive spawning. Upon spawning, eggs were collected, incubated, and sampled as above. Protocols involving live animals were approved by the Texas A&M University IACUC (protocol # 2017-0047, 2020-0033).

Gross Examination

A total of 100 individuals of *Ictalurus punctatus* (7.7 mm notochord length [NL] to 44.9 mm standard length [SL]) and 120 of *N. gyrinus* (5.4 mm SL to 26.4 mm SL) were cleared and double-stained (c&s) for bone and cartilage examination. Smaller specimens of *I. punctatus* (< 20 mm SL) were c&s using a modification of the acid-free

clearing and staining method of Kimmel and Walker (2007) and larger individuals of *I. punctatus* (~20 mm SL and larger) and all specimens of *N. gyrinus* were c&s following Taylor and Van dyke (1985). Once c&s, specimens were dissected and scored for the presence/absence of 328 (*I. punctatus*) and 286 (*N. gyrinus*) ossified skeletal elements under a ZEISS SteREO Discovery V20 stereomicroscope. For each individual specimen, bones were considered present at the first sign of alizarin red S staining and absent in the absence of alizarin red S staining. In the few cases in which it was not possible to confirm through stereomicroscopy whether a particular bone was stained with alizarin red S, specimens were examined at higher magnification using a Zeiss Primo Star compound microscope. The cartilage staining of Taylor and Van Dyke's (1985) c&s protocol relies on an acidic solution which has previously been reported to negatively affect the staining of bone (Walker & Kimmel, 2007), which could hinder the identification of bony elements, particularly during the earliest stages of development. In order to compensate for this as well as ensure that scoring of double-stained individuals was accurate, a small number of individuals of each species (45 *I. punctatus* [8.6 mm NL – 21.2 mm SL] and 38 *N. gyrinus* [5.8 mm SL – 13.1 mm SL]) were cleared and single stained with alizarin red S using a protocol modified from Taylor (1967), and scored for the presence and absence of bone. Bone presence/absence data of skeletal elements collected from double- or single-stained specimens were highly congruent and compiled in Microsoft Excel©. The length of the smallest individual in which a particular ossification was observed amongst the sampled individuals (minimum length) and the minimum length at which a particular ossification was observed in all sampled

individuals (fixed length) was determined for each bony element to generate the sequence of ossification for the entire skeleton as well as individual regions (following Cubbage & Mabee, 1996; Mattox, Britz, & Toledo-Piza, 2014). Select C&S specimens were photographed using a Zeiss Axiocam MRc5 digital camera attached to the aforementioned microscope. All images were processed using Adobe Photoshop CS5.1 and Illustrator CS5.1. Terminology of cartilages follows de Beer (1937). Osteological terminology follows that of Egge (2007). Weberian terminology follows that of Britz and Hoffman (2006). Pectoral-fin spine terminology follows that of Kubicek, Britz and Conway (2019). Sensory canal pores associated with particular skeletal elements were determined by counting individual pores in branches of the cephalic sensory canal from anterior to posterior. For example, the first anteriormost infraorbital sensory canal pore was counted as infraorbital sensory canal pore 1.

Material Examined

All material examined is deposited in the Collection of Fishes at the Biodiversity Research and Teaching Collections of Texas A&M University. *Ictalurus punctatus*: TCWC uncat., 100 specimens, 7.7 mm NL – 44.9 mm SL; TCWC uncat., 45 specimens, 8.6 mm NL – 21.2 mm SL. *Noturus gyrinus*: TCWC uncat., 120 specimens, 5.4 mm SL – 26.4 mm SL; TCWC uncat., 38 specimens, 5.8 mm SL – 13.1 mm SL; TCWC 19758.01, one specimen, 36.6 mm SL.

Results

Overview of Skeletal Development.

Approximately 328 and 286 individual elements (K. Kubicek personal observations; not including individual fin rays, gill rakers, or parapophyses) are present in the skeleton of *Ictalurus punctatus* and *Noturus gyrinus,* respectively. The total number of skeletal elements considered herein was condensed to 144 elements in *I. punctatus* and 137 elements in *N. gyrinus* by treating multiple serially repetitive elements as a single element. This included branchiostegal rays, vertebral elements posterior to vertebra 5 and anterior to preural vertebra 3, dorsal- and anal-fin proximal and distal radials (excluding dorsal-fin proximal radials 1 – 3), and post-Weberian ribs. All elements of the skeleton are ossified by 22.4 mm SL in *I. punctatus* (Fig. 2.1) and 14.1 mm SL in *N. gyrinus* (Fig. 2.2). The first bone to appear in both species is the cleithrum, which is present in the smallest specimens examined (7.7 mm NL in *I. punctatus* and 5.4 mm NL in *N. gyrinus*) with the maxilla, opercle, dentary and primary caudal-fin rays being the next elements to appear. The last bones to appear in *I. punctatus* include hypobranchial 2, the anal-fin distal radials, and the suprapreopercle. In *N. gyrinus*, the last bones to appear include hypobranchial 2, and the distal radials of the dorsal and anal fins. The dorsal- and anal-fin distal radials of *N. gyrinus* were absent from the developmental series compiled for the species but are present in larger specimens (36.6 mm SL; TCWC 19758.01). Comparison of the sequences generated for *I. punctatus* (Fig. 2.1) and *N. gyrinus* (Fig. 2.2) revealed differences in the order of appearance of particular bones (e.g., the prootic is the 38th bone to appear in the overall sequence for *I. punctatus* vs.

74th in *N. gyrinus*); however, when looking at the sequence of development by region (e.g., the neurocranium) these differences dissapear (e.g, the prootic is the first bone of the otic region to appear in both species; Fig. 2.3 – 2.4) except for preural centra 2 and 3, which are the 41st and 42nd bones to appear in *I. punctatus* and the 79th and 55th bones to appear in the whole skeleton and in the vertebral column are the 12th and 13th in *I. punctatus* and the 26th and 24th bones in *N. gyrinus*.

Skeletal development of Ictalurus punctatus

In the following sections, I provide a detailed overview of skeletal development for the cranium, paired fins, and Weberian apparatus of *Ictalurus punctatus*. For a detailed description of the post-Weberian axial skeleton in *I. punctatus* the reader is referred to Grande and Shardo (2002). For each region of the skeleton, the sequence of ossification for the bony elements of that region is provided first, followed by a description of development for each individual element in that region. Ossification sequences are arranged based on the length (NL/SL) at which each element becomes fixed. In instances where multiple elements of a region become fixed at the same length, elements are ordered based on length at first appearance (NL/SL) then alphabetically. I conclude each section with a brief overview of skeletal development in *N. gyrinus*, including the sequence of ossification for the bony elements of that region, and make note of any differences identified between the two species.

Neurocranium Ethmoid Region

The most common sequence of ossification: nasal (11.4 mm SL) – mesethmoid (12.2 mm SL) – lateral ethmoid (12.8 mm SL) – vomer (14.5 mm SL) (Fig. 2.5).

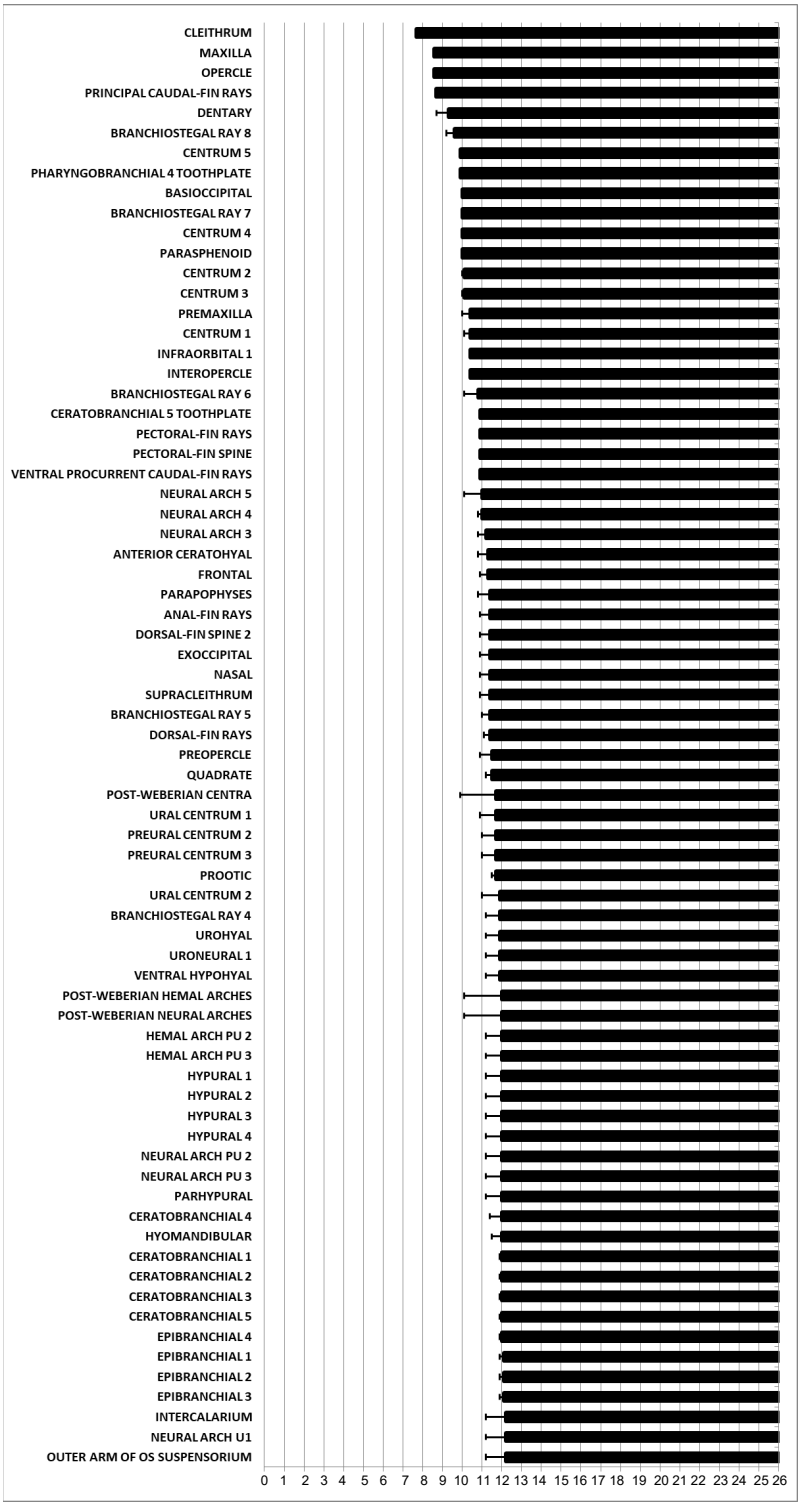

Figure 2.1. Ossification sequence of 144 skeletal elements of *Ictalurus punctatus*. Black bars along horizontal axis represent the length at which a particular ossification is present in all individuals (fixed). Error bars associated with black bars indicate the length at which a particular ossification is present in some but not all individuals. Vertical axis represents length in mm NL/SL. mm, Millimeters; NL, notochord length; SL, standard length.

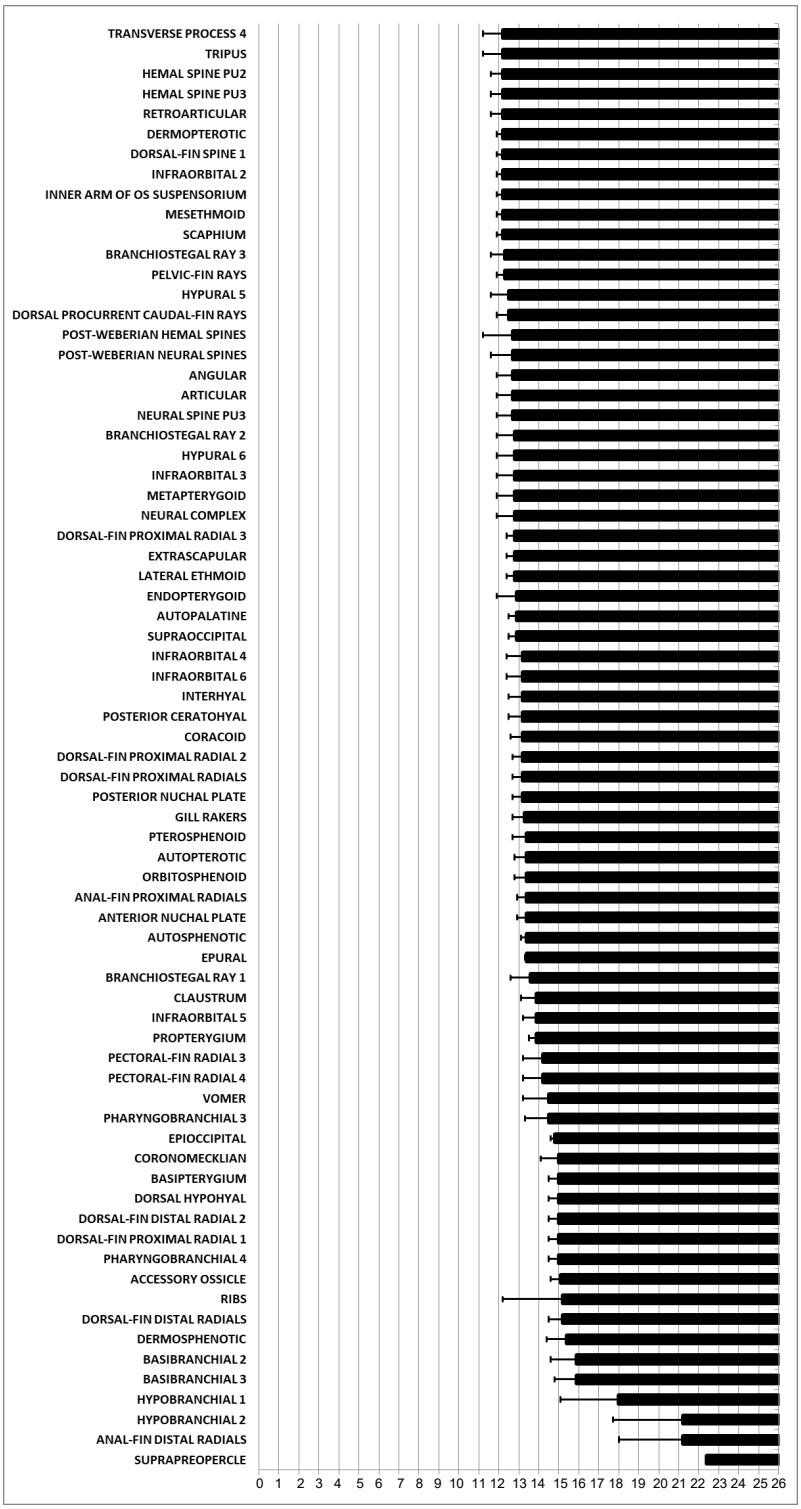

Figure 2.1. Continued

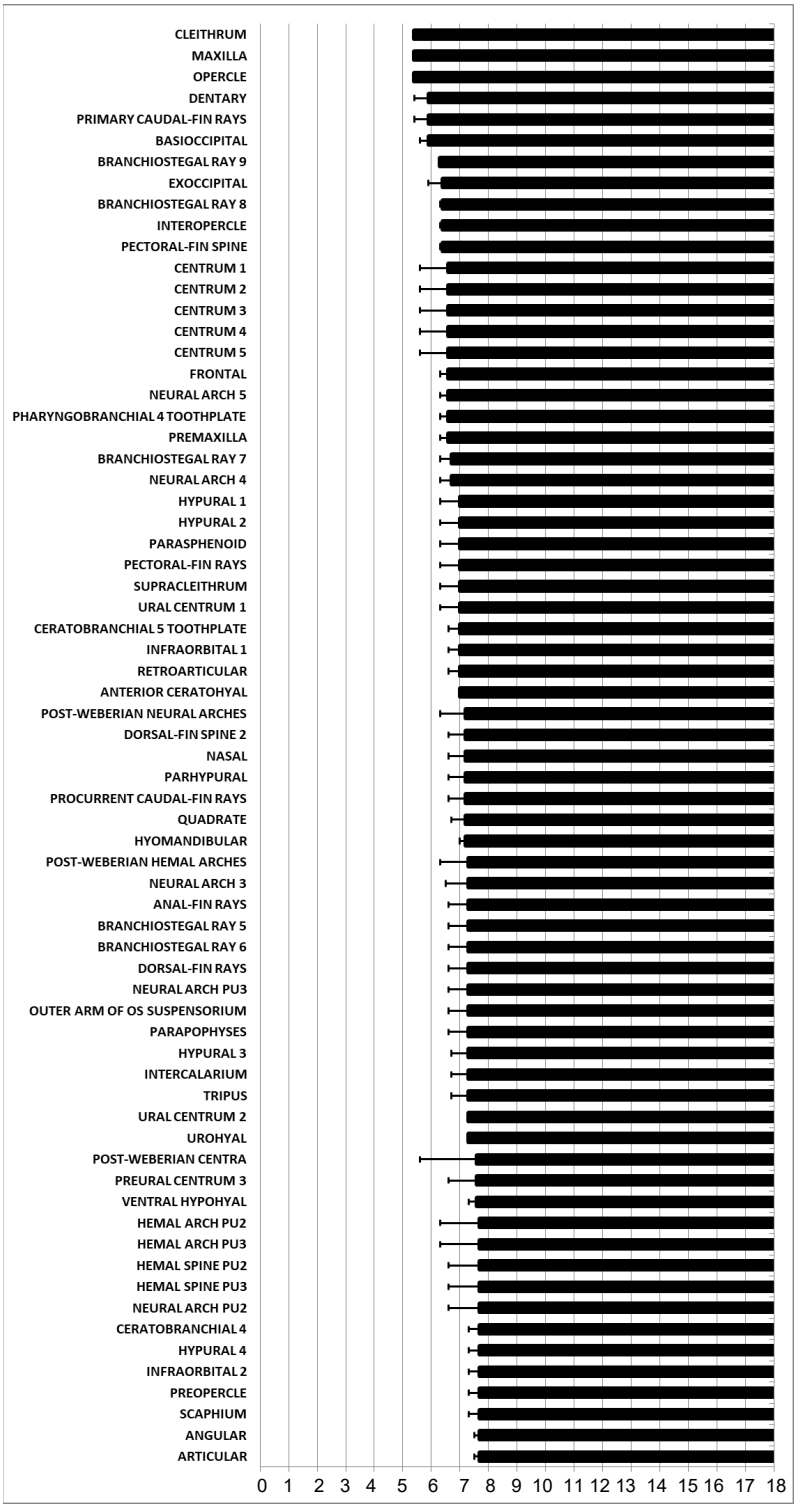

Figure 2.2. Ossification sequence of 137 skeletal elements of *Noturus gyrinus*. Black bars along horizontal axis represent the length at which a particular ossification is present in all individuals (fixed). Error bars associated with black bars indicate the length at which a particular ossification is present in some but not all individuals. Vertical axis represents length in mm SL. mm, Millimeters; SL, standard length.

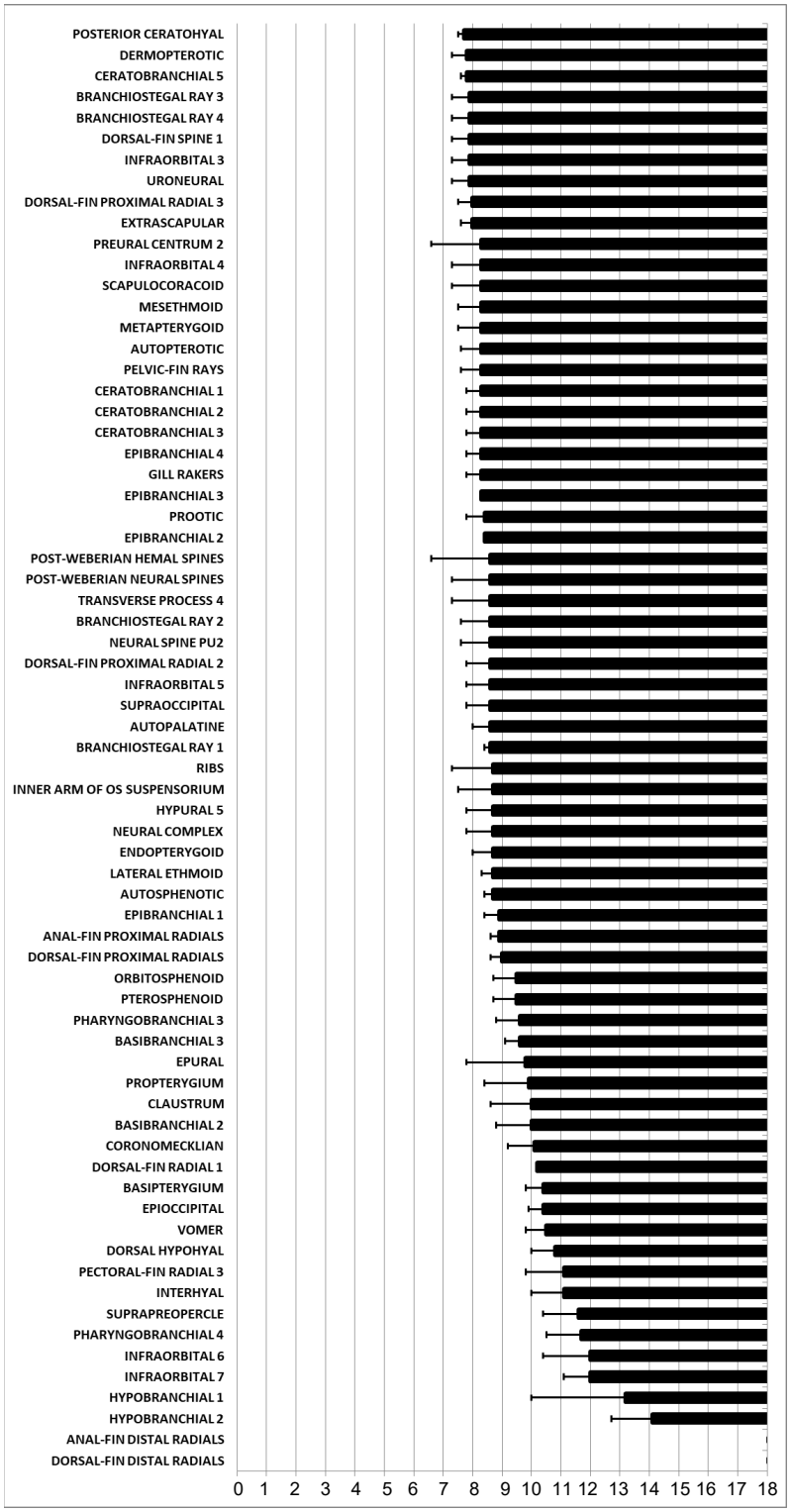

Figure 2.2. Continued

Figure 2.3. Ossification sequence of 144 skeletal elements of *Ictalurus punctatus* separated by skeletal region. Black bars along horizontal axis represent the length at which a particular ossification is present in all individuals (fixed). Error bars associated with black bars indicate the length at which a particular ossification is present in some but not all individuals. Vertical axis represents length in mm NL/SL. mm, Millimeters; NL, notochord length; SL, standard length.

Figure 2.3. Continued

Figure 2.4. Ossification sequence of 137 skeletal elements of *Noturus gyrinus* separated by skeletal region. Black bars along horizontal axis represent the length at which a particular ossification is present in all individuals (fixed). Error bars associated with black bars indicate the length at which a particular ossification is present in some but not all individuals. Vertical axis represents length in mm SL. mm, Millimeters; SL, standard length.

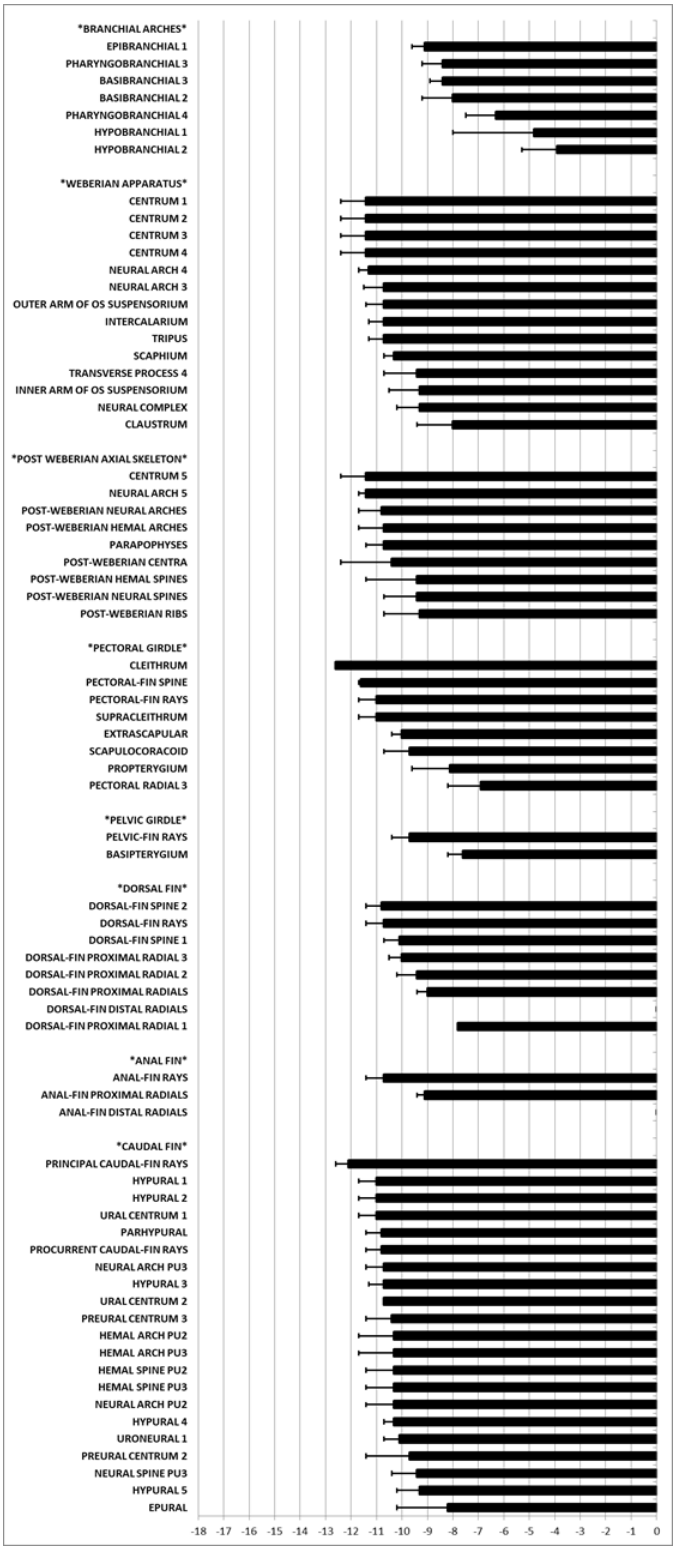

Figure 2.4. Continued

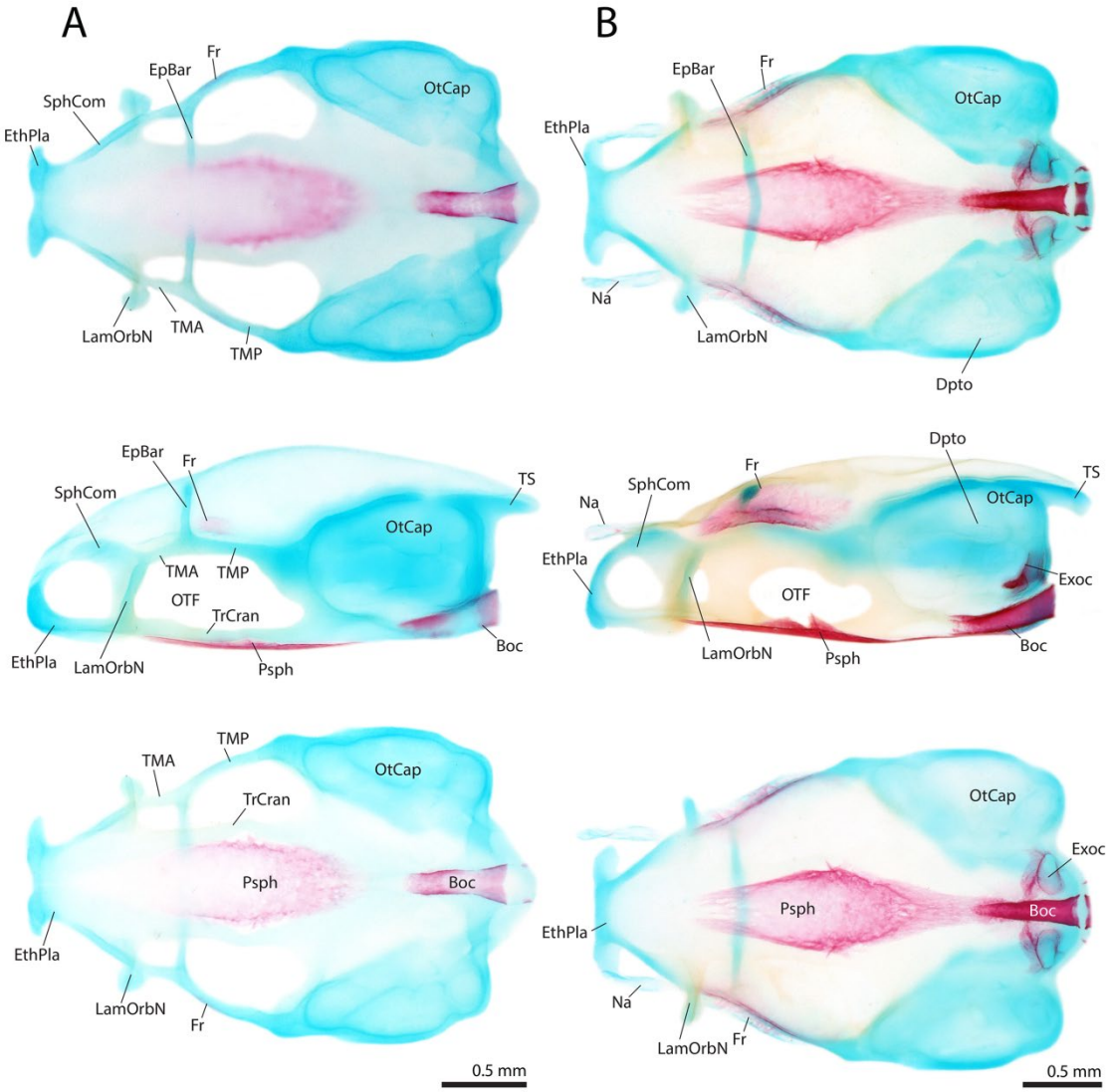

Figure 2.5. Ontogeny of the neurocranium of *Ictalurus punctatus* (**A**) 10.9 mm SL. (**B**) 12.2 mm SL. (**C**) 13.3 mm SL. (**D**) 18.0 mm SL. (**E**) 21.2 mm SL. (**F**) 44.9 mm SL. Arrows indicate segmentation. AExt, Additional extrascapular; Ast, Asteriscus; Boc, Basioccipital; Dpto, Dermopterotic; EpBar, Epiphysial bar; Epoc, Epioccipital; EthPla, Ethmoid plate; Exoc, Exoccipital; Ext, Extrascapular; Fr, Frontal; LamOrbN, Lamina orbitonasalis; Lap, Lapillus; LE, Lateral Ethmoid; ME, Mesethmoid; mm, Millimeters; Na, Nasal; Orsph, Orbitosphenoid; OtCap, Otic capsule; OpF, Optic foramen; OTF, Optico-trigemino-facial foramen; Pro, Prootic; Psph, Parasphenoid; Pto, Pterotic; Ptsph, Pterosphenoid; Sag, Sagitta; Soc, Supraoccipital; SphCom, Sphenoseptalis commissure; TMA, Taenia marginalis anterior; TMP, Taeniamarginalis posterior; TrCom, Trabecula cranii ;TrFaF, Trigemino-facial foramen; TS, Tectumsynoticum; TTM; Taenia tecti medialis; Vo, Vomer; SL, standard length.

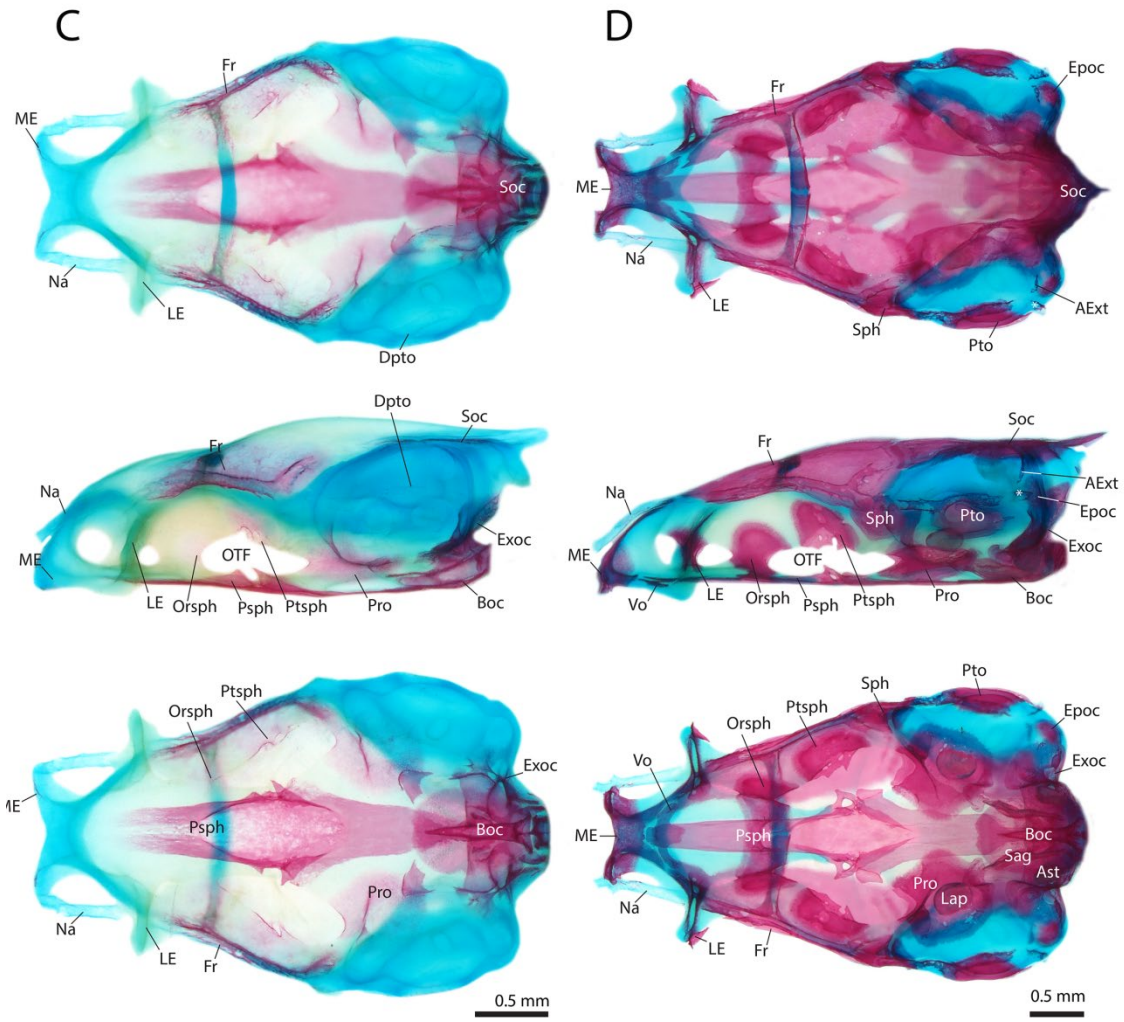

Figure 2.5. Continued

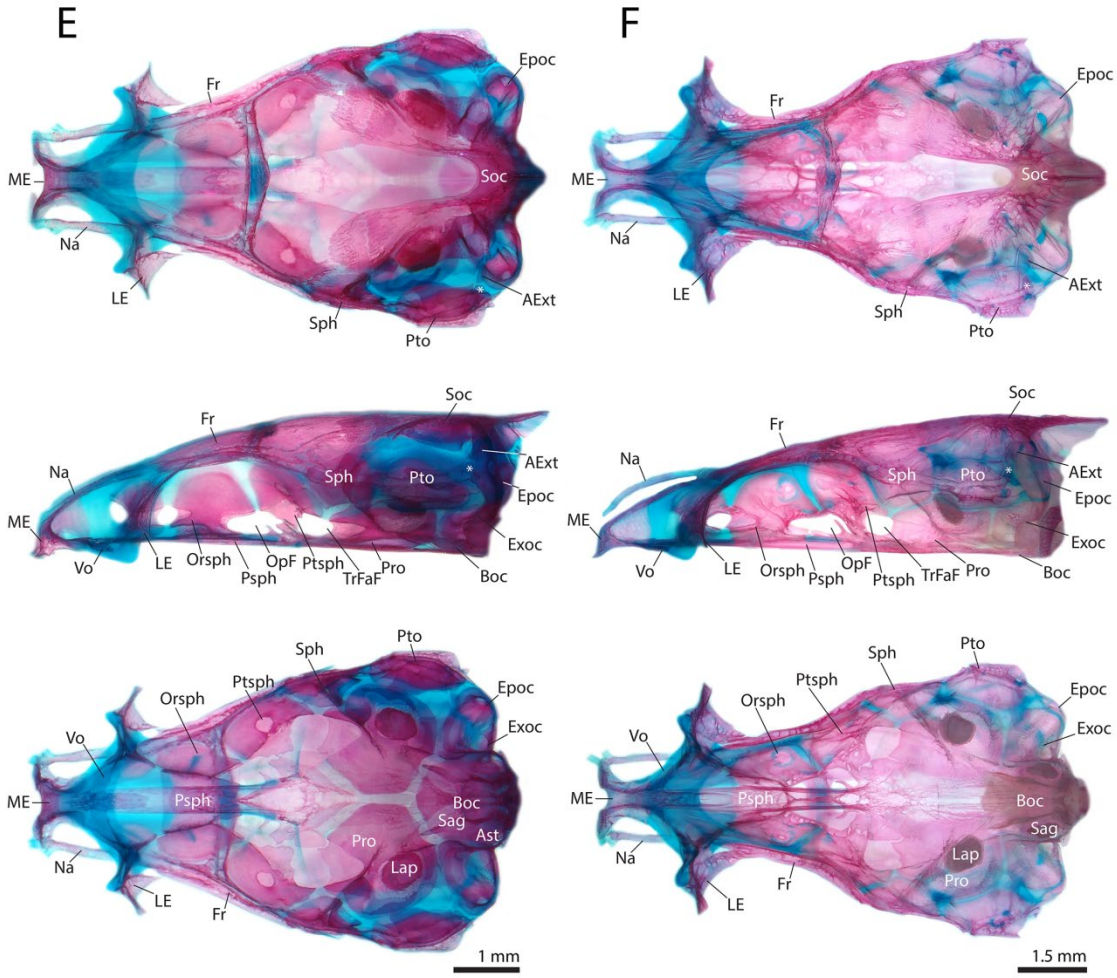

Figure 2.5. Continued.

Nasal: The nasal is a dermal ossification that first appears in some individuals of 10.9 mm SL (Fig. 2.5A) as a thin lamina of bone located laterally to the sphenoseptalis commissure. As the ossification expands it becomes trough-like and its length extends from just dorsal to the *lamina orbitonasalis* up to the anterior border of the ethmoid plate

(12.2 mm SL; Fig. 2.5B). The ossification begins to close dorsally forming a tube-like canal; however, a distinct opening in the ossification remains anterolaterally (13.3 mm SL; Fig 3C) which will eventually become an opening for supraorbital sensory pore 2 (K. Kubicek pers. obs.).

Mesethmoid: The mesethmoid first appears at 11.9 mm SL as a paired perichondral ossification located along the anterodorsal edge of the ethmoid cornua of the ethmoid plate. By 13.2 mm SL (Fig. 2.5C) the bone ossification has expanded ventrally to cover the anteroventral edge of the ethmoid cornua at the point of articulation with the premaxilla and shortly after, at 14.0 mm SL, the perichondral ossification has extended posteriorly along the ethmoid cartilage medial to the nasal capsule. The two separate ossifications continue to expand and, by 15.9 mm SL, meet each other medially over the anterodorsal surface of the ethmoid plate and fuse by 15.9 mm SL. At the same size, small flanges of membrane bone autogenous have arisen autogenously from the mesethmoid at the tips of the ethmoid cornua which extend towards and are connected to the premaxilla via dense connective tissue. At 18.0 mm SL (Fig. 2.5D), the mesethmoid covers much of the ethmoid plate which has begun to ossify endochondrally. By 44.9 mm SL (Fig. 2.5F), a stage closely resembling the adult condition, the mesethmoid is completely ossified and forms strong sutures with the frontals posterodorsally and the lateral ethmoids posteriorly. Posteroventrally, the mesethmoid extends dorsal to the anteriormost edge of the parasphenoid and the vomer.

Lateral Ethmoid: The paired lateral ethmoid first appears (12.4 mm SL) as a perichondral ossification of the *lamina orbitonasalis* at its mid-length near the

orbitonasal foramen. At 13.4 mm SL the ossification has expanded on both the anterior and posterior surface of the *lamina orbitonasalis*, both of which are connected by the orbitonasal foramen, which is now completely surrounded by bone. The lateral ethmoid continues to spread towards the taenia marginalis anterior and sphenoseptalis commissure dorsally and the ethmoid plate ventrally, and extends around the lateral edge of the *lamina orbitonasalis* by 15.9 mm SL. By 18.0 mm SL (Fig. 2.5D) the ossification has continued to expand around the posterior border the olfactory foramen anteriorly and the anterior border of the preoptic fontanelle in the orbit. A thin membrane bone extension of the lateral ethmoid has formed along the anterolateral edge of the bone forming an anterior rim for the orbit. By 44.9 mm SL (Fig. 2.5F), the lateral ethmoid now forms the entire anterior wall of the orbit, extending from the ventral surface of the mesethmoid and the frontal dorsally to the parasphenoid ventrally. Posteriorly it borders the orbitosphenoid, which remain separated by the preoptic fontanelle, which in adults becomes covered by bone.

Vomer: The vomer is a dermal ossification first appearing in some individuals as small as 13.2 mm SL (Fig. 2.5C) as a thin inverted U-shaped bone located ventrally on the ethmoid plate just anterior to the parasphenoid. At 16.5 mm SL, the lateral edges of the vomer have extended further posteriorly on either side of the parasphenoid. Medially, the vomer has gained a posterior process that extends ventral to the parasphenoid and a shorter rounded anterior process. In adult specimens, the vomer lies ventral to the overlapping parasphenoid and mesethmoid. The posterior extension of the

vomer has become much longer giving the bone its characteristic t-shape and the ventral surface of the bone exhibits sculpturing posteriorly.

Comparison. The most common sequence of ossification for this region in *Noturus gyrinus* is as follows: nasal (7.2 mm SL) – mesethmoid (8.3 mm SL) – lateral ethmoid (8.7 mm SL) – vomer (10.5 mm SL).

No differences in the sequence of ossification were identified between *Noturus gyrinus* and *Ictalurus punctatus* in the ethmoid region of the neurocranium. The ethmoid region of the neurocranium of *N. gyrinus* and *I. punctatus* are similar, and no major differences in adult morphology are observed in this region.

Neurocranium Orbital Region

The most common sequence of ossification: parasphenoid (10.0 mm SL) – frontal (11.3 mm SL) – pterosphenoid and orbitosphenoid (13.4 mm SL) (Fig. 2.5).

Parasphenoid: The parasphenoid first appears in individuals of 10.0 mm SL as a 'U' shaped splint of bone running medial to the *trabeculae cranii* that unite posteriorly in front of the otic capsule forming a thin plate of bone ventral to a portion of the hypoglossal foramen. By 11.3 mm SL, the parasphenoid has expanded anteriorly and posteriorly, now covering the entirety of the hypophyseal fenestra, with both ends tapering in width giving the bone a rhomboid appearance. Posteriorly it extends across the ventral surface of the otic capsule where it stops ventral to the anterior tip of the notochord and anteriorly it reaches the point of the *lamina orbitonasalis*. Two small ascending processes, represented by thin laminae of bone, have formed along the lateral margin near the widest point of the bone. At 13.3 mm SL (Fig. 2.5C), the anterior and

posterior ends have widened and the posterior margin now overlays the anteroventral surface of the basioccipital, in line with the notochord. The lateral ascending processes have grown larger and are located directly ventral to the newly formed pterosphenoid. The anterior margin of the parasphenoid extends dorsal to the vomer and reaches its anterior edge. At this point, the lateral margin of the parasphenoid posterior to the lateral ascending processes has expanded posterodorsally towards the anteroventral border of the prootic. The asending processes continue to expand dorsally towards the pterosphenoid, effectively separating the optico-trigemino-facial foramen into a separate optic foramen and trigemino-facial foramen by 21.2 mm SL (Fig. 2.5E) with the posterior process forming an interdigitating suture with it by 42.1 mm SL (Fig. 2.5D).

Frontal: The frontal is a paired dermal bone that first appears (10.9 mm SL; Fig. 2.5A) as a thin ossification forming around the frontal portion of the supraorbital sensory canal. It is located medial to the taenia marginalis and extends on both sides of the epiphyseal bar and is more heavily ossified just behind the epiphyseal bar. By 12.2 mm SL (Fig. 2.5B), the frontals run the length of the taenia marginalis reaching the sphenoseptalis commissure anteriorly and the anterior end of the otic capsule posteriorly. The underlying bone supporting the supraorbital canal has expanded medially forming a large flat plate of bone. As the frontal continues to expand, the canal supporting the parietal branch of the supraorbital canal has started to ossify (13.2 mm SL; Fig. 2.5D). At 15.9 mm SL, the frontals meet each other across the midline at the point of the epiphyseal bar. Posteriorly, the frontal contacts the anterior membrane bone extension of the supraoccipital and anteriorly it almost reaches the mesethmoid. The ossification

surrounding the supraorbital sensory canal is almost completely enclosed at this stage. By 21.2 mm SL (Fig. 2.5E), the frontal has formed an interdigitating suture with the mesethmoid anteriorly and overlaps the anterior margin of the supraoccipital and sphenotic. From this point on, the frontal changes little other than becoming more sculptured (44.9 mm SL; Fig. 2.5F) and expanding medially, which reduces the size of the anterior and posterior cranial fontanelles.

Pterosphenoid: The pterosphenoid first appears as a paired perichondral ossification on the dorsal margin of the common foramen for the passage of the Optic (II), Trigeminal (V) and Facial (VII) nerves at 12.7 mm SL, and its presence becomes fixed in development at 13.4 mm SL. By 14.2 mm SL, the perichondral ossification has expanded in size and become semicircular in shape. Membrane bone processes extend ventrally from the perichondral ossification leaving two openings, which (by 15.9 mm SL in most specimens) become surrounded by bone establishing the foramina for the passage of the ophthalmic branch of the trigeminal and facial nerves. The bone continues to expand in all directions and by 21.2 mm SL (Fig. 2.5E) the ventral margin almost reaches the ascending process of the parasphenoid, creating separate optic and trigemino-facial foramina. At 42.1 mm SL (Fig. 2.5F), it meets the frontal dorsally and has formed an interdigitating suture with the ascending process of the parasphenoid but still remains separate from the orbitosphenoid and sphenotic by a strip of cartilage.

Orbitosphenoid The paired orbitosphenoid originates as a small perichondral ossification along the anterior margin of the common foramen for the passage of the Optic (II), Trigeminal (V) and Facial (VII) nerves (12.8 mm SL, becoming fixed in

development at 13.4 mm SL). The perichondral ossification expands across the cartilage anteriorly and becomes crescent shaped in appearance by 14.2 mm SL. As the orbitosphenoid grows, it eventually meets its antimere ventrally and the two elements fuse into a single ossification (16.2 mm SL). At 18.0 mm SL (Fig. 2.5D), the orbitosphenoid has spread to the posterior margin of the preoptic fontanelle, and by 21.2 mm SL (Fig. 2.5F) a lamina of membrane bone extends anteriorly over part of the fontanelle. The orbitosphenoid continues to grow, replacing much of the cartilage immediately posterior to the *lamina orbitonasalis*. Interdigitated sutures have started to form with the lateral ethmoid anteriorly, dorsal to the preoptic fontanelle, the pterosphenoid posteriorly and the parasphenoid posteroventrally, dorsal and ventral to the optic foramen, respectively. However, much of the border between the orbitosphenoid and the surrounding elements, excluding the parasphenoid, remains separated by cartilage.

Comparison. The most common sequence of ossification for this region in *Noturus gyrinus* is as follows: frontal (6.6 mm SL) – parasphenoid (7.0 mm SL) – pterosphenoid and orbitosphenoid (9.5 mm SL).

The only difference observed in the sequence of ossification identified between *Noturus gyrinus* and *Ictalurus punctatus* in the orbital region of the neurocranium is that the frontal appears before the parasphenoid in *N. gyrinus* while the parasphenoid appears first in *I. punctatus*. The orbital regions of the neurocranium of *N. gyrinus* and *I. punctatus* are similar, and no major differences in adult morphology are observed in this region.

Neurocranium Otic Region

The most common sequence of ossification: prootic (11.7 mm SL) – pterotic (12.2 mm SL) – sphenotic (13.4 mm SL) (Fig. 2.5).

Prootic: The paired chondral prootic is one of the largest bones in the neurocranium. The bone first appears (11.5 mm SL) as a perichondral ossification on the ventrolateral surface of the otic capsule ventral to the utricular capsule, and is found in all individuals of 11.7 mm SL or larger. The prootic has started to endochondrally ossify and reaches the posterior edge of the common foramen for the passage of cranial nerves II, V, and VII anteriorly (13.3 mm SL; Fig. 2.5C). The bone has also expanded to cover part of the anterior surface of the anterior vertical semicircular canal and utricular capsule as well as the anterior portion of the saccular capsule. At 15.9 mm SL, the bone has expanded to contact the parasphenoid ventrally and a membranous extension covers a posterior portion of the common foramen for the passage of the Optic (II), Trigeminal (V) and Facial (VII) nerves. The prootic increases in size but changes little in shape and by 42.1 mm SL (Fig. 2.5F), the surface has become slightly sculptured. It has begun to form an interdigitated suture with the parasphenoid but still remains separate from the other elements by a thin strip of cartilage.

Pterotic: The compound pterotic is composed of both chondral (autopterotic) and dermal (dermopterotic) bones. The dermopterotic is the first to appear (11.9 mm SL) on the posterolateral surface of the otic capsule as two thin trough shaped ossifications of the pterotic portion of the otic sensory canal. By 13.3 mm SL (Fig. 2.5C), the autopterotic can be seen as a small perichondral ossification on the lateral surface of the

otic capsule, ventral to the dermopterotic. The sensory canal ossifications of the dermopterotic continue to expand towards each other and by 14.2 mm SL they have fused into a single trough of bone excluding an opening in the ventral wall which connects the otic sensory canal to the preoperculo-mandibular sensory canal. At the same stage, the autopterotic is oval shaped and has begun to endochondrally ossify. The autopterotic continues to grow and eventually meets the dermopterotic anterodorsally and the two elements fuse forming the pterotic (15.5 mm SL). Shortly after this (16.2 mm SL), a membranous lamina of bone has started to form along the lateral edge of the bone with a small pointed process extending posteriorly past the chondral portion of the bone. Additionally, the pterotic overlies the lateral border of the horizontal semicircular canal. Bone has started to enclose the roof of the pterotic portion of the otic sensory canal by 17.8 mm SL (Fig. 2.5D) and by 21.2 (Fig.5E) the canal is fully enclosed. At this stage, the lamina of bone has expanded lateroventrally where it comes into contact with the supracleithrum. Anteriorly, the pterotic has just reached the border of the sphenotic, although much of the border remains cartilaginous. The sensory canal has fused with the sphenotic portion of the otic canal anteriorly, and posteriorly it ends just anterior to the extracapular. At 42.1 mm SL (Fig. 2.5F), the pterotic forms a suture with the supraoccipital dorsally. Posteriorly it meets the extrascapular and lies ventral to a portion of the accessory ossicle. The pterotic remains separated by cartilage from the epiotic posteriorly and the exoccipital and the prootic ventrally. The medial surface of the bone forms the lateral surface of the utricular canal and the lateral surface has become slightly sculptured.

Sphenotic: The sphenotic is a compound element in catfishes resulting from the ontogenetic fusion of the endoskeletal autosphenotic and the dermal dermosphenotic. The autosphenotic is the first to appear at 13.1 mm SL as a perichondral ossification at the junction of the taenia marginalis and the otic capsule. By 14.2 mm SL, the autosphenotic has started to endochondrally ossify and by 15.4 mm SL it covers the anteroventral border of the anterior vertical semicircular canal and has expanded dorsally to the anterodorsal edge of the otic capsule where it meets the frontal. At this stage, the dermosphenotic has appeared as a trough shaped ossification of the sphenotic portion of the otic sensory canal that is fused to the autosphenotic, forming the sphenotic. The roof of the spenotic portion of the otic sensory canal has started to enclose in bone by 17.8 mm SL (Fig. 2.5D) and is fully enclosed and fused with the pterotic portion of the otic sensory canal by 21.2 mm SL (Fig. 2.5E). By 42.1 mm SL (Fig. 2.5F), the sphenotic has extended posteriorly and contacts the supraoccipital and the pterotic. It remains separated by a small strip of cartilage from the prootic and pterosphenoid ventrally. The sensory canal ossification ends anteriorly at the junction with the infraorbital and supraorbital sensory canals which sits at the border of the sphenotic and the frontal.

Comparison. The most common sequence of ossification for this region in *Noturus gyrinus* is as follows: prootic (8.4 mm SL) – pterotic (8.5 mm SL) – sphenotic (8.7 mm SL).

No differences in the sequence of ossification were identified between *Noturus gyrinus* and *Ictalurus punctatus* in the otic region of the neurocranium. The otic region

of the neurocranium of *N. gyrinus* and *I. punctatus* are similar, and no major differences in adult morphology are observed in this region.

Neurocranium Occipital Region

The most common sequence of ossification: basioccipital (10.0 mm SL) – exoccipital (11.4 mm SL) – extrascapular (12.8 mm SL) – supraoccipital (12.9 mm SL) – epioccipital (14.8 mm SL) – accessory ossicle (15.1 mm SL) (Fig. 2.5).

Basioccipital: The basioccipital originates as a perichordal ossification around the anterior tip of the notochord at the base of the cranium (10.0 mm NL). By 12.0 mm SL (Fig. 2.5B), the entire cranial portion of the notochord is covered in a thin ossification. The basioccipital extends lateroventrally from the notochord as a perichondral ossification on the ventral surface of the otic capsule. A small membranous lamina of bone has started to form on the dorsal surface of the perichordal ossification. At 14.2 mm SL, the membranous lamina has expanded anteriorly forming a flat sheet and posteriorly it has formed into a pointed process on either side of the notochord that extends dorsally towards the exoccipital forming part of the posterodorsal surface of the lagenar capsule. Ventrally, the perichondral ossification has expanded to form a circular ossification that extends from the back of the cranium to the anteriormost tip of the notochord, forming most of the ventral surface of the saccular capsule and the entirety of the ventral surface of the lagenar capsule. The anterior membranous extension has expanded anterolaterally towards the posteroventral margin of the prootic giving it a triangular appearance (15.4 mm SL). The basioccipital changes little in appearance and shape as it continues to grow, becoming slightly larger and having a sculptured surface

(42.1 mm SL; Fig. 2.5F). In the adult, it is bordered posterodorsally by the exoccipital and anteriorly by the prootic and the parasphenoid.

Exoccipital: The paired exoccipital is a chondral bone that first appears at 10.9 mm SL (Fig. 2.5A) and is fixed in development at 11.4 mm SL. It starts as a perichondral ossification around the occipital arches dorsolateral to the notochord. The ossification continues to spread over the occipital arch and by 12.2 mm SL (Fig. 2.5B) the exoccipital possesses a lamina of membrane bone anteriorly that forms a portion of the roof of the saccular and lagenar capsules. By 13.4 mm SL (Fig. 2.5C), the exoccipital covers most of the occipital arch forming the lateral margin of the foramen magnum. The posterior margin of the foramen for the passage of the Glossopharyngeal (IX) nerve and the entire rim of the foramen for the passage of the Vagus (X) nerve are perichondrally ossifying. A small membranous extension has formed on the dorsoposterior margin of the exoccipital directly anterior to the *concha* of the *scaphium*. At 15.4 mm SL, the foramina for the Glossopharyngeal (IX) and Vagal (X) nerves are completely surrounded by the exoccipital. The membranous bone along the posterior margin of the bone has grown ventrally and rejoins the exoccipital, creating the foramen for an occipital spinal nerve (16.2 mm SL). As the bone continues to expand it covers the lateral surface of the lagenar capsule (18.0 mm SL; Fig. 2.5D) but by 44.9 mm SL (Fig. 2.5F) it remains separated from all of the surrounding elements by a strip of cartilage.

Extrascapular: The extrascapular can first be observed in 12.4 mm SL individuals as a small weakly ossified trough of bone around the lateral line sensory

canal anterior to the supracleithrum and in line with the posterior margin of the chondrocranium. By 16.2 mm SL the roof of the sensory canal has begun to close with bone and by 21.2 mm SL (Fig. 2.5E) a small flange of bone has started to form from its anterodorsal margin. At 42.1 mm SL (Fig. 2.5F), the extrascapular is bordered by the pterotic anteriorly, the supracleithrum posteriorly and the accessory ossicle dorsally. The sensory canal ossification is completely enclosed, forming a tube, but still weakly ossified. The flange of bone extends dorsally over the posterior edge of the pterotic towards the accessory ossicle.

Supraoccipital: Whether this element is of compound origin (parietal+supraoccipital) or not has been a contentious subject in the past. Herein I refer to the element as the supraoccipital and further discuss the homology of this bone in the discussion. The supraoccipital originates as a pair of perichondral ossifications in the otic capsule on either side of the posterior cranial fontanelle (12.5 mm SL first appearance, 12.9 mm SL fixed length). Soon after (13.3 mm SL; Fig. 2.5C), the paired elements have expanded and are endochondrally ossifying. A small ridge of membrane bone extends laterally from the perichondral ossification over a groove in the otic capsule, which carries an accessory ramus of the facial nerve. This membranous ridge of bone runs the length of the supraoccipital and extends anteriorly beyond the margin of the otic capsule. By 14.1 mm SL, the paired ossifications have met and fused into a single U-shaped bone around the posterior margin of the posterior cranial fontanelle. The ridges of membrane bone on either side of the fontanelle extend posteromedially along the margin of the otic capsule and meet to form a point at the posterior tip of the *tectum*

synoticum. The anterior membranous extensions have expanded to meet the frontals (15.9 mm SL) with the anteriormost margin extending under the posterior edge of the frontals. At this size, the supraoccipital starts to expand around the anterodorsal and posterodorsal margin of the anterior and posterior vertical semicircular canals respectively. The groove for the passage of the accessory ramus of the facial nerve is completely enclosed in bone leaving a pair of foramina at the back of the cranium through which the nerve passes prior to extending along either side of the body. The posteromedial extensions of membrane bone completely cover the dorsal surface of the *tectum synoticum* giving the posterior margin of the bone a triangular point and by 18.0 mm SL, the supraoccipital extends beyond the posterior margin of the *tectum synoticum* and possesses a small ventral extension of membrane bone forming the supraoccipital crest. By 21.2 mm SL (Fig. 2.5E), the bone has retained the same relative shape but has grown in size, just meeting the epioccipital posterolaterally. The supraoccipital crest has continued to expand ventrally forming a triangular lamina of bone that extends to the posterior tip of the *tectum synoticum*. At 42.1 mm SL (Fig. 2.5F), the supraoccipital now forms the posterior third of the cranial roof. It forms a strong interdigitating suture with the frontal and now meets the sphenotic at its anterolateralmost corner and the pterotic along most of its lateral border. Posterolaterally, the supraoccipital also contacts the accessory ossicle and the anterodorsal tip of the supracleithrum and posteroventrally it still remains separated from the exoccipital by a thin strip of cartilage. Posteriorly the supraoccipital crest forms a connection with the first proximo-middle radial of the

dorsal-fin and ventral to this, two anterolateral projections of the neural complex of the Weberian apparatus contact the posterior surface of the supraoccipital.

Epioccipital: The epioccipital is a paired chondral bone that first appears in some individuals of 14.6 mm SL as a small circular perichondral ossification underlying the anterior arm of and situated just ventral to the tip of the anterior arm of the supracleithrum. It has started to endochondrally ossify by 15.6 mm SL and it continues to increase in size and extends ventrally to become more ovoid in shape and covers the posteroventral portion of the posterior vertical semicircular canal of the inner ear (21.2 mm SL; Fig. 2.5E). By 44.9 mm SL (Fig. 2.5F, it has increased in size but changed little in shape and remains separated from all surrounding bones by a thin strip of cartilage, except for the supraoccipital, which it meets anterodorsally.

Accessory ossicle: The homology of this element located on the dorsolateral surface of the cranium in some ictalurids has been contentious in the past (see Lundberg, 1975; Arratia & Gayet, 1995; Slobodian & Pastana, 2018). Due to the unknown homology of this element, it is referred to herein as the accessory ossicles. The accessory ossicle is a small dermal plate-like ossification that first appears at 14.6 mm SL as a small splint of bone anterior to the dorsal tip of the supracleithrum. At 21.2 mm SL (Fig. 2.5E) it has started to expand anteroventrally and by 42.1 mm SL (Fig. 2.5F) it forms a plate of bone overlying the ventral border between the supraoccipital and epioccipital. It tapers ventrally to meet the posterodorsal tip of the pterotic and the dorsal margin of the extrascapular.

Comparison. The most common sequence of ossification for this region in *Noturus gyrinus* is as follows: basioccipital (5.9 mm SL) – exoccipital (6.4 mm SL) – extrascapular (8.0 mm SL) – supraoccipital (8.6 mm SL) – epioccipital (10.4 mm SL).

No differences in the sequence of ossification were identified between *Noturus gyrinus* and *Ictalurus punctatus* in the occipital region of the neurocranium. The occipital region of *N. gyrinus* differs slightly from *I. punctatus* in that in the former the accessory ossicle is absent and the extracapular consists of only a canal ossification with no laminar portion.

Jaws

The most common sequence of ossification: maxilla (8.6 mm NL) – dentary (9.3 mm NL) – premaxilla (10.4 mm SL) – retroarticular (12.2 mm SL) – anguloarticular (12.7 mm SL) – coronomeckelian (15 mm SL) (Fig. 2.6).

Maxilla: The paired maxilla is one of the first three elements to ossify in the skeleton of *Ictalurus punctatus* (8.6 mm NL). It starts off as a slightly curved lamina located anteriorly to the pars autopalatina that extends laterally to cover the anteroproximal tip of the maxillary barbel cartilage. By 11.3 mm SL (Fig. 2.6A), the maxilla has become more heavily ossified but overall maintains the same shape. The medial edge is slightly concave and wraps around the lateroventral edge of an anterior process of the pars autopalatina while the lateral edge cups the anterior half of the base of the maxillary barbel. At around 17.8 mm SL (Fig., 6D), the maxilla's dorsalmost and ventralmost points of articulation with the pars autopalatina form small extensions of bone, each capped in cartilage, that increase the area of contact for articulation between

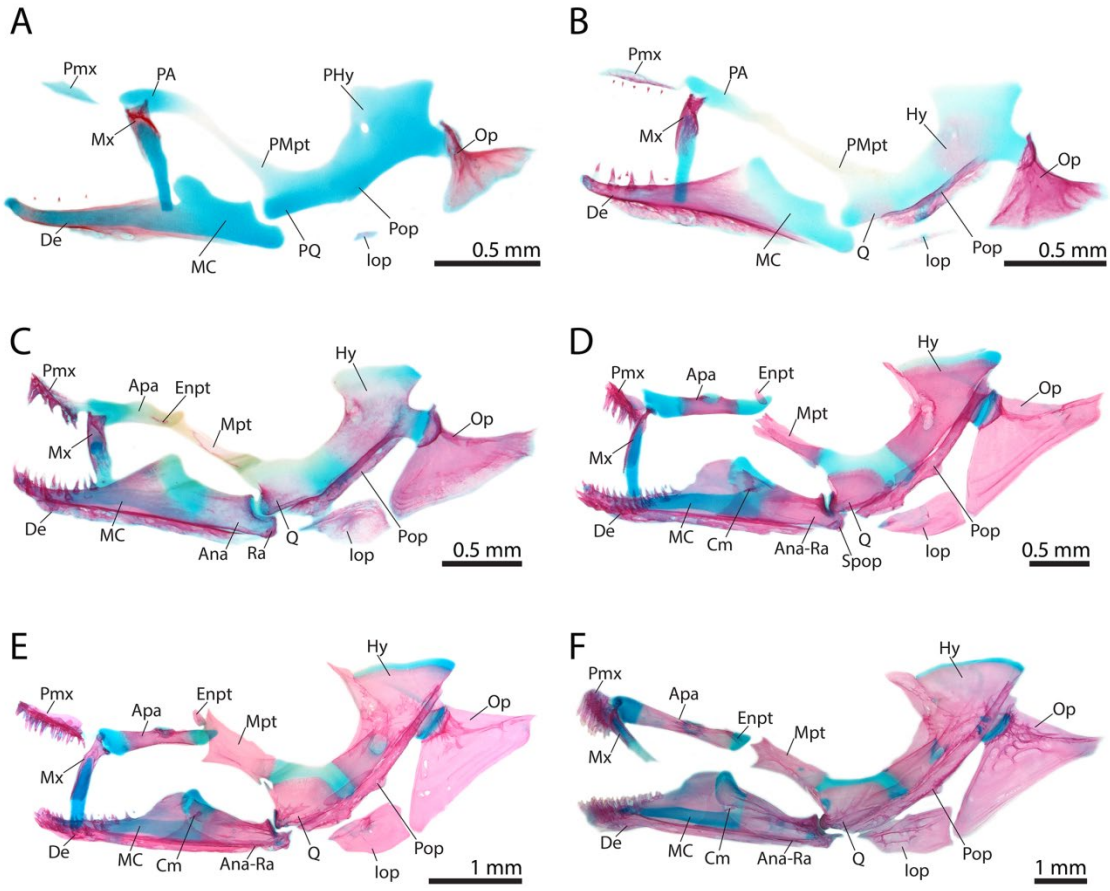

Figure 2.6. Ontogeny of the hyopalatine arch, jaws and opercular series of *Ictalurus punctatus*. (**A**) 11.2 mm SL. (**B**) 12.2 mm SL. (**C**) 13.3 mm SL. (**D**) 18.0 mm SL. (**E**) 21.5 mm SL. (**F**) 44.9 mm SL. Ana, Anguloarticular; Ana-Ra, Anguloarticular+retroarticular; Apa, Autopalatine; Cm, Coronomeckelian; De, Dentary; Enpt, Endopterygoid; Hy, Hyomandibular; Iop, Interopercle; MC,Meckel's cartilage; mm, Millimeters; Mpt, Metapterygoid; Mx,Maxilla; Op, Opercle; PA, Pars Autopalatina; PHy, Pars Hyomandibularis; PMpt, ParsMetapterygoidea; Pmx, Premaxilla; Pop, Preopercle; PQ, ParsQuadrata; Q, Quadrate; Ra, Retroarticular; Sop, Subopercle; Spop, Subpreopercle; SL, standard length.

the two elements. In adults, the maxilla has extended to cover the anterior half of the proximal 1/12th of the maxillary barbel cartilage and the lateralmost tip ends in a narrow pointed process.

Premaxilla: The paired premaxilla originates as small splint of bone located ventral to the tip of the ethmoid cornua (10.1–10.4 mm SL) with the first premaxillary teeth appearing shortly after this (11.5 mm SL). By 12.4 mm SL (Fig. 2.6B) the premaxilla has become a wider lamina of bone extending close to the midline of the ethmoid plate and it supports 6 conical teeth with additional teeth in development. By 14.1 mm SL, there are two distinctive rows of conical teeth with a third row beginning to develop behind them. Although a clear gap is still present between the premaxillae, they are already connected via dense connective tissue. At 15.9 mm SL, these paired bones have become rectangular in shape, support three irregular rows of conical teeth each and together span the distance between the medial edges of the pars autopalatina. Dorsally, they have a small process that extends towards membranous extensions of the mesethmoid to which they are strongly attached via dense connective tissue. As the specimens continue to grow, additional rows of teeth are added to the premaxillae, their ventral surface becoming almost brush-like in appearance and the symphysis becomes mostly obscured by the overlying teeth (44.9 mm SL; Fig. 2.6F).

Dentary: The dentary originates early on in development, appearing in specimens as small as 8.7 mm NL as a dermal lamina of bone lateral to Meckel's cartilage. The first few teeth can be seen in specimens of 10.4 mm SL at which point the dentary extends across the length of Meckel's cartilage up to the coronoid process. Shortly after this (11.2 mm SL (Fig. 2.6A), dermal bone of the mandibular portion of the preoperculo-mandibular sensory canal starts to form as a ventral extension at the midlength of the dentary. By 12.0 mm SL (Fig. 2.6B), there are four conical teeth ankylosed to the

dentary with several more teeth developing in the adjacent tissue (extraosseus). Posteriorly, the dentary has begun to expand towards the coronoid process of Meckel's cartilage dorsally, while ventrally it extends farther, below the anterior edge of the articular surface of the cartilage. The mandibular portion of the preoperculo-mandibular canal is a trough of bone that spans much of the ventral edge of the dentary before it begins to curve medially. At 14.1 mm SL, bone has started to enclose the roof of the sensory canal and the dentary possesses two distinct rows of conical teeth. The coronoid process of the dentary is fully formed by 17.7 mm SL (Fig. 2.6D) and the dentary now overlaps the anteriormost portion of the anguloarticular. The mandibular portion of the preoperculo-mandibular sensory canal is fully enclosed by 21.2 mm SL (Fig. 2.6E), except for four circular openings associated with the preoperculo-mandibular sensory canal pores 2–5 Three rows of conical teeth are present on the dentary by 44.9 mm SL (Fig. 2.6F) and there is minor sculpturing on the coronoid process.

Retroarticular: The retroarticular is first observed in specimens of 11.6 mm SL as a perichondral ossification at the point of attachment of the interoperculo-retroarticular ligament on the posteroventral-most tip of Meckel's cartilage. The retroarticular becomes more heavily ossified around the posterior tip of Meckel's cartilage and around 13.0 mm SL (Fig. 2.6C) it meets and fuses with the anguloarticular to become a compound element. It can still be readily distinguished as a highly ossified cap on the posterior edge of the anguloarticular up to 17.7 mm SL; however, it becomes less apparent in larger sizes until it is no longer distinguishable (21.5 mm SL (Fig. 2.6E).

Anguloarticular: The anguloarticular is a compound element composed of the dermal angular and the endoskeletal articular, although the two bones were not observed as separate ossifications. The element first appears as an ossification on the dorsal edge of Meckel's cartilage posterior to the coronoid process (11.9 mm SL). The anguloarticular proceeds to ossify in a dorsoventral direction becoming saddle-shaped in appearance at 12.5 mm SL. At 13.0 mm SL the bone completely encompasses the posterior end of Meckel's cartilage (Fig. 2.6C). Anteriorly, it lies dorsal to the dentary and posteriorly it has expanded to meet and fuse with the retroarticular. At 15.9 mm SL the posterior end of Meckel's cartilage is endochondrally ossifying with only a small portion of cartilage remaining at the point of articulation with the quadrate. The angular portion of the anguloarticular extends anteriorly where it lies medial to the posterior end of the dentary and posteriorly, a tiny recurved process can be seen on the posterodorsal tip of the bone. A subpreopercular bone (*sensu* Egge, 2007) forms around the mandibular portion of the preoperculo-mandibular sensory canal (17.7 mm SL, 2.6D) laterally to the anguloarticular and fuses with the underlying bone by 21.2 mm SL (Fig. 2.6E). By 44.9 mm SL (Fig. 2.6F) the anguloarticular completely covers the posterior remnant of Meckel's cartilage, meeting the coronoid process of the dentary anterodorsally. The surface of the bone that articulates with the quadrate has become enlarged and more posteriorly directed and the lateral surface of the bone is now slightly sculptured.

Coronomeckelian: The coronomeckelian is a small tendon bone that is first observed as a tiny ossification located medially to the coronoid process of Meckel's

cartilage at the tendinous insertion of the A3 adductor mandibulae (15.0 mm SL). It becomes triangular in shape shortly after ossifying (16.2 mm SL) and maintains this shape and position during ontogeny, only increasing in size.

Comparison. The most common sequence of ossification for this region in *Noturus gyrinus* is as follows: maxilla (5.4 mm NL) – dentary (5.9 mm NL) – premaxilla (6.6 mm SL) – retroarticular (7.0 mm SL) – anguloarticular (7.7 mm SL) – coronomeckelian (10.1 mm SL).

No differences in the sequence of ossification between *Noturus gyrinus* and *Ictalurus punctatus* were identified in the jaws. The only major difference observed in the jaws of *N. gyrinus* and *I. punctatus* is that the coronomeckelian is a larger lamina of bone that expands outward from the tendinous insertion of the A3 adductor mandibulae while in *I. punctatus* it is restricted to a small triangular ossification within the tendon.

Hyopalatine Arch

The most common sequence of ossification: quadrate (11.5 mm SL) – hyomandibular (12.0 mm SL) – metapterygoid (12.8 mm SL) – endopterygoid – autopalatine (12.9 mm SL) (Fig. 2.6).

Quadrate: the quadrate is an endoskeletal bone that first appears in some individuals of 11.2 mm SL (Fig. 2.6A) as a perichondral ossification along the ventral edge of the pars quadrata of the quadratometapterygoid portion of the palatoqudrate cartilage, which in catfishes is separate from the pars autopalatina and confluent with the hyosymplectic cartilage. The perichondral ossification extends dorsally to surround the anteroventral portion of the pars quadrata that articulates with the lower jaw and the

quadrate has begun to endochondrally ossify (12.2 mm SL (Fig. 2.6B). By 14.0 mm SL, the quadrate has expanded into a triangular bone and the posteroventral process of the quadrate (*sensu* Arratia and Schultze, 1991) runs ventral to the preopercle. A strip of membrane bone forms medial to the ventral portion of the preopercle (15.9 mm SL) and is joined with the posteroventral process anteriorly forming a shallow trough in which the dorsal edge of the overlapping preopercle rests. The quadrate has also become more heavily ossified near the connection with the lower jaw but remains cartilaginous at the joint. At 18.0 mm SL (Fig. 2.6D), the point of connection with the lower jaw is now restricted to an anteriorly directed articular facet and a thin lamina of membrane bone has formed along the anterior edge of the quadrate above the facet. By 21.5 mm SL (Fig. 2.6E) the anterior lamina has developed an anterodorsal spine-like process extending towards the posteroventral corner of the metapterygoid. The medial surface of the quadrate possesses some sculpturing near the articular facet. In individuals up to 44.9 mm SL (Fig. 2.6F), the quadrate has changed little and still remains separated from the hyomandibular and most of the metapterygoid by cartilage. The anterodorsal process now sits tightly between a similar posteroventral process and the chondral portion of the metapterygoid forming a rigid connection between the two. The quadrate also has started to form a more rigid connection with the preopercle posteriorly.

Hyomandibular: The hyomandibular originates as a perichondral ossification around the pars hyomandibularis near the foramen for the passage of the hyomandibular branch of the facial nerve and can appear as early as 11.5 mm SL. By 13.2 mm SL (Fig.6C) the bone has spread to cover most of the pars hyomandibularis excluding the

dorsal and posterior articular heads, which articulate with the neurocranium and opercle respectively, and the ventral arm which joins the pars quadratometapterygoidea. At 15.9 mm SL, two small flanges of membrane bone flank the shaft of the hyomandibular, one anterior to the foramen for the passage of the hyomandibular branch of the facial nerve and one posterior, directly above the posterior articular head. Additionally, a thin splint of membrane bone extends from the anterodorsalmost corner of the hyomandibular towards the pterosphenoid. A flange of membrane bone has formed on the posterior margin of the hyomandibular below the posterior articular head by 18.0 mm SL (Fig. 2.6D) and the cartilage is beginning to be fully replaced by bone near the foramen. By 21.2 mm SL (Fig. 2.6E) the anterodorsal extension of membrane bone forms a tight connection with a similar process on the pterosphenoid. The membrane bone along the posterior margin has formed a shelf for medial surface of the preopercle as it runs the length of the hyomandibular and cartilage has been fully replaced anteriorly. At 44.9 mm SL (Fig. 2.6F), the cartilage has been completely replaced by bone in the middle of the hyomandibular shaft with cartilage still remaining in the dorsal head and ventral arm. The surface of the bone has become lightly sculptured where only bone remains and the connection between the hyomandibular and the preopercle has become firmer.

Metapterygoid: The metapterygoid starts as a perichondral ossification around the middle of the anterior process of the pars metapterygoidea (11.9 mm SL), which in catfishes is shifted anteriorly towards the pars autopalatina. By 13.3 mm SL (Fig. 2.6C), the entire anterior process is covered in perichondral bone and a small membranous projection has appeared on the tip of the process and supports a connection to the

autopalatine and neurocranium in which the endopterygoid has ossified. The metapterygoid is endochondrally ossifying at 15.9 mm SL and a continuous lamina of membrane bone extends along the entire ventral length of the bone up to and around the middle of the dorsal edge. The lamina of bone extends the length of the dorsal margin and has expanded to take on a somewhat rectangular shape by 18.0 mm SL (Fig. 2.6D) and by 21.0 mm SL (Fig. 2.6E) possesses an anterior and a posterior ventral process, the posterior of which extends towards a similar process of the quadrate. By 44.9 mm SL (Fig. 2.6F), the metapterygoid has increased in size and the posteroventral process attaches to the anterodorsal projection of the quadrate. The anterior edge has three distinct points, the dorsal of which supports a ligamentous connection to the ventrolateral margin of the orbitosphenoid, the middle supports a ligamentous connection to the endopterygoid and the ventralmost supports a ligamentous connection to the lateral edge of the autopalatine.

Endopterygoid: The endopterygoid is a small ossification that first appears as a thin splint of bone in the ligamentous connection between the metapterygoid, autopalatine and neurocranium in individuals as small as 11.9 mm SL. The bone expands into a thin lamina of bone (14.1 mm SL) and by 15.6 mm SL it has become large enough to replace the portion of the ligament in which it has formed resulting in three ligamentous connections to the metaperygoid posteriorly, the autopalatine laterally and the vomer anteriorly. An additional ligament connecting the endopterygoid to the vomer has been previously reported (Arratia, 1992) although this connection was not observed in the largest C&S specimen studied here (44.9 mm SL).

Autopalatine: The autopalatine starts as a perichondral ossification (12.5 mm SL) around the middle of the cylindrical pars autopalatina, which originates as an independent cartilage separate from the rest of the palatoquadrate. By 13.9 mm SL it has expanded into a cylindrical ossification around the middle third of the pars autopalatina excluding a dorsomedial facet for the articulation with the lateral ethmoid. Anteriorly, the cartilaginous head of the autopalatine possesses a ventrolateral groove for the articulation of the maxilla. The pars autopalatinea has increased in size with the posterior tip extending almost to the metapterygoid by 18 mm SL (Fig. 2.6D) and by 21.2 mm SL (Fig. 2.6E) the autopalatine has started to endochondrally ossify. Light sculpturing is present around the articular facet for the lateral ethmoid and a lateral and medial flange of membrane bone has formed on the posterior half of the bone. By 44.9 mm SL (Fig. 2.6F), the autopalatine has become more elongate and is completely ossified, except for the anterior and posterior tips as well as the dorsomedial articular facet for the lateral ethmoid, and the middle of the bone is more heavily sculptured.

Comparison. The most common sequence of ossification for this region in *Noturus gyrinus* is: quadrate and hyomandibular (7.2 mm SL) – metapterygoid (8.3 mm SL) – autopalatine (8.6 mm SL) – endopterygoid (8.7 mm SL).

The only difference in the sequence of ossification identified between *Noturus gyrinus* and *Ictalurus punctatus* in the hyopalatine arch is that the autopalatine appears before the endopterygoid in *N. gyrinus* while in *I. punctatus*, despite being fixed in development at the same size, the endopterygoid was present before the autopalatine in

some individuals. The hyopalatine arch of *N. gyrinus* and *I. punctatus* are similar, and no major differences in adult morphology are observed in this region.

Opercular Series

The most common sequence of ossification is: opercle (8.6 mm NL) – interopercle (10.4 mm SL) – preopercle (11.5 mm SL) – suprapreopercle (22.4 mm SL) (Fig. 2.6).

Opercle: The opercle is one of the first skeletal elements to appear in *Ictalurus punctatus* (8.6 mm NL) and was first observed as a thin dermal ossification extending posteroventrally from the posterior condyle of the pars hyomandibularis of the hyosymplectic cartilage. At 9.6 mm NL, the posterior end of the ossification begins to widen and by 10.8 mm SL the opercle has become fan-shaped with a concave anterior and dorsal edge, the latter of which is more heavily ossified. As the opercle continues to expand, the anteroventral edge becomes more rounded as it gets closer to the posterior margin of the interopercle while the posterior dorsal tip ends in a sharp point (13.0 mm SL; Fig. 2.6C). The cup-shaped articular surface of the opercle completely surrounds the posterior condyle of the pars hyomandibularis. A thin lamina of bone begins to form along the dorsal edge by 15.0 mm SL and by 21.5 mm SL (Fig. 2.6E) extends to the posteriormost tip of the opercle resulting in a straight dorsal margin. In adult specimens, the lateral surface has become sculptured proximally while the distal edge remains smooth.

Interopercle: The interopercle is a dermal ossification that first appears at 10.4 mm SL as a small splint of bone lateral to the connection between the ceratohyal

cartilage and the interhyal cartilage. By 13.3 mm SL (Fig. 2.6C), the interopercle has grown in length, almost meeting the anterior edge of the opercle. The bone has widened posteriorly while anteriorly it terminates in a fine point, which accommodates the posterior end of the interoperculo-retroarticular ligament. The interopercle takes on a rhomboid shape as the bone continues to grow (18.6 mm SL) and the posterior edge becomes curved around the margin of the opercle where the two bones approach each other (21.5 mm SL; Fig. 2.6E). In adult specimens, the lateral surface is sculptured and the overall shape has changed little from the earlier stages.

Preopercle: The preopercle forms as a splint of bone (10.9 mm SL) along the posterior margin of the confluent pars hyomandibularis and pars quadrata cartilages at the point of contact with the interhyal cartilage. At 12.2 mm SL (Fig. 2.6B), the ossification has expanded dorsally to cover the posterior margin of the pars hyomandibularis up to the posterior condyle and has formed into a trough-shaped canal, the preopercular portion of the preoperculo-mandibular sensory canal, with three small foramina associated with the innervation of neuromasts. The walls of the canal begin expanding to cover the canal (14.1 mm SL) which becomes completely enclosed by 15.9 mm SL except for two openings for the preoperculo-mandibular sensory canal pores 8 and 9, the first located lateral to the interhyal cartilage and the second opening posteriorly in line with the border of the opercle and interopercle. Additionally, a posteroventral lamina of bone is present between the anterior opening of the canal and the posterior of the two pores and an anterodorsal lamina is forming at the junction of the hyomandibular and the quadrate. At 44.9 mm SL (Fig. 2.6F), the preopercle extends

almost the entire length of the posterior margins of the quadrate and hyomandibular. The posteroventral lamina of membrane bone has expanded and runs almost the entire length of the preopercle and is heavily sculptured while the anterodorsal lamina has only expanded slightly.

Suprapreopercle: The suprapreopercle is the last element to appear in the skeleton of *Ictalurus punctatus* (22.4 mm SL) and is first observed as a small ossification located between the preopercle and the pterotic. In the largest specimen observed (44.9 mm SL; Fig. 2.6F) it is a weakly ossified trough of bone that forms around the preoperculo-mandibular in the gap between the pterotic and preopercle just after it branches off the otic canal.

Comparison. The most common sequence of ossification for the opercular bones in *Noturus gyrinus* is as follows: opercle (5.4 mm NL) – interopercle (6.4 mm SL) – preopercle (7.7 mm SL) – suprapreopercle (11.6 mm SL).

No differences in the sequence of ossification were identified between *Noturus gyrinus* and *Ictalurus punctatus* in the opercular series. The opercular series of *N. gyrinus* and *I. punctatus* are similar, and no major differences in adult morphology are observed in this region.

Infraorbitals

The most common sequence of ossification is: lacrimal (10.4 mm SL) – infraorbital 2 (12.2 mm SL) – infraorbital 3 (12.8 mm SL) – infraorbital 4 and 6 (13.2 mm SL) – infraorbital 5 (13.9 mm SL) (Fig. 2.7).

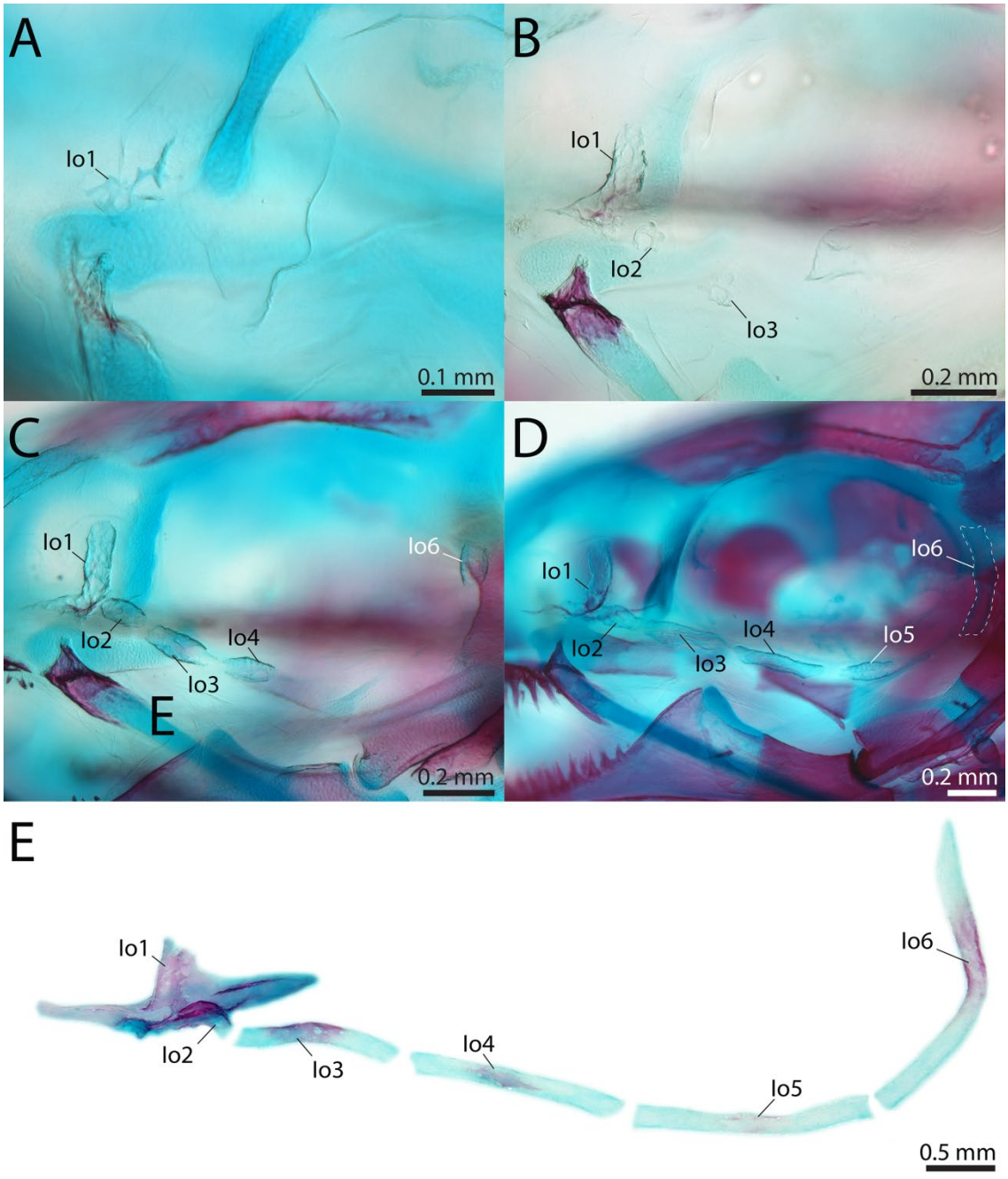

Figure 2.7. Ontogeny of the infraorbitals of *Ictalurus punctatus*. (**A**) 11.2 mm SL. (**B**) 12.7 mm SL. (**C**) 13.2 mm SL. (**D**) 15.0 mm SL. (**E**) 44.9 mm SL. Io, Infraorbital; mm, Millimeters; SL, standard length.

Infraorbital 1: Infraorbital 1 (the lacrimal) first appears at 10.4 mm SL as a small dermal bone located dorsal to the articulation between the maxilla and pars autopalatina and anterior to the *lamina orbitonasalis* (Fig. 2.7A). By 11.5 mm SL it expands dorsally and ventrally giving the bone a distinct L shape. The anterior and posterior edges of the dorsal process have just started to form roughly in the shape of a trough. At 12.5 mm SL (Fig. 2.7B), the roof of the infraorbital sensory canal has begun to close in the dorsal portion of the lacrimal. The anterior process has become triangular, ending in a distinct point, and a small posteriorly directed process has just formed. By 14.1 mm SL, the dorsal portion of the bone is represented solely by a fully enclosed canal ossification and the posterior process extends to the *lamina orbitonasalis* resulting in a roughly rhomboid lamina of bone ventral to the canal ossification. The lacrimal increases in size and changes little until 21.2 mm SL at which point the ventral lamina of bone expands dorsally on either side of the ventral third of the canal ossification. The posterior projection continues to widen, becomes ovoid in shape, and is closely associated with the remnant of the *lamina orbitonasalis* and with the lateral ethmoid posteriorly.

Infraorbital 2: Infraorbital 2 first appears as small trough of bone just posterior to the lacrimal at 11.9 mm SL. A single foramen associated with neuromast innervation in the infraorbital sensory canal is present in the center of the ossification. At 13.2 mm SL (Fig. 2.7C), bone starts to cover the roof of the canal and by 14.0 mm SL the canal bone becomes enclosed and sits directly lateral to the posterior process of the lacrimal. By 44.9 mm SL (Fig. 2.7E), infraorbital 2 is closely associated with the posterior process of the lacrimal but remains separate.

Infraorbital 3: Infraorbital 3 first appears (11.9 mm SL, Fig. 2.7B) as a small dermal bone surrounding a foramen associated with neuromast innervation in the infraorbital sensory canal. It is located just posterior to infraorbital 2 and in line with the posterior margin of the *lamina orbitonasalis*. By 14.1 mm SL, the bone has started to lengthen and completely surrounds the infraorbital sensory. By 44.9 mm SL (Fig. 2.7E), infraorbital 3 resembles the adult condition and extends beyond the posterior extension of the lacrimal and almost reaches the anterior rim of the orbit.

Infraorbital 4: Infraorbital 4 first appears (in some individuals as small as 12.4 mm SL) as a small lamina of bone around a foramen associated with neuromast innervation ventral to the anterior quarter of the eye. It becomes trough shaped shortly after this (13.1 mm SL (Fig. 2.7C) and by 14.1 mm SL it has become completely enclosed by bone. By 44.9 mm SL (Fig. 2.7E), it resembles the adult condition and sits ventral to the anterior half of the eye.

Infraorbital 6: Infraorbital 6 is the largest infraorbital in the series. It appears directly ventral to the junction of the supraorbital, infraorbital and otic sensory canals near the vertical midline of the eye at approximately the same time as infraorbital 4 (12.4 mm SL). It becomes enclosed in bone by 14.1 mm SL and continues to expand in length. By 44.9 mm SL (Fig. 2.7E), it expands from just below the frontal down to the posteroventral extent of the eye forming the posterior rim of the orbit resembling the adult condition.

Infraorbital 5: Infraorbital 5 forms around a foramen associated with neuromast innervation in individuals as small as 13.2 mm SL (Fig. 2.7C) in line with the posterior

quarter of the eye. The canal ossification is enclosed by 14.6 mm SL (Fig. 2.7D) and the bone continues to expand until it spans the posterior half of the eye forming the ventral border of the orbit along with infraorbital 4 resembling the adult condition (44.9 mm SL; Fig. 2.7E).

Comparison. The most common sequence of ossification for this region in *Noturus gyrinus* is as follows: lacrimal (7.0 mm SL) – infraorbital 2 (7.7 mm SL) – infraorbital 3 (7.9 mm SL) – infraorbital 4 (8.3 mm SL) – infraorbital 5 (8.6 mm SL) – infraorbital 6 and 7 (12 mm SL).

The only difference in the infraorbitals observed in the sequence of ossification between *Noturus gyrinus* and *Ictalurus punctatus* in the infraorbitals was that infraorbital 5 appears before infraorbital 6 in *N. gyrinus* while it appears after infraorbital 6 in *I. punctatus*. The infraorbitals of *N. gyrinus* and *I. punctatus* are generally similar except for *N. gyrinus* possessing an additional element, infraorbital 7. The only difference noted is the shape of the lacrimal in *N. gyrinus* in which the anterior process in more elongate and the posterior process is a narrow splint that does not reach the *lamina orbitonasalis*.

Hyoid Bar

The most common sequence of ossification: branchiostegal ray 8 (9.6 mm NL) – branchiostegal ray 7 (10.0 mm SL) – branchiostegal ray 6 (10.8 mm SL) – anterior ceratohyal (11.3 mm SL) – branchiostegal ray 5 (11.4 mm SL) – branchiostegal ray 4, urohyal and ventral hypohyal (11.9 mm SL) – branchiostegal ray 3 (12.3 mm SL) – branchiostegal ray 2 (12.8 mm SL) – interhyal and posterior ceratohyal (13.2 mm SL) – branchiostegal ray 1 (13.6 mm SL) – dorsal hypohyal (15.0 mm SL) (Fig. 2.8).

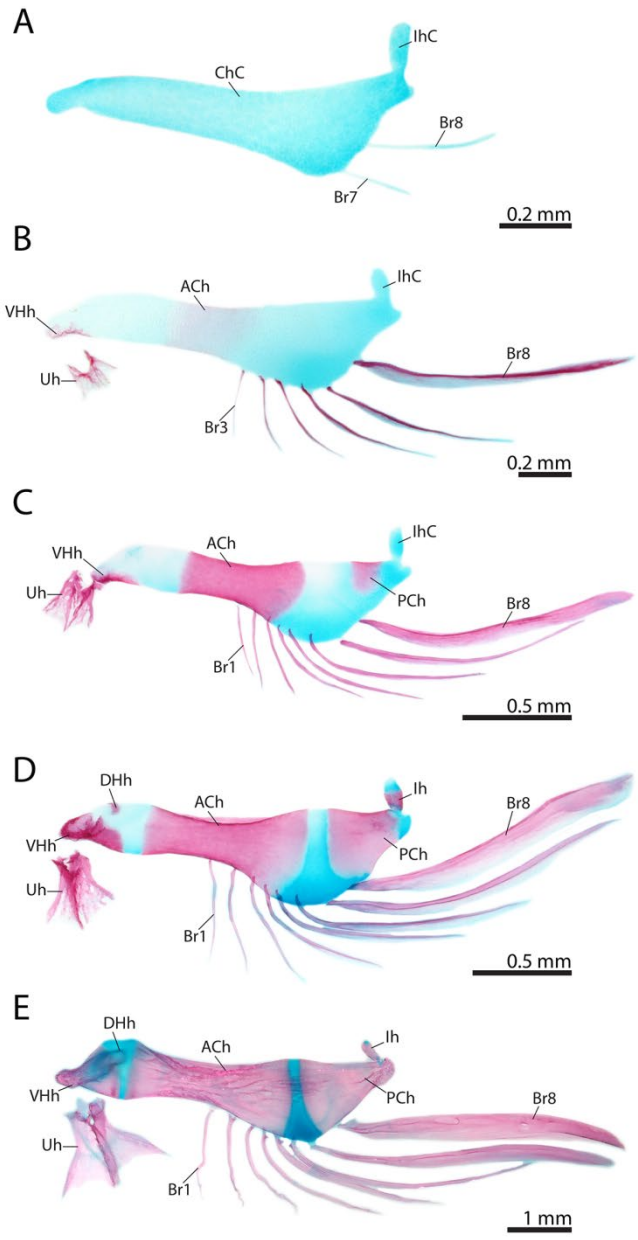

Figure 2.8. Ontogeny of the hyoid bar of *Ictalurus punctatus*. (**A**) 10 mm NL. (**B**) 12.5 mm SL. (**C**) 13.3 mm SL. (**D**) 15.0 mm SL. (**E**) 44.9 mm SL. ACh, Anterior ceratohyal; Br, Branchiostegal ray; DHh, Dorsal hypohyal; Ih, Interhyal; IhC, Interhyal cartilage; mm, Millimeters; PCh, Posterior ceratohyal; Uh, Urohyal; VHh, Ventral hypohyal; NL, notochord length; SL, standard length.

Branchiostegal Rays: The branchiostegal rays appear as thin dermal ossifications extending posteroventrally from the hyoid bar. The first branchiostegal ray to develop is the posteriormost, branchiostegal ray 8 (9.2 mm NL) along the posteroventral margin of the deepest portion of the ceratohyal cartilage. The next three branchiostegal rays to appear are branchiostegal rays 7 (10.0 mm SL; Fig. 2.8A), 6 (10.1 mm SL), and 5 (11.2 mm SL), which are associated with the ventral edge of the deepest portion of the ceratohyal cartilage. By the appearance of branchiostegal ray 5, branchiostegal ray 8 now reaches the midline of the opercle but remains a thin splint of bone. The branchiostegal rays continue to develop in an posteroanterior direction with branchiostegal ray 1 appearing by 12.6 mm SL. At this point the branchiostegal ray 8 has started to widen posteriorly and now reaches the posterior point of and connects to the opercle via dense connective tissue. By 15.9 mm SL, all of the branchiostegal rays are recurved posteriorly with branchiostegal rays 5–8 now widened into thin sheets of bone. By 21.2 mm SL, all eight branchiostegal rays are at a stage resembling the adult condition. Branchiostegal rays 1–5 articulate with the medioventral edge of the anterior ceratohyal, branchiostegal rays 6 and 7 articulate with the ventral margin of the remaining ceratohyal cartilage, between the anterior and posterior ceratohyal, and branchiostegal ray 8 articulates with the lateral surface of the posterior ceratohyal. The last two branchiostegal rays are closely associated with the opercular series, forming a close connection with the posterior margin of the opercle.

Anterior Ceratohyal: The anterior ceratohyal is a chondral bone that develops (10.8 mm SL) as a perichondral ossification around the middle of the slender anterior

portion of the ceratohyal cartilage. The cylindrical ossification extends anteriorly and posteriorly until it covers the middle third of the ceratohyal cartilage (12.5 mm SL; Fig. 2.8B). A thin lamina of membrane bone appears along the dorsal edge of the anterior ceratohyal where it is narrowest (14.0 mm SL), and by 16.2 mm SL a similar extension of membrane bone flanks the ventral margin. At this stage, the ossification has started to spread onto the deeper portion of the ceratohyal cartilage posteriorly giving the bone a more hourglass shape. By 17.7 mm SL, the anterior ceratohyal almost covers the entirety of the anterior half of the deepest portion of the ceratohyal cartilage, of which only a thin strip remains between the anterior and posterior ceratohyal. The middle of the anterior ceratohyal is now endochondrally ossified and the medial surface has become lightly sculptured. By 44.9 mm SL (Fig. 2.8E), the anterior ceratohyal sutures with the posterior ceratohyal across the medial surface of the ceratohyal cartilage remnant and anteriorly remains separated from the ventral hypohyal by a thin strip of cartilage. The surface of the bone has become more heavily sculptured.

Urohyal: The urohyal originates as a pair of ossifications in the posterior portion of the sternohyoideus tendons that insert on the medial surface of the anteriormost point of the ceratohyal cartilage (11.2 mm SL). The two ossifications expand in a fan-like direction posteriorly and fuse by 12.2 mm SL, forming a sheet of bone ventrally. By 13.2 mm SL (Fig. 2.8C), a ‘Y’ shaped dorsal extension of bone has appeared medially running the length of the bone and the lateral margins also extend posteriorly giving the bone three distinct points along the posterior edge. The two anterior tips in the dorsal flange of bone have started to expand laterodorsally and medioventrally forming two

angled surfaces of bone (16.2 mm SL). By 21.5 mm SL, the aforementioned flanges have joined medially forming a slightly anterior facing cup like process. At 44.9 mm SL (Fig. 2.8E), the anterior tip of the anterior basibranchial copula extends dorsal to the posterior edge of the cup-like process; however, it does not yet fully receive and articulate with the parurohyal as has been reported previously for larger individuals of *Ictalurus punctatus* (Arratia & Schultze, 1990).

Ventral Hypohyal: The ventral hypohyal is a paired chondral bone that develops (11.2 mm SL) ventrally on the medioventral process of the anterior head of the ceratohyal cartilage that supports the insertion of the sternohyoideus tendons. At 12.5 mm SL (Fig. 2.8B), the ossification has spread anteriorly to cover the entire ventral surface of the anteromedial process while posteriorly it has started to expand along the medial edge of the ceratohyal cartilage. Just dorsal to the middle of the bone, a foramen for the afferent hyoidean artery has formed in the cartilage. The bone has started to spread dorsally, cupping the ventral edge of the anteromedial process (14.0 mm SL) and by 15.9 mm SL it covers the anterolateral tips of the cartilage and even expands onto the dorsal surface of the anteromedial process by 15.9 mm SL. At this stage, the ventral hypohyal continues to spread posteriorly covering much of the anterior head of the ceratohyal cartilage ventrally. The foramen for the afferent hyoidean artery has become dorsoventrally elongated with the ventral hypohyal forming the border of the ventral half of the opening. By 18.0 mm SL, the ventral hypohyal covers the ventral half of the anterior head of the ceratohyal cartilage and the opening for the afferent hyoidean artery has expanded further dorsally where it forms a circular opening in the cartilage above

the ventral hypohyal. By 21.5 mm SL, the bone has endochondrally ossified anteroventrally and forms a tight connection with its antimere across the midline. The ventral elongate portion of the opening for the afferent hyoidean artery has begun to fill with bone and by 44.9 mm SL (Fig. 2.8E) only the dorsal rounded portion of the foramen remains. The bone is lightly sculptured anteroventrally and still remains separated by cartilage from the dorsal hypohyal and the anterior ceratohyal.

Interhyal: The small interhyal cartilage forms a connection between and is continuous with the ceratohyal and the pars quadrata-hyomandibularis cartilages. The interhyal first appears as perichondral ossification around the interhyal cartilage in some individuals as small as 12.5 mm SL, shortly after the cartilaginous connections with the ceratohyal and pars quadrata-hyomandibularis cartilage begins to regress. By 14.0 mm SL, the perichondral ossification covers most of the interhyal cartilage which is now an independent cartilage with connective tissue replacing its previously cartilaginous dorsal and ventral connections. It continues to become more heavily ossified (21.2 mm SL) and by 44.9 mm SL (Fig. 2.8E) it has become slightly more elongate, started to endochondrally ossify yet retains cartilage at its dorsal and ventral tips. A small ridge of membrane bone has started to form along the anterior edge.

Posterior Ceratohyal: The posterior ceratohyal develops in individuals as small as 12.5 mm SL as a perichondral ossification on the lateral surface of the ceratohyal cartilage just anterior to its ligamentous connection with the interopercle. Shortly after (13.1 mm SL; Fig. 2.8C), it expands into a saddle shaped ossification in the dorsal half of the cartilage and by 15.9 mm SL the perichondral ossification has expanded around

the entire posterior end of the ceratohyal cartilage excluding the point of articulation with the interhyal. At 21.5 mm SL, the posterior ceratohyal is endochondrally ossifying and a ridge of membrane bone has formed on the posterioventral edge of the bone. Anteriorly it remains separated from the anterior ceratohyal by a thin strip of cartilage. On the medial surface, the posterior ceratohyal has started to extend across this cartilage and by 44.9 mm SL (Fig. 2.8E), it forms an interdigitating suture with the anterior ceratohyal. The ridge of membrane bone has become curved and the posterior tip of the bone is now sculptured.

Dorsal Hypohyal: the dorsal hypohyal originates as a perichondral ossification medially on the posterodorsal process of the anterior head of the ceratohyal cartilage (14.5 mm SL). The bone forms a saddle shaped ossification (15.9 mm SL) and slowly expands to incorporate the entire medial edge of the posterodorsal process (21.5 mm SL). By 44.9 mm SL, the dorsal hypohyal has changed little in shape but has expanded ventrally towards the ventral hypohyal, from which it remains separated by cartilage.

Comparison. The most common sequence of ossification for this region in *Noturus gyrinus* is as follows: branchiostegal ray 9 (6.3 mm NL) – branchiostegal ray 8 (6.4 mm NL) – branchiostegal ray 7 (6.7 mm SL) – anterior ceratohyal (7.0 mm SL) – branchiostegal ray 5 and 6 (7.3 mm SL) – urohyal (7.3 mm SL) – ventral hypohyal (7.6 mm SL) – posterior ceratohyal (7.7 mm SL) – branchiostegal ray 3 and 4 (7.9 mm SL) – branchiostegal ray 2 and 1 (8.6 mm SL) – dorsal hypohyal (10.8 mm SL) – interhyal (11.1 mm SL).

The sequence of ossification in the hyoid bar differs between *Noturus gyrinus* and *Ictalurus punctatus* in that the interhyal is the last element to appear in *N. gyrinus* while in *I. punctatus* it appears before the dorsal hypohyal at the same time as the posterior ceratohyal. The hyoid bar of *N. gyrinus* and *I. punctatus* are similar, and no major differences in adult morphology are observed in this region.

Branchial Skeleton

The most common sequence of ossification: pharyngobranchial 4 toothplate (9.9 mm NL) – ceratobranchial 5 toothplate (10.9 mm SL) – ceratobranchial 1, 2, 3, 4, 5 and epibranchial 4 (12.0 mm SL) – epibranchial 1, 2 and 3 (12.1 mm SL) – gill rakers (13.3 mm SL) – pharyngobranchial 3 (14.5 mm SL) – pharyngobranchial 4 (15.0 mm SL) – basibranchial 2 and 3 (15.9 mm SL) – hypobranchial 1 (18.0 mm SL) – hypobranchial 2 (21.2 mm SL) (Fig. 2.9).

Ceratobranchials: The ceratobranchials start as perichondral ossifications around the middle of their respective cartilages. The first to ossify is ceratobranchial 4 (11.4 mm SL) with the remaining ceratobranchials ossifying shortly after (11.8 mm SL). The perichondral ossification proceeds to expand towards the tips of the cartilages and the teeth associated with the lower pharyngeal jaws are ankylosed to ceratobranchial 5 toothplate which has already fused with ceratobranchial 5 (12.9 mm SL; Fig. 2.9B). By 14.1 mm SL, ceratobranchials 1–5 are completely ossified perichondrally except for the tips and at 15.0 mm SL (Fig. 2.9C), flanges of membrane bone have appeared on the anterior and posterior edges of the ceratobranchials. By 20.6 mm SL (Fig. 2.9D), the

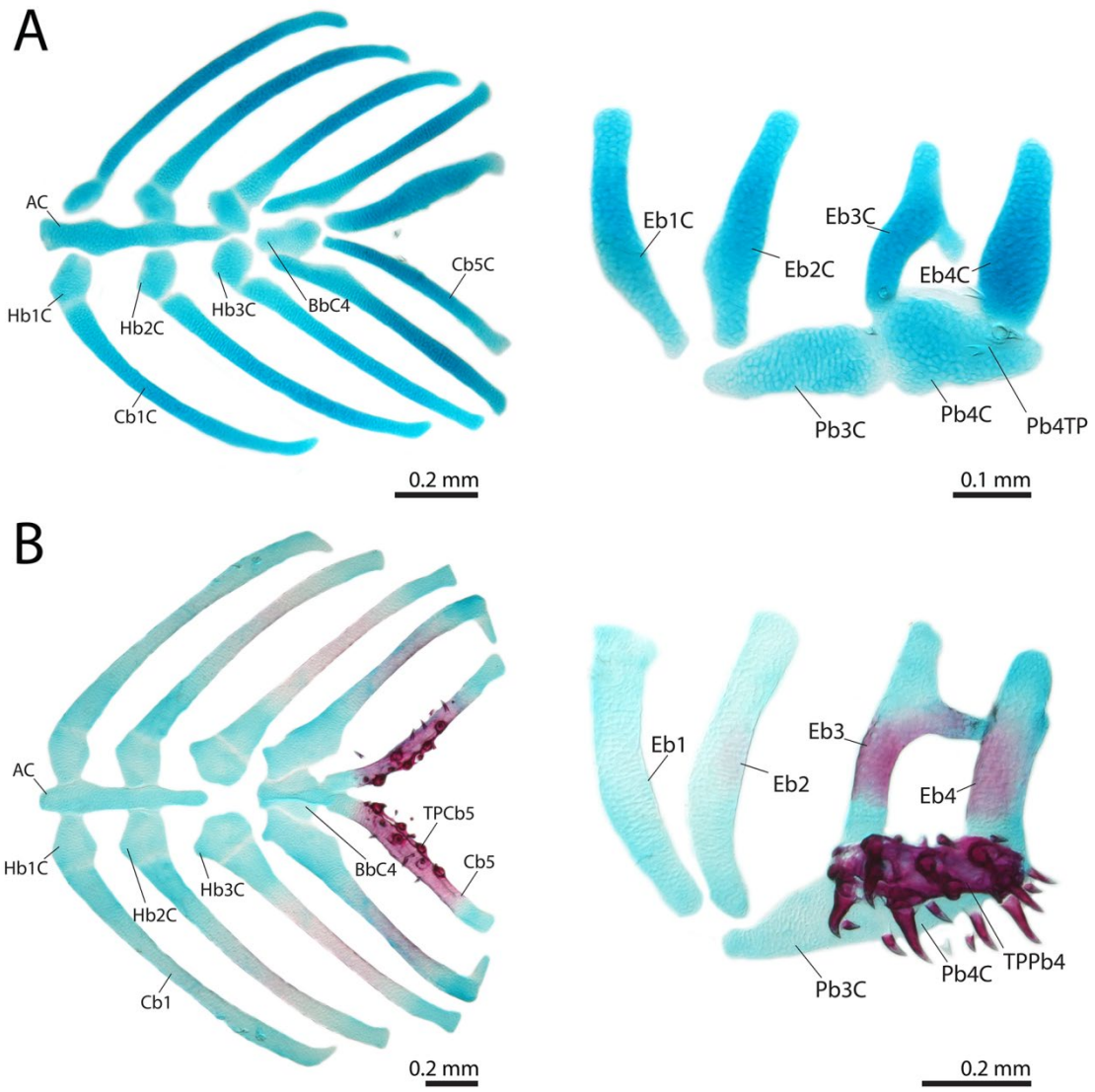

Figure 2.9. Ontogeny of the branchial skeleton of *Ictalurus punctatus*. (**A**) 10.9 mm SL. (**B**) 12.9 mm SL. (**C**) 15.0 mm SL. (**D**) 20.6 mm SL. AC, Anterior copula ;Bb, Basibranchial; BbC, Basibranchial cartilage; Cb, Ceratobranchial; Cb, Ceratobranchial cartilage; Eb, Epibranchial; EbC, Epibranchial cartilage; Hb, Hypobranchial; HbC, Hypobranchial cartilage; Pb, Pharyngobranchial; PbC, Pharyngobranchial cartilage; TPCb, Toothplate of ceratobranchial; TPPb, Toothplate of pharyngobranchial; SL, standard length.

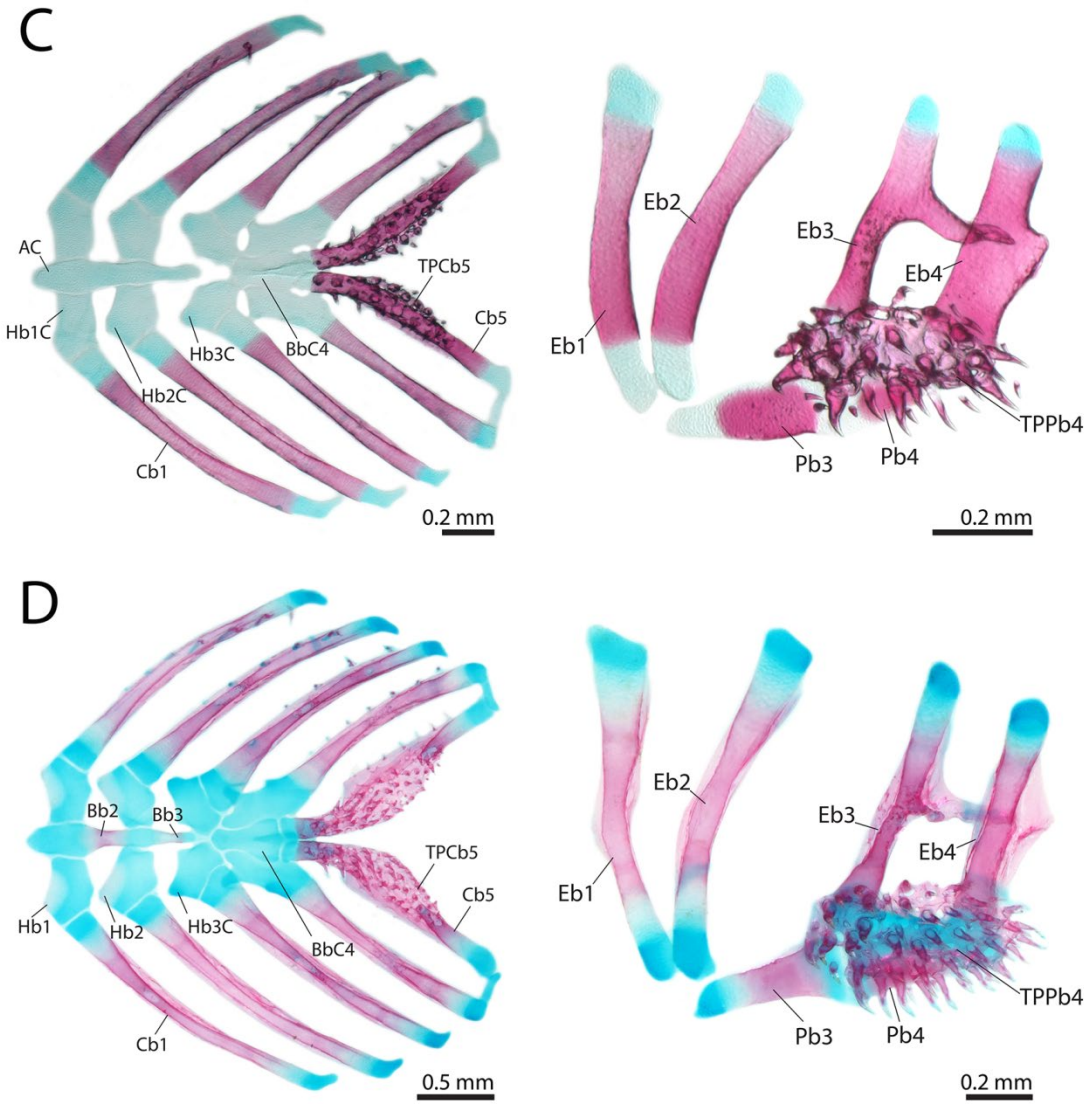

Figure 2.9. Continued

ceratobranchials are endochondrally ossifying at the centerand by 44.9 mm SL, the ceratobranchials are fully ossified and resemble the adult condition.

Epibranchials: Epibranchials 1–4 ossify perichondrally around the midline of the epibranchial cartilages and, like the ceratobranchials, the ossification proceeds to spread across the entirety of the cartilages, excluding the tips which remain cartilaginous. They ossify rapidly with all of the epibranchials first appearing in individuals as small as 11.9 mm SL with epibranchial 4 being the first to become fixed in development at 12.0 mm SL. Additionally a posterior to anterior direction of ossification is suggested by a single specimen (11.9 mm SL) in which only epibranchials 3 and 4 are present. By 15.0 mm SL (Fig. 2.9C), all four epibranchials are completely perichondrally ossified including the uncinate process of epibranchial 3 which is connected to the anterodorsal surface of epibranchial 4 via connective tissue, and possesses a pointed flange of membrane bone at its tip. By 20.6 mm SL (Fig. 2.9D), all four epibranchials have begun to endochondrally ossify and possess flanges of membrane bone along their anterior and posterior margins. By 44.9 mm SL, the posterior flange of epibranchial 4 has expanded posteordorsally forming a large sheet of bone.

Gill Rakers: The gill rakers first appear on ceratobranchial 1 in individuals as small as 12.7 mm SL and by 13.3 mm SL, at least one gill raker is associated with all five ceratobranchials. By 15.9 mm SL, 5–6 gill rakers are present on each ceratobranchial and a single gill raker is associated with epibranchials 1 and 2. At 20.6 mm SL (Fig. 2.9D), the gill rakers along the anterior margin of ceratobranchial 1 have become more elongate, an additional gill raker is associated with epibranchials 1 and 2 and a single gill raker has formed on epibranchial 3. At 44.9 mm SL, 6-8 gill rakers are present on the anterior margin of all five ceratobranchials and the posterior edge of

ceratobranchials 3 and 4. Epibranchials 1 and 2 possess four gill rakers and epibranchials 3 and 4 possess only one each.

Pharyngobranchials: Only two pharyngobranchial cartilages, pharyngobranchials 3 and 4, are present in *Ictalurus punctatus*. Teeth associated with pharyngobranchial 4 toothplate can be seen in individuals as small as 9.9 mm SL ventral to pharyngobranchial 4 cartilage (Fig. 2.9A). Pharyngobranchial 3 is the first of the two to ossify in individuals as small as 13.3 mm SL with pharyngobranchial 4 first appearing at 14.5 mm SL. Both start as perichondral ossifications around the medial edge of the middle of the pharyngobranchial cartilages. By 16.2 mm SL, pharyngobranchial 3 completely encircles the middle of pharyngobranchial 3 cartilage and by 20.6 mm SL (Fig. 2.9D) a small flange of membrane bone has started to form on its lateral margin. At the same size, pharyngobranchial 4 has expanded into a larger semicircular perichondral ossification but remains cartilaginous laterally. A flange of membrane bone is present on its medial margin as well. By 44. 9 mm SL, flanges of bone border the length of pharyngobranchial 3 on the lateral and medial edges and pharyngobranchial 4 remains relatively unchanged.

Basibranchials: Only two basibranchials, basibranchial 2 and 3, are present in *Ictalurus punctatus*. These form as perichondral bands of bone around the middle and posterior end of the anterior basibranchial copula. Both ossifications appear at approximately the same time with basibranchial 2 appearing slightly earlier (basibranchial 2, 14.6 mm SL; basibranchial 3, 14.8 mm SL). The basibranchials become more elongate (20.6 mm SL; Fig. 2.9D) and by 44.9 mm SL they have increased in size

but changed little in shape. The dorsal surface of basibranchial 2 is lightly sculptured at this size.

Hypobranchials: The hypobranchials are some of the last bones to ossify in *Ictalurus punctatus*. Hypobranchial 1 first appears at 15.1 mm SL and hypobranchial 2 at 17.7 mm SL. Both start as perichondral ossifications at the anterolateral tips of hyobranchial cartilages 1 and 2. By 20.6 mm SL (Fig. 2.9D), the perichondral ossifications have expanded medially and are now semicircular in shape and the anterolateral tips are more heavily ossified. By 44.9 mm SL, the hypobranchials have grown posteriorly but still only cover the anterior 2/3^{rds} of the cartilages and the anterolateral tips have become more heavily ossified. Though hypobranchial 3 cartilage is present in *I. punctatus*, hypobranchial 3 does not ossify and is absent.

Comparison. The most common sequence of ossification for this region in *Noturus gyrinus* is as follows: pharyngobranchial 4 toothplate (6.6 mm NL) – ceratobranchial 5 toothplate (7.0 mm SL) – ceratobranchial 4 (7.7 mm SL) – ceratobranchial 5 (7.8 mm SL) – ceratobranchial 1, 2 and 3, epibranchial 4 and 3, and gill rakers (8.3 mm SL) – epibranchial 2 (8.4 mm SL) – epibranchial 1 (8.9 mm SL), pharyngobranchial 3 and basibranchial 3 (9.6 mm SL) – basibranchial 2 (10.0 mm SL) – pharyngobranchial 4 (11.7 mm SL) – hypobranchial 1 (13.2 mm SL) – hypobranchial 2 (14.1 mm SL).

The sequence of ossification in the branchial skeleton differed between *Noturus gyrinus* and *Ictalurus punctatus* in that the gill rakers appear before epibranchials 1 and 2 in *N. gyrinus* rather and phayryngobranchial 4 appears after basibranchials 3 and 2.

The sequence of ossification was better resolved in *N. gyrinus* with a general posterior to anterior direction of development in the ceratobranchials and epibranchials. Although this could not be determined in *I. punctatus* based off of initial ossification, the same pattern could be observed based off of how well ossified the bones were in the earliest stages of appearance. The branchial skeleton of *N. gyrinus* and *I. punctatus* are similar, and the only difference observed was in the relative size of the gill rakers which were much larger in *N. gyrinus*.

Weberian Apparatus and Associated Centra

The most common sequence of ossification: centrum 4 (10.0 mm SL) – centrum 2 and 3 (10.1 mm SL) – centrum 1 (10.4 mm SL) – neural arch 4 (11.0 mm SL) – neural arch 3 (11.2 mm SL) – intercalarium, outer arm of the os suspensorium, tripus, inner arm of the os suspensorium and scaphium (12.2 mm SL) – claustrum (13.9 mm SL) (Fig. 2.10).

Centra 1–4: Although the first four centra appear in a posterior to anterior direction starting with centrum 4, all four centra were present in some individuals of 10.0 mm SL, the smallest size in which centra were observed. All four centra originate as a pair of parachordal ossifications on the lateroventral margin of the notochord which proceed to expand and meet at the dorsal and ventral midlines. At 10.6 mm SL (Fig. 2.10A), the transverse process of the fourth vertebra is present between the basidorsal and basiventral and by 11.8 mm SL, a small process representing the rudiment of the transverse process of the third vertebra is present on the dorsolateral surface of the third centrum ventral to the basidorsal. At 12.2 mm SL (Fig. 2.10B), the fourth centrum is the

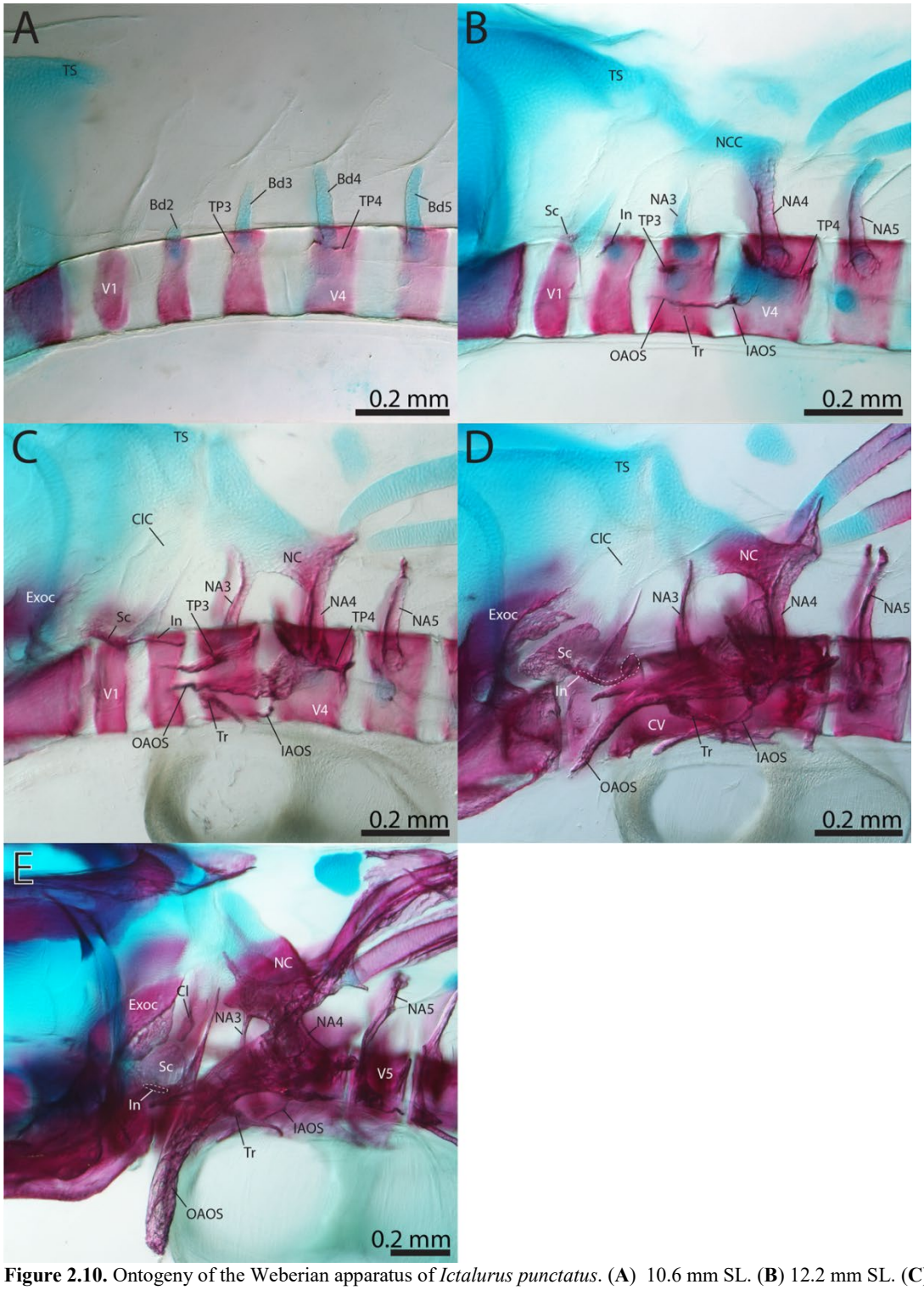

Figure 2.10. Ontogeny of the Weberian apparatus of *Ictalurus punctatus*. (**A**) 10.6 mm SL. (**B**) 12.2 mm SL. (**C**) 12.7 mm SL. (**D**) 13.3 mm SL. (**E**) 15.0 mm SL. Bd, Basidorsal; Cl, Claustrum; ClC, Claustrum cartilage; Exoc, Exoccipital; IAOS, Inner arm of Os Suspensorium; In, Intercalarium; mm, Millimeters; NA, Neural arch; NC, Neural complex; NCC, Neural complex cartilage; OAOS, Outer arm of Os Suspensorium; Sc, Scaphium; Tr, Tripus; TS, Tectum synoticum; TP, Transverse Process; V, Vertebral centrum; SL, standard length.

longest of the four centra, being slightly longer than the post Weberian centra, followed by centrum 3 and centra 1 and 2 which are approximately half the width of a regular centrum. By 12.7 mm SL (Fig. 2.10C), the transverse process of vertebra 4 has expanded laterally and is in the process of fusing to the os suspensorium. The transverse process of centrum 3 spans the length of the centrum and possesses an anterior process which extends out past the transformator process of the tripus. Centra 3 and 4 both possess a pair of ventral bony ridges that extend the length of the centra where they contact the swimbladder. By 13.1 mm SL, centra 2–4 have started to fuse ventrally and the anterior projection of the transverse process of the third vertebra has met and fused to the transformator process of the tripus. At 15 mm SL (Fig. 2.10E), centra 2–4 are completely fused forming a compound centrum which possesses two prominent ventral ridges of bone at the point of attachment to the swimbladder. Centrum 1 remains separate and is significantly shorter than other centra. In the

Neural Arches 3 and 4: The neural arches of vertebrae 3 and 4 first appear (10.8 mm SL) as perichondral ossification of the pair of basidorsal cartilages of centrum 3 and 4. By 12.2 mm SL (Fig 8B), neural arch 4 has expanded to cover basidorsals 4, except for the dorsal end which is confluent with the neural complex cartialge. Neural arch 3 is almost completely perichondrally ossified around basidorsals 3, and possesses a small dorsal process of membrane bone. The neural complex cartilage extends anteriorly from basidorsal 4 above, but not contacting, neural arch 3, and then medially where it meets its counterpart, forming a ‘U’-shaped cartilage. A dorsomedial extension of cartilage arises from the anterior midline of the neural complex cartilage towards the *tectum*

synoticum. At 12.7 mm SL (Fig. 2.10C), membranous processes extend from the dorsal tips of neural arch 4 on either side of the ventral tip of the dorsal-fin proximal radial 2 and a small lamina of membrane bone is forming on the anterior edge of neural arch 4. The ossification from neural arch 4 has begun to spread anteriorly onto the neural complex and the dorsal tips of neural arch 3 now contact the neural complex cartilage medially. The ossification of the neural complex spans the gap between the tips of neural arches 3 and 4 by 13.3 mm SL (Fig. 2.10D), and the anteromedial process of the neural complex cartilage is directed more dorsally. The posterodorsal membranous tips of neural arch 4 have expanded to become triangular in shape and the anterior laminae of membrane bone meets and joins with an anterodorsal process of the transverse process of vertebra 4. The perichondral ossification of the neural complex spreads medially over the posterior halve of the cartilage and by 15.0 mm SL (Fig. 2.10E), meets and fuses with its counterpart across the midline. The posterodorsal processes of neural arch 4 have extended dorsally with the tips reaching lateral to the anterior nuchal process of dorsal-fin proximal radial 2. A pair of anterodorsal processes dorsal to neural arch 3 are extending towards the back of the cranium on either side of the anterodorsal process of the neural complex cartilage. A median crest of bone has appeared on the dorsal surface of the neural complex ossification (17.8 mm SL) and by 21.2 mm SL has expanded to reach across the length of the bone, branching posteriorly to meet the posterodorsal processes on either side of dorsal-fin proximal radial 2. These posteordorsal processes form a close connection with the anterior nuchal plate via dense connective tissue. The lateral gap between neural arches 3 and 4 has completely been filled in with bone and

the whole structure forms a tunnel around the spinal cord. By 44.9 mm SL, the posterodorsalmost point of the median crest of bone contacts the ventral process of dorsal-fin proximal radial 1 and the tips of the anterodorsal processes dorsal to neural arch 3 contact the posterior surface of the supraoccipital. The whole neural complex has become heavily sculpture.

Intercalarium: The *intercalarium* first appears as perichondral ossification around the basidorsal of vertebra 2 in individuals as small as 11.2 mm SL. At 12.2 mm SL (Fig. 2.10B), an anterolateral process, the *manubrium*, has formed from the perichondral ossification and by 12.7 mm SL (Fig. 2.10C) it extends laterally to the *scaphium*. The perichondral ossification of the *intercalarium* along with the basidorsal become reduced and were no longer observed by 13.3 mm SL (Fig. 2.10D), leaving only the *manubrium* of the *intercalarium*, the tip of which lies in the interossicular ligament. By 15.0 mm SL (Fig. 2.10E), the *manubrium* starts to reduce in size and begins to break down, except for the tip which remains in the interossicular ligament between the tripus and the scaphium. By 17.7 mm SL, the tip of the *manubrium* is all that remains resembling the condition observed in adults.

Os suspensorium: The *os suspensorium* first appears as a perichondral ossification around the tip of basiventral 4 (11.2 mm SL) in which the outer arm is already present as a thin anterior directed process. By 12.2 mm SL (Fig. 2.10B), the outer arm has extended lateral to the anterior margin of vertebra 3 and an additional small process, the inner arm, is present on the tip of basiventral 4 ventromedial to the outer arm. The outer arm of the *os suspensorium* extends anterolaterally towards the

pectoral girdle while the inner arm has expanded anteromedially towards the vertebral column where it curves anteriorly and lies parallel to the dorsal surface of the swimbladder and medial to the transformator process of the tripus. The perichondral ossification of the *os suspensorium* expands medially covering much of the basiventral cartilage and in some individuals of this size, meets and begins to fuse with the transverse process of vertebra 4 posteriorly. This fusion is complete by 13.3 mm SL (Fig. 2.10D), with laminar expansions of bone forming anterior and posteriorly from the perichondral ossification of the *os suspensorium*. The outer arm now reaches and forms a close association with the medial surface of the cleithrum. At 15.0 mm SL (Fig. 2.10E), the outer arm has become more robust and its surface is now sculptured. A posterolateral process has formed along the posterior margin of the outer arm at this size and by 17.8 mm SL, bone has formed between this process and the posterior margin of the centrum creating a large sheet of bone. The outer arm has formed a firm connection with the medial arm of the supracleithrum. By 44.9 mm SL, the laminar sheets of bone forming from the *os suspensorium* have grown in size and now appear as large wing-shaped expansions, covering much of vertebral column just posterior to the cranium. The inner arm has expanded in width but remains otherwise unchanged.

Tripus: The *tripus* originates as a perichondral ossification around the tip of basiventral 3 with a small membranous posteriorly directed process, the transformator process (11.2 mm SL). As the transformator process grows it curves ventromedially (12.7 mm SL; Fig 8C) and by 13.3 mm SL (Fig. 2.10D) the tip of the process reaches towards the inner arm of the *os suspensorium* and sits dorsal to the swimbladder. At this

size, an anteriorly directed process extending from the transverse process of centrum 3 begins to fuse to the base of the *tripus* at the tip of the basiventral process and forms the anteriormost extent of the *tripus*. By 14.1 mm SL, a thin lamina of bone has formed lateral from this point of fusion filling the gap between the anteriormost tip of the *tripus* and the lateralmost extent of the transformator process, giving the anterior half a distinct triangular shape. The transformator process is now semicircular in shape extending posteriorly to the inner arm of the *os suspensorium* and rests on the dorsal surface of the swimbladder. By 15.0 mm SL (Fig. 2.10E), the anteriormost tip of the *tripus* reaches lateral to and is connected via an interossicular ligament to the anterior tip of the *manubrium* of the *intercalarium* and the *scaphium*, resembling the adult condition.

Scaphium: The *scaphium* appears in individuals as small as 11.9 mm SL as a perichondral ossification around the dorsal half of basidorsal 1 and a small membrane bone process can be seen extending anteriorly from the middle of the basidorsal cartilage by 12.2 mm SL (Fig. 2.10B). The perichondral ossification covers the entirety of the dorsal half of basidorsal 1 by 12.7 mm SL (Fig. 2.10C) and possesses a thin process of membrane bone from its dorsal tip, forming the ascending process of the *scaphium*. At this size, the anterior process is more robust, extends almost to the back of the cranium and a thin lamina of bone has started to form at the anterior tip of the process. By 13.3 mm SL (Fig. 2.10D), this lamina has expanded into a large disc, the *concha scaphium*, but still remains separate from the ascending process. The *concha* posteriorly meets and joins with the ascending process (14.1 mm SL) and by 15.0 mm SL (Fig. 2.10E) the

concha abuts the back of the cranium almost contacting the posterior membranous extension of the exoccipital, resembling the adult condition.

Claustrum: The *claustrum* is a chondral bone located between the ascending process of the *scaphium* and the back of the cranium. It first appears as a perichondral ossification on the anteroventral edge of the supradorsal cartilage of vertebra 1 (Britz & Hoffman, 2006) from which a membrane bone process extends towards the *concha scaphium* (13.1 mm SL). By 15 mm SL (Fig. 2.10E), the *claustrum* expands dorsally to cover the ventral half of the supradorsal cartilage and by 44.9 mm SL, the ossification has expanded to fill most of the gap between the ascending process of the *scaphium* and the back of the cranium although at this stage, the dorsal third of the supradorsal cartilage remains unossified.

Comparison. The most common sequence of ossification for this region in *Noturus gyrinus* is as follows: centrum 1, 2, 3 and 4 (6.6. mm SL) – neural arch 4 (6.7 mm SL) – neural arch 3, outer arm of the os suspensorium, intercalarium, and tripus (7.3 mm SL) – scaphium (7.7 mm SL) – inner arm of the os suspensorium (8.7 mm SL) – claustrum (10.0 mm SL).

No differences in the sequence of ossification were identified between *Noturus gyrinus* and *Ictalurus punctatus* in the Weberian apparatus. The Weberian apparatus of *N. gyrinus* and *I. punctatus* are similar, and no major differences in adult morphology are observed in this region.

Pectoral Girdle

The most common sequence of ossification: cleithrum (7.7 mm NL) – pectoral-fin rays (10.9 mm SL) – supracleithrum (11.4 mm SL) – scapulocoracoid (13.2 mm SL) – propterygium (13.9 mm SL) – pectoral-fin radial 3 and 4 (14.2 mm SL) (Fig. 2.11).

Cleithrum: The cleithrum is a dermal bone and the first ossification to appear in *Ictalurus punctatus* in individuals as small as 7.7 mm SL. It starts off as a slightly curved, thin split of bone just posterior to the cranium and anterodorsal to the yolk-sac. By 10.0 mm SL (Fig. 2.11A), the bone is now 'L' shaped with the ventral third of the bone directed anteromedially. The bone is widest at its midpoint where it possesses a small rounded posterior extension with additional bone forming dorsal and medial to this widened portion. By 11.9 mm SL (Fig. 2.11B), the reduction of the yolk-sac has brought the cleithra closer together but they do not make contact across the ventral midline. The bone has widened with laminae of bone extending both anterior and posterior to the original splint like ossification, which appears as a median ridge of bone. At 12.8 mm SL, the bone continues to widen at its center and its posterior edge now extends lateral to much of the scapulocoracoid cartilage. The humeral process is starting to form on the posterior edge just dorsal to the scapulocoracoid cartilage and a small process has formed on the posterodorsalmost point of the bone. A posterolateral curved expansion of bone starts to form ventral to the humeral process (14.3 mm SL) and by 15.0 mm SL (Fig. 2.11D) it forms the spinal fossa, a groove on the posteromedial surface of the cleithrum for the articulation of the dorsal head of the pectoral-fin spine. Posteroventrally, the cleithrum meets the *abductor coracoid lamina* (*sensu* Fine et al.,

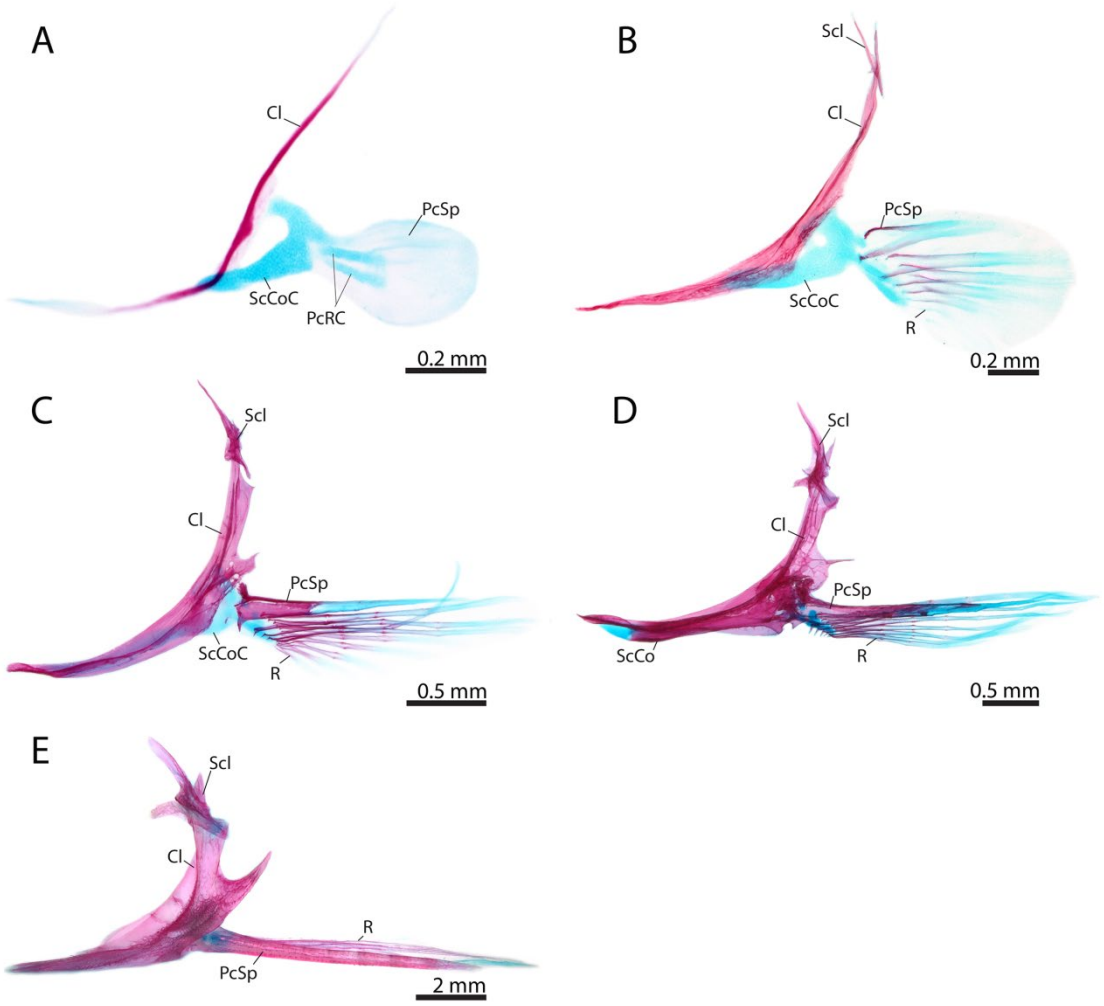

Figure 2.11. Ontogeny of the dermal pectoral girdle of *Ictalurus punctatus*. (**A**) 10.0 mm NL. (**B**) 11.8 mm SL. (**C**) 13.3 mm SL. (**D**) 15.0 mm SL. (**E**) 44.9 mm SL. Cl, Cleithrum; mm, Millimeters; Pcl, Postcleithrum; PcRC, Pectoral radial cartilage; PcSp, Pectoral-fin spine; R, Pectoral-fin ray; ScCo, Scapulocoracoid; ScCoC, Scapulocoracoid cartilage; Scl, Supracleithrum; NL, notochord length; SL, standard length.

1997) which along with the spinal fossa serves as part of the spine locking mechanism. At the same stage, the cleithrum joins its antimere ventrally and is attached firmly to the ventral arm of the coracoid via dense connective tissue. The humeral process and

posterior dorsal process continue to expand and a small cartilage, herein referred to as the cleithral cartilage, appears medially to the latter near its articulation with the supracleithrum and the outer arm of the os suspensorium. At 21.5 mm SL, the ventral portion of the cleithrum is directed medially almost at a right angle to the dorsal half and forms a tight connection with its counterpart. The connections between the coracoid and the cleithrum are near inseparable and sculpturing is present over the entire surface of the bone at this stage. At 44.9 mm SL (Fig. 2.11E) the cleithrum is heavily ossified and the humeral process has become significantly larger.

Pectoral-Fin Rays: The pectoral fin is the second fin to develop in *Ictalurus punctatus* with the first two fin rays appearing at 10.9 mm SL. The anteriormost pectoral-fin ray which will become the pectoral-fin spine is approximately twice the size of the subsequent fin rays and its dorsal hemitrichium is closely associated with the propterygium. Four more fin-rays have appeared by 12.0 mm SL and the first four are now segmented. The dorsal and ventral hemitrichia of the first segment of the anteiormost fin ray have started to fuse across the anterior edge and eight-fin rays (including the spine) have formed. A second segment has fused to the spine proper and the propterygium has perichondrally ossified and is fused to the proximal head of the upper hemitrichia of the spine at 14.1 mm SL. At approximately the same time as a third segment is added to the spine proper (15.0 mm SL; Fig. 2.11D), the spine is capable of locking. At this size, the tenth and final fin ray has just formed. By 15.9 mm SL the number of pectoral fin-rays equals that of the adult (i.9) and all fin rays are segmented. The pectoral fin-spine possesses serrations along the posterior edge associated with each

segment and the anterior margin has gained several denticuli (a more detailed account of pectoral-fin spine development is provided by Kubicek, Britz and Conway, 2019).

Supracleithrum: Whether this element is of compound origin (posttemporal+supracleithrum) or not has been a contentious subject in the past. Herein we refer to the element as the supracleithrum and further discuss the homology of this element below (see discussion). The supracleithrum is a dermal ossification that first appears as a thin splint of bone anterolateral to the dorsal tip of the cleithrum (10.9 mm SL; Fig. 2.11B). By 12.2 mm SL, an anteroventral process has started to form giving the bone a triangular shape and a medially directed process has appeared and extends anterior to the dorsal tip of the cleithrum. Ridges of bone arise on the lateral surface of the supraoccipital forming a trough around the lateral line sensory canal. Shortly after this (12.8 mm SL), the median process of the supracleithrum wraps around the cleithrum and is connected to the base of the chondrocranium via a newly formed Baudelot's ligament. The dorsal tip of the supracleithrum lies over the posterodorsal surface of the otic capsule and the roof of the lateral line sensory canal associated with the supracleithrum is fully enclosed in bone. At 15.0 mm SL (Fig. 2.11D), the medial process continues to lengthen replacing Baudelot's ligament with bone. Posteroventrally, the supracleithrum extends laterally to the small cleithral cartilage and the dorsal posterior process of the cleithrum strengthening the connection with the cleithrum. Anteriorly, a lamina of membrane bone has formed between the dorsal tip of the bone and the anteroventral process which almost reaches the posterolateral surface of the chondrocranium. By 21.5 mm SL, Baudelot's ligament has been entirely replaced by the

medial process of the supracleithrum except for a small portion between the process and the basioccipital. The anteroventral process reaches and lies ventral to the lateral lamina of membrane bone of the pterotic and the dorsal arm overlies the epioccipital. At 44.9 mm SL (Fig. 2.11E, the supracleithrum has changed only in size and its lateral surface has become sculptured. The tip of the dorsal arm forms an attachment to and is covered by the accessory ossicle.

Scapulocoracoid: The scapulocoracoid first appears as a perichondral ossification around the proximal end of the ventral arm of the scapulocoracoid cartilage (12.6 mm SL). By 13.1 mm SL (Fig. 2.12A), the ventral portion of the ventral arm of the scapulocoracoid cartilage has widened and the scapulocoracoid spreads posterodorsally around the scapular foramen (enabling passage of a branch of the pterygial nerve) to the anterodorsalmost point of the scapulocoracoid cartilage. At this size, a small ridge of membrane bone is present on the concave margin of the scapulocoracoid cartilage dorsal to the ventral arm. A small projection of membrane bone extends from the posterior edge of the scapulocoracoid on the lateral surface of the scapulocoracoid cartilage. By 14.1 mm SL, the scapulocoracoid has started to spread down the ventral arm and over the posterior surface of the scapulocoracoid cartilage. The ventral arm of the scapulocoracoid rotates roughly 90 degrees with dorsal and ventral edges of smaller stages making up the posterior and anterior margins respectively. Two membranous processes, one at both the dorsal and ventralmost tip of the posterior edge, extend towards each other on the medial side of the bone. The projection of membrane bone on the lateral surface of the scapulocoracoid extends anteriorly towards the posteroventral

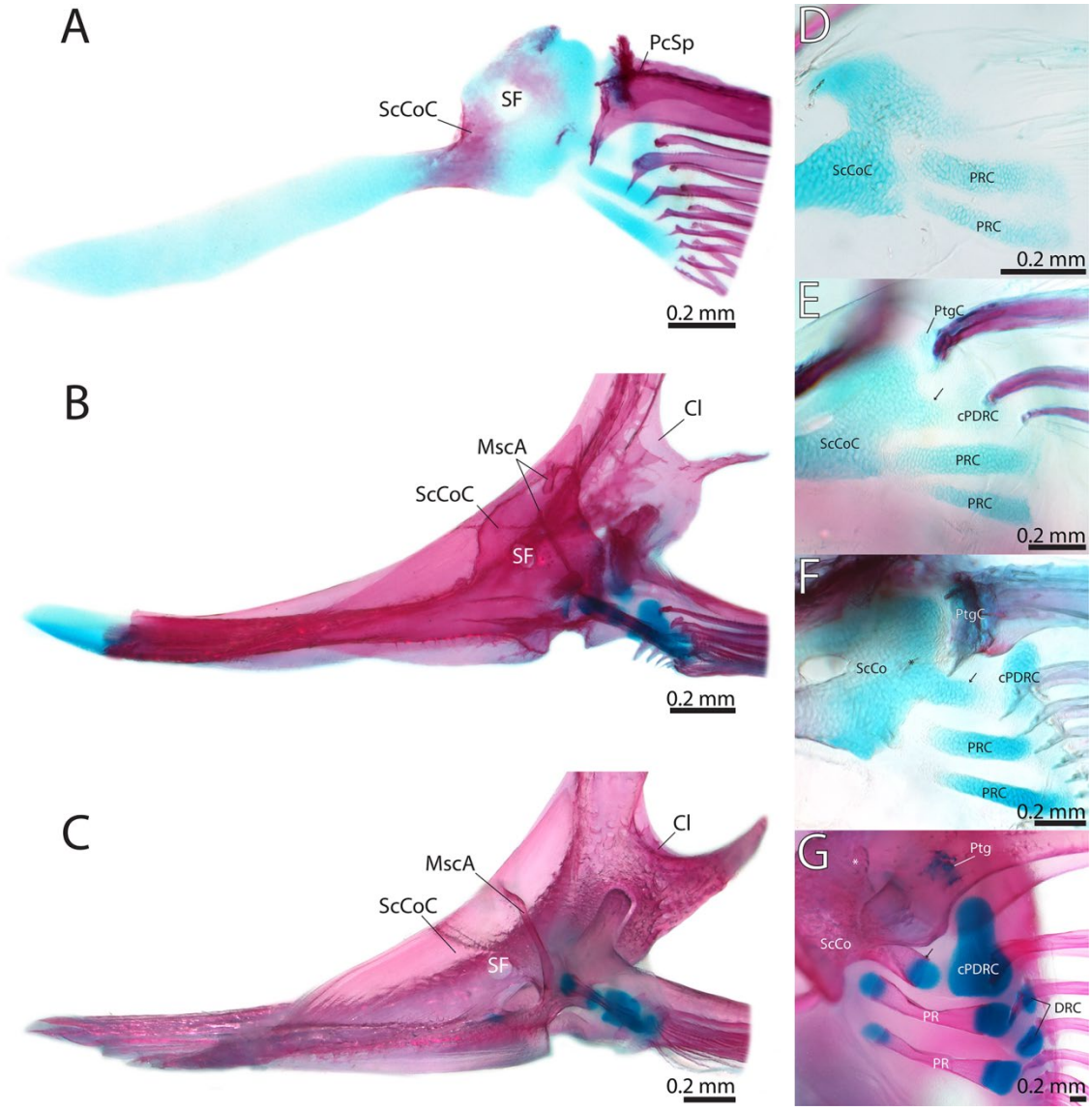

Figure 2.12. Ontogeny of the endoskeletal pectoral girdle (A-C, scapulocoracoid; D-G, pectoral radials) of *Ictalurus punctatus* (**A**) 13.3 mm SL. (**B**) 15.0 mm SL. (**C**) 44.9 mm SL. (**D**) 10.0 mm NL. (**E**) 10.8 mm SL. (**F**) 12.9 mm SL. (**G**) 44.9 mm SL. Asterisk indicates abductor coracoid lamina. Black arrows indicated scapular process of scapulocoracoid. Cl, Cleithrum; cPDRC, complex pectoral distal radial cartilage; DRC, distal radial cartilage; mm, Millimeters; MscA, Mesocoracoid arch; PcSp, Pectoral-fin spine; PR, Pectoral radial; PRC, Pectoral radial cartilage; Ptg, Propterygium; PtgC, Propterygial cartilage; ScCo, Scapulocoracoid; ScCoC, Scapulocoracoid cartilage; SF, Scapular foramen; NL, notochord length; SL, standard length.

corner of the cleithrum and by 15.0 mm SL (Fig. 2.12B) it reaches and forms a tight connection with the cleithrum forming the *abductor coracoid lamina* of the spine locking mechanism. At this stage the scapulocoracoid extends over the entirety of the scapulocoracoid cartilage except for the anteroventral tip of the ventral arm, the posterodorsal margin at the point of articulation with the propterygium, as well as the tip of the scapular process (*sensu* Brousseu, 1976), which articulates with the complex distal radial cartilage. The ventral arm has widened considerably, increasing the area of contact with its antimere. The lamina of bone originating on the posterodorsal edge of the ventral arm extends to its tip where it overlaps slightly with its counterpart across the midline. A second ridge of lamina bone is present on the ventral surface of the bone extending from the posteroventralmost point towards the midlength of its anterior edge. The medial membranous processes of the dorsal and ventral tips of the posterior margin of the scapulocoracoid continue to grow towards each other and by 16.2 mm SL, these processes have fused together forming the mesocoracoid arch. The scapulocoracoid has started to endochondrally ossify and forms a weakly interdigitated suture with its counterpart across the midline. At 21.2 mm SL, the entire bone is endochondrally ossified and the tip of the ventral arm is more heavily sutured with its antimere. The scapulocoracoid and cleithrum have strengthened in their connection and an interdigitating suture is forming at the point of contact between the cleithrum and the *abductor coracoid lamina*.

Pectoral-Fin Radials: Two small cartilaginous pectoral radials are present by 10.0 mm SL (Fig. 2.12D), although they remain connected by a thin layer of cartilage

distally and proximally where they are continuous with the scapulocoracoid cartilage. By 11.0 mm SL (Fig. 2.12E) the two pectoral radial cartilages are separated from the scapulocoracoid cartilage and have fully differentiated into independent cartilages. The complex distal radial cartilage has appeared at the base of pectoral-fin ray 2 and is confluent with the scapular process of the scapulocoracoid cartilage. Both pectoral-radial cartilages start to perichondrally ossify around their midline in individuals as small as 13.2 mm SL. By this size, the complex pectoral distal radial cartilage has separated from and now articulates with the scapular process. At 16.2 mm SL, the perichondral ossification covers all but the distal and proximal tips of the two radials. The complex pectoral distal radial cartilage extends anteriorly into the posterior edge of the spine where it articulates with a remnant of the propterygium cartilage and two distal radials have formed distal to the pectoral radials. In a stage resembling the adult (44.9 mm SL (Fig. 2.12G), the pectoral radials are endochondrally ossified and possess lateral flanges of membrane bone and the complex pectoral distal radial remains cartilaginous.

Comparison. The most common sequence of ossification for this region in *Noturus gyrinus* is as follows: cleithrum (5.4 mm NL) – pectoral-fin rays (6.4 mm SL) – supracleithrum (7.0 mm SL) – scapulocoracoid (8.3 mm SL) – propterygium (9.9 mm SL) – pectoral-fin radial 3+4 (11.1 mm SL).

No differences in the sequence of ossification were identified between *Noturus gyrinus* and *Ictalurus punctatus* in the pectoral girdle. The pectoral girdle of *N. gyrinus* and *I. punctatus* are similar, except for the shape of the pectoral-fin spine, which lacks posterior serrations and anterior dentations in *N. gyrinus*, and the pectoral-fin radials, in

which there is only a single pectoral-radial element in *N. gyrinus* which is a compound element consisting of pectoral radials 3 and 4.

Pelvic Girdle

The most common sequence of ossification: pelvic-fin rays (12.3 mm SL) – basypterygium (15.0 mm SL) (Fig. 2.13).

Pelvic-Fin Rays: The pelvic fin is the last of the fins to develop with fin rays first appearing in individuals of 11.9 mm SL on the posterolateral margin of the yolk-sac. By 12.6 mm SL, the resorption of the yolk-sac has resulted in the fins sitting in their normal position on the ventral margin of the body anterior to the anus. At this size, five small fin rays are present but remain unsegmented. At 14.1 mm SL, the number of pelvic-fin rays equals that of adults (i.7), the first six of which are segmented. A small pelvic splint (not included in the ossification sequence) has appeared on the lateral margin of the fin and all eight fin rays are segmented by 15.9 mm SL.

Basipterigium: The basipterigium starts as a perichondral ossification of the basipterygium cartilage between the anterior foramen and the anterior edge of the cartilage between the lateral and medial processes (14.5 mm SL; Fig. 2.13B). By 16.2 mm SL, the ossification has spread to cover most of the basipterygium cartilage excluding the the posterior edge (which serves as a point of articulation for the pelvic-fin rays), the ischiac processes, and the medial edge (where it abuts its counterpart), and the tips of the anterior lateral and medial processes. Laminae of membrane bone have formed on either side of the anterior processes by 21.5 mm SL. At 44.9 mm SL (Fig

.

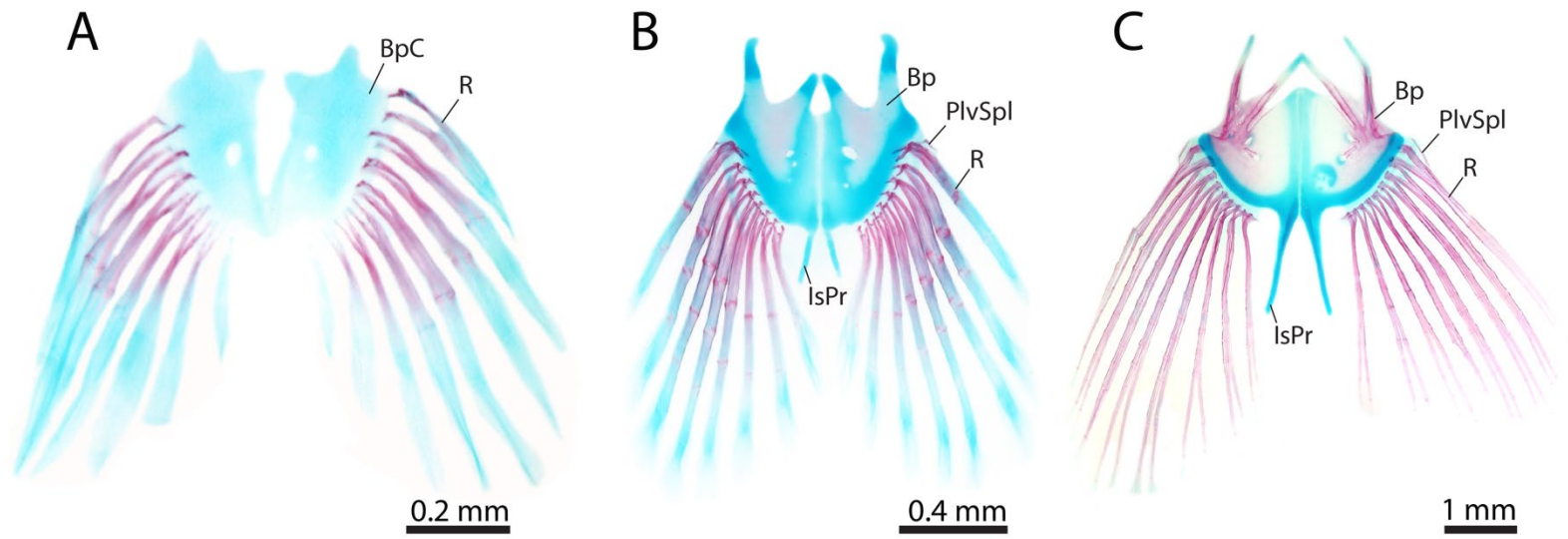

Figure 2.13. Ontogeny of the pelvic girdle of *Ictalurus punctatus*. (**A**) 13.3 mm SL. (**B**) 15.0 mm SL. (**C**) 44.9 mm SL. Bp, Basipterygium; BpC, Basipterygial cartilage; mm, Millimeters; PlvSpl, Pelvic splint; R, Pelvic-fin ray; SL, standard length

2.13C), the basipterygium is endochondrally ossifiying and the surface of the bone near the base of the anterior processes is lightly sculptured.

Comparison. The most common sequence of ossification for this region in *Noturus gyrinus* is as follows: pelvic-fin rays (8.3 mm SL) – basypterygium (10.4 mm SL).

No differences in the sequence of ossification were identified between *Noturus gyrinus* and *Ictalurus punctatus* in the pelvic girdle. The pelvic girdle of *N. gyrinus* and *I. punctatus* are similar, except for the ischiac processes which are much shorter and the outer edge of the basipterygia which reaches approximately half the distance of the lateral anterior process in *N. gyrinus*.

Comparison with other Otophysans

Although there have been numerous studies of skeletal development in otophysans, most of these have focused only on a subsection of the skeleton (e.g., cranium and paired fins, post-cranial skeleton, Weberian apparatus; Kindred, 1919; Bamford, 1948; Cubbage & Mabee, 1996; Bird & Mabee, 2003; Britz & Hoffman, 2006). Studies that provide information on the development of the entire skeleton are available for only three other otophysans, the cypriniforms *Danio rerio* (Cubbage & Mabee, 1996; Bird & Mabee, 2003; see Chapter IV) and *Enteromius holotaenia* (Conway, Kubicek & Britz, 2017), and the characiform *Salminus brasiliensis* (Mattox, Toledo-Piza & Britz, 2014). In the following section I compare the ossification sequence data collected herein with that available for *D. rerio*, *E. holotaenia*, and *S. brasiliensis*. Due to the similarity between the sequence of ossification compiled for *Ictalurus*

punctatus and *Noturus gyrinus*, I focus here only on the sequence compiled for *I. punctatus*. Some skeletal elements found in other otophysans are not present in ictalurids (and vice versa) so only those elements present in all four species could be compared.

Danio rerio* and *Enteromius holotaenia

Comparing *Ictalurus punctatus* to the two cypriniforms revealed seven major differences in the sequence of ossification of cranial elements, five of which are shared between *Danio rerio* and *Enteromius holotaenia*. In the ethmoid region, the nasal is the first bone to appear in *I. punctatus* and appears much earlier in the entire sequence of ossification compared to *D. rerio* and *E. holotaenia,* in which it does not appear until much later in development and is the last bone in the region to appear. The lateral ethmoid appears later in *I. punctatus* (towards the beginning of the final third of elements within the sequence) while it is the first bone to appear in the ethmoid region of *D. rerio* and is present much earlier in the entire sequence of ossification. *E. holotaenia* does not exhibit this shift in the lateral ethmoid and instead, the first bone of the ethmoid region to appear is the vomer compared to it being the last bone to appear in the region in *I. punctatus*. In the otic region, the dermopterotic is the second element of the region to appear in *I. punctatus*, after the prootic and before the autopterotic and autosphenotic. In the cypriniforms, the dermopterotic is the last element to appear in the region and is one of the last to appear in the overall sequence of ossification. In the occipital region of *I. punctatus*, the extrascapular appears before the supraoccipital while in *D. rerio* and *E. holotaenia*, it is the last element in the region to ossify, after both the supraoccipital and epioccipital. In the suspensorium of *I. punctatus*, both the hyomandibular and

endopterygoid appear much later in the regional sequence as well as the entire ossification sequence when compared to that of *D. rerio,* in which both ossifications represent some of the first bones to appear in the sequence of ossification. Unfortunately, in *E. holotaenia* the smallest individual observed possessed 14 elements which included many of the elements of the hyopalatine arch, jaws, and opercular series so it is not possible to compare the sequence of development in most of this region. It should also be mentioned that, despite appearing at roughly the same position in the overall sequence of development, both the premaxilla and the preopercle appear earlier in *I. punctatus*, being the fourth and sixth respective elements of the hyopalatine arch, jaws, and opercular series to appear while in *D. rerio* they appear later being the ninth and twelfth elements to appear respectively. The last major difference of the cranium in *I. punctatus* compared to the cypriniforms is ceratobranchial 5 which does not vary in the regional sequence but is one of the first few bones to appear in cypriniforms while in *I. punctatus* it appears much later, after 61 other elements. In *E. holotaenia*, basibranchials 2 and 3 appear relatively early in the sequence and before epibranchials 1 and 2 have ossified. In *I. punctatus*, the basibranchials appear much later and are among the last elements to appear in the skeleton. The sequence of ossification of the elements of the hyoid bar of *I. punctatus* differed from *E. holotaenia* in the earlier appearance of the urohyal and interhyal and the later appearance of the dorsal hypohyal. The urohyal is the third element of the region to appear in *I. punctatus* while it is the second to last to appear in *E. holotaenia*. The interhyal appears at approximately the same time as the posterior ceratohyal in *I. punctatus* but well after all other elements of the hyoid bar in *E.*

holotaenia. The dorsal hypohyal, despite being one of the last three elements to appear in the hyoid bar region, ossifies before approximately 2/3rds of the skeleton while it appears towards the end of the sequence in *I. punctatus*.

In the post-cranial skeleton, the pectoral- and dorsal-fin rays appear early in the ossification sequence of *Ictalurus punctatus* while in the cypriniforms they ossify much later in the entire sequence of ossification. In the case of the procurrent caudal-fin rays, the ventral-procurrent caudal-fin rays of *I. punctatus* appear very early on in the sequence of ossification while the dorsal-procurrent caudal-fin rays appear much later in the overall sequence. In *Danio rerio* and *Enteromius holotaenia*, both the dorsal- and ventral-procurrent caudal-fin rays appear at approximately the same time in the middle of the sequence. It is also worth noting that in *I. punctatus* the fin rays associated with all fins (except for the pelvic fin) ossify before the endoskeletal elements of the caudal-fin, while in the cypriniforms most of the caudal skeleton is ossified before any of the other fins-rays start to develop. In the vertebral column the most notable difference observed between *I. punctatus* and the cypriniforms is the early appearance of the parapophyses, which start to ossify before all of the post-Weberian vertebral centra in *I. punctatus*, but do not start to ossify until almost the entire vertebral column (excluding some of the hemal and neural spines and ural centrum 2) has formed in *D. rerio* and *E. holotaenia*. The outer arm of the os suspensorium is the second of the Weberian elements to ossify in *I. puncatusus* while in *D. rerio* and *E. holotaenia* it is the second to last, just before the claustrum. Additionally, the intercalarium, inner arm of the os suspensorium, scaphium and tripus all start to ossify slightly later in the overall sequence of *I.*

punctatus when compared to that of the two cypriniforms. Additionally, the centra associated with the caudal skeleton (preural centra 2 and 3 and ural centra 1 and 2) appeared earlier in the sequence of ossification of *I. punctatus* before the Weberian ossicles and some of the hemal and neural arches, in *E. holotaenia* these centra were some of the last elements of the vertebral column to ossify.

Salminus brasiliensis

There were seven major differences in the cranial skeleton between *Ictalurus punctatus* and *Salminus brasiliensis*. The nasal, dermopterotic and extrascapular all appeared much earlier in the regional sequences of ossification as well as that of the whole skeleton in *I. punctatus* compared to *S. brasiliensis*. Likewise, the hyomandibular and the endopterygoid appeared much later in *I. punctatus* while both of these appeared very early in the sequence of *S. brasiliensis*. The gill rakers of *S. brasiliensis* ossified very early in development, before ceratobranchial 4 or any of the epibranchials had appeared compared to *I. punctatus* in which they appeared much later in the sequence after all of the ceratobranchials and epibranchials were ossified. Additionally, the interhyal in *S. brasiliensis* towards the end of the sequence, well after the other elements of the hyoid bar had ossified. In *I. punctatus* the interhyal appears slightly earlier in the overall sequence at the same time as the posterior ceratohyal and before the dorsal hypohyal.

In the postcranial skeleton, the pectoral-fin rays and the parapophyses showed the same pattern of appearing much earlier in the sequence of *Ictalurus punctatus* when compared to *Salminus brasiliensis*. The ventral procurrent caudal-fin rays appear much

earlier in *I. punctatus* while the dorsal procurrent caudal-fin rays appear at roughly the same place in the sequence as *S. brasiliensis*. Neural arches 3 and 4 also appear much earlier in the sequence of *I. punctatus*, ossifiying before most of elements of the vertebral column while in *S. brasiliensis* they do not ossify until after most of the vertebral column is present. Finally, like what was observed in the comparison with *E. holotaenia*, the four centra supporting the caudal skeleton were some of the last elements of the vertebral column to appear while in *I. punctatus* they appear much earlier in the sequence of ossification.

Discussion

Skeletal development in Ictalurus punctatus *and* Noturus gyrinus

The development of the skeleton in *Ictalurus punctatus* and *Noturus gyrinus* occurred over a relatively short period of growth, with all elements of the skeleton (excluding the dorsal- and anal-fin distal radials in *N. gyrinus*) present by 22.4 and 14.1 mm SL, respectively. Dorsal- and anal-fin distal radials, which are present in the adult stage of *N. gyrinus* (Pers. Obs.; TCWC 19758.01), are absent from the developmental series compiled for this study suggesting that these elements form later in development, at sizes larger than that of the material examined herein (max size 26.4 mm SL). Elements of the skeleton typically appeared at smaller sizes in *N. gyrinus* compared to *I. punctatus*, which is not surprising given that the former is much smaller than the latter (it is generally observed that smaller bodied species develop quicker than closely related, larger bodied species; Reiss, 1989; Block & Mabee, 2012; Kubicek & Conway, 2016). Despite the difference in the size at which a particular element ossifies, the sequence of

ossification did not differ significantly between the two species except for preural centra 2 and 3, which appear later in the sequence of *N. gyrinus* (both in sequence for the entire skeleton and the elements of the vertebral column).

Low levels of intraspecific variation in the total number of certain serial elements was observed in both species. Variation in the total number of elements of the vertebral column was observed in both *Ictalurus punctatus* and *Noturus gyrinus*. In *I. punctatus*, 11 post-Weberian ribs associated with vertebrae 5–15 was the most common condition although in a small number of individuals (n=11) an additional rib associated with vertebra 16 was observed. The majority of individuals examined possessed 20 abdominal vertebrae and 29 caudal vertebrae for a total of 51 independent vertebrae including the two ural centra although individuals with 19 abdominal central and 28 or 30 caudal centra were observed, resulting in a total vertebral count ranging 49–52. In *N. gyrinus*, the number of post Weberian ribs, starting at vertebra 5, varied between seven and nine in total with seven being the most commonly observed condition (n=45) followed by eight (n=39). The number of vertebral centra also varied with the most commonly observed condition being 13 abdominal vertebrae and 25 caudal vertebrae for a total of 40 individual vertebrae, including the two ural centra. The number of abdominal vertebrae observed ranged from 13–15 and the number of caudal vertebrae ranged from 24 to 28 for a total range of 40–43 vertebrae. In addition to elements of the vertebral column, variation was also observed in the number of branchiostegal rays and hypurals present in individuals of *N. gyrinus*. In a small number of individuals (n=16) an additional branchiostegal ray was observed anterior to the remaining nine branchiostegal

rays (asymmetry of this element was also observed in a single individual, in which it was present on the right side only). Most individuals of *N. gyrinus* possessed five hypurals; however, in a few individuals a sixth hypural is present and ossified. The intraspecific variation observed here for *N. gyrinus* in the total number of vertebrae, branchiostegal rays and hypurals was also observed by Taylor (1969). The variation observed for the post-Weberian ribs differed from that reported by Taylor, in which six was the most commonly observed count. The rib associated with vertebra five is typically much smaller than those associated with more posterior vertebrae and it is possible that this element was overlooked by Taylor (1969) or that it was excluded from the total count (Taylor also excluded vertebra five from his vertebral counts).

Homology

Parieto-supraoccipital

The parieto-supraoccipital is one of several elements in the skeleton of catfishes which have previously been purported to represent a compound element, resulting from the fusion of the parietal and supraoccipital (Arratia & Gayet, 1995). Prior to 1948, the parietal was either interpreted to be absent in catfishes with the supraoccipital extending anteriorly on either side of the postcranial fontanelle to occupy the space left in its absence (McMurrich, 1884) or to have possibly fused with the supraoccipital (Kindred, 1919). Evidence of a fusion between these two elements was first reported by Bamford (1948) in a developmental study of the cranium in the ariid catfish *Ariopsis felis*. Using serial sections of a limited series of specimens (six individuals ranging from 8–50 mm), Bamford described the supraoccipital as originating from three separate ossifications,

which he interpreted as the parietal, post-parietal and a paired supraoccipital, which is typically a median bone. These three bones then proceeded to fuse on either side of the postcranial fontanelle into paired compound elements before subsequently fusing across the midline into the single 'U'-shaped element observed in adults (e.g., see figures 4 and 6; Bamford, 1948). A small paired element interpreted to represent the parietal has also been reported in juvenile individuals of the trichomycterids *Hatcheria* and *Bullockia* (Arratia, Chang, Menu-Marque & Rojas, 1978; Arratia & Menu-Marque, 1981). This small paired element is located between the supraoccipital, frontal and sphenotic and is reported to subsequently fuse to the supraoccipital in adult individuals. In addition to these reported cases of fusion, Arratia and Gayet (1995) argued that the elements that surround and suture with the 'supraoccipital' of catfishes are also those elements that surround and suture with the parietals and supraoccipital in other teleosts, providing what they viewed as an additional line of evidence in support of the compound nature of this element.

At no point in the development of the supraoccipital in *Ictalurus punctatus* and *Noturus gyrinus* were two separate ossification centers on one side of the postcranial fontanelle observed (see description of supraoccipital development in *I. punctatus*; Fig. 2.14). In both species, development of the supraoccipital starts as a paired perichondral ossification of the otic capsule on either side of the posterior fontanelle (Fig. 2.14A). As development continues, an anterior extension of membrane bone confluent with the perichondral ossification of the supraoccipital forms on the edge of the otic capsule (13.2 mm SL, Fig. 2.14B) and this paired ossification then fuses across the midline, along the

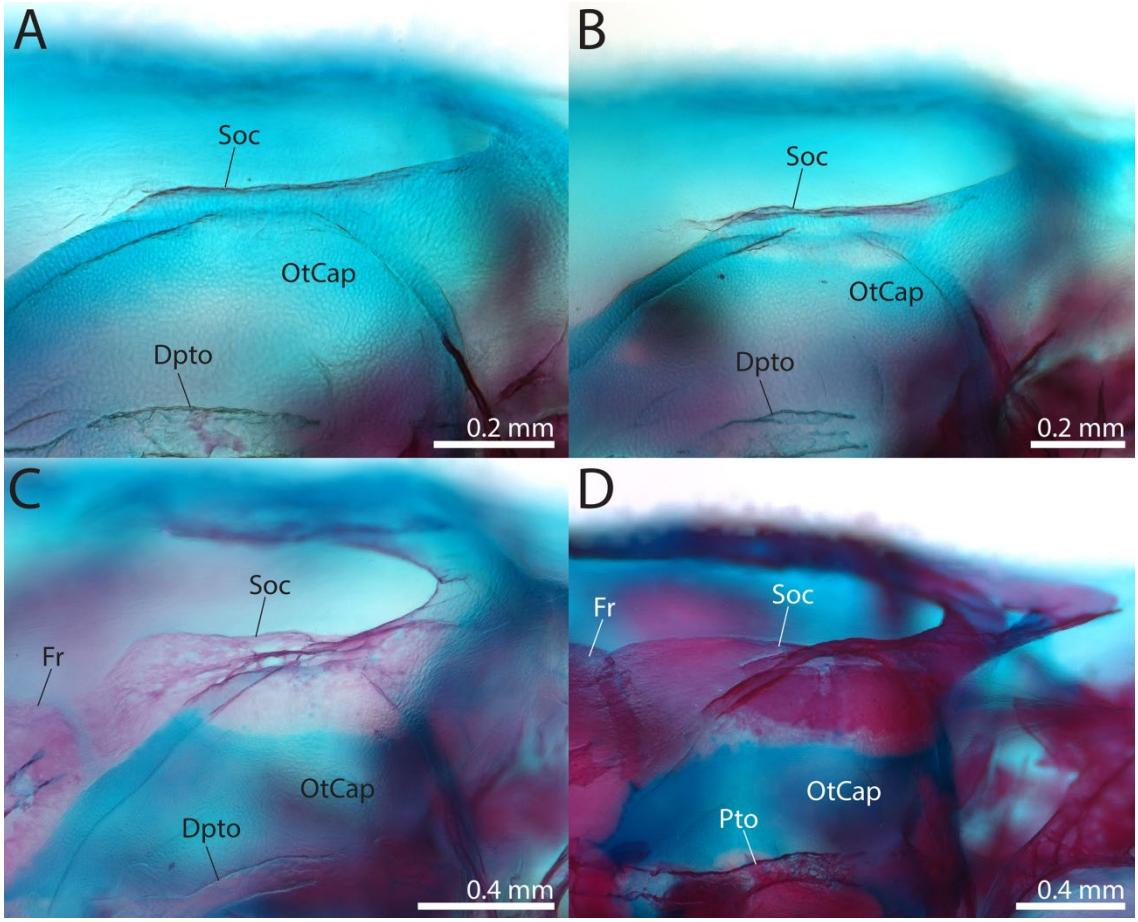

Figure 2.14. Ontogeny of the supraoccipital of *Ictalurus punctatus*. (**A**) 12.7 mm SL. (**B**) 13.2 mm SL. (**C**) 14.1 mm SL. (**D**) 15.4 mm SL. Dpto, Dermopterotic; Fr, Frontal; mm, Millimeters; OtCap, Otic capsule; Pto, Pterotic; Soc, Supraoccipital; SL, standard length.

posterior border of the cranial fontanelle (14.1 mm SL, Fig. 2.14C). The anterior extensions of this now median ossification widen and continue to expand anteriorly until they meet and suture with the paired frontal, at which point the bone resembles the adult condition (15.4 mm SL, Fig. 2.14D). Given that this element arises through endochondral ossification of the otic capsule, it is interpreted herein to represent a highly

modified supraoccipital. The parietals are interpreted to be absent. The absence of a separate parietal that fuses with the supraoccipital ontogenetically has also been noted in studies of the Clariidae (Adriaens & Verraes, 1998), Callichthyidae (Huysentruyt, et al., 2011) Heteropneustidae (Srinivasachar, 1958), and Loricariidae (Geerinckx, Brunain, & Adriaens, 2007). The origin of the chondral supraoccipital as a paired ossification is consistent with what has been reported in *Ariopsis felis* (Bamford, 1948) and *Ancistrus* cf. *triradiatus* (Geerinckx, Brunain, & Adriaens, 2007), which appears to be a mode of development unique to catfishes. Based on his descriptions and accompanying illustrations, the element Bamford interprets as the post-parietal most likely represents the perichondral ossification of the supraoccipital, implying a fusion of only two elements, the parietal and supraoccipital, rather than three as was originally reported. However, it should be mentioned that only a single center of ossification was reported in *Heteropneustes fossilis* (Srinivasachar, 1958) and *Corydoras paleatus* (Huysentruyt, et al., 2011) suggesting that the way in which this bone develops may vary across catfishes.

Posttemporo-supracleithrum

Unlike other teleosts which typically possess three main dermal components of the pectoral girdle (cleithrum, supracleithrum, and posttemporal), siluriformes only possess two major dermal bones in the pectoral-girdle elements, the cleithrum and an upper element which shares characteristics of both the supracleithrum and the posttemporal. As a result, the homology of this element has been contested and three hypotheses regarding the homology of this element have been proposed: (1) the supracleithrum is lost and the posttemporal contacts the cleithrum (Kindred, 1919;

Alexander, 1965); (2) the posttemporal is lost and the supracleithrum is modified and now contacts the skull (Taylor, 1969); and (3) the bone is a compound element resulting from the fusion of the posttemporal and supracleithrum (Fink & Fink, 1981). The latter hypothesis of ontogenetic fusion was originally proposed by Fink and Fink (1981), because the element in question possesses characteristics of both the supracleithrum (Baudelot's ligament, which typically inserts on the supracleithrum in other teleosts, inserts on this element) and posttemporal (a distinct dorsal arm that connects the pectoral-girdle to the back of the cranium, which is typically present on the posttemporal in other teleosts). Additionally, they also noted that there was a general lack of ontogenetic material available for study that could provide further insight on this homology problem. In the two species of ictalurids examined herein, the upper element of the pectoral-girdle originates from a single ossification that forms lateral to the dorsal tip of the cleithrum and no evidence of fusion during the ontogeny of this element was observed (Fig. 2.11). This corroborates what has previously been observed in the development of *Clarias gariepinnus* (Adriaens & Verraes, 1998) and *Ancistrus* cf. *triradiatus* (Geerinckx, Brunain, & Adriaens, 2007), and supports the hypothesis that one of the elements of the upper pectoral-girdle is lost. Given that Baudelot's ligament only attaches to the supracleithrum in most other otophysans and teleosts (Fink & Fink, 1981), the upper element of the pectoral-girdle in ictalurids likely represents a modified supracleithrum that has become expanded anterodorsally to occupy the typical location of the posttemporal.

Scapulocoracoid

The single endoskeletal element in the pectoral-girdle of catfishes has been assumed to represent the product of ontogenetic fusion between three endochondral ossifications, including the coracoid, scapula and mesocoracoid. This is based primarily on a comparison of the adult skeleton of catfishes with other teleosts in which the coracoid, scapula, and mesocoracoid are three separate bones (Stark, 1930; Alexander, 1966). Based on a small developmental series of *Ictalurus punctatus*, Arratia (2003b) observed only a single ossification within the scapulocoracoid cartilage, though in the supporting figure this ossification was shown to cover much of the scapulocoracoid cartilage. As reported by Arratia (2003b), in the material studied herein the scapulocoracoid originates from a single center of ossification within the scapulocoracoid cartilage. Ossification starts around the ventral arm of scapulocoracoid cartilage, which corresponds to the typical location of the coracoid in other teleosts. The ossification proceeds to spread posterodorsally to surround the portion of the scapulocoracoid in which the scapula typically ossifies, adjacent to the foramen for the passage of a branch of the pterygial nerve. A separate mesocoracoid is absent in both of the species of ictalurids examined herein and instead the 'mesocoracoid' arch forms from two separate extensions, one dorsal and one ventral, which meet and fuse. Based on the location of the initial center of ossification, the coracoid is the only ossification that could be confirmed to be present. Due to the relatively rapid ossification of the scapulocoracoid cartilage and only a small number of specimens available during this

ossification, the presence of the scapula cannot be ruled out without the examination of additional individuals. The mesocoracoid is absent as a separate ossification.

Urohyal

The urohyal of catfishes (parurohyal of Arratia & Schultze, 1990) has been shown in loricarioid catfishes to be a compound element of the tendon ossification of a typical urohyal and an ossification of the anterior basibranchial copula cartilage (Arratia & Schultz, 1990; Geerinckx, Brunain & Adriaens, 2007). In siluroid catfishes, this element has been described as articulating with the anterior tip of the basibranchial cartilage and fusion between these elements has been proposed in these taxa based on the observation of 'chondroid bone' fused to the dorsal portion of the urohyal in skeletonized material of adult individuals of *Ictalurus* (Arratia & Schultz, 1990). In the developmental series examined herein, the urohyal forms a close articulation with the anterior tip of the anterior basibranchial copula; however, no ossification or subsequent fusion between the two elements was observed. This could be due to the fusion occurring later in development as suggested by Arratia and Schultz (1990) or it is possible that variation exists within the development of the urohyal across catfishes and that in ictalurids the urohyal is not a compound element.

Lacrimal

The infraorbital elements of catfishes are greatly reduced, represented by simple tube-like ossifications around the infraorbital sensory canal except for the anteriormost infraorbital element (lacrimal), which exhbits a laminar portion that underlies the canal ossification. As a result, some studies have proposed that the anteriormost infraorbital is

the result of a fusion between the lacrimal and the antorbital, which is generally considered to be absent in siluriforms (de Pinna, Reis, & Britski, 2020). The development of the anteriormost infraorbital in *Ictalurus punctatus* (Fig. 2.5) and *Noturus gyrinus* shows only a single bone is present which gives rise to both the canal and laminar ossification of the element. Based on this information, I consider the anteriormost infraorbital element to be homologous to the lacrimal of other teleosts, and consider the antorbital to be absent.

Comparison of Skeletal Development with other Otophysans

The relative timing of appearance for bony skeletal elements varied between *Ictalurus punctatus* and the three non-siluriform otophysans. Most of this variation was restricted to only slight shifts in the relative position of skeletal elements in either regional sequences or the entire sequence. However, several major differences were observed between the ossification sequence compiled for *I. punctatus* and those for all three non-siluriform otophysan species, several of which were consistent across all three comparisons. In the neurocranium, elements associated with the cephalic lateral line sensory canals (e.g., nasal, dermopterotic, and extrascapular) all appear much earlier in the development of *I. punctatus*. This also applies to infraorbital 1, another element associated with the cephalic lateral line sensory system, which is one of the first elements to appear in *I. punctatus* but does not make an appearance until much later in development in the three other species of otophysan. The hyomandibular and endopterygoid also appear later in the sequence of ossification of *I. punctatus*. It should be noted that the homology of the element identified as the endopterygoid in catfishes

also has been previously debated (Arratia, 1992) and development of the element identified as the endopterygoid differs markedly between siluriforms and non-siluriform otophysans. In cypriniforms (Arratia, 1992; Cubbage & Mabee, 1996; Conway, Kubicek, & Britz, 2017) and characiforms (Arratia, 1992; Mattox, Britz, & Toledo-Piza, 2014) the endopterygoid is a dermal bone that forms along the dorsomedial edge of the palatoquadrate cartilage between the pars autopalatina and the pars metapterygoidea. In catfishes, the endopterygoid ossifies within a ligament connecting the pars metapterygoidea to the pars autopalatina, which is separate from the rest of the palatoquadrate. Given that the element is still located medial to the palatoquadrate between the metapterygoid and autopalatine I consider these elements to be homologous herein.

In the post-cranial skeleton, the pectoral-fin rays, ventral procurrent caudal-fin rays, and the parapophyses all appear very early in the sequence of ossification compiled for *Ictalurus* compared to the three non-siluriform otophysans. Of particular interest is the much earlier appearance of the pectoral-fin rays in the two ictalurids, which are the 21st or the 11th bone to appear in the sequence of *I. punctatus* and *Noturus gyrinus*, respectively, versus the 100th to 125th element to ossify in the three non-siluriform otophysans. The anteriormost pectoral-fin ray of most catfishes is modified into a robust lockable spine that exhibits a remarkable amount of morphological variation (e.g., Reed, 1924; Vanscoy, Lundberg, & Luckenbill, 2015; Kubicek, Britz, & Conway, 2019). A similar shift is observed in the dorsal-fin rays, in which the two anteriormost fin-rays are

modified into spines as well, when compared to the two cyprininforms, but not in comparison to the characiform *Salminus brasiliensis*.

Although the aforementioned differences in the appearance of ossifications were consistently observed in comparisons between *Ictalurus punctatus* and the three non-siluriform otophysans, it is not possible to tell if these consistent patterns are due to chance, as variation exists throughout the entire ossification sequence of these taxa, or if these differences in the timing of appearance of these elements could be a derived characteristic of ictalurids or even siluriformes. In other groups of vertebrates (e.g., amphibians, squamates, birds, and mammals; Harrington, Harrison, & Sheil, 2013; Werneburg, & Sánchez-Villagra, 2015; Carril, & Tambussi, 2017; Sánchez-Villagra et al., 2008), shifts in the relative timing of developmental events, or sequence heterochrony, has been shown to be connected with major changes in morphology, life-history and function (e.g., the earlier development of the cranial and forelimb skeleton in marsupial vs. placental mammals; ; Goswami, Weisbecker, & Sánchez-Villagra, 2009; Keyte & Smith, 2010). Given that certain elements, like the pectoral-fin spine, appear to be significantly shifted in the development of catfishes, an examination of sequence heterochrony between siluriforms and non-siluriform otophysans could help to clarify if these elements vary in their relative position due to random chance or if the early appearance of these elements is the product of heterochrony (See Chapter IV).

Conclusion

This study is the first to document skeletogenesis throughout the entire skeleton for a representative of the order Siluriformes, and it introduces two novel sequences of

ossification for the order. No major differences were observed in the sequences of the two species (*Ictalurus punctatus* and *Noturus gyrinus*) examined herein. In ictalurids, all five of the bones that have previously been proposed to represent compound elements resulting from the result of ontogenetic fusion of elements that are typically separate in other teleosts are shown to develop from only a single *anlage*. It should be mentioned that in some instances (e.g., urohyal, supraoccipital; Bamford, 1948; Geerinckx, Brunain & Adriaens, 2007) evidence or accounts exist which may suggest that ontogenetic fusion in these elements is variable among catfishes. As a result, developmental studies of additional catfishes are needed to fully understand what variation, if any, exists in the development of these highly-modified skeletal elements and whether or not this variation may represent novel morphological information to be used in systematic studies of the order. Several differences were observed when the sequence of *I. punctatus* was compared to those available for other otophysan fishes. This includes the earlier appearance of the dermopterotic, extrascapular, lacrimal, nasal, parapophyses, and pectoral-fin rays and the later ossification of the endopterygoid and hyomandibular in *I. punctatus* compared to the other otophysans. Whether or not the early or late appearance of these elements is widespread across siluriforms, or are characteristic only of ictalurids, remains uncertain without additional data on skeletogenesis in other catfishes. A future study of sequence heterochrony could reveal whether these differences in the relative timing of initial ossification are due to random variation or if they are representative of ictalurids, or even the order Siluriformes.

CHAPTER III

ONTOGENY OF THE CATFISH PECTORAL-FIN SPINE (TELEOSTEI: SILURIFORMES)*

Introduction

The order Siluriformes (catfishes) is a diverse (3,873 species/~43 families; Nelson, Grande, & Wilson, 2016; Eschmeyer and Fong, 2018) and globally distributed group of vertebrates with extant representatives in fresh and shallow coastal waters on all continents, excluding Antarctica, from where only fossilized remains are known (Grande and Eastman, 1986). As a group, catfishes vary greatly in body shape and size, with maximum lengths ranging from as large as 3 meters in *Silurus glanis* (Copp et al., 2009) to less than 2cm (e.g., Friel and Lundberg, 1996; Schaefer, Provenzano, Pinna, & Baskin, 2005). Several skeletal synapomorphies characterize this group, including the modification of the anteriormost pectoral-fin ray into a robust, lockable spine (Fink and Fink, 1981; Fig. 3.1). Morphology of the spinous pectoral-fin ray varies significantly across the order (Fig. 3.2) with some species sporting large saw-like projections along the anterior and/or posterior edge of the spine (Fig. 3.2C,D,H,I), some with smooth, blade-like spines (Fig. 3.2B,F) and others with cylindrical spines that are covered with odontodes (Fig. 3.2K,L), tooth-like structures composed of dentine with an enamel cap (Peyer 1922; Reed, 1924; Alexander, 1966; Ørvig, 1967; Sire & Huysseune, 1996;

---

* Reprinted with permission from "Ontogeny of the Catfish Pectoral-fin Spine (Teleostei: Siluriformes)" by Kubicek, K. M., Britz, R. and Conway, K. W. 2019. *Journal of Morphology*, 280, 339–359, 2019 Wiley Periodicals, Inc.

Arratia, 2003; Vanscoy, Lundberg, & Luckenbill, 2015). In some groups, such as the highly rheophilic sisorids and amphiliids, the anteriormost pectoral-fin ray has been

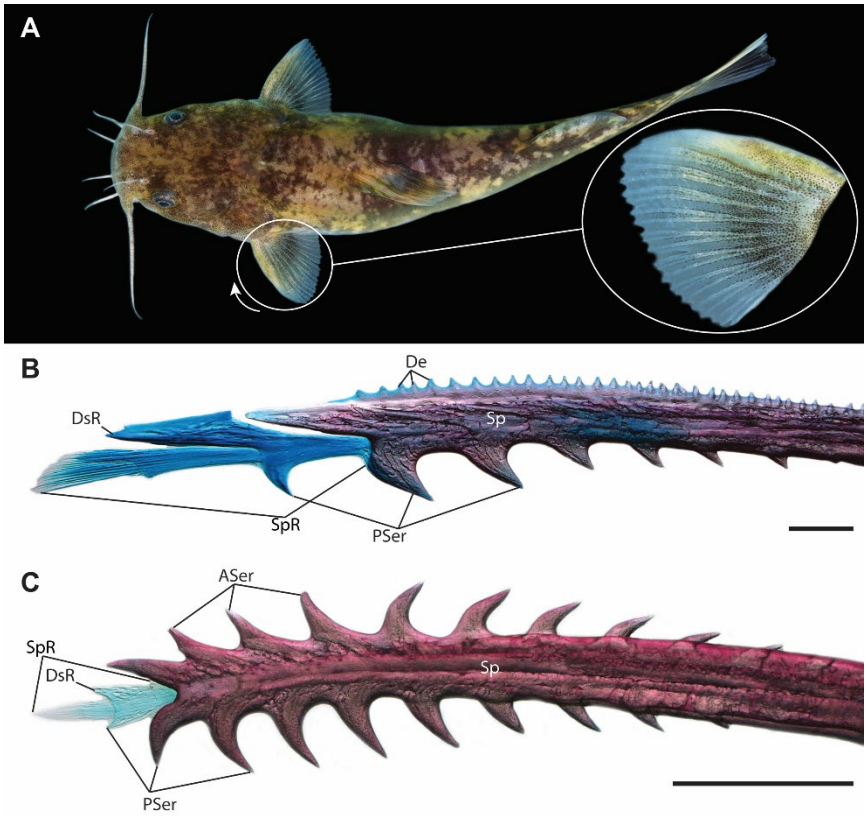

Figure 3.1. Pectoral-fin spine of Catfishes. (**A**)*Pylodictis olivaris*, pectoral fin with spines erected. Pectoral-fin spines of (**B**) *Ictalurus punctatus*, TCWC 19757.01, and (**C**) *Pseudobunocephalus lundbergi*, ANSP 168810, exhibiting the different types of ornamentation. Scale bars equal to 1 mm. Abbreviations: ASer; anterior serra; De, denticulus; DsR, distal ramus; PSer, posterior serra; Sp, spine proper; SpR, spurious ray. Reprinted from Kubicek, Britz & Conway, 2019.

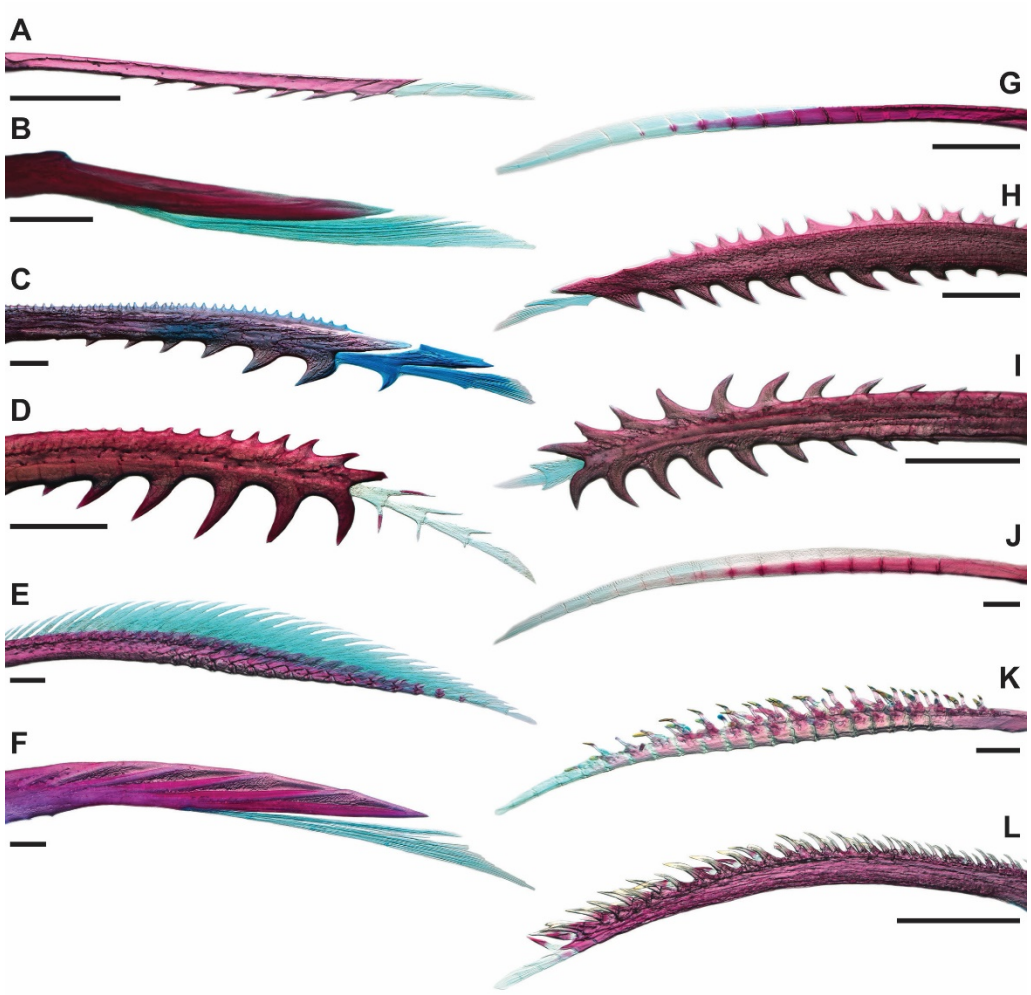

Figure 3.2. Morphological diversity of pectoral-fin spines in adult Siluriformes. Images were taken in a dorsal view with the anterior edge towards the top and distal edge towards the center of the page. (**A)** *Parailia pellucida*, Schilbeidae (USNM 229794, 30.3 mm SL). (**B**) *Akysis vespa*, Akysidae (TCWC 19739.01, 36.5 mm SL). (**C**) *Ictalurus punctatus*, Ictaluridae (TCWC 19757.01, 31.3 mm SL). (**D**) *Pseudolaguvia kapuri*, Erethistidae (CAS 50294, 25.1 mm SL). (**E**) *Amphilius uranoscopus*, Amphiliidae (CU 93740, 41.8 mm SL). (**F**) *Noturus gyrinus*, Ictaluridae (TCWC 19758.01, 36.6 mm SL). (**G**) *Helogenes marmoratus*, Cetopsidae (ANSP 177185, 31.87 mm SL). (**H**) *Pimelodus pictus*, Pimelodidae (TCWC 19761.01, 33.09 mm SL). (**I**) *Pseudobunocephalus lundbergi*, Aspredinidae (ANSP 168810, 24.73 mm SL). (**J**) *Henonemus* sp., Trichomycteridae (TCWC 13989.19, 69.7 mm SL). (**K**) *Astroblepus* sp., Astroblepidae (CU 78811, 32.2 mm SL). (**L**) *Ancistrus* sp., Loricariidae (TCWC 19759.01, 16.5 mm SL). Scale bars equal to 1 mm. Note the absence of ornamentation in F, G and J. Reprinted from Kubicek, Britz & Conway, 2019.

modified to form a flat and highly flexible structure that is heavily pinnate and provides support to a thick, keratinized skin pad (Fig 2E; Hora, 1922; Annandale, 1923; Conway, Lujan, Lundberg, Mayden, & Siegel 2012) and in others, such as the trichomycterids, malapterurids and the monotypic Kryptoglanidae, has even been reduced to a state resembling that of a more typical fin ray (Fig. 3.2J; Britz, Kakkassery, & Raghavan, 2014; Lundberg, Luckenbill, Babu and Ng, 2014; Vanscoy et al., 2015). Additionally, an association between the pectoral-fin spine and toxin producing cells is common and may have evolved independently multiple times within the order (Wright, 2009). Numerous studies have focused on different aspects of pectoral-fin spine morphology and function in adult stages of catfishes, including investigation of the spine locking mechanism (Fine et al., 1997) and the involvement of the spine in the production of sound (e.g., Fine et al., 1996; Kaatz, Stewart, Rice, & Lobel, 2010).

Given this complexity and variation, the utility of the pectoral-fin spine in systematic investigations has long been recognized. Typically this has involved the use of pectoral-fin spine characters for species diagnosis in studies of both extant (e.g., Ng and Kottelat, 1998; Ng and Tan, 1999; Thomas and Burr, 2004; Rocha, Oliveira, & Py-Daniel, 2008; Carvalho and Reis, 2009; Rodiles-Hernández, Lundberg, & Sullivan 2010) and extinct taxa (e.g., Hubbs and Hibbard, 1951; Lundberg & Case, 1970; Grande & Lundberg, 1988; Pinton, Fara, & Otero 2006), but apomorphic characters of pectoral-fin spine anatomy have also been used as evidence to support monophyletic groups of catfishes (e.g., Schaefer, 1991, Ng, 2015; Vanscoy et al., 2015). Despite this previous use of morphological characters of the pectoral-fin spine in systematic studies, the

usefulness of such characters has been undermined by an inconsistent application of terminology. Terms such as dentations, serrations and denticulations have been used interchangeably in reference to ornamentations on either the anterior or posterior margin of the spine in different species (e.g., Hubbs and Hibbard, 1951; Arratia, 2003; Thomas and Burr, 2004), or in some cases the same species (e.g. *Ictalurus punctatus*; Fine et al., 1997; Egge and Simons, 2011), and without consideration of the homology of such ornamentation. Vanscoy et al. (2015) recognized these issues and made the first attempt at standardizing the terminology in order to facilitate the usage of pectoral-fin spine morphological characters in systematic studies; however, they used a single term only, dentations, to identify two clearly different defined types of ornamentation (posterior dentations that form as part of the individual lepidotrichial segments and anterior dentations that form independent of these segments.

Most previous studies of catfish pectoral-fin spine morphology have focused largely on the adult anatomy, and only a handful of studies have provided ontogenetic information for this unique character complex (Peyer, 1922; Reed, 1924; Grande & Shardo, 2002; Arratia, 2003; Vanscoy et al., 2015). Peyer (1922) was the first to study ontogenetic changes of the pectoral-fin spine from juveniles to adults in *Silurus* and reported spine growth to be the result of the addition of new segments to the tip of the spine. In the same study, he examined the diversity of fin spines in 19 families of catfishes and confirmed Hertwig's (1876) observation that most loricarioids have tooth-like structures, now called odontodes, on their spines and body and that other spine extensions in many other catfishes (i.e. serrae and denticuli, as described below) are not

tooth-like elements but just projections of bone. Reed (1924), based on the examination of histological sections and oil cleared specimens, hypothesized that the pectoral-fin spine was a highly modified, dichotomously branching (i.e. branching in a bilaterally symmetrical pattern), segmented fin-ray. He, like Peyer (1922), concluded that formation of the spine occurred through the successive fusion of fin-ray segments into a single structure, the spine proper. Reed (1924) termed the flexible, segmented portion of the fin ray, located distal to the tip of the spine proper, the spurious ray (Fig. 3.1B,C). Arratia (2003) came to the same conclusion as Reed (1924); however, disagreed with his assessment of the spurious ray as possessing the same structure and segmentation as a typical fin ray. Arratia (2003: pg. 135-137) instead hypothesized that the spurious ray is formed from a connective tissue that stains with Alcian Blue, which would imply that the pectoral-fin spine develops from a tissue possessing high levels of mucopolysaccharides (Scott and Dorling, 1965) and not from typical dermal bone. These previous ontogenetic studies were also limited in the taxa examined, utilizing only siluroid catfishes and primarily focusing on the family Ictaluridae. As a result, our knowledge on development of the pectoral-fin spine across catfishes is limited and there is no information currently available on the development of the pectoral-fin spine in loricarioids, which comprise 40% (1,576 species) of all known catfishes (Eschmeyer and Fong, 2018). Given the remarkable diversity of pectoral-fin spines across catfishes, a better understanding of development would greatly aid systematic research and potentially provide novel insight into the evolution of this unique structure.

In order to determine whether the morphologically diverse pectoral-fin spine in different groups of catfishes results from a similar ontogenetic pathway I document the development of the pectoral-fin spine in four siluroid (*Ictalurus punctatus*, *Noturus gyrinus*, *Silurus glanis* and *Akysis vespa*) and two loricarioid catfishes (*Corydoras panda* and *Ancistrus* sp.). The major goals of my study are to resolve the issues of homology associated with the components of the spurious ray, standardize the terminology of the pectoral-fin spine morphology based on homology and identify which differences, if any, exist in the early formation of the pectoral-fin spine across catfishes. I accomplish this via examining ontogenetic series of the aforementioned four taxa as well as juvenile and adult specimens of species representing 41 of the currently recognized 43 families.

Materials and Methods

Ontogenetic Series

Small groups (N = 3–6 adult individuals) of select species of catfishes were obtained via either field collection (*Noturus gyrinus*) or through the aquarium trade (*Akysis vespa*, *Corydoras panda*, and *Ancistrus* sp.) and maintained in 40 L aquaria (pH 7.5–8.0; temperature 26°C ± 1°C). Upon spawning, eggs were collected and incubated until hatching at which point they were transferred to 20 L aquaria where they were raised until sampling. Eggs were treated with Paraguard (Seachem Laboratories, Madison, GA) to prevent fungus. Larval fishes were fed a mixture of decapsulated brine shrimp eggs, crushed blackworm pellets, *Artemia* nauplii and microworms. Individuals were sampled daily from 5 days pre-hatch up to 30 days post-hatch (dph) and every third day from 30 dph to 60 dph when possible. Once collected, specimens were euthanized

with an overdose of tricaine methanosulfonate (MS222) and subsequently fixed in a solution of 10% buffered paraformaldehyde for 24 hours. After fixation, individuals were transferred to a 70% solution of EtOH for final storage. Eggs of *Ictalurus punctatus* also were obtained from the Texas A&M Aquatic Research and Teaching Facility. Embryos and larvae were sampled as above. A developmental series of *Silurus glanis* as well as smaller series (n= 2–5) of species representing 41 families of catfishes were compiled opportunistically from material housed in museum collections. All aspects of the research undertaken are in compliance with the protocol approved by the Texas A&M Institutional Animal Care and Use Committee (AUP: IACUC 2017-0047).

Gross and Histological Examination

Specimens were cleared and doubled stained (C&S) for bone and cartilage following Taylor and Van Dyke (1985) and examined using a ZEISS SteReo Discovery V20 stereomicroscope (Carl Zeiss Inc., Thornwood, NY). Select C&S specimens were photographed using a Zeiss Axiocam MRc5 digital camera attached to the aforementioned microscope. Whole pectoral fins also were removed from a number of specimens and prepared for serial sectioning. In the case of larger individuals, a smaller portion of the pectoral fin or just the pectoral-fin spine was removed. Dissected pectoral fins and spines were rinsed for 1 h in DI water, decalcified in RDO-GOLD (Apex Engineering Products Corp., Aurora, IL) for 7 h, rinsed for 1 h in DI water, and dehydrated through a graded series of EtOH (30%, 50%, 70% and 95%, for 1 h each, 100%, two cycles for 30 min each). Specimens were then cleared in Toluene (two cycles for 20 min each) and subsequently embedded in paraffin blocks. Sagittal sections, 9 µm

thick, were cut and affixed to albumenized slides. Slides were stained with Hall-Brunt Quadruple (HBQ) stain (following Hall, 1986). Slides were examined using a Zeiss Primo Star compound microscope. Select specimens were photographed using a Zeiss Axiocam MRc5 digital camera attached to the aforementioned microscope. All images were improved for print reproduction using Adobe Photoshop CS5.1 and Illustrator CS5.1 (Adobe Inc., San Jose, CA).

Terminology for components of the pectoral-fin spine is as follows (Fig. 3.1B,C): I use the term spurious ray as defined by Reed (1924). Serra (equivalent to posterior dentation of Vanscoy et al. 2015) is a pointed extension that forms at the posterior margin of each hemitrichial segment, initially bilaterally paired, dorsal and ventral halves of the serra fuse subsequently. When several lepidotrichial segments each with a single serra have fused into the spine proper, the spine carries several serrae, which together form a posterior serration. In this case the spine is called posteriorly serrate. The distal ramus is an anterodistally developed process on each hemitrichial segment (equivalent to anterior projections/branches of Vanscoy et al., 2015), with dorsal and ventral halves of the distal ramus fusing in subsequent development. If the tip of the distal ramus extends beyond the margin of the spine and forms a recurved process, I refer to this as an anterior serra (see anterior distal serrae of Vanscoy et al., 2015). When several anterior serrae bearing segments have fused to the spine proper, the spine possesses an anterior serration or is anteriorly serrate. Denticuli (equivalent to anterior dentations of Vanscoy et al., 2015) are short pointed processes at the anterior or posterior margin of the spine, which may or may not be regularly spaced and form on the

shaft of the spine proper after lepidotrichial segments have fused to it. I refer to the spine as denticulate or as having a denticulation.

Materials Examined

The following specimens, listed alphabetically by family, genus and species were examined during the course of this study. For each species, the collection numbers along with the total number of individuals from each lot examined and the size range of those specimens are listed. Individuals examined are whole mount C&S unless otherwise denoted. Museum Abbreviations: AMNH, American Museum of Natural History, New York; ANSP, Academy of Natural Sciences, Philadelphia; BMNH, Natural History Museum, London; CAS/CAS-SU, California Academy of Sciences, San Francisco; CU, Cornell University, Ichthyology Collection, Ithaca; FMNH, Field Museum of Natural History, Chicago; LACM, Natural History Museum of Los Angeles County, Los Angeles; MZUSP, Museu de Zoologia da Universidade de São Paulo, São Paulo; TCWC, Biodiversity Research and Teaching Collections, College Station; UMMZ, University of Michigan Museum of Zoology, Ann Arbor; USNM, Smithsonian Institution National Museum of Natural History, Washington D.C.

Ailiidae: *Ailia coila*, UMMZ 208353, 1 examined (ex.), 91.6 mm SL; UMMZ 208442, 4 ex., 79.5-123.7 mm SL. — Akysidae: *Akysis vespa*, TCWC 19739.01, 8 ex., 3.5-41.6 mm NL/SL; TCWC 19739.02, 1 pectoral fin sectioned (pect.), 34.0 mm SL. — Amblycipitidae: *Amblyceps cerinum*, UMMZ 248835, 2 ex., 67.4-74.1 mm SL; *Amblyceps mangois*, UMMZ 244866, 2 ex., 36.5-37.8 mm SL; *Amblyceps* sp., ANSP 178675, 1 ex., 53.3 mm SL; *Liobagrus somjinensis,* TCWC uncat., 1 ex., 42.8 mm SL.

— Amphiliidae: *Amphilius uranoscopus*, CU 93740, 2 ex., 41.8-55.8 mm SL; CU 95213, 1 ex., 41.7 mm SL. — Anchariidae: *Ancharius fuscus*, AMNH 93702, 1 ex., 88.4 mm SL. — Ariidae: *Ariopsis felis*, TCWC 19690.02, 2 ex. (dissected pectoral fins only), 61.8-80.7 mm SL; *Arius jordani*, TCWC 19740.01, 2 ex., 50.0-51.1 mm SL; *Bagre marinus*, TCWC 547.07, 1 ex., 79.7 mm SL; TCWC 19690.03, 3 ex. (dissected pectoral fins only), 98.9-118.6 mm SL. — Aspredinidae: *Bunocephalus* sp., TCWC 19741.01, 2 ex., 33.8-43.4 mm SL; *Pseudobunocephalus lundbergi*, ANSP 168810, 5 ex., 20.1-22.7 mm SL. — Astroblepidae: *Astroblepus* sp., CU 78735, 2 ex., 32.1-54.4 mm SL; CU 78811, 2 ex., 27.8-30.0 mm SL. — Auchenipteridae: *Tatia intermedia*, TCWC 19752.01, 4 ex., 37.6-60.8 mm SL; *Trachycorystes* sp., FMNH 85945, 3 ex. , 55.7-65.8 mm SL. — Auchenoglanididae: *Auchenoglanis occidentalis*, CU 90478, 2 ex., 26.4-35.8 mm SL. — Austroglanididae: *Austroglanis gilli*, ANSP 177966, 1 ex., 71.8 mm SL. — Bagridae: *Pseudomystus siamensis*, CAS 94782, 5 ex., 35.5-58.0 mm SL. — Callicthyidae: *Corydoras panda*, TCWC 19753.01, 6 ex., 8.7-18.9 mm SL; TCWC 19753.02, 2 pect., 18.5-19.5 mm SL. — Cetopsidae: *Cetopsis coecutiens*, FMNH 97324, 1 ex. (pectoral fin dissected), 198.0 mm SL; FMNH 100000, 1 ex. (pectoral fin dissected), 119.0 mm SL; *Helogenes marmoratus*, ANSP 175833, 1 ex., 50.7 mm SL; ANSP 177185, 4 ex., 30.9-36.7 mm SL. — Chacidae: *Chaca chaca*, UMMZ 208728, 1 ex., 156.0 mm SL. — Clariidae: *Clarias batrachus*, UMMZ 217578, 3 ex., 99.7-105.2 mm SL; *Clarias gariepinus* TCWC 15276.09, 2 ex., 62.5-71.3 mm SL. — Claroteidae: *Chrysichthys mabusi*, CU 91692, 2 ex., 58.0-80.7 mm SL. — Cranoglanididae: *Cranoglanis bouderius*, CAS-SU 69758, 1 ex., 97.0 mm SL. — Diplomystidae: *Diplomystes*

chilensis, AMNH 55327, 1 ex., 64.4 mm SL; CAS 13706, 1 ex., 144.5 mm SL; *Diplomystes papillosus*, CAS 81539, 1 ex., 118.0 mm SL. — Doradidae: *Ossanocora punctata*, TCWC 16723.16, 2 ex., 34.9-51.8 mm SL; *Platydoras armatulus*, TCWC 19754.01, 1 ex., , 45.1 mm SL. — Erethistidae: *Pseudolaguvia kapuri*, CAS 50294, 4 ex., 23.4-26.6 mm SL. — Heptateridae: *Goeldiella eques*, ANSP 177187, 2 ex., 99.2-104.5 mm SL. — Heteropneustidae: *Heteropneustes fossilis*, CAS 29627, 2 ex., 122.3-123.2 mm SL. — Horabagridae: *Horabagrus brachysoma*, TCWC 19755.01, 2 ex., 53.2-56.1 mm SL. — Ictaluridae: *Ameirus melas* TCWC 15355.08, 1 ex., 66.0 mm SL; *Ictalurus furcatus* TCWC 19756.01, 4 ex., 64.9-70.8 mm SL; *Ictalurus punctatus*, TCWC 19757.01, 7 ex., 11.7-36.2 mm SL; *Noturus flavus* UAIC 14314.07, 1 ex., 73.4 mm SL; *Noturus gyrinus*, TCWC 15438.13, 1 ex., 41.5 mm SL; TCWC 19758.01, 6 ex., 8.6-36.6 mm SL; TCWC 19758.02, 2 pect., 72.5-78.0 mm SL; *Pylodictis olivaris* TCWC 7834.10, 1 ex., 61.1 mm SL. — Kryptoglanidae: *Kryptoglanis shajii*, BMNH uncat., 1 ex., 60.0 mm SL — Loricariidae: *Ancistrus* sp., TCWC 19759.01, 5 ex., 5.6-16.5 mm SL; *Hemipsilichthys vestigipinnis*, USNM 314657, 3 ex., 45.2-59.8 mm SL. — Malapteruridae: *Malapterurus oguensis*, CU 92271, 1 ex., 49.9 mm SL; CU 95140, 1 ex., 56.4 mm SL. — Mochokidae: *Microsynodontis* sp., TCWC 19760.01, 1 ex., 26.2 mm SL. — Nematogenyidae: *Nematogenys inermis*, UMMZ 212697, 1 ex. (pectoral fin dissected), 68.0 mm SL; USNM 84343, 1 ex., 25.8 mm SL. — Pangasiidae: *Pangasius macronema*, CAS 29360, 3 ex., 50.5-66.5 mm SL; UMMZ 214029, 2 ex., 103.9-104.7 mm SL. — Phreatobiidae: *Phreatobius sanguijuela* MZUSP 118607, 1 ex. (photograph only), 40.2 mm SL. — Pimelodidae: *Pimelodus ornatus*, LACM 41735.022; LACM

41740.015; *Pimelodus pictus*, TCWC 19761.01, 2 ex., 33.1-37.6 mm SL. — Plotosidae: *Plotosus lineatus*, FMNH 110269, 5 ex., 21.0-66.7 mm SL. — Pseudopimelodidae: *Microglanis poecilus*, AMNH 54973, 2 ex., 23.1-23.9 mm SL. — Ritidae: *Rita rita*, CAS-SU 34866, 1 ex., 85.0 mm SL. — Schilbeidae: *Parailia congica*, AMNH 246178, 2 ex., 60.5-60.8; *Parailia pellucida*, USNM 229794, 3 ex., 29.9-32.3 mm SL; *Schilbe intermedius* TCWC 15286.18, 3 ex., 57.6-72.7 mm SL. — Scoloplacidae: *Scoloplax empousa*, FMNH 108610, 5 ex., 12.8-19.1 mm SL. — Siluridae: *Silurus asotus*, ANSP 185139, 3 ex., 51.2-67.5 mm SL; *Silurus glanis,* BMNH 2005.7.5.944-1034, 4 ex., 17.2-85.0 mm SL; *Wallago attu*, CAS 92824, 2 ex., 69.2-71.0. — Sisoridae: *Glyptothorax sinensis*, UMMZ 246438, 1 ex., 60.7 mm SL; *Parachiloglanis hodgarti*, CAS50170; KU 29549; KU 40556. — Trichomycteridae: *Henonemus* sp., TCWC 13989.19, 1 ex., 69.7 mm SL; *Trichomycterus hasemani*, ANSP 175851, 3 ex., 13.2-13.9 mm SL.

Results

Development of the Pectoral-Fin Spine in Siluroid Catfishes

Ictalurus punctatus *(Ictaluridae)*

In the earliest stages of *Ictalurus punctatus* examined (11.3 mm SL, Fig. 3.3A), the anteriormost, or first pectoral-fin ray is twice the size of, but comparable in structure to, more posterior pectoral-fin rays. This anteriormost ray consists of two separate hemitrichia, one dorsal and one ventral, each with a mineralized proximal segment and a second segment forming distally. Each hemitrichium overlays bundles of actinotrichia which extend beyond the fin ray distally and fan out to form the anterodistal edge of the developing pectoral fin. The more anterior actinotrichia, those of the leading edge of the

first fin ray, are much shorter than those situated posteriorly, resulting in a distal edge that is uneven (Fig. 3.4A) and unlike the symmetrical edge seen in the actinotrichia bundles of the remaining pectoral-fin rays (Fig. 3.4B).

By 12.3 mm SL (Fig. 3.3B) the first pectoral-fin ray has begun to deviate from the remaining pectoral-fin rays in appearance. The line of demarcation between segments of the first ray, unlike that of other pectoral-fin rays, is not straight but curves distally towards the anterior edge of the ray (Fig. 3.4A). This results in an anterodistal extension, or distal ramus, of each lepidotrichial segment. A distal ramus is present in the first two segments at this stage of 12.3 mm and also marks the point of fusion across the anterior midline of the dorsal and ventral half of each lepidotrichial segment (Fig. 3.3C). The distal most tips of dorsal and ventral hemitrichial segments are the first to meet in the midline, with fusion continuing proximally from this point along each pair of hemitrichial segments.

By 13.5 mm SL (Fig. 3.3D), the proximalmost segment has completely fused across the anterior midline, forming the start of the spine proper. The second most proximal segment has almost completely fused to the spine proper at this stage. A lamina of bone extends from the anterior midline of the spine proper and retrorse extensions, or serrae, have developed along the posterior edge of the second and third segment. As with the distal ramus, these serrae correspond with the point of initial fusion between the hemitrichia of each segment, in this case across the posterior midline (Fig. 3.3E).

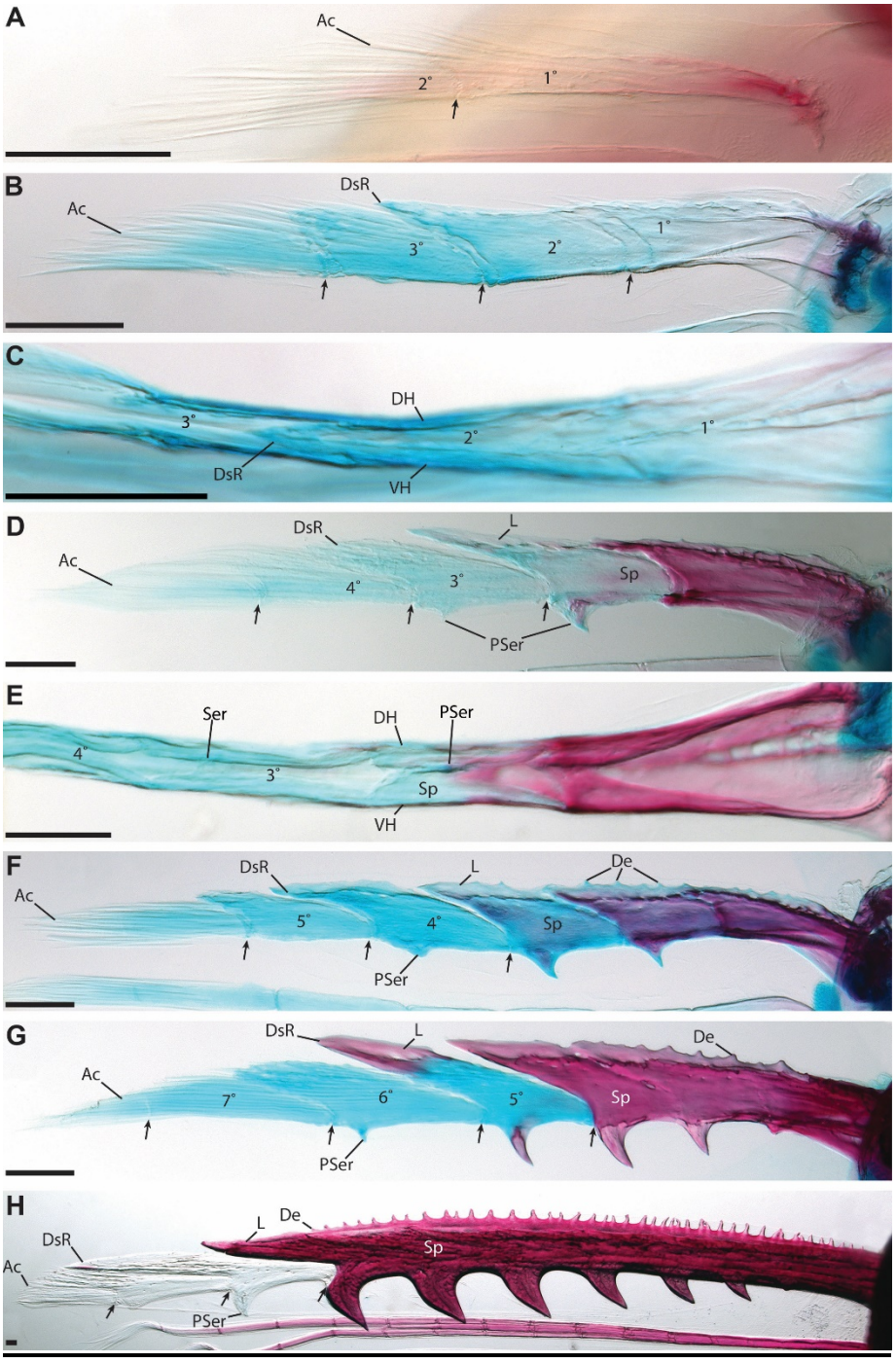

Figure 3.3. Ontogeny of the pectoral-fin spine of *Ictalurus punctatus* (TCWC 19757.01). (**A**) 11.7 mm SL. (**B**) 12.3 mm SL. (**C**) Anterior view of B showing fusion of hemitrichia at the distalmost tip of the distal ramus. (**D**) 13.5 mm SL. (**E**) Posterior view of D showing fusion of hemitrichia at the point of posterior serrations. (**F**) 14.1 mm SL. (**G**) 15.1 mm SL. (**H**) 36.2 mm SL. Arrows indicate segmentation. N° indicates segment number in stages where the total number of segments is known with 1° being the proximalmost. Scale bars equal to 0.2 mm. Abbreviations: Ac, actinotrichia bundle; De, denticulus; DH, dorsal hemitrichium; DsR, distal ramus; L, lamina of bone; PSer, posterior serra; Sp, spine proper; VH, ventral hemitrichium. Reprinted from Kubicek, Britz & Conway, 2019.

By 14.1 mm SL (Fig. 3.3F), fusion of the third segment to the spine proper (which consists of two fused segments at this point) is underway. The lamina of bone running along the anterior edge of the spine proper has attained a series of irregular saw-

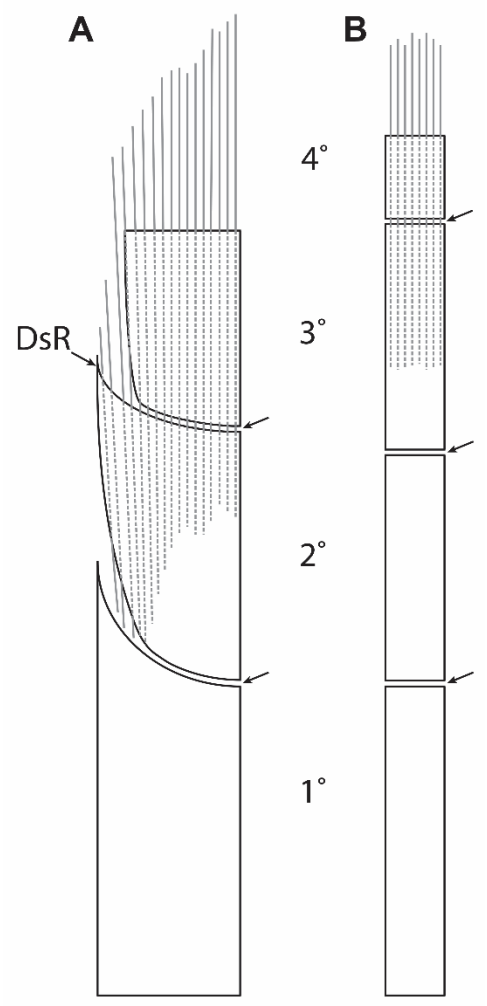

Figure 3.4. Diagrammatic and simplified representation of the developing first (**A**) and second (**B**) pectoral-fin rays of *Ictalurus punctatus* (anterior to left) illustrating differences in segmentation and fields of actinotrichia. Thin grey lines represent actinotrichia. Arrows indicate segmentation. N° indicates segment number with 1° being the proximalmost. Abbreviations: DsR, distal ramus. Reprinted from Kubicek, Britz & Conway, 2019.

like projections, or denticuli. These denticuli appear to be the result of either the addition of bone to or bone remodeling of the existing bone lamina.

At 15.1 mm SL (Fig. 3.3G), the fourth segment is almost completely fused to the three segments that form now the spine proper. The fifth segment, which is now the proximalmost segment of the spurious ray, is larger in size when compared to the previous four segments, primarily in the length of the distal ramus (ca. 63% of segment length vs. ca. 25% in the first segment to appear; 3B). This segment appears to have two centers of increased ossification, as evidenced by a much darker staining with Alizarin Red, one at the tip of the distal ramus and the other at the posterior serra. The previously formed posterior serrae of the fourth and third fused in segments have increased in size and become more recurved.

In a specimen of 36.2mm SL (Fig. 3.3H), the spine is similar to that of an adult. The serrae along the posterior edge have become much larger in size with the proximalmost serrae in the process of being resorbed/incorporated into the shaft of the spine. A full row of denticuli is present along the anterior edge of the spine proper excluding the area of the leading edge occupied by the distalmost fused segment. The segments under development (consistently three) in the spurious ray have increased in not only size but also asymmetry when compared to the earlier larval stages and no longer resemble segments of a typical fin ray.

Noturus gyrinus *(Ictaluridae)*

The development of the pectoral-fin spine in *Noturus gyrinus* is very similar to that described for *Ictalurus punctatus*. In the earliest stage examined (8.6 mm SL; Fig.

3.5A), the anteriormost, first, pectoral-fin ray is twice the width of the remaining pectoral-fin rays, and consists of two separate hemitrichia in which the distal ramus of the first segment is just starting to form.

By 9.9 mm SL (Fig. 3.5B) the first segment is complete including its distal ramus which accounts for over half (ca. 59%) of the length of the segment, rendering it comparatively longer than that of *I. punctatus* (ca. 25% of first segment length; 4B). Fusion across the anterior midline of the dorsal and ventral halves of the proximalmost segment is complete forming the spine proper and two additional segments are discernable with the development of the distal ramus underway in the second segment.

By 11.6 mm SL (Fig. 3.5C), the proximalmost segment is well ossified with a serra present on its posterodistal margin and ossification of the second segment has started distally. The distal ramus of the second segment is complete, and a thin lamina of bone extends off of the anterodistal midline of the segment, similar to the condition in *I. punctatus*.

By 13.1 mm SL (Fig. 3.5D) the second segment has become more heavily ossified distally but has yet to undergo fusion to the spine proper. The thickness of the spine proper has increased and the posterior edge of the distal ramus has gained a vertically extending dorsal and ventral ridge of bone.

By 19.8 mm SL (Fig. 3.5E), these aforementioned ridges of bone demarcate the posterior limit of each segment that has been added to the spine proper. Upon fusion, the thin lamina of bone present on the distal ramus thickens along its anterior margin and fills the gap between the posterior ridges of the fusing segment and the ridge along the

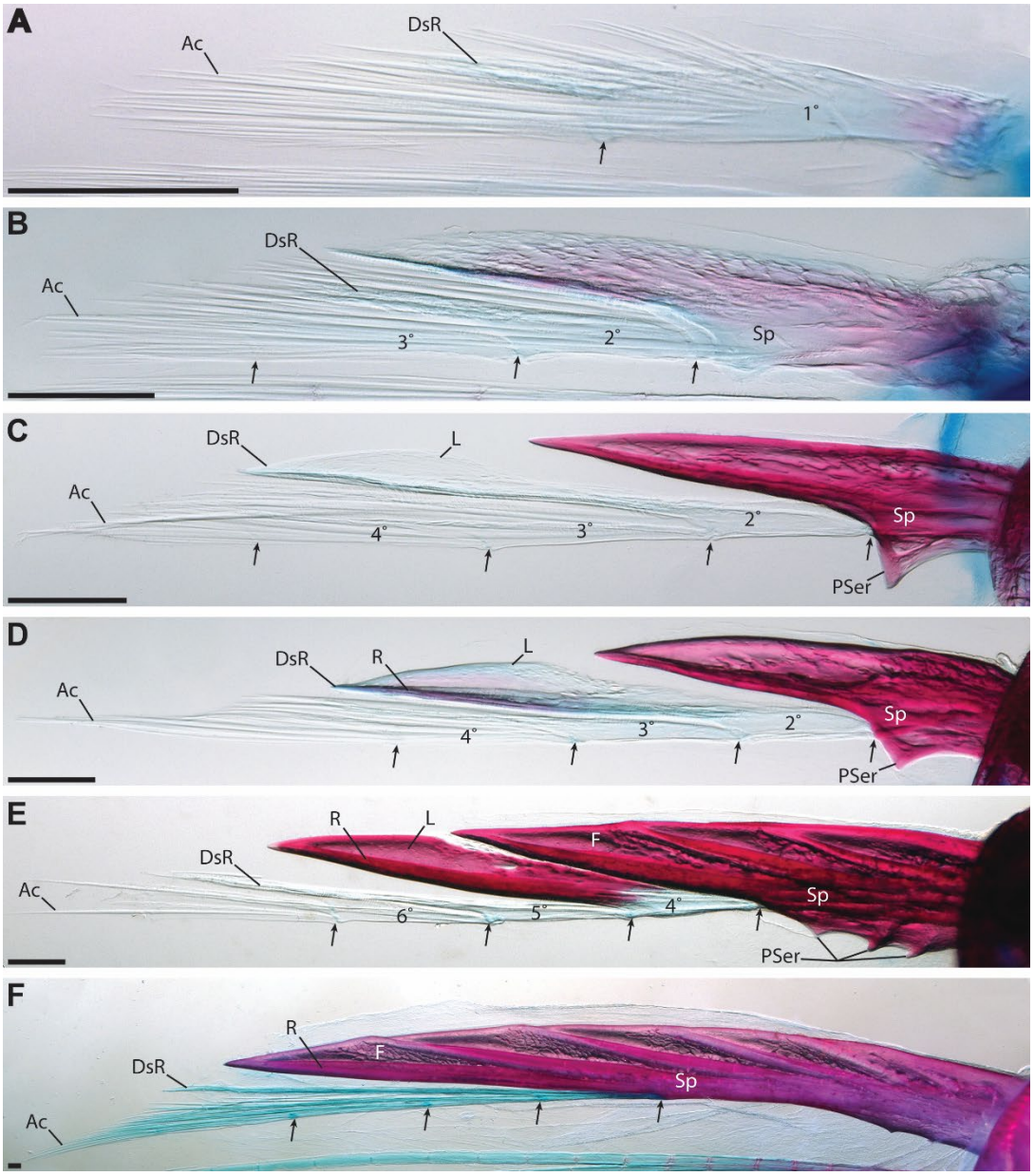

Figure 3.5. Ontogeny of the pectoral-fin spine of *Noturus gyrinus* (TCWC 19758.01). (**A**) 8.6 mm SL. (**B**) 9.9 mm SL. (**C**) 11.6 mm SL. (**D**) 13.1 mm SL. (**E**) 19.8 mm SL. (**F**) 36.6 mm SL. Arrows indicate segmentation. N° indicates segment number in stages where the total number of segments is known with 1° being the proximalmost. Scale bars equal to 0.2 mm. Abbreviations: Ac, actinotrichia bundle; DsR, distal ramus; F, furrow; L, lamina of bone; R, dorsal and ventral ridges of bone; PSer, posterior serra; Sp, spine proper. Reprinted from Kubicek, Britz & Conway, 2019.

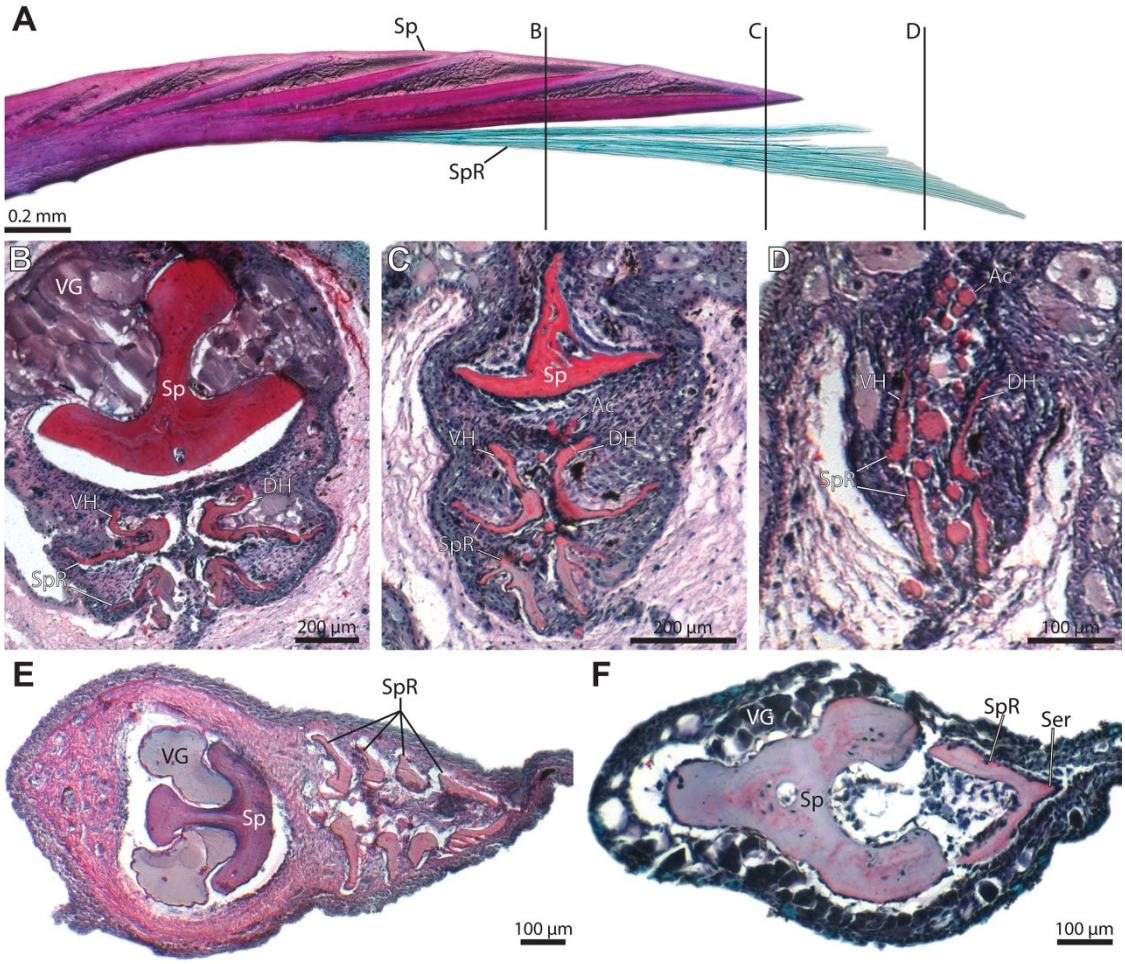

Figure 3.6. Sagittal sections through the pectoral-fin spines of *Noturus gyrinus* (A, TCWC 19758.01, 36.6 mm SL; B-E, TCWC 19758.02, 80.5 mm SL), *Akysis vespa* (TCWC 19739.02, 34 mm SL) and *Corydoras panda* (TCWC 19753.02, 19.5 mm SL). (**A**) Spine of *Noturus gyrinus* with lines representing approximate locations of sections shown in B, C and D. (**B**) Proximal section through the pectoral-fin spine. (**C**) Section through the pectoral-fin spine near the distal tip of the spine proper. (**D**) Section through the distal end of the spurious ray. (**E**) Pectoral-fin spine in *Akysis vespa*. (**F**) Section through the pectoral-fin spine of *Corydoras panda*. Anterior to top of page in B-D, to left in E, F. Abbreviations: DH, dorsal hemitrichium; PSer, posterior serra; Sp, spine proper; SpR, Spurious ray; VG, Venom glands; VH, ventral hemitrichium. Reprinted from Kubicek, Britz & Conway, 2019.

posterior distal edge of the spine proper, resulting in a series of furrows along the anterior edge, in which the toxin cells reside (Fig. 3.6B). Serrae are associated with the three proximalmost segments that make up the spine proper. As in *I. punctatus*, each segment of the spurious ray appears to increase in ossification in a distal to proximal direction.

By 36.6 mm SL (Fig. 3.5F), a stage resembling the adult condition, the pectoral-fin spine has become slightly recurved and is more blade-like in appearance. The distal ramus of each developing segment has become longer (ca. 88% of the proximalmost segment in the spurious ray vs. ca. 59% of the first segment to appear; 6B) resulting in longer furrows distally. As the spine continues to grow the proximalmost furrows fill in with bone, causing them to decrease in size until they disappear. These furrows, along with the dorsal and ventral ridges give the spine proper an anchor-like appearance in cross section and are the result of a modification in shape to the hemitrichia of the segments in the spurious ray (Fig. 3.6B-D). These modifications become more pronounced as they develop until the hemitrichial segments finally become strongly concave prior to the point of fusion to the spine proper (Fig. 3.6C). No additional serrae formed after the first three which, at this stage, have almost been fully incorporated into the body of the spine proper by addition of bone to its girth.

Silurus glanis *(Siluridae)*

The development of the pectoral-fin spine in *Silurus glanis* is almost identical to that of *I. punctatus*, with only a few obvious differences. In the earliest stage illustrated (17.2 mm SL; Fig. 3.7A) the first pectoral-fin ray is indistinguishable in size, shape and

composition from the other pectoral-fin rays. By 24.0 mm SL (Fig. 3.7B), distal rami have formed on the three most proximal segments of the first pectoral-fin ray and a total of five segments are currently under development. In a specimen of 36.0 mm SL (Fig. 3.7C), fusion of the proximal two segments across the anterior midline is complete, with the second segment in the process of fusing to the spine proper. The developing segments are similar in shape to those of *I. punctatus* except for the lack of serrae and denticuli in

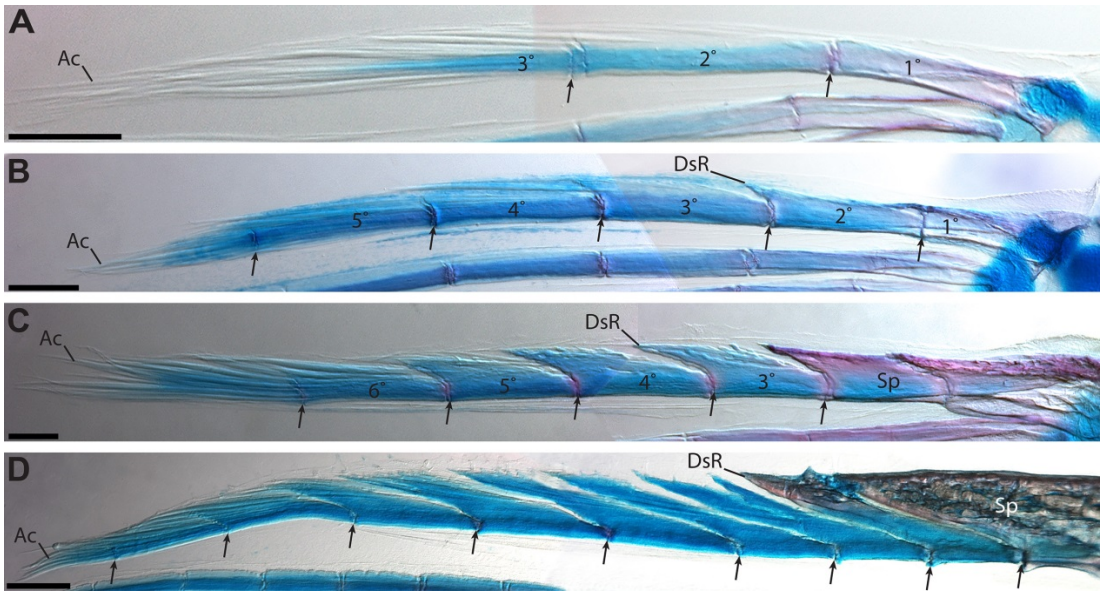

Figure 3.7. Ontogeny of the pectoral-fin spine of *Silurus glanis* (BMNH 2005.7.5.944-1034). (**A**) 17.2 mm SL. (**B**) 24.0 mm SL. (**C**) 36.0 mm SL. (**D**) 85.0 mm SL. Arrows indicate segmentation. N° indicates segment number in stages where the total number of segments is known with 1° being the proximalmost. Scale bars equal to 0.5 mm. Abbreviations: Ac, actinotrichia bundle; DsR, distal ramus; Sp, spine proper. Reprinted from Kubicek, Britz & Conway, 2019.

S. glanis. In a stage resembling the adult (85.0 mm SL; Fig. 3.7D), the length of the distal rami have increased significantly (ca. 68% of the proximalmost segment of the spurious ray vs. 23% in the first segment to appear; 7B), and there are 8 segments under development in the spurious ray. The consistently higher number of free developing segments in *Silurus*, when compared to ictalurids, results in a spurious ray that makes up ca. 55% of the total length of the pectoral-fin spine. This, along with the absence of ornamentation, results in a spine proper that is relatively short and is simple and stout in appearance.

Akysis vespa *(Akysidae)*

Development of the pectoral-fin spine in *Akysis vespa* is similar to that described for *N. gyrinus*. In the earliest stage illustrated (4.5 mm SL; Fig. 3.8A), the distal ramus of the first segment is complete and makes up ca. 40% of the segment length. Two additional segments are apparent, with the distal ramus starting to form on the second, and a third segment is represented by a small plate-like bone.

At 6.2 mm SL (Fig. 3.8B), the dorsal and ventral halves of the first segment have completely fused anteriorly to form the spine proper. The dorsal and ventral halves of the second segment, in which the distal ramus is heavily ossified, have also completely fused anteriorly and a well-developed lamina of bone has formed along its anterior edge and a dorsal and ventral ridge of bone have appeared along its posterior edge. Three additional segments are visible in the spurious ray with distal rami present in the third and fourth segments. The lengths of the forming distal rami are relatively larger when

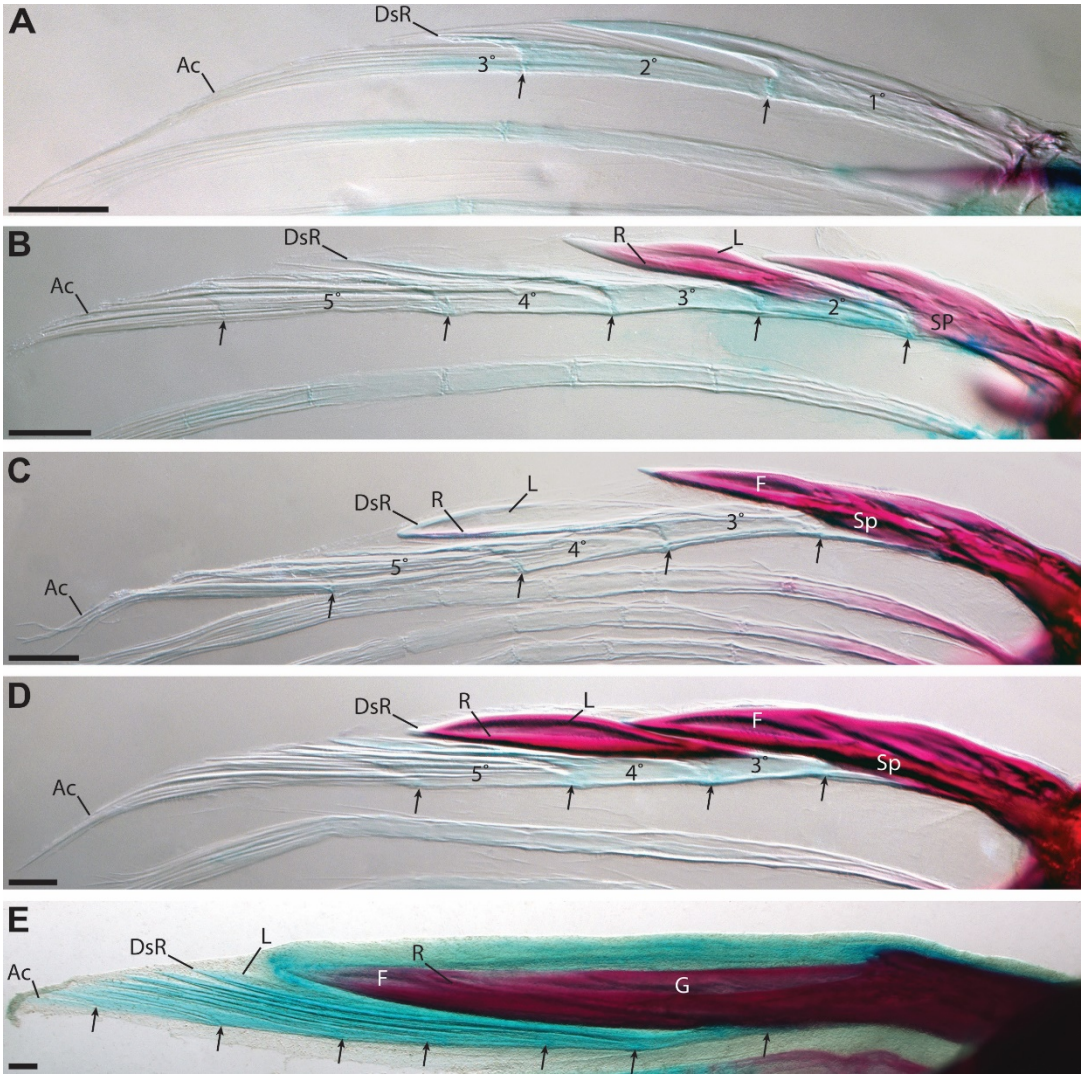

Figure 3.8. Ontogeny of the pectoral-fin spine of *Akysis vespa* (TCWC 19739.01). (**A**) 4.5 mm SL. (**B**) 6.2 mm SL. (**C**) 6.6 mm SL. (**D**) 7.3 mm SL. (**E**) 36.5 mm SL. Arrows indicate segmentation. N° indicates segment number in stages where the total number of segments is known with 1° being the proximalmost. Scale bars equal to 0.2 mm. Abbreviations: Ac, actinotrichia bundle; DsR, distal ramus; F, furrow; G, groove; L, lamina of bone; R, dorsal and ventral ridges of bone; Sp, spine proper. Reprinted from Kubicek, Britz & Conway, 2019.

compared to the first two segments with the distal ramus on the third segment contributing to ca. 65% of the total length of the segment.

By 6.6 mm SL (Fig. 3.8C), the spine proper exhibits a slight curvature and the fusion of the second segment to the spine proper is complete. As a result of this fusion, a furrow similar to that in *N. gyrinus* is present along the anterodistal edge of the spine proper. As the spine continues to grow, additional furrows appear as new segments are added to the spine proper (7.3 mm SL; Fig. 3.8D).

By the time the spine reaches the adult condition (as observed in a specimen of 36.5 mm SL; Fig. 3.8E), it is markedly different from the earlier developmental stages. Only a single furrow, representing the proximalmost fused segment, is present at the distal end of the spine proper. The ridges of bone that demarcated the furrows of previously fused segments appear to have been resorbed during development leaving a single shelf of bone projecting from the anterior midline of the spine proper. This shelf of bone separates two longitudinal grooves that extend across almost the full length of the spine and support the large toxin containing cells (Fig. 3.6E). The spine proper is now curved slightly anteriorly, with up to six segments under development in the spurious ray. The distal rami are exceptionally long in the adult and in the proximalmost segment the distal ramus accounts for ca. 87% of its total length.

Development of the Pectoral-Fin Spine in Loricarioid Catfishes

Corydoras panda *(Callicthyidae)*

In *Corydoras panda*, development of the pectoral-fin spine is similar to that described above for the siluroids, in particular *I. punctatus* and *S. glanis*, with only a few minor differences observed. In the earliest stage examined (8.7 mm SL, Fig. 3.9A), the first pectoral-fin ray is indistinguishable from other pectoral-fin rays. By 9.1 mm SL

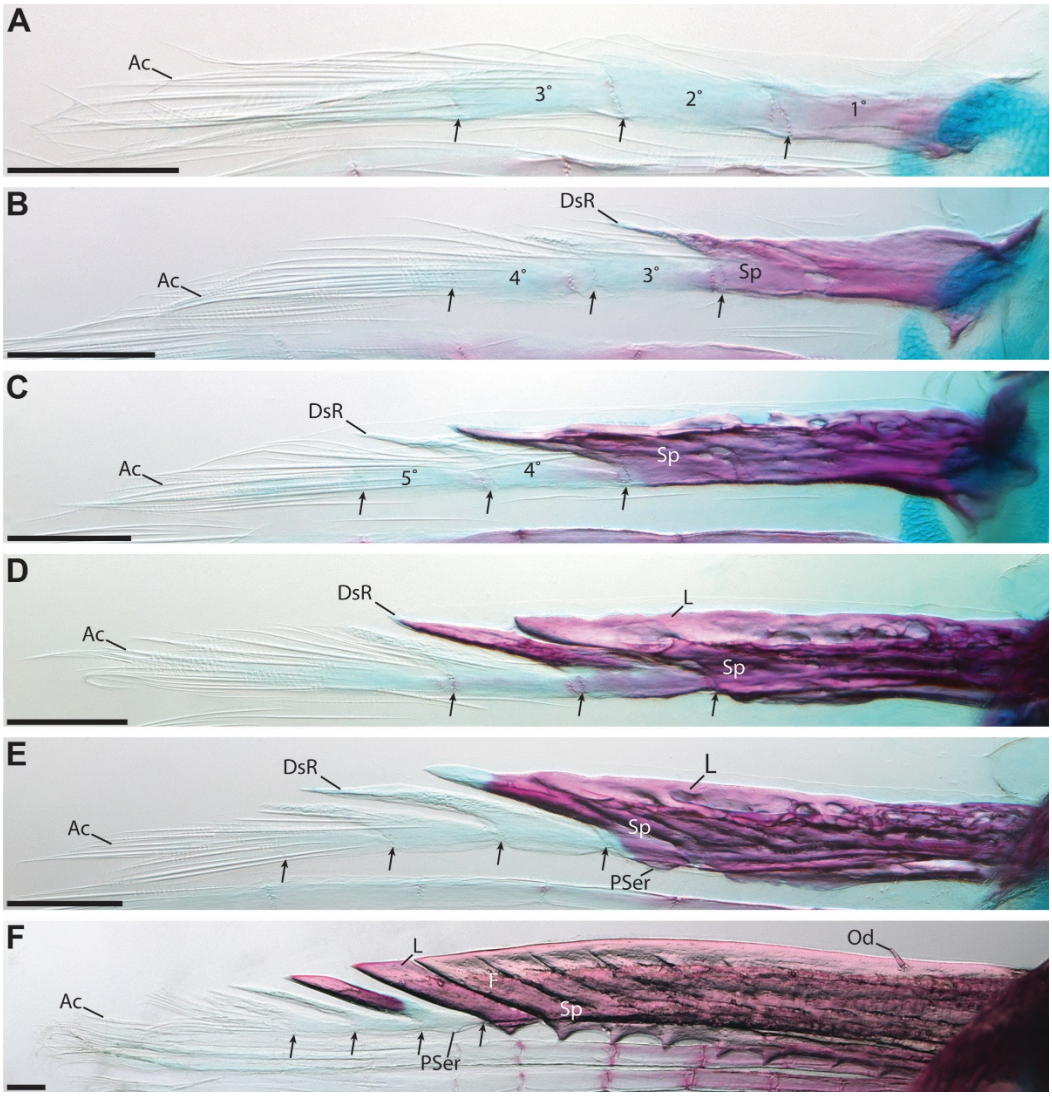

Figure 3.9. Ontogeny of the pectoral-fin spine of *Corydoras panda* (TCWC 19753.01). (**A**) 8.7 mm SL. (**B**) 9.1 mm SL. (**C**) 9.6 mm SL. (**D**) 10.4 mm SL. (**E**) 10.9 mm SL. (**F**) 18.9 mm SL. Arrows indicate segmentation. N° indicates segment number in stages where the total number of segments is known with 1° being the proximalmost. Scale bars equal to 0.2 mm. Abbreviations: Ac, actinotrichia bundle; DsR, distal ramus; F, furrow; L, lamina of bone; Od, odontode; PSer, posterior serra; Sp, spine proper. Reprinted from Kubicek, Britz & Conway, 2019.

(Fig. 3.9B), distal rami are present on the three most proximal segments. The spine proper consists of the proximalmost segments in which the dorsal and ventral halves

have fused anteriorly. Increased ossification of the spine proper is indicated by the presence of sculpturing by 9.6 mm SL (Fig. 3.9C). By 10.4 mm SL (Fig. 3.9D), a lamina of bone is present along the anterior edge of the spine proper, which itself is now stouter. A small posterior serra has formed on the segment undergoing fusion to the spine proper in a specimen of 10.9 mm SL (Fig. 3.9E). The small segmental serrae of *C. panda* do not develop until the segment has started to fuse to the spine proper. As in *I. punctatus,* the first point of fusion between the dorsal and ventral hemitrichia of an individual segment across the posterior midline occurs at the point of the serra (Fig. 3.6F). By 18.9 mm SL (Fig. 3.9F), the spine is similar to that of an adult. The lamina of bone along the anterior edge extends the length of the spine and supports a single pair of odontodes proximally. Bone is forming between each of the serrae, filling in the spaces, along the posterior edge of the spine proper. The bone has almost completely enveloped the proximalmost part of the serration at this point. Near the distal tip of the spine proper, a few shallow furrows are present with the posterior edge of the most recently fused segments forming the ridges separating them.

Ancistrus *sp. (Loricariidae)*

In the earliest stage of *Ancistrus* sp. illustrated (5.6 mm SL, Fig. 3.10A), the first pectoral-fin ray is similar to the other pectoral-fin rays in general appearance, but is slightly wider and longer. A pair of odontodes is present on the anterior edge of the fin ray with one located on the dorsal hemitrichium and the other on the ventral hemitrichium, similarly to but at a much earlier stage of development compared to *Corydoras panda*.

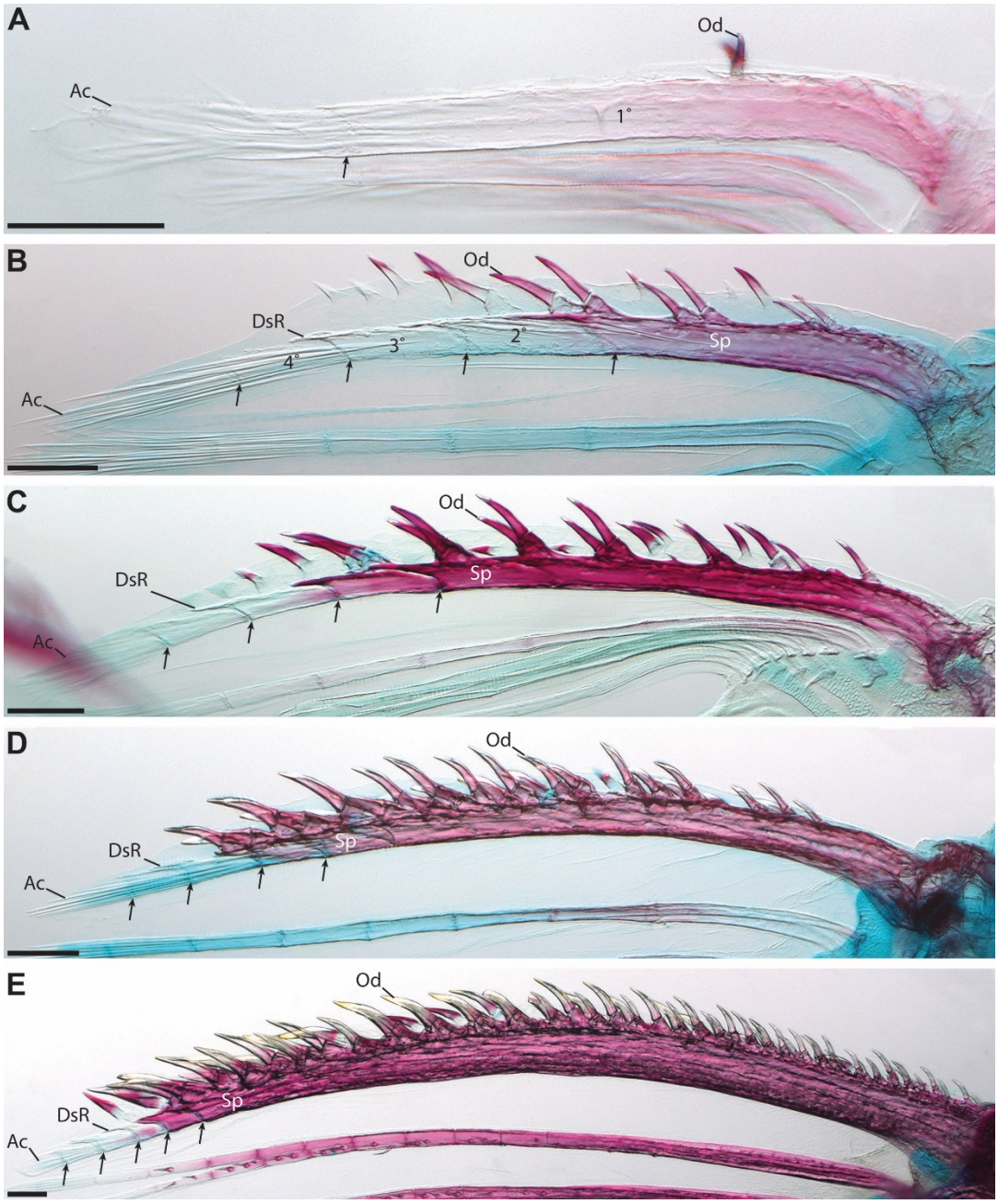

Figure 3.10. Ontogeny of the pectoral-fin spine of *Ancistrus* sp. (TCWC 19759.01). (**A**) 5.6 mm SL. (**B**) 9.7 mm SL. (**C**) 10.1 mm SL. (**D**) 10.8 mm SL. (**E**) 16.5 mm SL. Arrows indicate segmentation. N° indicates segment number in stages where the total number of segments is known with 1° being the proximalmost. Scale bars equal to 0.2 mm. Abbreviations: Ac, actinotrichia bundle; DsR, distal ramus; Od, odontode; Sp, spine proper. Reprinted from Kubicek, Britz & Conway, 2019.

At 9.7 mm SL (Fig. 3.10B) the dorsal and ventral halves of the proximalmost segment have fused across the anterior midline to form the spine proper and a second segment is in the process of fusing to the spine proper. Distal rami are present on the two proximalmost segments of the spurious ray. Several more odontodes have appeared with two additional pairs located on the proximalmost segment and several more developing in the epithelium anterior to the spine.

By 10.1 mm SL (Fig. 3.10C) the spine has continued to elongate but has not yet increased much in diameter. At this point in development, each segment possesses a single pair of larger odontodes with several smaller odontodes forming between these pairs along the length of the spine.

At 10.8 mm SL (Fig. 3.10D), the spine proper has become more heavily ossified and is now covered in odontodes making the aforementioned pairs of odontodes indistinguishable from the others. Unlike the other catfishes examined, the segments of the spurious ray in *Ancistrus* sp. do not increase in size as the spine grows but instead each new segment that is formed is approximately the same size, 0.2 mm, as the preceding one.

In the largest specimen illustrated (16.5 mm SL; Fig. 3.10E), the spine is similar to that of an adult. The spine proper has increased significantly in size and odontodes extend the full length of the spine. The largest odontodes are located distally on the spine and gradually decrease in size proximally. The segments of the spurious ray are only slightly larger than those of the other pectoral-fin rays and, unlike those of the other catfishes examined, do not contribute to the growth in circumference of the spine proper.

Instead, growth seems to occur entirely from deposition of new bone. The spurious ray instead becomes increasing smaller relative to the size of the spine. These differences result in a remarkably different spine morphology when compared to that of the other catfishes described herein.

Overview of Pectoral-Fin Spine morphology in Siluriformes

The adult morphology of the first pectoral-fin ray was examined in adults and juveniles of 62 species, representing 41 of 43 families of catfishes, and development was inferred through the examination of the spurious ray (Fig. 3.11-3.12) and summarized in Table 3.1. Members of four families (Kryptoglanidae, Malapteruridae, Phreatobiidae and Trichomycteridae) do not possess spines. Of the 37 families examined that include members with pectoral-fin spines, 34 (54 species) exhibit distal rami and 28 (38 species) exhibit posterior serrations. *Nematogenys inermis* was the only species examined that possessed segments in the spurious ray with posterior serrae but lacked distal rami. Denticulations were found only in members of 13 families (15 species). Anterior serrae were observed in 16 families (25 species), just under half of the species possessing distal rami, with most present only on the distal end of the spine proper. Odontodes were observed on the pectoral-fin spines of all the loricarioid species, excluding those of the family Trichomycteridae.

Discussion

Fin spines, i.e. unpaired, unsegemented, spinous fin rays have evolved several times independently among ray-finned fishes. Polypterids have dorsal-fin spines that form from ontogenetic fusion of paired dorsal-fin hemitrichial segments (Sewertzoff,

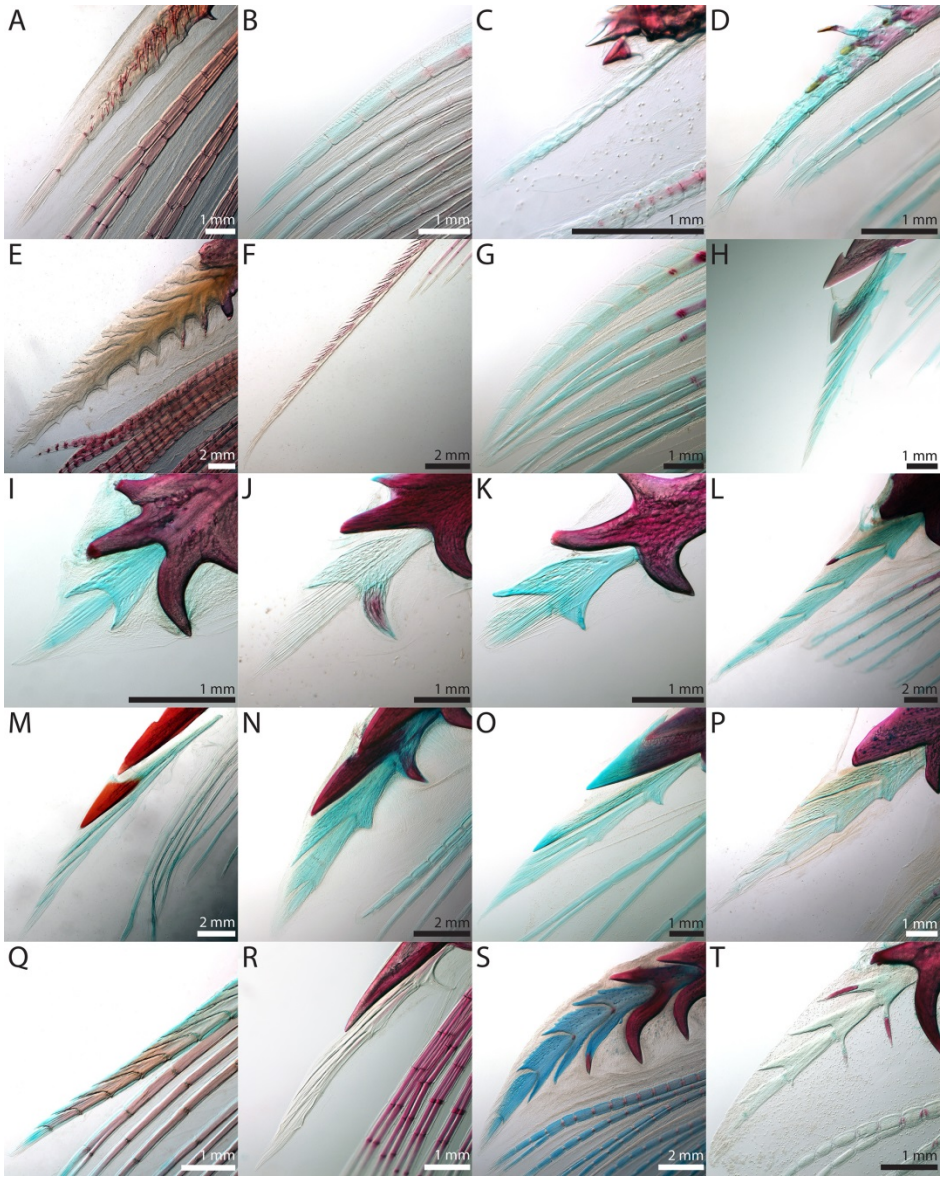

Figure 3.11. Spurious ray of the left or right (image reversed) pectoral-fin spine in select members of the Siluriformes. (**A**) *Nematogenys inermis*, Nematogenyidae (UMMZ 212697, 68.0 mm SL). (**B**) *Henonemus* sp., Trichomycteridae (TCWC 13989.19, 69.7 mm SL). (**C**) *Scoloplax empousa*, Scoloplacidae (FMNH 108610, 19.1 mm SL). (**D**) *Astroblepus* sp., Astroblepidae (CU 78811, 32.2 mm SL). (**E**) *Diplomystes chilensis*, Diplomystidae (CAS 13706, 144.5 mm SL). (**F**) *Cetopsis coecutiens*, Cetopsidae (FMNH 10000, 119 mm SL). (**G**) *Helogenes marmoratus* (ANSP 177185, 31.9 mm SL). (**H**) *Pangasius macronema*, Pangasiidae (CAS 29360, 62.9 mm SL). (**I**) *Pseudobunocephalus lundbergi*, Aspredinidae (ANSP 168810, 24.7 mm SL). (**J**) *Ossanocora punctata*, Doradidae (TCWC 16723.16, 46.1 mm SL). (**K**) *Tatia intermedia*, Auchenipteridae (TCWC 19752.01, 37.6 mm SL). (**L**) *Rita rita*, Ritidae (CAS-SU 34866, 85 mm SL). (**M**) *Cranoglanis bouderius*, Cranoglanididae (CAS-SU 69758, 97.0 mm SL). (**N**) *Austroglanis gilli*, Austroglanididae (ANSP 177966, 71.8 mm SL). (**O**) *Horabagrus brachysoma*, Horabagridae (TCWC 19755.01, 56.1 mm SL). (**P**) *Pseudomystus siamensis*, Bagridae (CAS 94782, 58.0 mm SL). (**Q**) *Ailia coila*, Ailiidae (UMMZ 208353, 91.6 mm SL). (**R**) *Liobagrus somjinensis*, Amblycipitidae (TCWC uncat., 42.8 mm SL). (**S**) *Glyptothorax sinensis*, Sisoridae (UMMZ 246438, 60.7 mm SL). (**T**) *Pseudolaguvia kapuri*, Erethistidae (CAS 50294, 25.1 mm SL). Reprinted from Kubicek, Britz & Conway, 2019.

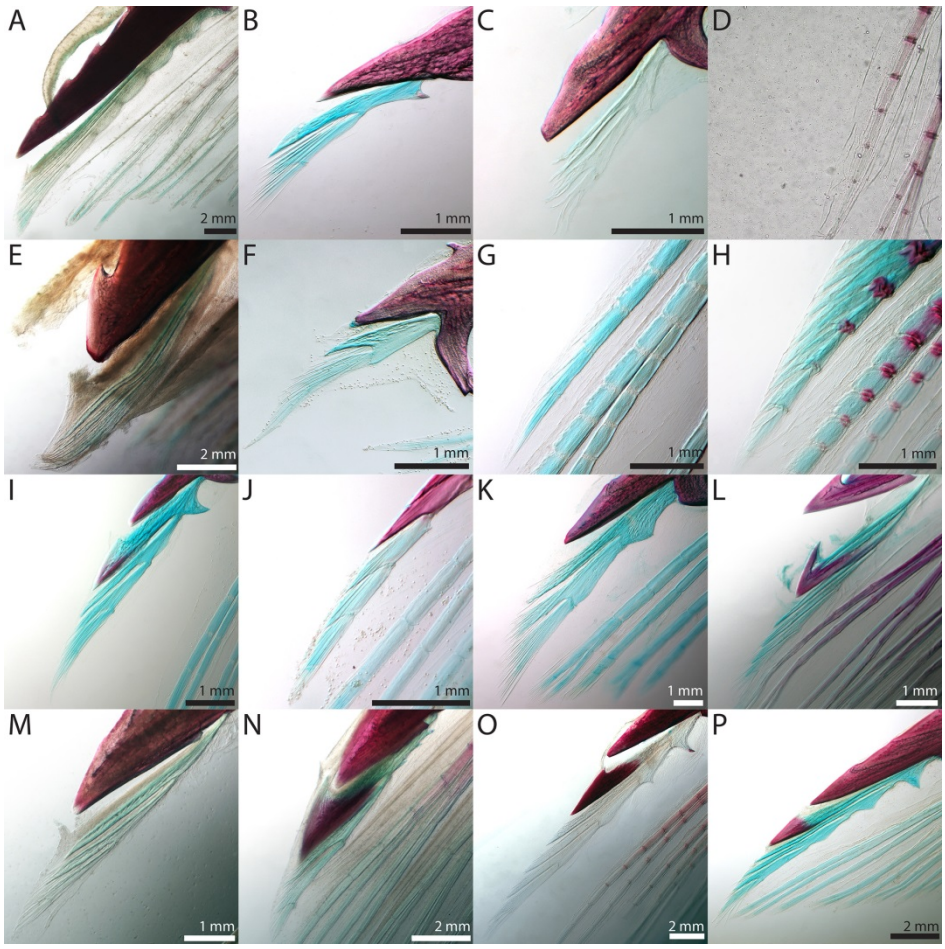

Figure 3.12. Spurious ray of the left or right (image reversed) pectoral-fin spine in select members of the Siluriformes. (**A**) *Goeldiella eques*, Heptapteridae (ANSP 177187, 99.2 mm SL). (**B**) *Pimelodus pictus*, Pimelodidae (TCWC 19761.01, 33.1 mm SL). (**C**) *Microglanis poecilus*, Pseudopimelodidae (AMNH 54973, 25.2 mm SL). (**D**) *Kryptoglanis shajii*, Kryptoglanidae (BMNH uncat., 60.0 mm SL). (**E**) *Chaca chaca*, Chacidae (UMMZ 208728, 156.0 mm SL). (**F**) *Microsynodontis* sp., Mochokidae (TCWC 19760.01, 26.2 mm SL). (**G**) *Malapterurus oguensis*, Malapteruridae (CU 95140, 56.4 mm SL). (**H**) *Amphilius uranoscopus*, Amphiliidae (CU 93740, 41.8 mm SL). (**I**) *Auchenoglanis occidentalis*, Auchenoglanididae (CU 90478, 35.8 mm SL). (**J**) *Parailia pellucida*, Schilbeidae (USNM 229794, 30.3 mm SL). (**K**) *Chrysichthys mabusi*, Claroteidae (CU 91692, 58.0 mm SL). (**L**) *Plotosus lineatus*, Plotosidae (FMNH 110269, 66.7 mm SL). (**M**) *Heteropneustes fossilis*, Heteropneustidae (CAS 29627, 122.3 mm SL). (**N**) *Clarias batrachus*, Clariidae (UMMZ 217578, 105.2 mm SL). (**O**) *Ancharius fuscus*, Anchariidae (AMNH 93702, 88.4 mm SL). (**P**) *Arius jordani*, Ariidae (TCWC 19740.01, 51.1 mm SL). Reprinted from Kubicek, Britz & Conway, 2019.

Table 3.1. Summary of diversity in the anteriormost pectoral-fin ray in members of the order Siluriformes examined in this study. Reprinted from Kubicek, Britz & Conway, 2019.

Family	Species	Number examined	Ray Type	Distal Rami	Posterior Serrae	Denticuli	Anterior Serrae	Odontodes	Dorsal Fin
	Loricarioidea								
Astroblepidae	*Astroblepus* sp.	4	Spine	Absent	Absent	Absent	Absent	Present	Same
Callichthyidae	*Corydoras panda*	6	Spine	Present	Present	Absent	Absent	Present	Same
Loricariidae	*Ancistrus* sp.	5	Spine	Present	Absent	Absent	Absent	Present	Same
	Hemipsilichthys vestigipinnis	3	Spine	Present	Absent	Absent	Absent	Present	Same
Nematogenyidae	*Nematogenys inermis*	2	Spine	Absent	Present	Absent	Absent	Present	–
Scoloplacidae	*Scoloplax empousa*	5	Spine	Absent	Absent	Absent	Absent	Present	Same
Trichomycteridae	*Henonemus* sp.	1	Normal	Absent	Absent	Absent	Absent	Absent	Same
	Trichomycterus hasemani	3	Normal	Absent	Absent	Absent	Absent	Absent	Same
	Diplomystoidea								
Diplomystidae	*Diplomystes chilensis*	2	Spine	Present	Present	Absent	Absent	Absent	Same
	Siluroidea								
Akysidae	*Akysis vespa*	8	Spine	Present	Absent	Absent	Absent	Absent	Same
Amblycipitidae	*Amblyceps cerinum*	2	Spine	Present	Absent	Absent	Absent	Absent	Same
	A. mangois	2	Spine	Present	Absent	Absent	Absent	Absent	Same
	Liobagrus somjinensis	1	Spine	Present	Present	Absent	Absent	Absent	No posterior serrae
Ailiidae	*Ailia coilia*	5	Spine	Present	Absent	Absent	Absent	Absent	No spine
Amphiliidae	*Amphilius uranoscopus*	3	Spine	Present	Absent	Absent	Absent	Absent	Same
Anchariidae	*Ancharias fuscus*	1	Spine	Present	Present	Absent	Absent	Absent	Same
Ariidae	*Ariopsis felis*	2	Spine	Present	Present	Absent	Present	Absent	Same
	Arius jordani	2	Spine	Present	Present	Absent	Absent	Absent	Same
	Bagre marinus	4	Spine	Present	Present	Absent	Present	Absent	Same
Aspredinidae	*Bunocephalus* sp.	2	Spine	Present	Present	Absent	Present	Absent	No serrae
	Pseudobunocephalus lundbergi	5	Spine	Present	Present	Absent	Present	Absent	No serrae
Auchenipteridae	*Tatia intermedia*	4	Spine	Present	Present	Absent	Present	Absent	No posterior serrae
	Trachycorystes sp.	3	Spine	Present	Present	Absent	Present	Absent	Same
Auchenoglanididae	*Auchenoglanis occidentalis*	2	Spine	Present	Present	Present	Present	Absent	Same
Austroglanididae	*Austroglanis gilli*	1	Spine	Present	Present	Absent	Absent	Absent	Same
Bagridae	*Pseudomystus siamensis*	5	Spine	Present	Present	Absent	Absent	Absent	Same

Table 3.1. Continued

Family	Species	Number examined	Ray Type	Distal Rami	Posterior Serrae	Denticuli	Anterior Serrae	Odontodes	Dorsal Fin
Cetopsidae	*Cetopsis coecutiens*	2	Spine	Present	Absent	Absent	Absent	Absent	Same
	Helogenes marmoratus	5	Spine	Present	Absent	Absent	Absent	Absent	Same
Chacidae	*Chaca chaca*	1	Spine	Present	Absent	Present	Present	Absent	No denticulations
Clariidae	*Clarias batrachus*	3	Spine	Present	Present	Present	Present	Absent	No distal rami, serrae or denticulations
	C. gariepinus	2	Spine	Present	Present	Present	Present	Absent	No distal rami, serrae or denticulations
Claroteidae	*Chrysichthys mabusi*	2	Spine	Present	Present	Present	Present	Absent	No denticulations
Cranoglanididae	*Crangolanis bouderius*	1	Spine	Present	Present	Present	Present	Absent	Same
Doradidae	*Ossanocora punctata*	2	Spine	Present	Present	Absent	Present	Absent	No anterior serrae; denticulations present
	Platydoras armatulus	1	Spine	Present	Present	Absent	Present	Absent	Same
Erethistidae	*Pseudolaguvia kapuri*	4	Spine	Present	Present	Present	Absent	Absent	No denticulations
Heptapteridae	*Goeldiella eques*	2	Spine	Present	Present	Present	Present	Absent	No posterior serrae or denticulations
Heteropneustidae	*Heteropneustes fossilis*	2	Spine	Present	Present	Absent	Present	Absent	No spine
Horabagridae	*Horabagrus brachysoma*	2	Spine	Present	Present	Present	Present	Absent	No denticulations
Ictaluridae	*Ameiurus melas*	1	Spine	Present	Present	Absent	Present	Absent	No posterior serrae
	Ictalurus furcatus	4	Spine	Present	Present	Present	Absent	Absent	No denticulations
	I. punctatus	7	Spine	Present	Present	Present	Absent	Absent	Same
	Noturus flavus	1	Spine	Present	Absent	Absent	Present	Absent	Same
	N. gyrinus	7	Spine	Present	Absent	Absent	Absent	Absent	Same

Table 3.1. Continued

Family	Species	Number examined	Ray Type	Distal Rami	Posterior Serrae	Denticuli	Anterior Serrae	Odontodes	Dorsal Fin
Ictaluridae	*Pylodictis olivaris*	1	Spine	Present	Present	Absent	Present	Absent	No serrae
Kryptoglanidae	*Kryptoglanis shajii*	1	Normal	Absent	Absent	Absent	Absent	Absent	Absent
Malapteruridae	*Malapterurus oguensis*	2	Normal	Absent	Absent	Absent	Absent	Absent	Same
Mochokidae	*Microsynodontis* sp.	1	Spine	Present	Present	Present	Absent	Absent	No denticulations
Pangasiidae	*Pangasius macronema*	5	Spine	Present	Present	Present	Present	Absent	Same
Phreatobiidae	*Phreatobius sanguijuela*	1	Normal	Absent	Absent	Absent	Absent	Absent	–
Pimelodidae	*Pimelodus pictus*	2	Spine	Present	Present	Present	Present	Absent	No Denticulations
Plotosidae	*Plotosus lineatus*	5	Spine	Present	Present	Absent	Present	Absent	Same
Pseudopimelodidae	*Microglanis poecilus*	2	Spine	Present	Present	Present	Absent	Absent	No denticulations
Ritaidae	*Rita rita*	1	Spine	Present	Present	Absent	Present	Absent	No anterior serrae
Schilbeidae	*Parailia congica*	2	Spine	Present	Absent	Absent	Absent	Absent	Absent
	P. pellucida	3	Spine	Present	Present	Absent	Absent	Absent	Absent
	Schilbe intermedius	3	Spine	Present	Present	Absent	Present	Absent	Same
Siluridae	*Silurus asotus*	3	Spine	Present	Absent	Absent	Present	Absent	No spine
	S. glanis	4	Spine	Present	Absent	Absent	Absent	Absent	No spine
	Wallago attu	2	Spine	Present	Absent	Absent	Absent	Absent	Same
Sisoridae	*Glyptothorax sinensis*	1	Spine	Present	Present	Absent	Absent	Absent	Same
	Parachiloglanis hodgarti	6	Spine	Present	Absent	Absent	Absent	Absent	Same

1924; Bartsch & Gemballa, 1992). The pectoral-fin spine of sturgeons also forms from paired hemitrichia that fuse early in development and subsequently incorporate up to two pectoral-fin rays (Hilton et al., 2011; Dillman & Hilton, 2015). Fin spines are more prevalent among teleosts and are found in several groups including the Notacanthidae (McDowall, 1973; Johnson & Patterson, 1993), where they are present as a series of dorsal and anal-fin spines. Among otophysans they are known from Cyprinidae, in which a single large spine may be located anteriorly in either the dorsal fin alone, or in combination with a single spine in the anal or the pelvic fins (Cope, 1874; Peyer, 1922; Miller & Hubbs, 1960), and from the siluriforms as pectoral- and dorsal-fin spines. Additionally, fin spines are almost ubiquitiously developed in members of the Acanthomorpha (Bridge, 1896; Johnson & Patterson, 1993), a large speciose group for which they are the name-giving anatomical structure and a putative synapomorphy of this group. Here they are developed as a series of dorsal- and anal-fin spines. The pelvic fin may also carry a fin spine and its presence is a putative synapomorphy of Acanthopterygii (Johnson & Patterson, 1993). This short overview shows that among teleosts the presence of a pectoral-fin spine is exceptional and a convincing synapomorphy of the Siluriformes.

As pointed out previously by Reed (1924) and Arratia (2003) the pectoral-fin spine of catfishes is a modification of the first pectoral-fin ray. In his detailed ontogenetic treatment of the pectoral-fin spine, Reed (1924) noted that growth of the spine is achieved via the fusion of subsequent segments of the spurious ray to the distal tip of the spine proper. However, Reed (1924) interpreted the distal ramus of each

hemitrichial segment of the spurious ray as an anterior branch in a dichotomously branching soft fin ray. This interpretation is unlikely given that the first pectoral-fin ray in teleost fishes is invariably unbranched (Lundberg & Marsh, 1976; Pers. Obs., present authors) and, as I have shown herein, the distal ramus represents the anterodistal most region of an individual hemitrichial segment that forms during the process of segmentation across the field of actinotrichia at the distal tip of the spine. The conclusion of Arratia (2003), that the segments of the spurious ray are "formed by a mass that stains blue with Alcian Blue and that corresponds to some kind of connective tissue [sic]", is also inaccurate. Although the segments of the spurious ray frequently stain with Alcian Blue (Fig. 3.11-3.12), this is likely an artifact of the clearing and staining process and unlikely to be associated with the presence of mucopolysaccharides. I have reached this conclusion because: (1) specimens of *Ictalurus punctatus* (Fig. 3.2C and Fig. 3.3H) examined in this study exhibited variable levels of Alcian Blue uptake despite being stained with the same protocol (Taylor and van Dyke, 1985), albeit on two separate occasions; (2) serial sections prepared from the pectoral-fin spine (Fig. 3.6B-F) of individuals representing a number of different species confirm that the segments of the spurious ray comprise a bone matrix that is histologically identical to the bone matrix of the well-ossified spine proper; and (3) segments of the spurious ray in the aforementioned serial sections did not take up Alcian Blue when stained using a protocol that utilizes this stain (Hall, 1986).

No major differences were observed in the earliest stages of pectoral-fin spine development in any of the species examined, including loricarioid catfishes. This, in

addition to information gained through the examination of the spurious ray in adult and juveniles of 41 families (Fig. 3.11-3.12), suggests that the earliest stages in the development of the morphologically diverse pectoral-fin spine of catfishes are greatly conserved. The morphological variation of the pectoral-fin spine observed in the siluriforms examined instead appears to be related to the presence/absence of three primary traits (distal rami, anterior and posterior serrations), which are formed as a part of the developing fin ray segments, and two secondary traits (denticulations and odontodes), which appear after fusion of the segments to the spine proper has occurred. Variation observed between species includes the relative length of distal rami (e.g., compare *Pseudolaguvia kapuri* Fig. 3.11T vs. *Arius jordani* Fig. 3.12P), size and position of serrae on segments (e.g., compare *Parailia pellucida* Fig. 3.2A vs. *Pseudobunocephalus lundbergi* Fig. 3.2I), size of denticuli (e.g., compare *Ictalurus punctatus* Fig. 3.2C vs. *Pimelodus pictus* Fig. 3.2H), and distribution of odontodes. In addition there are many other secondary traits that affect the morphology of the pectoral-fin that were not mentioned herein but should be considered (e.g. sculpturing of the shaft of the spine proper and multicuspid posterior serrae; Rodiles-Hernández et al., 2010; Vanscoy et al., 2015). It should also be noted that development of the dorsal-fin spine in catfishes is very similar to that of the pectoral-fin spine and in all but one of the specimens examined, the dorsal-fin spine possessed either equal or less ornamentation than that of the pectoral-fin spine (Table 3.1). In the case of the doradid *Ossanocora punctata*, the ornamentation of the dorsal-fin spine differs from that of the pectoral-fin spine in that it possesses anterior denticuli and lacks anterior serrae.

Of the 41 families examined in this study, 34 had representatives in which distal rami were present on the hemitrichial segments of the spurious ray and 28 of those also possessed posterior serrae on these segments. This was the most frequent pattern observed and was found throughout the order, including Diplomystidae (Fig. 3.11E), a family that has long been hypothesized to represent a more basal member of the Siluriformes (Lundberg & Case, 1970; Arratia, 1987). This would suggest that presence of hemitrichial segments of the spurious ray that combine a distal ramus anterodistally with a serra posteriorly is the plesiomorphic condition at the level of the Siluriformes with subsequent modifications (e.g., see below) representing derived conditions of more inclusive groups of catfishes. It should be noted that the pectoral-fin spine ornamentation in the species examined does not encompass the entirety of morphological variation found within each family. Ornamentation within a single family can vary greatly, particularly in the presence/absence of denticuli and serrae (e.g. Ictaluridae; Table 3.1; Egge and Simmons, 2010; Vanscoy et al., 2015).

Although development of the pectoral-fin spine is similar across the order, there were some species in which novel development and variation was observed. For example, in *Cetopsis coecutiens* (Fig. 3.11F), the distal rami of the segments in the spurious ray first appear as four to five individual splints along the anterior edge of each hemitrichial segment. As the segment develops, its dorsal and ventral halves fuse and subsequently its associated four to five individual splints fuse together through the deposition of bone between them to form the distal ramus of the segment. This condition was not observed in *Helogenes marmoratus*, another member within the family

Cetopsidae (de Pinna, Ferraris & Vari, 2007), which possesses a relatively short distal ramus that forms from a single extension of bone as is the case in the majority of the other taxa examined (Fig. 3.11G). *Clarias batrachus* (Fig. 3.12N) provides another example of novelty in the process of spine formation. This species possesses two to three posterior serrae variably on each segment of the spurious ray. This condition is unique in that all other species in which a posteriorly serrated spine was observed only possessed a single posterior serra per segment including the other member of Clariidae examined, *C. gariepinnus*.

Variation was also observed in the pattern of fusion between dorsal and ventral hemitrichia. Although the locations of distal rami and posterior serrae appear to correspond with points of fusion, the members of Astroblepidae (Fig. 3.11D) and Scoloplacidae (Fig. 3.11C) examined did not appear to possess distal rami or posterior serrae. In the scoloplacid I studied, the process of fusion could not be determined due to the proximalmost segments of the spurious ray being obscured from view by the considerably larger spine proper. Previously, it has been reported that some scoloplacids possess posterior serrations (e.g. *Scoloplax baskini*; Rocha et al., 2008); however, whether this species possesses true serrae or something more similar to denticuli could not be determined. In astroblepids (Fig. 3.2K, 11D), fusion between the dorsal and ventral hemitrichia occurs with the addition of bone in no discernable pattern across the anterior edge of the segment after the hemitrichial segments fuse to those of the spine proper. *Nematogenys inermis*, which also lacks distal rami, has a similar mechanism of forming its pectoral-fin spine proper through bone deposition along its anterior margin.

This suggests that the distal ramus is not required for the formation of the spine proper but when present corresponds to the first point of fusion. Variation in the histological structure of the spurious ray was also observed, even between species that exhibit a similar spine morphology. For example, *Noturus gyrinus* and *Akysis vespa* possess spines that are blade-like and anchor-shaped in cross section. However, when studied histologically the hemitrichial segments in the spurious rays of the two species differ markedly in their shape (Fig. 3.6B-E): *N. gyrinus* has hemitrichial segments that are strongly concave while those of *A. vespa* appear to be simply expand dorsally and ventrally. This variation in shape and formation of the hemitrichia has, to the best of my knowledge, not been reported previously and this and other aspects of spine development could potentially serve as a source of morphological characters for future phylogenetic studies focused on the intrarelationships of catfishes once the variation has been properly documented.

I have shown that the early development of the pectoral-fin spine of the Siluriformes is greatly conserved and through only slight developmental modification has resulted in the morphologically diverse structure that has long generated interest from vertebrate anatomists and ichthyologists. Further understanding of how this unique structure has evolved will likely be gained through the investigation of the genetic mechanisms underpinning the formation of pectoral fin-rays, such as the expression of genes controlling segmentation of lepidotrichia (e.g. homeobox transcription factor Evx1; Schulte, Allen, England, Juárez-Morales & Lewis, 2011)). Additionally, as shown by Vanscoy et al. (2015), and further supported in this paper, information on pectoral-fin

spine development can be inferred, to a certain extent, through the examination of the developing segments of the spurious ray. Given that herein I have assessed the morphology of the pectoral-fin spine in less than 2% of the total number of catfishes described to date, it is likely that additional morphological variation will continue to be documented from this unique feature of the Siluriformes.

CHAPTER IV

CHANGES IN THE RELATIVE TIMING OF SKELETAL DEVELOPMENT IN CATFISHES (TELEOSTEI: SILURIFORMES)

Introduction

Heterochrony, or changes in the relative timing of developmental events in a descendent relative to an ancestor (Haeckel, 1874; Gould, 1977), has been cited as one of the major underlying processes resulting in evolutionary change (de Beer, 1930; Gould, 1977). Heterochrony can be divided into two subcategories (Smith, 2001): 1) changes in developmental rates which affect shape and size, or growth heterochrony, and 2) changes in the relative timing of a developmental event in a sequence relative to all other events in that sequence, or sequence heterochrony. By utilizing a developmental sequence as a method of standardization, sequence heterochrony analyses allow for the inclusion of multiple types of developmental data (e.g., appearance of distinct morphological characters, onset of gene expression, differentiation of tissue types) and, unlike growth heterochrony, are not restricted to whole body events (e.g., paedomorphosis, Denoël & Joly, 2000; Britz and Conway, 2009) or relatively late processes that depend on shape and size as reference points (Smith, 2001; Esquerré, Sherratt & Keogh, 2017). Studies of sequence heterochrony have been conducted using developmental sequence data collected for a number of different groups of tetrapods, including amphibians (Weisbecker & Mitgutsch, 2010; Harrington, Harrison, & Sheil, 2013), squamates (Hugi, Hutchinson, Koyabu, & Sánchez-Villagra, 2012; Ziermann, Mitgutsch, & Olsson, 2014; Werneburg, & Sánchez-Villagra, 2015), turtles (Werneburg,

Hugi, Müller, & Sánchez-Villagra, 2009; Sánchez-Villagra et al., 2009), crocodylians (Larsson, 1998), birds (Maxwell, Harrison, & Larsson, 2010; Carril, & Tambussi, 2017), and mammals (Nunn and Smith, 1998; Sánchez-Villagra et al., 2008; Weisbecker, V., Goswami, A., Wroe, S., & Sánchez-Villagra, 2008; Hautier et al., 2011, 2013). These studies have revealed that relative changes in the timing of skeletogenesis are widespread, both within and among the major groups of tetrapods, with some of the most notable examples of heterochrony in the vertebrate skeleton being associated with (and potentially responsible for) major evolutionary changes in morphology, life history, and function (e.g., the accelerated development of the cranial and forelimb skeleton in marsupials relative to placental mammals; Goswami, Weisbecker, & Sánchez-Villagra, 2009; Sears, 2009; Keyte & Smith, 2010).

Astonishingly, given the diversity (~ 35,000 species; Fricke, Eschmeyer, & Fong, 2020) and the relatively easier access to developmental material through captive rearing, comparable studies on sequence heterochrony in bony fishes are rare (Mabee & Trendler, 1996; Ito, Matsumoto, & Hirata, 2019). The skeleton of bony fishes is more complex, contains a higher number of elements, and exhibits a wider degree of morphological diversity when compared to that of tetrapods, and as a result, the skeleton of bony fishes has a greater potential for heterochronic shifts to occur. To date, there have only been two studies of sequence heterochrony in bony fishes (Mabee & Trendler, 1996; Ito, Matsumoto, & Hirata, 2019), with Mabee and Trendler (1996) being one of the first attempts to study sequence heterochrony within a phylogenetic framework. However, comparisons made in both of these studies were restricted to information

available from the literature and as a result focused on distantly related taxa, making it difficult to interpret any recovered heterochronic shifts within a broader evolutionary context.

The Order Silurformes is a highly diverse group of otophysan fishes (3,992 species; Fricke, Eschmeyer, & Fong, 2020) accounting for ~11% of the global ichthyofauna and are distributed globally in both fresh and coastal marine waters (Nelson, Grande, & Wilson, 2016). In addition to being speciose, members of this order also exhibit a large amount of morphological diversity, both in shape and size (ranging in length from less than 20 mm to greater than 3 meters; Friel & Lundberg, 1996; de Pinna & Winemiller, 2000; Schaefer, Provenzano, Pinna, & Baskin, 2005; Copp et al., 2009). Despite this diversity, siluriforms are one of the morphologically best-defined groups of bony fishes, with several synapomorphies supporting their monophyly (Fink & Fink, 1981). In many cases these synapomorphies represent greatly modified skeletal elements, such as the modification of the anteriormost pectoral-fin ray into a stout, lockable spine (Fink & Fink, 1981; Fine et al., 1997; Kubicek, Britz, & Conway, 2019). Relationships between siluriforms and the other three orders of otophysan fishes (viz. Cypriniformes, Characiformes and Gymnotiformes) have been well studied (Fink & Fink, 1981; Arcila et al., 2017). Although developmental information available for otophysan fishes has been primarily restricted to particular parts of the skeleton (e.g., the Weberian apparatus; Coburn & Grubach, 1998; Britz & Hoffman, 2006), complete information on the sequence of skeletal development is available for five species of otophysan fishes. This includes two species of cypriniform (*D. rerio* and *Enteromius*

holotaenia; Cubbage & Mabee, 1996; Bird and Mabee, 2003; Conway, Kubicek & Britz, 2017), one characiform (*Salminus brasiliensis*; Mattox, Britz, & Toledo-Piza, 2014), and two siluriforms belonging to the suborder Siluroidei (*Ictalurus punctatus* and *Noturus gyrinus*; see chapter II).

Given the diversity of catfishes as well as the availability of information on the ontogeny of the skeleton in otophysan fishes, the order Siluriformes is an excellent group in which to investigate heterochrony and the role that this process may have played in the evolution of the group. A study of sequence heterochrony within siluriform fishes would not only determine which heterochronic shifts, if any, characterize the order but also provide an opportunity to assess whether heterochrony has played a role in the evolution of derived characteristics of the skeleton, such as the morphologically diverse but developmentally conserved pectoral-fin spine (Kubicek, Britz, & Conway, 2019).

In order to determine the role of sequence heterochrony in the evolution of siluriforms, I conduct sequence heterochrony analyses using ossification sequences currently available for otophysans as well as novel sequences generated herein for two additional siluriforms (*Corydoras panda* and *Ancistrus* sp.) which belong to the suborder Loricarioidei (Sullivan, Lundberg, & Hardman, 2006). Additionally, a new sequence of ossification is generated for *D. rerio*, to address shortcomings with a previously published sequenced. The major goals of this study are to identify which, if any, heterochronic shifts characterize the Order Siluriformes and if any of the key synapomorphies of the group, such as the pectoral-fin spine, exhibit heterochronic shifts

compared to non-siluriform otophysans. I accomplish this by conducting sequence heterochrony analyses using the aforementioned ossification sequences for the entire skeleton as well as multiple subcomponents of the skeleton.

Materials and Methods

Data Collection

Small groups (N = 3–8 adult individuals) of *D. rerio* (Cypriniformes), *C. panda* and *Ancistrus* sp. (Siluriformes) were obtained through the aquarium trade and maintained in 40 L aquaria (pH 7.5–8.0; temperature 26°C ± 1°C). Upon spawning, eggs were collected and incubated until hatching, at which point they were transferred to 20 L aquaria where they were raised until sampling. Eggs were treated with Paraguard (Seachem Laboratories, Madison, GA) to prevent fungus. Larval fishes were fed a mixture of decapsulated brine shrimp eggs, crushed blackworm pellets, *Artemia* nauplii and microworms. Individuals were sampled daily from either 5 days pre-hatch (catfishes) or hatching (*D. rerio*), up to 30 days post-hatch (dph) and every third day from 30 dph to 60 dph when possible. Once collected, specimens were euthanized with an overdose of tricaine methanosulfonate (MS222) delivered in a buffered solution of aquarium water, and subsequently fixed in a solution of 10% buffered paraformaldehyde for 24 hours. After fixation, individuals were transferred to a 70% solution of EtOH for final storage. Protocols involving live animals were approved by the Texas A&M University IACUC (protocol # 2017-0047, 2020-0033).

A total of 81 *D. rerio* (3.0 mm notochord length [NL] to 30.0 mm standard length [SL]), 106 *C. panda* (5.2 mm NL to 21.7 mm SL), and 130 *Ancistrus* sp. (5.4 mm

SL to 26.3 mm SL) were cleared and double-stained (c&s) for bone and cartilage examination. Specimens of *D. rerio* were c&s following Taylor and Van Dyke (1985) and specimens of *C. panda* and *Ancistrus* sp. were c&s using a modification of the acid-free clearing and staining method of Kimmel and Walker (2007). Once c&s, specimens were dissected and scored for the presence/absence of 267 (*D. rerio*), 202 (*C. panda*), and 218 (*Ancistrus* sp.) ossified skeletal elements under a ZEISS SteREO Discovery V20 stereomicroscope. For each individual specimen, bones were considered present at the first sign of alizarin red S staining and absent in the absence of alizarin red S staining. In the few cases in which it was not possible to confirm through stereomicroscopy whether a particular bone was stained with alizarin red S, specimens were examined at higher magnification using a Zeiss Primo Star compound microscope. The cartilage staining of Taylor and Van Dyke's (1985) c&s protocol relies on an acidic solution which has previously been reported to negatively affect the staining of bone (Walker & Kimmel, 2007), which could hinder the identification of bony elements, particularly during the earliest stages of development. In order to compensate for this as well as ensure that scoring of double-stained individuals was accurate, a small number of individuals of each species (69 *D. rerio* [3.4 mm NL – 15.0 mm SL], 30 *C. panda* [5.6 mm NL – 14.9 mm SL], and 21 *Ancistrus* sp. [5.4 mm SL – 14.0 mm SL]) were cleared and single stained for with alizarin red S using a protocol modified from Taylor (1967) and scored for the presence and absence of bone. Bone presence/absence data of skeletal elements collected from double- or single-stained specimens were highly congruent and combined into a single data set in Microsoft Excel©. The length of the smallest

individual in which a particular ossification was observed amongst the sampled individuals (minimum length) and the minimum length at which a particular ossification was observed in all sampled individuals (fixed length) was determined for each bony element to generate the sequence of ossification for each species (following Cubbage & Mabee, 1996; Mattox, Britz, & Toledo-Piza, 2014). Sequences generated for *D. rerio* (Fig. 4.1), *C. panda* (Fig. 4.2), and *Ancistrus* sp (Fig. 4.3). included 159, 129, and 136 skeletal elements, respectively, with some of the elements in the sequence representing multiple serial elements in the skeleton (e.g., branchiostegal rays or vertebral centra). Although ossification sequence information already exists for *D. rerio* (Cubbage and Mabee, 1996; Bird and Mabee, 1996), a new sequence was generated due to a lack of comparative information on the fixed relative timing in the skeletal elements of the paired fins.

Sequence Heterochrony Analysis

Ossification sequences obtained herein along with all others available for members of the Otophysi, *E. holotaenia* (Kubicek, Britz, & Conway, 2017), *S. brasiliensis* (Mattox, Britz, & Toledo-Piza, 2014), *I. punctatus*, and *N. gyrinus* (Chapter II), were used to conduct sequence heterochrony analyses. The ossification sequences were trimmed to ensure that only elements present in the skeleton of all seven species were represented and a final dataset of 93 skeletal elements was produced. Given that sequence heterochrony analyses identify shifts in events relative to all other events in a sequence, changing the number of events included in a sequence can affect whether a particular event is observed to have shifted in one sequence compared to another. To

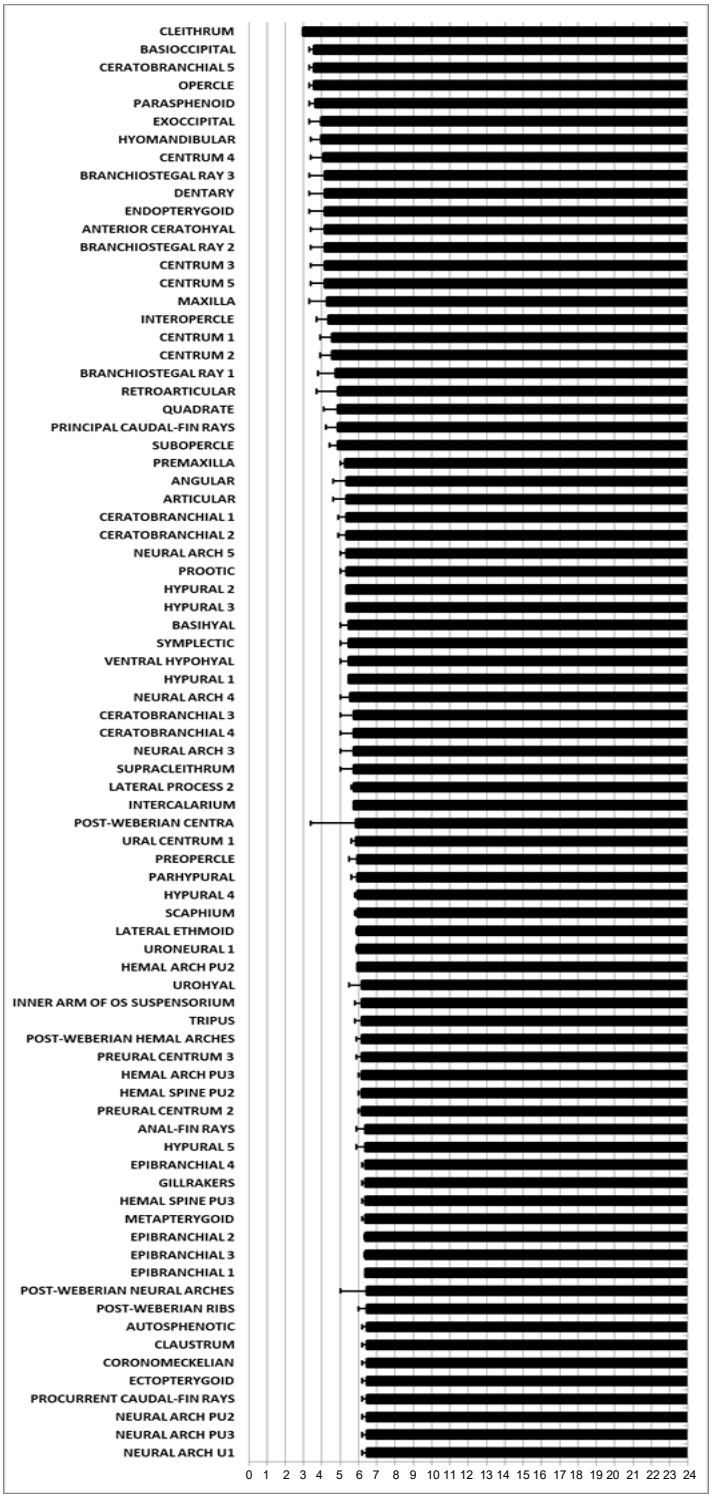

Figure 4.1. Ossification sequence of 159 skeletal elements of *Danio rerio*. Black bars along horizontal axis represent the length at which a particular ossification is present in all individuals (fixed). Error bars associated with black bars indicate the length at which a particular ossification is present in some but not all individuals. Vertical axis represents length in mm NL/SL. Mm, Millimeters; NL, notochord length; SL, standard length.

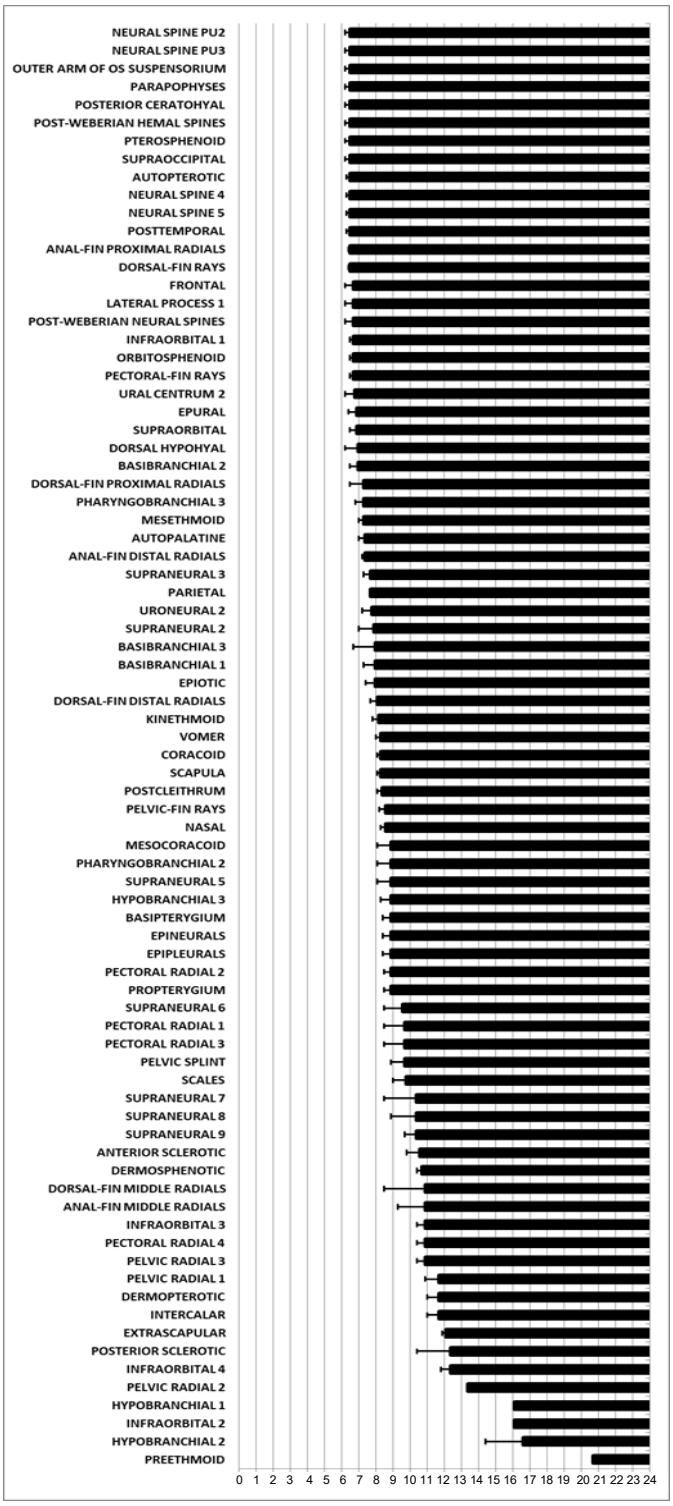

Figure 4.1. Continued

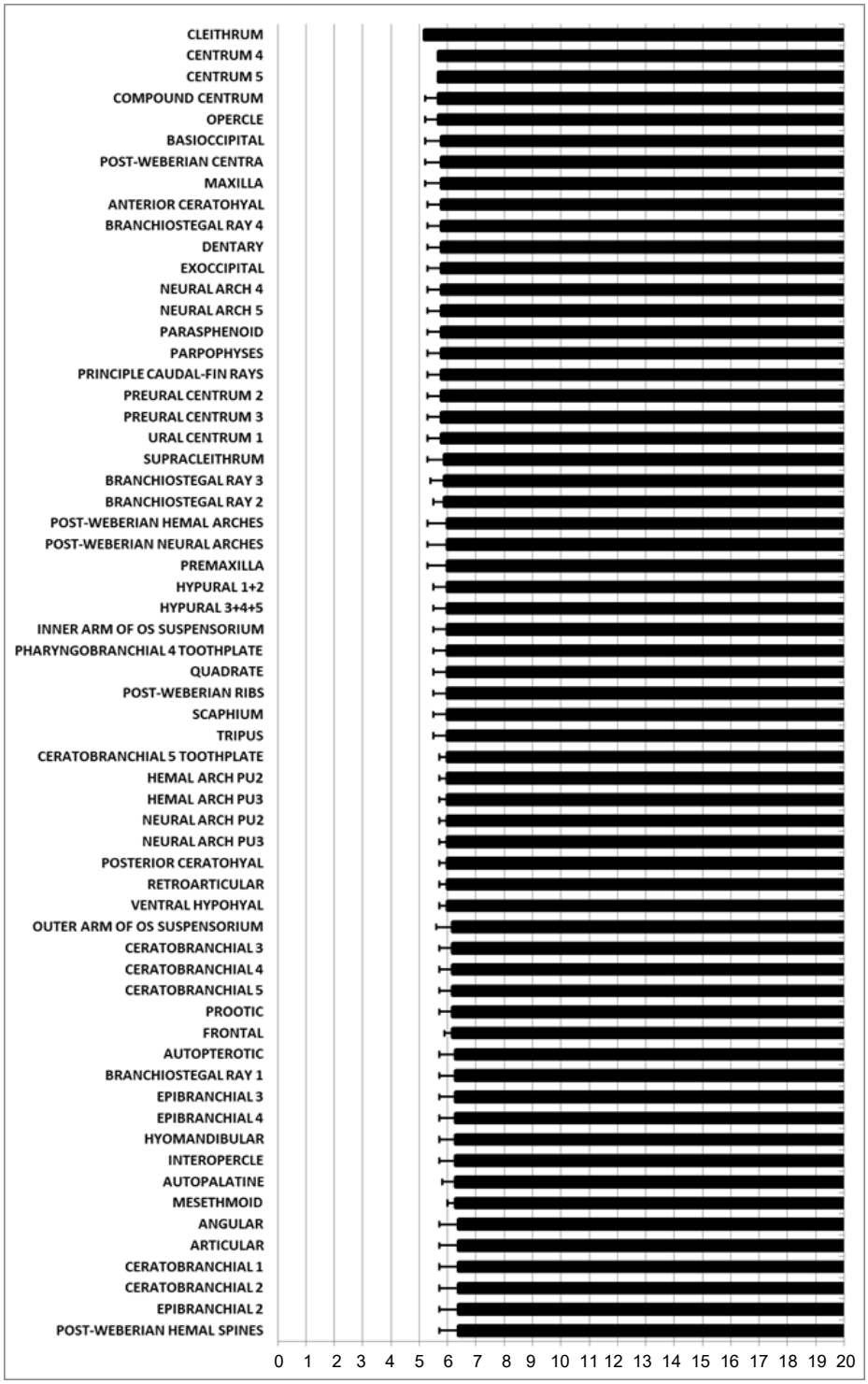

Figure 4.2. Ossification sequence of 129 skeletal elements of *Corydoras panda*. Black bars along horizontal axis represent the length at which a particular ossification is present in all individuals (fixed). Error bars associated with black bars indicate the length at which a particular ossification is present in some but not all individuals. Vertical axis represents length in mm NL/SL. mm, Millimeters; NL, notochord length; SL, standard length.

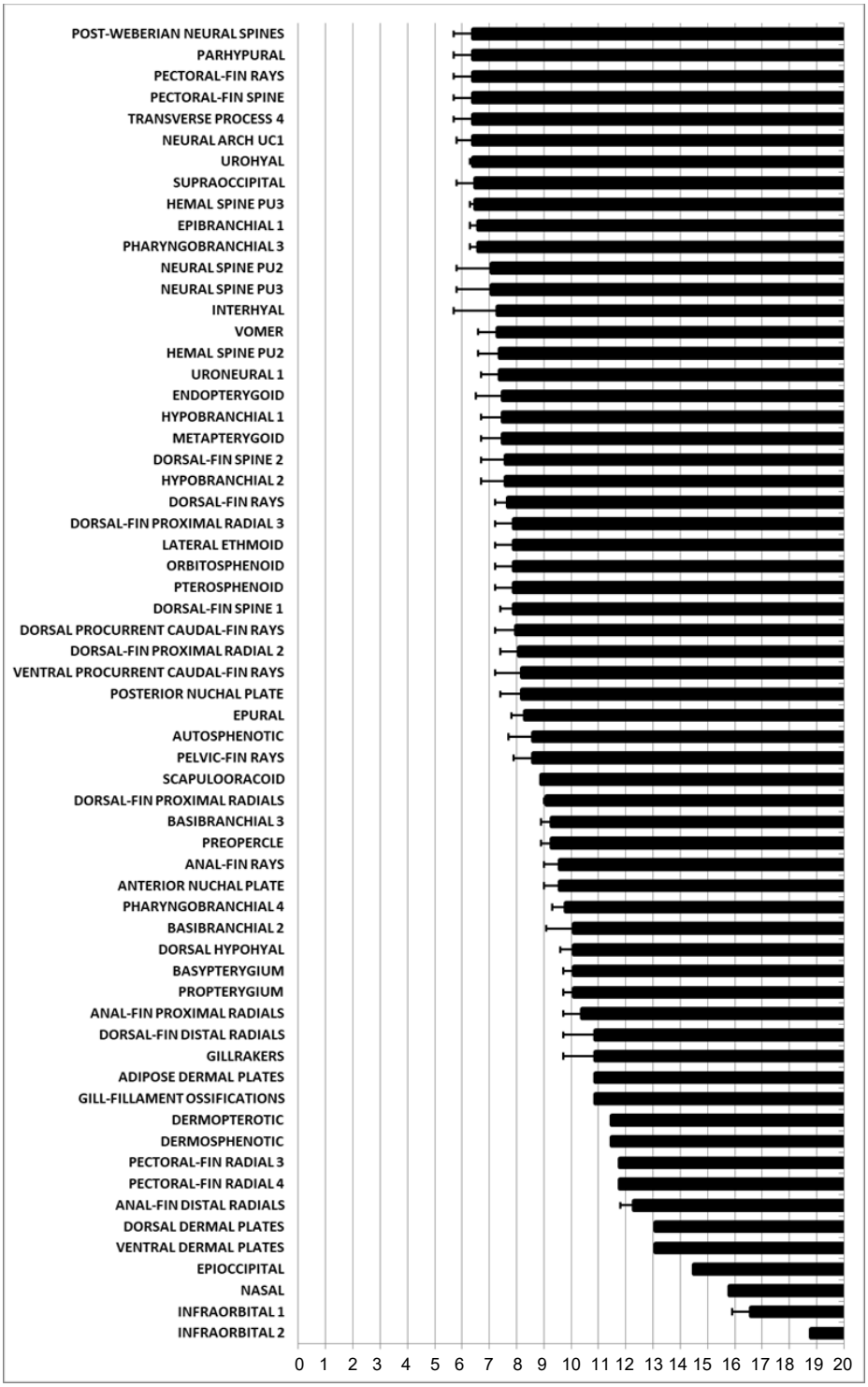

Figure 4.2. Continued

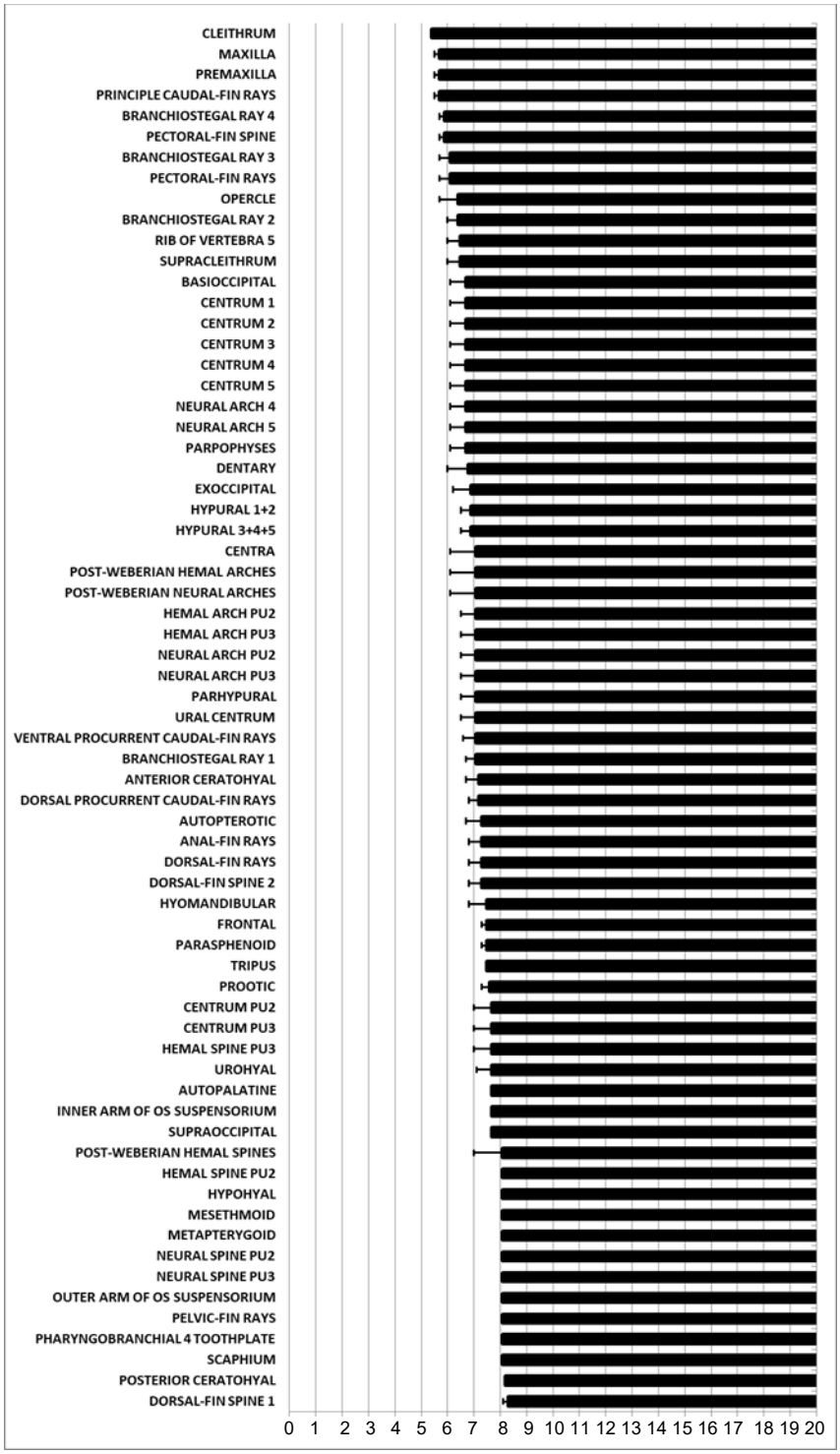

Figure 4.3. Ossification sequence of 136 skeletal elements of *Ancistrus* sp. Black bars along horizontal axis represent the length at which a particular ossification is present in all individuals (fixed). Error bars associated with black bars indicate the length at which a particular ossification is present in some but not all individuals. Vertical axis represents length in mm SL. mm, Millimeters; SL, standard length.

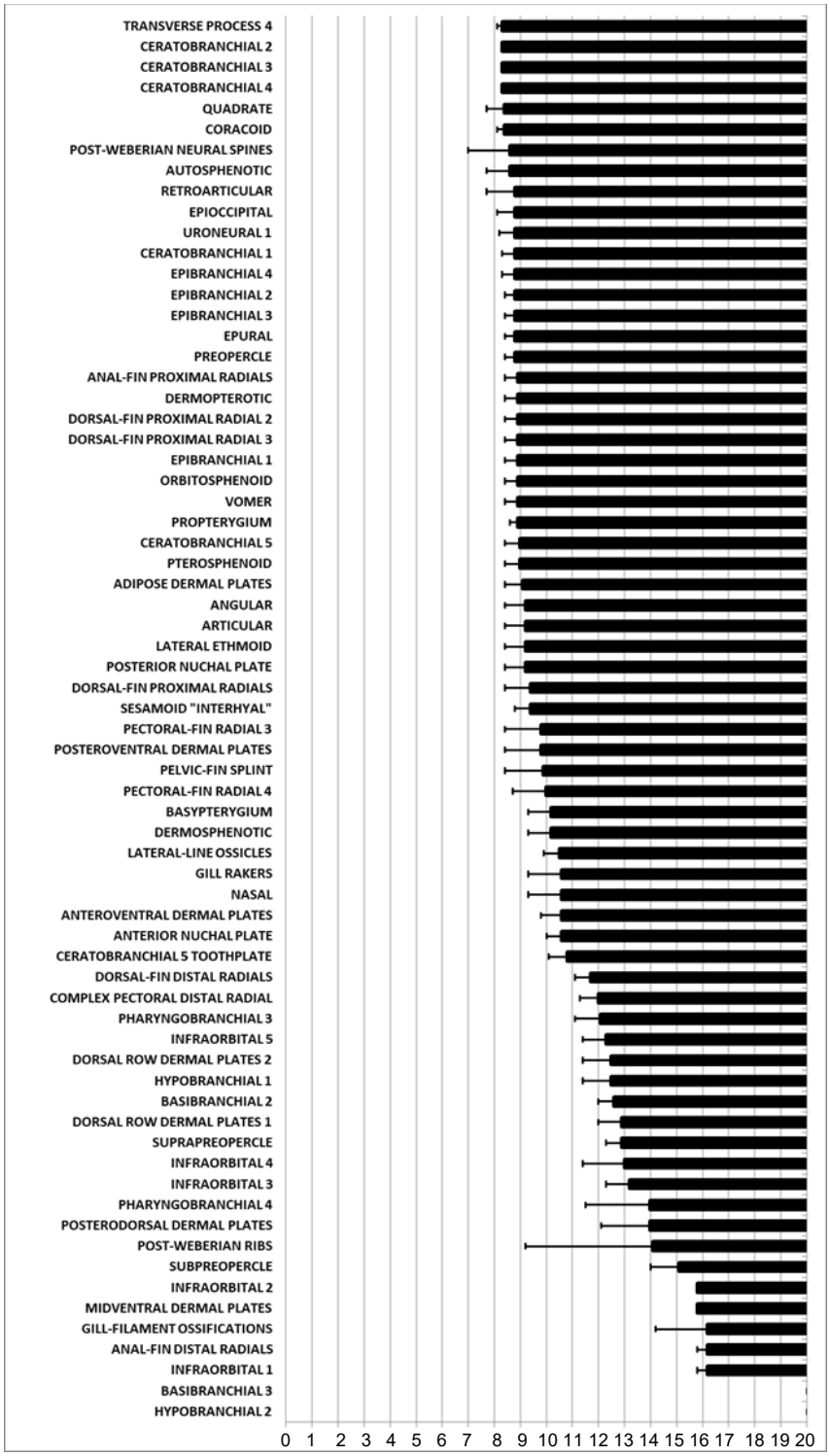

Figure 4.3. Continued

identify which ossifications are clearly shifted regardless of the number of elements included in the analysis, sequences representing six sub-regions of the skeleton were also produced from the whole-skeleton dataset. These include datasets of approximately half of the skeleton (the cranium [48 elements] and postcranial skeleton [45 elements]) as well as smaller regional subcomponents (neurocranium [17 elements], splanchnocranium and associated dermal bones [31 elements], vertebral column [31 elements], and the median and paired fins [29 elements]). Each skeletal element was included in a total of three hierarchical datasets (e.g., the whole skeleton, cranium, and neurocranium), except for the supporting elements of the caudal skeleton (elements of preural vertebrae 2 and 3, ural centra, uroneural 1, hypurals, and epural 1), which were included in two regional datasets (the vertebral column and median and paired-fin skeleton) for a total of four analyses. Data sets were used to analyze sequence heterochrony using two different methods, Sequence analysis of variance (ANOVA) (Nunn & Smith, 1998; Hautier et al., 2013) and Parsimov-based genetic inference (PGi; Harrison & Larsson, 2008).

Sequence-ANOVA

Sequence-ANOVA, developed by Nunn and Smith (1998), is a statistical approach to analyzing sequence data. Before this analysis can be performed, sequence data must be converted into a series of ranks, from 1–*N* (*N* being the total number of elements) based on their order of appearance in the sequence. In the case of a simultaneous appearance of two or more ossifications, an average rank is applied to each element (following Smith, 2001). For example, the sequence of ossification of the neurocranium contains 17 elements, each of which receives a rank from 1 to 17, with 17

being the last element to appear. Tied elements, those that appear simultaneously in development or at the same size in the material examined for each species, receive a mean rank (e.g., the autosphenotic, pterosphenoid and supraoccipital in *D. rerio* receive a mean rank of 7 because all three appear simultaneously after the 5th element in the sequence). The rank-ordered sequence data were divided into two groups for comparison, including: (1) siluriforms (including *I. punctatus*, *N. gyrinus*, *C. panda*, and *Ancistrus* sp.); and (2) non-siluriform otophysans (including *D. rerio*, *E. holotaenia*, and *S. brasiliensis*). A one-way ANOVA was conducted in Microsoft Excel© on the rank data of each individual element within the sequence in order to identify which elements show a greater significance in rank position between rather than within groups (Nunn and Smith, 1998; Smith, 2001; Hautier et al., 2013). This was repeated for each of the seven data sets to identify significant differences in the whole, cranial/postcranial, and regional skeleton. Due to the inherent nature of the sequence-ANOVA, it allows only for the determination of a shift in the sequence but does not reveal which elements are shifting and in which direction (i.e., earlier or later). This means that a significant difference in the rank of an element between two groups may be the result of shifts in the relative timing of other elements in the sequence and as a result this analysis should only be used to identify sequence heterochronies in conjunction with an analysis that can pinpoint which elements are shifting within a sequence, and in which direction (e.g., PGi; Harrison & Larsson, 2008).

PGi Analysis

The PGi method of Harrison and Larsson (2008) is an evolutionary-based approach that reconstructs heterochronic shifts on a given phylogenetic tree. Additionally, this method allows for the inclusion of simultaneous events in a sequence unlike other evolutionary methods (e.g., event-pairing, Parsimov; Jeffery, Bininda-Emonds, Coates, & Richardson, 2005). This method treats an entire sequence as one single, complex character and uses the Parsimov algorithm as an edit-cost function to optimize ancestral states and sequence heterochronies. Rank-ordered data of the whole skeleton and the six sub-regions were analyzed using the PGi method in R version 3.6.3 (R Core Team, 2020) using the R package "pgi2" (Harrison and Larsson, 2008). PGi analyses were run on a constrained tree [((*D. rerio*, *E. holotaenia*), (*S. brasiliensis*, ((*I. punctatus*, *N. gyrinus*), (*C. panda*, *Ancistrus* sp.))))] constructed using available phylogenetic hypotheses for the Otophysi (Fink & Fink, 1981; Arcila et al., 2017) and with the following parameters: 100 replicates, 100 cycles, and 100 sequences retained at each node. Due to the size of the data sets, a semi-exhaustive search of 2000 (whole skeleton, cranium, and postcranial skeleton) or 10,000 (neurocranium, splanchnocranium and associated dermal bones, vertebral column, and median and paired fins) permutations per node was performed. Ten independent runs were conducted for each dataset, except for the whole skeleton in which 20 independent runs were conducted, and the resulting solutions were combined into a superconsensus tree with heterochronic shifts recovered in more than 50% of all runs reported.

Material Examined.

All material examined is deposited in the Collection of Fishes at the Biodiversity Research and Teaching Collections of Texas A&M University. *Danio rerio*: TCWC uncat., 81 specimens, 3.0 mm NL – 30.0 mm SL; TCWC uncat., 69 specimens, 3.4 mm NL – 15.0 mm SL. *Corydoras panda*: TCWC uncat., 106 specimens, 5.2 mm NL – 21.7 mm SL, TCWC uncat., 30 specimens, 5.6 mm NL – 21.7 mm SL. *Ancistrus* sp.: TCWC uncat., 130 specimens, 5.5 mm SL –26.3 mm SL; TCWC uncat., 21 specimens, 5.4 mm SL – 14.0 mm SL.

Results

Sequence-ANOVA

For the whole skeleton data set, the onset of ossification in 26 of 93 skeletal elements was found to be significantly different in siluriforms when compared to that of non-siluriform otophysans at a p-value ≤ 0.05 (Fig. 4.4). Relative to non-siluriform otophysans, the onset of ossification of 14 bones in catfishes is delayed, all of which are chondral elements of the suspensorium (anguloarticular, anterior ceratohyal, basibranchials 2 and 3, ceratobranchials 1–5, hyomandibular, metapterygoid, quadrate, retroarticular, and ventral hypohyal). The remaining 12 bones were recovered as occurring significantly earlier in catfishes and include elements of the fins (coracoid, pectoral-fin rays, pelvic-fin rays and principle caudal-fin rays), vertebral column (the hemal arches, neural arches of centrum 4 and 5 and preural centrum 3, parapophyses, preural centrum 3, and ural centrum 1) and neurocranium (frontal). Of the

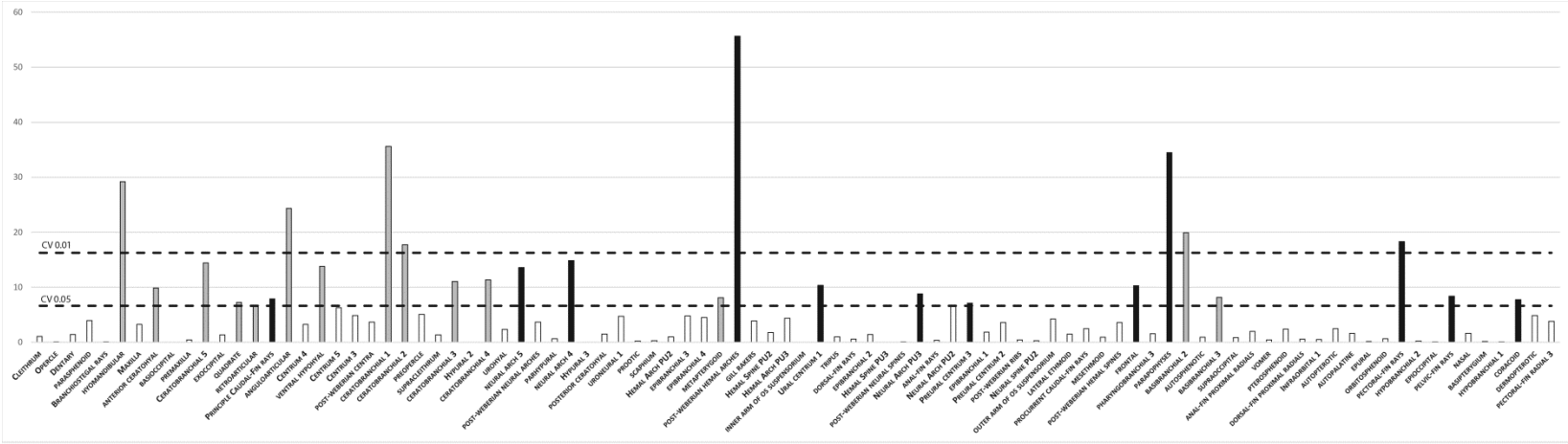

Figure 4.4. Results of the analysis of variances of the entire ossification sequence (93 elements) between siluriforms and non-siluriform otophysans. Bars represent F-statistic. The dotted lines denote the critical value, CV, required for elelments to be considered statistically significant with a $P \leq 0.05$ (lower) and $P \leq 0.01$ (upper). Shifts that can be observed between the two groups are statistically significant when they exceed the dotted line. Elements found to be significant which ossify later in siluriforms relative to non-siluriform otophysans are grey and those which ossify earlier in siluriforms relative to non-siluriform otophysans are black.

aforementioned 26 bones, eight were significant at a p-value ≤ 0.01, including the anguloarticular, basibranchial 2, ceratobranchials 1 and 2, hemal arches, hyomandibular, parapophyses and pectoral-fin rays. In the cranium and postcranial skeleton, a total of nine ossifications were recovered as significantly different between siluriforms and non-siluriform otophysans at a p-value ≤ 0.05 (basibranchial 3, ceratobranchial 2, hemal and neural spine of preural centrum 2, hyomandibular, maxilla, pectoral-fin rays, pelvic-fin rays, and uroneural 1) and an additional five elements significant at a p-value ≤ 0.01 (basibranchial 2, ceratobranchial 1, frontal, hemal arches and parapophyses) (Fig. 4.5). Of the four elements that were not also found to be significant in the whole skeleton analysis, three ossify later in the timing of ossification of siluriforms relative to non-siluriform otophysans (the hemal and neural spine of preural centrum 2 and uroneural 1) and one, the maxilla, is accelerated in the onset of ossification of siluriforms relative to the non-siluriform otophysans.

Sequence-ANOVA analysis of the four regional subcomponents of the skeleton identified 18 elements that significantly differed (p-value ≤ 0.05) in the timing of ossification between siluriforms and non-siluriform otophysans, six of which were identified to be significant at a p-value ≤ 0.01 (hemal arches, hemal spine of preural centrum 2, maxilla, pectoral-fin rays, parapophyses and the ventral hypohyal) (Fig. 4.6, 4.7). Six of the 18 bones were not previously recovered as significant in analyses of either the whole skeleton or the cranial/postcranial skeleton. Three of these bones were determined to ossify significantly earlier (anal-fin proximal radials, branchiostegal rays,

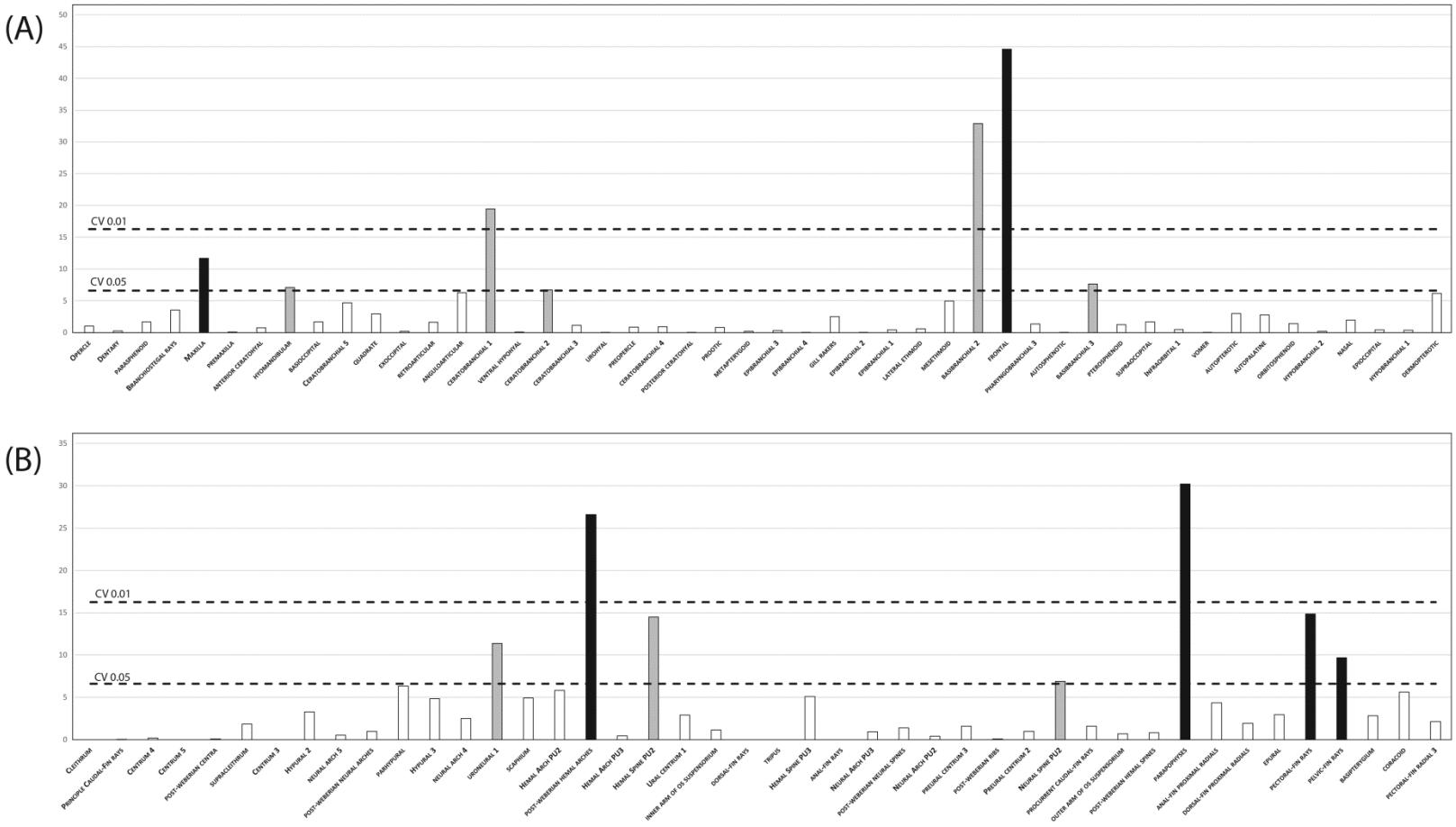

Figure 4.5. Results of the analysis of variances of the (**A**) cranial (48 elements) and (**B**) postcranial skeleton (45 elements) between siluriforms and non-siluriform otophysans. Bars represent F-statistic. The dotted lines denote the critical value, CV, required for elelments to be considered statistically significant with a $P \leq 0.05$ (lower) and $P \leq 0.01$ (upper). Shifts that can be observed between the two groups are statistically significant when they exceed the dotted line. Elements found to be significant which ossify later in siluriforms relative to non-siluriform otophysans are grey and those which ossify earlier in siluriforms relative to non-siluriform otophysans are black.

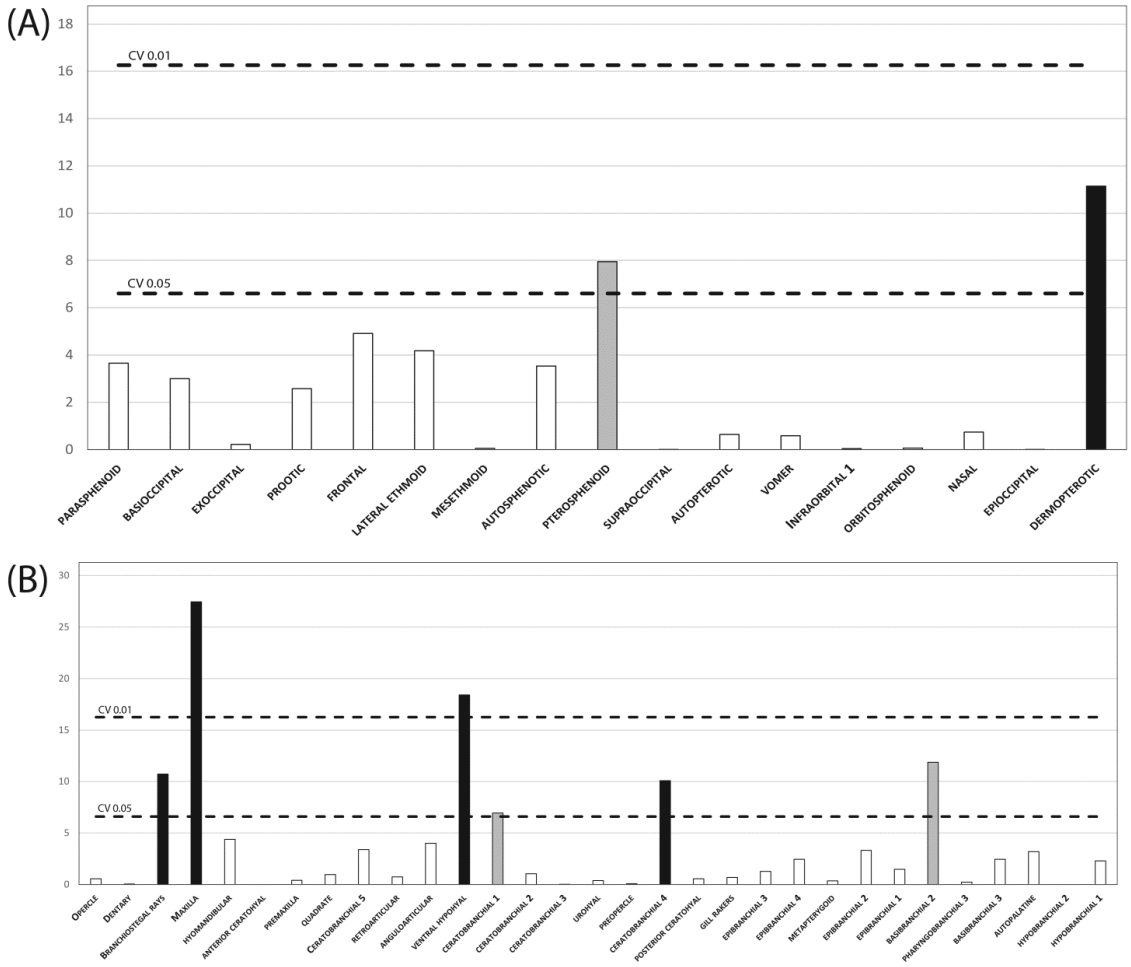

Figure 4.6. Results of the analysis of variances of the (**A**) neurocranium (17 elements) and (**B**) splanchnocranium and associated dermal bones (31 elements) between siluriforms and non-siluriform otophysans. Bars represent F-statistic. The dotted lines denote the critical value, CV, required for elelments to be considered statistically significant with a $P \leq 0.05$ (lower) and $P \leq 0.01$ (upper). Shifts that can be observed between the two groups and are statistically significant when they exceed the dotted line. Elements found to be significant which ossify later in siluriforms relative to non-siluriform otophysans are grey and those which ossify earlier in siluriforms relative to non-siluriform otophysans are black.

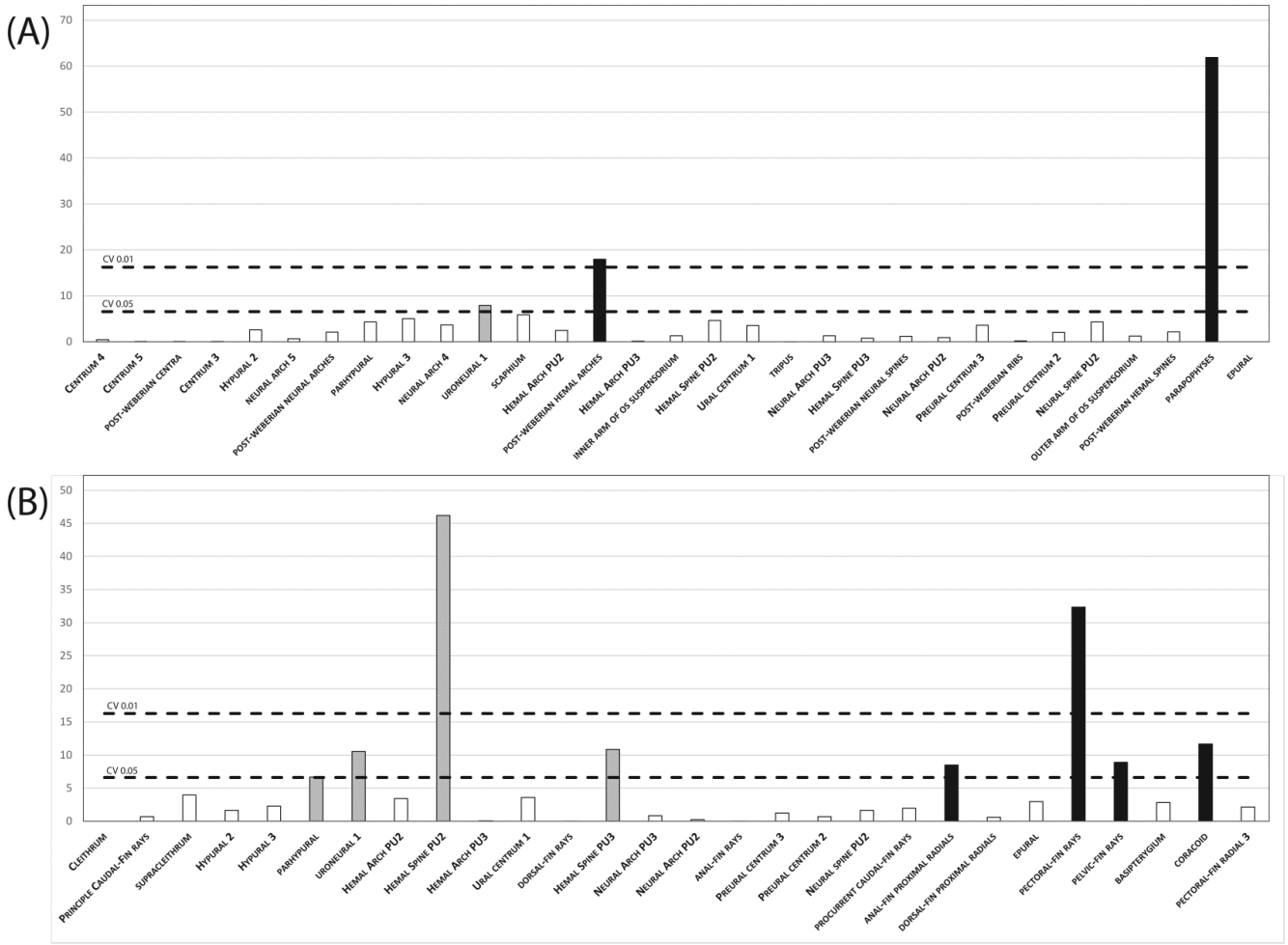

Figure 4.7. Results of the analysis of variances of the (**A**) vertebral column (31 elements) and (**B**) median and paired fins (29 elements) between siluriforms and non-siluriform otophysans. Bars represent F-statistic. The dotted lines denote the critical value, CV, required for elelments to be considered statistically significant with a $P \leq 0.05$ (lower) and $P \leq 0.01$ (upper). Shifts that can be observed between the two groups and are statistically significant when they exceed the dotted line. Elements found to be significant which ossify later in siluriforms relative to non-siluriform otophysans are grey and those which ossify earlier in siluriforms relative to non-siluriform otophysans are black.

and dermopterotic), and three were significantly delayed in the onset of ossification (hemal spine of preural centrum 3, parhypural, and pterosphenoid) in siluriforms compared to non-siluriform otophysans. Two elements which were previously recovered as significantly ossifying later in siluriforms in the whole skeleton analysis (ceratobranchial 4 and ventral hypohyal) were found to ossify significantly earlier compared to non-siluriform otophysans in the analysis of the suspensorium and associated dermal bones.

A summary of all elements recovered as being significantly different in siluriforms relative to non-siluriform otophysans in the results of the sequence-ANOVA analyses is provided in Table 4.1. A total of 36 different bones (~ 39% of the elements analyzed) were recovered as significantly different in siluriforms compared to non-siluriform otophysans; however, 20 of these were only found to be significant at one hierarchical level of the skeleton (six regional, one cranial/postcranial, and 13 whole). Of the remaining 16 elements, 10 were found to be significant in two of the three hierarchical analyses (basibranchial 3, ceratobranchials 2 and 4, coracoid, frontal, hemal spine of preural centrum 2, hyomandibular, maxilla, uroneural 1 and the ventral hypohyal). The remaining six (basibranchial 2, ceratobranchial 1, hemal arches, parapophyses, pectoral-fin rays and pelvic fin rays) were recovered as significantly different in all of the analyses, five (all but the pelvic-fin rays) of which were significant at a p-value ≤ 0.01 in at least two of the three analyses.

Table 4.1. Summary of elements recovered by the sequence-ANOVA analyses as significantly different in the relative timing of ossification between siluriform and non-siluriform otophysans for the whole skeleton, cranial/postcranial skeleton, and regional skeleton (Neurocranium, Splanchnocranium, Vertebral Column, and Median and Paired Fins) datasets.

Bone	Regional Skeleton	Cranial/Postcranial Skeleton	Whole Skeleton
Basibranchial 2	*	**	**
Ceratobranchial 1	*	**	**
Hemal Arches	**	**	**
Parapophyses	**	**	**
Pectoral-Fin Rays	**	*	**
Pelvic-Fin Rays	*	*	*
Uroneural 1	*	*	
Hemal Spine of Preural Centrum 2	**	*	
Maxilla	**	*	
Ceratobranchial 4	*		*
Coracoid	*		*
Ventral Hypohyal	**		*
Basibranchial 3		*	*
Ceratobranchial 2		*	**
Frontal		**	*
Hyomandibular		*	**
Anal-Fin Proximal Radials	*		
Hemal Spine of Preural Centrum 3	*		
Parhypural	*		
Branchiostegal Rays	*		
Dermopterotic	*		
Pterosphenoid	*		
Neural Spine of Preural Centrum 2		*	
Anguloarticular			**
Anterior Ceratohyal			*
Ceratobranchial 3			*
Ceratobranchial 5			*
Metapterygoid			*
Neural Arch 4			*
Neural Arch 5			*
Neural Arch Preural Centrum 3			*
Prinicpal Caudal-Fin rays			*
Preural Centrum 3			*
Quadrate			*
Retroarticular			*
Ural Centrum 1			*
Basibranchial 2			

*P-value ≤ 0.05, **P-value ≤ 0.01

PGi

All 93 skeletal elements were designated an event number which is used as a placeholder for the name of the bone in the analysis (Table. 4.2). In the analysis of the entire skeleton 15 sequence heterochronies were recovered on the branch leading to the most recent common ancestor (MRCA) of the siluriforms included in this analysis (Fig. 4.8). The dermopterotic, frontal, mesethemoid, pectoral-fin rays, pelvic-fin rays and principle caudal-fin rays were recovered as accelerated in the onset of ossification of the MCRA of siluriforms while the anguloarticular, anterior ceratohyal, basibranchial 2, ceratobranchial 4, hemal arches, hyomandibular, preopercle, quadrate and supraoccipital were shifted later in the sequence of ossification of the MCRA of siluriforms. The results of the cranium/post-cranial skeletal analyses also recovered 15 sequence heterochronies on the branch leading to the MRCA the siluriforms. The dermopterotic, hemal arches, pectoral-fin rays and preopercle, which were also recovered as shifts in the whole skeleton analysis, were recovered again as shifts in the cranial/postcranial PGi analysis; however, the hemal arches were inferred to be accelerated in the onset of ossification rather than delayed, as was found in the analysis of the whole sequence. The remaining 11 heterochronic shifts recovered include an acceleration in the onset of ossification of the autopalatine, basioccipital, coracoid, infraorbital 1, and parapophyses, and a delay in the onset of ossification of the ceratobranchial 2, dentary, dorsal-fin rays, epibranchial 2, hypural 2 and the opercle. 13 sequence heterochronies were recovered on the branch leading to the MRCA of the siluriforms. The autopalatine, basibranchial 2, ceratobranchial 2, dentary, dermopterotic and parapophyses were again inferred as

Table 4.2. List of skeletal elements sorted according to event number in the PGi Analysis.

Bone	No. of Event	Bone	No. of Event
Cleithrum	1	Hemal Spine of Preural Centrum 3	48
Opercle	2	Metapterygoid	49
Basioccipital	3	Post-Weberian Neural Spines	50
Ceratobranchial 5	4	Epibranchial 4	51
Parasphenoid	5	Gillrakers	52
Exoccipital	6	Epibranchial 3	53
Hyomandibular	7	Epibranchial 2	54
Centrum 4	8	Dorsal-fin Rays	55
Branchiostegal Rays	9	Epibranchial 1	56
Dentary	10	Anal-fin Rays	57
Centrum 5	11	Post-Weberian Ribs	58
Centrum 3	12	Parapophyses	59
Anterior Ceratohyal	13	Neural Arch of Preural Centrum 3	60
Maxilla	14	Neural Arch of Preural Centrum 2	61
Centra	15	Procurrent Caudal-fin Rays	62
Retroarticular	16	Supraoccipital	63
Quadrate	17	Hemal Spines	64
Principle Caudal-fin Rays	18	Outer Arm Os Suspensorium	65
Premaxilla	19	Neural Spine of Preural Centrum 2	66
Angulararticular	20	Posterior Ceratohyal	67
Ceratobranchial 2	21	Autosphenotic	68
Ceratobranchial 1	22	Pterosphenoid	69
Neural Arch 5	23	Autopterotic	70
Post-Weberian Neural Arches	24	Anal-fin Proximal Radials	71
Prootic	25	Frontal	72
Hypural 2	26	Pectoral-fin Rays	73
Hypural 3	27	Orbitosphenoid	74
Ventral Hypohyal	28	Infraorbital 1	75
Neural Arch 4	29	Epural	76
Supracleithrum	30	Basibranchial 2	77
Ceratobranchial 4	31	Dorsal-fin Proximal Radials	78
Ceratobranchial 3	32	Pharyngobranchial 3	79
Ural Centrum	33	Mesethmoid	80
Preopercle	34	Autopalatine	81
Parhypural	35	Basibranchial 3	82
Scaphium	36	Epioccipital	83
Uroneural 1	37	Vomer	84
Lateral Eethmoid	38	Coracoid	85
Hemal Arch of Preural Centrum 2	39	Scapula	86
Urohyal	40	Pelvic-fin Rays	87
Tripus	41	Nasal	88
Inner Arm of Os Suspensorium	42	Basypterygia	89
Hemal Arches	43	Pectoral Radial 3	90
Preural Centrum 3	44	Dermopterotic	91
Hemal Arch of Preural Centrum 3	45	Hypobranchial 1	92
Preural Centrum 2	46	Hypobranchial 2	93
Hemal Spine of Preural Centrum 2	47	Hemal Spine of Preural Centrum 3	48

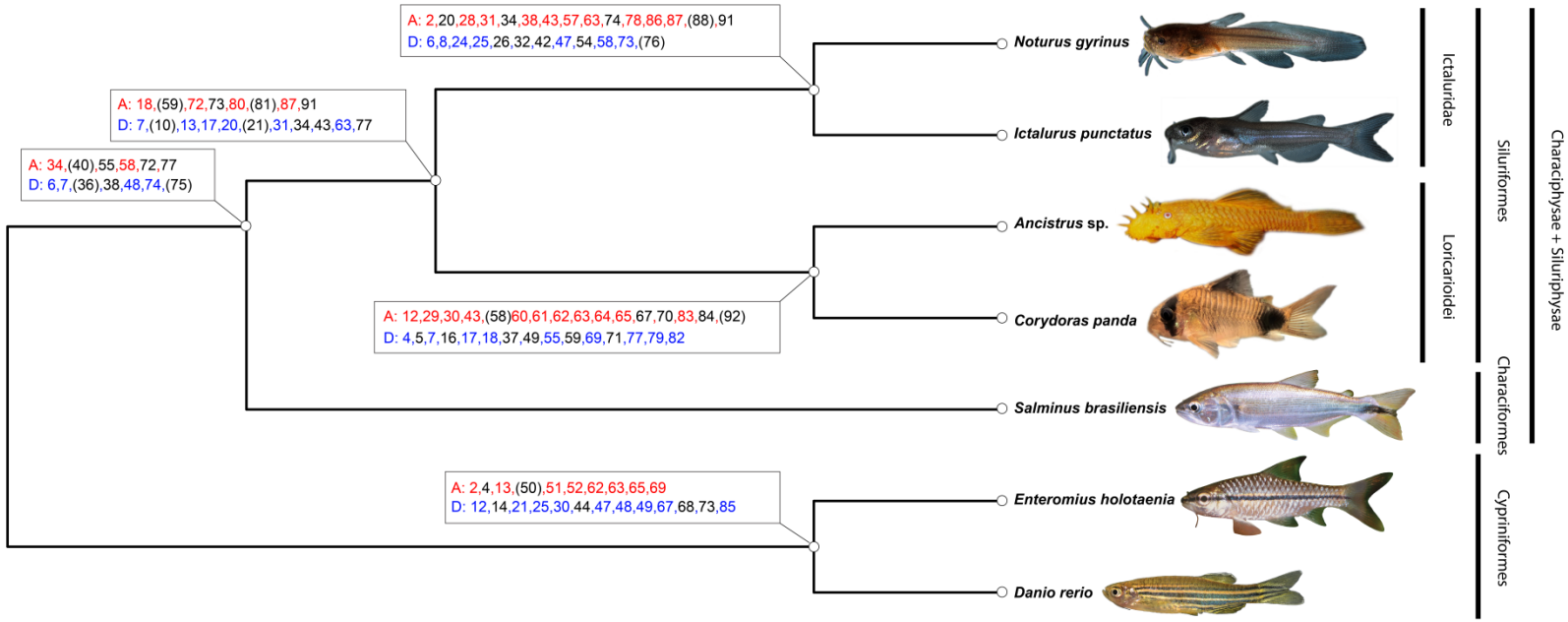

Figure 4.8. Sequence heterochronies at ancestral nodes resulting from the Parsimov analysis of 108 bony elements of the siluriforms, *Ictalurus punctatus*, *Noturus gyrinus*, *Corydoras panda*, and *Ancistrus* sp., the characiform *Salminus brasiliensis*, and the cyprinids, *Danio rerio* and *Enteromius holotaenia*. Numbers correspond to individual elements (see Table 2). Elements inferred as accelerated (A) or delayed (D) in relation to the ancestral node are shown in red or blue, respectively. Elements inferred as shifted in relation to the ancestral node in two or more PGi analyses are in black with those in brackets not inferred to be shifted in the whole skeleton analysis.

heterochronic shifts. Additionally, the autopterotic, metapterygoid and pectoral-radial 3 were recovered as shifting earlier in the development of catfishes while ceratobranchial 1, hemal arch of preural centrum 2, parasphenoid and premaxilla were delayed in the onset of ossification

In total, 33 distinct skeletal elements (~35 % of those included in the dataset) were inferred to have shifted along the branch leading from the MRCA of the Characiphysae+Siluriphysae (excluding Gymnotiformes) to the MRCA of the Siluriformes in at least one of the three separate PGi analyses in which they were included. Of the 33 elements, nine were inferred to have shifted in two of three PGi analyses (autopalatine, basibranchial 2, ceratobranchial 2, dentary, hemal arches, parapophyses, pectoral-fin rays, pelvic-fin rays and preopercle) (Fig. 4.8). Only a single element, the dermopterotic, was inferred to have shifted along the branch leading from the MRCA of the Characiphysae+Siluriphysae to the MRCA of the Siluriformes in all three of the PGi analyses in which this element was included (Fig. 4.8).

In addition to the heterochronic shifts that characterize Siluriformes, the PGi analyses also recovered several shifts, in at least two of the three analyses, that occurred on the branches leading to the MRCA of Cypriniformes, MRCA of Characiphysae+Siluriphysae, MRCA of Ictaluridae, and MRCA of Loricarioidei (Fig. 4.8). This includes the inferred earlier shift of ceratobranchial 5 and the post-Weberian neural spines, and the inferred delay in the onset of ossification of the autosphenotic, maxilla, pectoral-fin rays and preural centrum 3 on the branch leading from the MRCA of Otophysi to the MRCA of Cypriniformes. On the branch leading to the common

ancestor of Characiphysae+Siluriphysae, the dorsal-fin rays, frontal and urohyal were inferred to be accelerated in the onset of ossification and the hyomandibular, infraorbital 1, lateral ethmoid and scaphium inferred to be delayed in the onset of ossfication. A shift in the position of the frontal and hyomandibular were recovered in all three analyses while the remaining five shifts were only found in two out of three analyses. A total of nine sequence heterochronies were consistently recovered in two out of three analyses for the Ictaluridae, five of which were shifting earlier in the sequence of the MRCA of the group (anguloarticular, dermopterotic, nasal, orbitosphenoid, and preopercle) while the remaining four were delayed in the onset of ossification (ceratobranchial 3, epural, hypural 2, and the inner arm of the os suspensorium). Finally, 11 shifts were recovered on the branch leading from the MRCA of the Siluriformes to the MRCA of the Loricarioidei in relation to the MRCA of Siluriformes. These included the autopterotic, hypobranchial 1, posterior ceratohyal, ribs and vomer being accelerated in the onset of ossification and the anal-fin proximal radials, metapterygoid, parasphenoid, retroarticular, and uroneural 1 being delayed in the onset of ossification. Of these, the shifts in the posterior ceratohyal, uroneural 1 and vomer were found in all three analyses.

Discussion

Comparison of Methods

The sequence-ANOVA and the PGi analyses were variable in their results and both analyses recovered several shifts in elements in at least one of three hierarchical analyses (19 in the ANOVA and 14 in the PGi analysis) that were not recovered using the alternative methodology. 17 skeletal elements were identified as changing in their

relative timing of ossification in catfishes relative to non-siluriform otophysans in both the sequence-ANOVA and PGi analyses. Of the 17, 14 were consistent in the change in relative timing of appearance compared to non-siluriform otophysans (i.e., earlier, later) with seven being accelerated in the onset of ossification of catfishes (the coracoid, dermopterotic, frontal, parapophyses, pectoral-fin rays, pelvic-fin rays, and principle caudal-fin rays). The other seven were delayed in the onset of ossification (angulocarticular, anterior ceratohyal, basibranchial 2, ceratobranchials 1 and 2, hyomandibular and the quadrate), all of which are chondral components of the splanchnocranium. The remaining three elements (metapterygoid, hemal arches, ceratobranchial 4) showed variation in the change of relative timing recovered by the analyses. The metapterygoid was recovered as appearing significantly later in the ossification sequence catfishes compared to non-siluriform otophysans in the whole skeleton sequence-ANOVA while it is inferred as accelerating in the onset of ossification in the regional PGi analysis. This can be explained when looking at the ranked data of the catfishes in which the ranks for the ictalurids are higher than the non-siluriform otophysans while the ranks in the loricarioids are lower than the non-siluriform otophysans. As a result, it is clear that this is likely not a shift common to catfishes but rather due to artifacts of the analyses (discussed in more detail below). A similar issue is in the hemal arches, which appears significantly earlier in the sequence of ossification of catfishes in all three sequence-ANOVA analyses as well as the postcranial PGi analysis but as a later shift in the whole skeleton PGi analysis. The delay of the hemal arches recovered on the branch leading to catfishes in the whole skeleton

analysis is followed by an acceleration on the branches leading to ictalurids and loricarioid catfishes that was recovered in 100 % of runs used to generate the superconsensus tree. This is likely an artifact of the PGi analysis due to the limitations placed on the analysis to prevent excessive computing time (discussed in more detail below). Ceratobranchial 4 is a more interesting case and is recovered as appearing significantly later in catfishes compared to non-siluriform otophysans in both the sequence-ANOVA and PGi analysis of the whole skeleton and appearing significantly earlier in the regional sequence-ANOVA analysis. In relation to the whole skeleton, there is a consistent trend of a later appearance in several chondral elements of the splanchnocranium and this may also be the case for ceratobranchial 4. However, when comparing this element to others within the same region of the skeleton, the result of the earlier appearance coincides with the order of ossification of the ceratobranchials in catfishes in which ceratobranchial 4 is the first to appear (see chapter II).

A large number of the elements included in the dataset were recovered to be either significantly different in siluriforms compared to non-silurform otophysans (36 of 93 for sequence-ANOVA) or as shifts on the branch leading to the MRCA of catfishes (33 of 93 for PGi anlyses). By running multiple hierarchical analyses, it becomes clear that most of the shifts (20 of 36 for sequence-ANOVA and 24 of 33 for PGi) occurred only in a single hierarchical level of the skeleton (whole, cranial/postcranial, or regional) and although they potentially represent actual differences (or shifts) in developmental timing between species, they could also represent artifacts of the different methods of analysis. For example, sequence-ANOVA of Nunn and Smith (1998) is a parametric

statistical analysis which assumes a normal distribution of the data; however, the rank-ordered sequence data is not normally distributed and as a result the probability of rejecting a true null hypothesis (Type I error) is increased. In order to test the consequences of violating non-normality, Nunn and Smith (1998) ran a series of simulations to determine the effect of the number of taxa and developmental events on Type I and Type II errors and although they recovered only slightly increased Type I error rates, they showed that Type I error increased with both the number of taxa and elements added to the analysis. Some authors (Hautier et. al; 2011, 2013) have attempted to mitigate the increase in Type 1 error by analyzing their data using the non-parametric Mann-Whitney U test to corroborate the results of the sequence-ANOVA. Unfortunately, due to the small number of taxa in the present study (n=7), a Mann-Whitney U test could not be run. Given that most of the elements recovered to be significantly different in only one of the three hierarchical levels had F-statistics only slightly above the critical value for a p-value ≤ 0.05, it is possible that these differences are the result of Type 1 error and should not be considered as potential sequence heterochronies.

The way in which the PGi analysis computes sequence heterochronies can also lead to artifacts. When calculating the sequence heterochronies along branches from the reconstructed ancestral sequences, the program will run through every possible combination of sequence heterochronies in order to determine the lowest number of heterochronies that can explain the change in the sequence between two nodes (Harrison & Larsson, 208). Although this is not an issue with smaller datasets, when the number of

elements is increased the number of possible solutions increases exponentially. As a result, only a semi-exhaustive search is conducted by setting a limit on the number of times the analysis will traverse each branch in order to compute the result in a reasonable period of time (<1 month, Harrington, Harrison, & Sheil, 2013). Although Harrington et al. (2013) compared the results of the semi-exhaustive search with a fully exhaustive search on smaller data sets and recovered similar results, due to the limits caused by the semi-exhaustive search, the shifts that are recovered in individual runs may not be reflective of actual shifts in the sequences, especially in larger datasets. This is compounded by the heuristic nature of the analysis which significantly reduces the number of possible solutions to be searched. Although this can be mitigated by combining multiple independent runs into a superconsensus for a more robust result (Harrison & Larsson; 2008; Harrington, Harrison, & Scheil, 2013; Maxwell, Harrison, & Larsson, 2010), only those shifts that are found in multiple analyses should be considered to represent potential heterochronic shifts.

Sequence Heterochrony in Siluriformes

As a result of the issues mentioned above, only those bones that are identified to have shifted in the inferred sequence of MRCA of Siluriformes in at least four of the six different analyses are considered herein as potential sequence heterochronies within catfishes. Eight different bones meet this requirement (Table 4.3), including the dermopterotic, basibranchial 2, ceratobranchials 1 and 2, hemal arches, parapophyses, pectoral-fin rays and pelvic-fin rays. The dermopterotic and pelvic-fin rays were interesting in that they were both recovered in all three analyses using the PGi and

Table 4.3. Skeletal elements recovered as sequence heterochronies from a combination of both sequence-ANOVA and PGi analysis using regional, cranial/postcranial, and whole-skeleton data sets.

	Sequence-ANOVA			PGi		
Bone	**R**	**C/P**	**W**	**R**	**C/P**	**W**
Hemal Arches	**	**	**		Earlier	Later
Parapophyses	**	**	**	Earlier	Earlier	
Pectoral-Fin Rays	**	*	**		Earlier	Earlier
Basibranchial 2	*	**	**	Later		Later
Pelvic-Fin Rays	*	**	**			Earlier
Ceratobranchial 1	*	**	**	Later		
Ceratobranchial 2		*	**	Later	Later	
Dermopterotic	*			Earlier	Earlier	Earlier

*P-value ≤ 0.05, **P-value ≤ 0.01

sequence-ANOVA methods respectively but only one out of three analyses using the alternative methodology. The individual ranks of the dermopterotic and pelvic-fin rays for the catfishes reveal that although they do appear earlier in *I. punctatus*, *N. gyrinus*, and *Ancistrus* sp., they appear in *C. panda* at a similar position to that of the non-siluriform otophysans. This would imply that either a secondary shift has occurred in *C. panda*, resulting in a position convergent with the non-siluriform otophysans, or that the shift in these two elements may in fact be representative of multiple independent shifts of these two elements earlier in the sequence of ossification within the different groups of catfishes. Basibranchial 2 and ceratobranchials 1 and 2 were interpreted to appear later in the development of catfishes compared to other otophysans in the results of the PGi analysis. In addition to this, several other elements of the gill arches were also variably interpreted as appearing later in the development of siluriforms compared to

non-siluriform otophysans in the analysis of the whole skeleton data set using both methodologies. Catfishes typically possess an enlarged yolk-sac that can persist for several days after hatching (ranging from ~3 days in *C. panda* to ~ 9 days in *N. gyrinus*; Pers. Obs.) with exogenous feeding starting around complete resorption of the yolk-sac (Kozarić, 2008; de Amorim et al., 2009). This delay in active feeding may explain the pattern of ossifications appearing later in the overall sequence of ossification of siluriforms compared to-non siluriform otophysans. There also appears to be an acceleration in the appearance of the ossification of the post-Weberian basiventral cartilages, as both the post-Weberian parapophyses and hemal arches (which develop from the basiventral cartilage precursors) were consistently recovered as shifted and the most significantly different elements between the siluriform and non-siluriform otophysans in the sequence-ANOVA analyses.

Finally, the pectoral-fin rays were found consistently to be associated with an accelerated appearance in the sequence of skeletal development in catfishes. The anteriormost pectoral-fin ray is highly modified into a robust lockable spine in catfishes, which is known to exhibit large amounts of morphological variation (Vanscoy, Lundberg, & Luckenbill, 2015; Kubicek, Britz & Conway, 2019) and is commonly associated with venom glands (Wright, 2009). Despite the morphological diversity observed in the pectoral-fin spine, it has been shown to develop from a single common ontogenetic pathway (Kubicek, Britz, & Conway, 2020). This structure is known to serve a multitude of different functions in catfishes, including defense (Alexander, 1966; Bosher, Newton, &Fine, 2006; Wright, 2009), sound production (Fine et al.,1996;

Pruzsinszky, & Ladich, 1998; Kaatz, Stewart, Rice & Lobel, 2010), terrestrial locomotion (Johnels, 1957), and has even been reported to play a role in reproductive behavior, including male territorial defense (Winemiller, 1987; Pruzsinszky, & Ladich, 1998). Considering the presumed rapid diversification of catfishes (Hardman, 2002, 2005; Sullivan, Lundberg, & Hardman, 2006) as well as the variety of important functions associated with the remarkably diverse structure, the pectoral-fin spine of catfishes may represent a key innovation (sensu Hunter, 1998). Heterochrony has previously been shown in other groups of vertebrates to be associated with major changes to morphology, life history, and function, some of which are frequently considered within the context of evolutionary key innovations (e.g., the accelerated development of the cranial and forelimb skeleton in marsupials relative to placental mammals; Goswami, Weisbecker, & Sánchez-Villagra, 2009; Sears, 2009; Keyte & Smith, 2010). In this context, the accelerated appearance of the pectoral-fin rays in catfishes compared to other non-siluriform otophysans may provide another rare example of the link between heterochrony and the evolution of morphological innovation.

Conclusions

This study represents one of the first modern studies of sequence heterochrony to focus on a group of bony fishes, the catfishes. The results of the analysis herein revealed several different patterns of development within catfishes and recovered potential sequence heterochronies for several elements. This includes an association between heterochrony and the pectoral-fin spine of catfishes, which represents a remarkable

innovation of this highly successful group. Additionally, I show that running sequence analyses on multiple hierarchical subcomponents of the skeleton, rather than only a single dataset as is common among previous studies (e.g., Sánchez-Villagra et al., 2008; Weisbecker, Goswami, Wroe, & Sánchez-Villagra, 2008; Hautier et al., 2011, 2013; Werneburg & Sánchez-Villagra, 2015), can reveal elements that may exhibit different patterns of development at small vs. large scales (e.g., ceratobranchial 4). Additionally, running different analyses on multiple hierarchical datasets can help to elucidate which elements are shifting regardless of the data set, increasing the likelihood of identifying actual shifts in developmental timing.

CHAPTER V

CONCLUSION

Studies of skeletal ontogeny, in addition to furthering our general knowledge of skeletogenesis in fishes, have shown to be effective in resolving issues of homology (e.g., Britz & Hoffman, 2006; Hilton & Johnson, 2007; Britz & Johnson, 2012), providing novel morphological information for systematic studies (e.g., Johnson, 1983; Johnson & Washington, 1987; Kubicek & Conway, 2016), and identifying changes in developmental timing that may have played a major role in generating the tremendous morphological diversity that exists among and between different groups of bony fishes (Mabee & Trendler, 1996; Mattox, Britz & Toledo-Piza, 2016). The catfishes (order Siluriformes) exhibit a highly modified skeleton in comparison to other groups of bony fishes and this fascinating anatomical structure has been the subject of dozens of studies (Alexander, 1966; Rao, & Lakshmi 1984; Brown & Ferraris, 1987; Diogo, Oliveira, & Chardon, 2001; Arratia, 2003a,b; Huysentruyt & Adriaens, 2005; Rodiles-Hernández, Hendrickson, Lundberg, & Humphries, 2005; Egge, 2007; Vigliotta, 2008; Britz, Kakkassery, & Raghavan, 2014 Carvalho, & Reis, 2020). Despite this interest, the homology of many elements of the catfish skeleton have remained contentious (Lundberg, 1975; Arratia & Gayet, 1995; Slobodian and Pastana, 2018), likely because studies examining early developmental stages are few (in comparison to the number of studies conducted on adults), focused only on a specific part of the skeleton, and limited in the breadth of taxa studied (e.g., ~7 of 43 valid families; Kindred, 1919; Bamford,

1948; Srinivasachar, 1958; Adriaens & Verraes, 1998; Grande & Shardo, 2002; Arratia, 2003a,b; Geerinckx, Brunain, & Adriaens, 2007; Huysentruyt, Geerinckx, Brunain, & Adriaens, 2011).

In this dissertation, I conducted three separate studies that further our understanding of the catfish skeleton, and the skeleton of bony fishes in general. This includes: (1) a detailed developmental study of the entire skeleton in two species of catfishes (both family Ictaluridae) in order to address long standing issues of homology; (2) a detailed comparative study of the development of the morphologically diverse pectoral-fin spine in both siluroid and loricarioid taxa with the goal to standardize pectoral-fin spine terminology for systematic studies; and (3) the first modern study of sequence heterochrony in a close related group of bony fishes (Otophysi).

In Chapter II, I describe in detail the development of the skeleton in *Ictalurus punctatus* and *Noturus gyrinus* and provide a high quality photographic atlas to illustrate select aspects of skeletal development. Catfishes possesses several elements which have previously been proposed to represent the developmental fusion of two elements which are separate in other teleosts, including the parieto-supraoccipital, posttemporo-supracleithrum, scapulocoracoid, urohyal, and lacrimal (infraorbital 1). Throughout the development of both species, no evidence for ontogenetic fusion was observed and the parietal, posttemporal and antorbital are interpreted as absent in ictalurid catfishes. For some of these elements (supraoccipital, urohyal; Bamford, 1948; Arratia & Schultze, 1990; Geerinckx, Brunain & Adriaens, 2007), evidence or accounts exist which may suggest that ontogenetic fusion in these elements is variable within catfishes. The

supraoccipital, typically a median element that arises from a single center of ossification in most teleosts (Cubbage & Mabee, 1996; Mattox, Britz & Toledo-Piza, 2014; Kubicek & Conway, 2016), exhibits a unique ontogeny in some catfishes, in which it arises as a pair of ossifications which later fuse into a single median element (Bamford, 1948; Geerinckx, Brunain, & Adriaens, 2007; Chapter II). Given that most of the information available on skeletogenesis in siluriforms is limited to a few species, developmental studies of additional species representing different families of catfishes are needed to fully understand the variation that exists in the development of these highly modified skeletal elements and whether or not this variation may represent novel information that can be utilized in future systematic studies.

In Chapter III, the examination of the earliest stages of development in four siluroid (*Akysis vespa*, *I. punctatus*, *N. gyrinus*, and *Silurus glanis*) and two loricarioid catfishes (*Corydoras panda* and *Ancistrus* sp.) revealed that the earliest stages in the ontogeny of the morphologically diverse pectoral-fin spine are greatly conserved across these taxa. Despite being an important source of information for the systematic studies of extant (Ng and Kottelat, 1998; Ng and Tan, 1999; Thomas and Burr, 2004; Rocha, Oliveira, & Py-Daniel, 2008; Carvalho and Reis, 2009; Rodiles-Hernández, Lundberg, & Sullivan 2010) and extinct (Hubbs and Hibbard, 1951; Lundberg & Case, 1970; Grande & Lundberg, 1988; Pinton, Fara, & Otero 2006) catfishes, the terminology (dentations, serrations, and denticulations) used in descriptions of the pectoral-fin spine ornamentation have been inconsistently applied, undermining the usefulness of this character source. By applying a common terminology based on the homology of

pectoral-fin spine morphology, the information that can be utilized in systematic studies not only becomes reliable but also increases due to the variable combination and morphology of pectoral-fin spine ornamentation (Vanscoy, Lundberg, & Luckenbill, 2015; Kubicek, Britz, & Conway, 2019). Additionally, as the pectoral-fin spine continuous to grow throughout the life of a catfish, the ontogeny of this element can be inferred even in later stages through examination of the spurious ray, the distal developing portion of the spine that houses developing segments that have yet to fuse to the spine proper. This allows for the use of a morphological character source based on development that is not constrained by the difficulty of obtaining early developmental stages. Given that the early development of the pectoral-fin spine in catfishes is greatly conserved, the morphological diversity of this structure appears to have resulted through only slight modifications in development. Obtaining a better understanding of the underlying genetic mechanisms of pectoral-fin ray formation (e.g., expression of genes controlling segmentation of lepidotrichia; Schulte, Allen, England, Juárez-Morales & Lewis, 2011) will likely be the next step needed to further our understanding of this remarkable morphological structure and shed additional light on how it has evolved.

In Chapter III, I examine the role of heterochrony in the evolution of the skeleton of catfishes. Studies of sequence heterochrony, or changes in the relative timing of developmental events in a sequence relative to all other events in the sequence (Smith, 2001), have been conducted using developmental sequence data in a variety of tetrapods (e.g., amphibians [Weisbecker & Mitgutsch, 2010; Harrington, Harrison, & Sheil, 2013], squamates [Hugi, Hutchinson, Koyabu, & Sánchez-Villagra, 2012; Ziermann,

Mitgutsch, & Olsson, 2014; Werneburg, & Sánchez-Villagra, 2015], crocodylians [Larsson, 1998], birds [Maxwell, Harrison, & Larsson, 2010; Carril, & Tambussi, 2017], and mammals [Nunn and Smith, 1998; Sánchez-Villagra et al., 2008; Weisbecker, Goswami, Wroe, & Sánchez-Villagra, 2008; Hautier et al., 2011]). These studies have revealed that heterochronic shifts during skeletogenesis are widespread among and between major groups of tetrapods and in many cases are associated with major changes to morphology, life history, and function (Goswami, Weisbecker, & Sánchez-Villagra, 2009; Sears, 2009; Keyte & Smith, 2010). Despite representing greater than half of all vertebrates (Nelson, Grande, & Wilson, 2016) having a greater potential of exhibiting sequence heterochronies due to possessing a more complex skeleton with a larger number of elements, studies of sequence heterochrony in fishes is rare (Mabee & Trendler, 1996; Ito, Matsumoto, & Hirata, 2019). I conduct the first modern study of sequence heterochrony on a closely related group of fishes (the Otophysi) in which the relationships are well studied (Fink & Fink, 1981; Arcila et al., 2017) in order to determine which heterochronic shifts, if any, are characteristic of catfishes and whether an association exists between heterochrony and the highly modified skeletal elements that represent synapormorphies of the Siluriformes. This study of sequence heterochrony, unlike most others that are available (e.g., Weisbecker & Mitgutsch, 2010; Hugi, Hutchinson, Koyabu, & Sánchez-Villagra, 2012; Werneburg, Hugi, Müller, & Sánchez-Villagra, 2009; Hautier et al., 2011, 2013) utilizes mulitple hierarchichal datasets (e.g., whole, cranial/postcranial, and regional skeleton) in order to identify which elements are consistently recovered as exhibiting changes in their relative timing

of appearance. This helps to mitigate the incorrect identification of events as being shifted in one sequence compared to another resulting from different methods of analysis. Additionally, different types of analyses have their own potential benefits and drawbacks, and as a result only those elements which are consistently identified by multiple analyses to have changed in their relative timing of appearance within a developmental sequence should be considered to represent potential heterochronic shifts. Of the eight different bones which were identified as potential heterochronic shifts in the early evolution of catfishes, the accelerated appearance of the pectoral-fin rays, of which the anteriormost is modified into the morphologically diverse pectoral-fin spine, provides evidence for the association of heterochrony with a remarkable morphological innovation in a highly successful group of fishes. However, sequence ossification data for additional otophysan taxa, particularly those which represent groups missing in our analyses (e.g., Gymnotiformes) are required in order to more accurately assess whether these recovered heterochronic shifts are indeed characteristic of catfishes. By obtaining additional data on the skeletogenesis of not only otophysan fishes, but actinopterygian fishes as a whole, we can gain a better understanding of the underlying evolutionary mechanisms responsible for generating the tremendous morphological diversity exhibited by this highly speciose and successful group of vertebrates. This would also allow us to identify whether heterochrony has played a role in the evolution of other potential key innovations of the Otophysi, including the Weberian apparatus (Bird & Mabee, 2013; D'Anatro, Giorello, Feijoo, & Lessa, 2017).

REFERENCES

Adriaens, D., & Verraes, W. (1998). Ontogeny of the osteocranium in the African catfish, *Clarias gariepinus* Burchell (1822) (Siluriformes: Clariidae): ossification sequence as a response to functional demands. *Journal of Morphology*, *235*, 183–237.

Alexander, R. McN. (1966). Structure and function in the catfish. *Journal of Zoology*, *148*, 88–152.

Alfaro, M. E., Santini, F., Brock, C., Alamillo, H., Dornburg, A., Rabosky, D. L., Carnevale, G. & Harmon, L. J. (2009). Nine exceptional radiations plus high turnover explain species diversity in jawed vertebrates. *Proceedings of the National Academy of Sciences*, *106*, 13410–13414.

de Amorim, M. P., Gomes, B. V. C., Martins, Y. S., Sato, Y., Rizzo, E., & Bazzoli, N. (2009). Early development of the silver catfish *Rhamdia quelen* (Quoy & Gaimard, 1824) (Pisces: Heptapteridae) from the São Francisco River Basin, Brazil. *Aquaculture Research*, *40*, 172–180.

Annandale, N. (1923). LVIII.—The classification of the Siluroid fishes belonging to the genus *Glyptosternum* and allied genera. *Journal of Natural History*, *12*, 573–577.

Arcila, D., Ortí, G., Vari, R., Armbruster, J. W., Stiassny, M. L., Ko, K. D., Sabaj, M. H., Lundberg, J., Revell, L. J., & Betancur-R, R. (2017). Genome-wide interrogation advances resolution of recalcitrant groups in the tree of life. *Nature Ecology & Evolution*, *1*, 1–10.

Arratia, G. (1987). Description of the primitive family Diplomystidae (Siluriformes, Teleostei, Pisces): morphology, taxonomy and phylogenetic implications. *Bonner Zoologische Monographien*, *24*, 1–120

Arratia, G. (1992) Development and variation of the suspensorium of primitive Catfishes (Teleostei: Ostariophysi) and their phylogenetic relationships. *Bonner Zoologische Monographien*, *32*, 1–149.

Arratia, G. (2003a). Catfish head skeleton—an overview. In: Arratia, G., Kapoor, B.G., Chardon, M., Diogo, R. (Eds.), *Catfishes*, vol.1. Science Publishers, Enfield, NH, pp. 3–46.

Arratia, G. (2003b). The siluriform postcranial skeleton—an overview. In: Arratia, G., Kapoor, B.G., Chardon, M., Diogo, R. (Eds.), *Catfishes*, vol. 1. Science Publishers, Enfield, NH, pp. 121–158.

Arratia, G., Chang G, A., Menu-Marque, S. M., & Rojas M, G. (1978). About *Bullockia* gen. nov., *Trichomycterus mendozensis* n. sp. and revision of the family Trichomycteridae (Pisces, Siluriformes). *Studies on Neotropical Fauna and Environment*, *13*, 157–194.

Arratia, G., & Gayet, M. (1995). Sensory canals and related bones of tertiary siluriform crania from Bolivia and North America and comparison with recent forms. *Journal of Vertebrate Paleontology*, *15*, 482–505.

Arratia, G. & Menu-Marque, S., (1981). Revision of the freshwater catfishes of the genus *Hatcheria* (Siluriformes, Trichomycteridae) with commentaries on ecology and biogeography. *Zoologischer Anzeiger*, *207*, 88–111.

Arratia, G., & Schultze, H. P. (1990). The urohyal: development and homology within osteichthyans. *Journal of Morphology*, *203*, 247–282.

Arratia, G., & Schultze, H. P. (1991). Palatoquadrate and its ossifications: development and homology within osteichthyans. *Journal of Morphology*, *208*, 1–81.

Bamford, T. W. (1948). Cranial development of *Galeichthys felis*. *Proceedings of the Zoological Society of London*, *118*, 364–391.

Ballen, G. A., Pastana, M. N., & Peixoto, L. A. (2016). A new species of *Farlowella* (Siluriformes: Loricariidae) of the *F. nattereri* species-group from the rio Xingu basin, Mato Grosso, Brazil, with comments on *Farlowella jauruensis*, a poorly-known species from the upper rio Paraguai basin. *Neotropical Ichthyology*, *14*(3).

Barbieri, L. R., dos Santos, R. P., & Andreata, J. V. (1992). Reproductive biology of the marine catfish, Genidens genidens (Siluriformes, Ariidae), in the Jacarepaguá Lagoon system, Rio de Janeiro, Brazil. *Environmental Biology of Fishes*, *35*, 23–35.

Bartsch, P., & Gemballa, S. (1992). On the anatomy and development of the vertebral column and pterygiophores in *Polypterus senegalus* Cuvier, 1829 ('Pisces', Polypteriformes). *Zoologische Jahrbücher. Abteilung für Anatomie und Ontogenie der Tiere*, *122*, 497–529.

de Beer, G. R. (1930). *Embryology and evolution*. Clarendon Press, Oxford.

de Beer, G. R. (1937). *The development of the vertebrate skull*. Clarendon Press, Oxford

Bird, N. C., & Mabee, P. M. (2003). Developmental morphology of the axial skeleton of the zebrafish, *Danio rerio* (Ostariophysi: Cyprinidae). *Developmental Dynamics*, *228*, 337–357.

Birindelli, J. L., Sousa, L. M., & Pérez, M. H. S. (2008). New species of thorny catfish, genus *Leptodoras* Boulenger (Siluriformes: Doradidae), from Tapajós and Xingu basins, Brazil. *Neotropical Ichthyology*, *6*, 465–480.

Block, A. J., & Mabee, P. M. (2012). Development of the mandibular, hyoid arch and gill arch skeleton in the Chinese barb *Puntius semifasciolatus*: comparisons of ossification sequences among Cypriniformes. *Journal of Fish Biology*, *81*, 54–80.

Bosher, B. T., Newton, S. H., & Fine, M. L. (2006). The spines of the channel catfish, *Ictalurus punctatus*, as an anti-predator adaptation: an experimental study. *Ethology*, *112*, 188–195.

Bridge, T. W. (1896). The Mesial Fins of Ganoids and Teleosts. *Zoological Journal of the Linnean Society*, *25*, 530–602.

Britz, R., & Conway, K. W. (2009). Osteology of *Paedocypris*, a miniature and highly developmentally truncated fish (Teleostei: Ostariophysi: Cyprinidae). *Journal of Morphology*, *270*, 389–412.

Britz, R., & Hoffmann, M. (2006). Ontogeny and homology of the claustra in otophysan Ostariophysi (Teleostei). *Journal of Morphology*, *267*, 909–923.

Britz, R., & Johnson, G. D. (2012). Ontogeny and homology of the skeletal elements that form the sucking disc of remoras (Teleostei, Echeneoidei, Echeneidae). *Journal of Morphology*, *273*, 1353–1366.

Britz, R., Kakkassery, F., & Raghavan, R. (2014). Osteology of *Kryptoglanis shajii*, a stygobitic catfish (Teleostei: Siluriformes) from Peninsular India with a diagnosis of the new family Kryptoglanidae. *Ichthyological Exploration of Freshwaters*, *24*, 193–207.

Brown, B. A., & Ferraris, C. J. (1988). Comparative osteology of the Asian catfish family Chacidae: with the description of a new species from Burma. *American Museum Novitates*, *1988*(2907), 1–16.

Calegari, B. B., Vari, R. P., & Reis, R. E. (2019). Phylogenetic systematics of the driftwood catfishes (Siluriformes: Auchenipteridae): a combined morphological and molecular analysis. *Zoological Journal of the Linnean Society*, *187*, 661–773.

Carril, J., & Tambussi, C. P. (2017). Skeletogenesis of *Myiopsitta monachus* (Psittaciformes) and sequence heterochronies in Aves. *Evolution & Development*, *19*, 17–28.

Carvalho, T. P., & Reis, R. E. (2009). Four new species of *Hisonotus* (Siluriformes: Loricariidae) from the upper rio Uruguay, southeastern South America, with a review of the genus in the rio Uruguay basin. *Zootaxa*, *2113*, 1–40.

Carvalho, T. P., & Reis, R. E. (2020). A New Miniature Species of *Acanthobunocephalus* (Silurifomes: Aspredinidae) from the Lower Purus River Basin, Amazon Basin, Brazil. *Copeia* (2020), 347–357.

Coburn, M. M., & Grubach, P. G. (1998). Ontogeny of the Weberian apparatus in the armored catfish *Corydoras paleatus* (Siluriformes: Callichthyidae). *Copeia* (1998), 301–311.

Conway, K. W., Kubicek, K. M., & Britz, R. (2017). Morphological novelty and modest developmental truncation in *Barboides*, Africa's smallest vertebrates (Teleostei: Cyprinidae). *Journal of Morphology*, *278*, 750–767.

Cope, E. D. (1874). On the Plagopterinae and the ichthyology of Utah. *Proceedings of the American Philosophical Society*, *14*, 129–139.

Copp, G. H., Robert Britton, J., Cucherousset, J., García-Berthou, E., Kirk, R., Peeler, E., & Stakėnas, S. (2009). Voracious invader or benign feline? A review of the

environmental biology of European catfish *Silurus glanis* in its native and introduced ranges. *Fish and Fisheries*, *10*, 252–282.

Cubbage, C. C., & Mabee, P. M. (1996). Development of the cranium and paired fins in the zebrafish *Danio rerio* (Ostariophysi, Cyprinidae). *Journal of Morphology*, *229*, 121–160.

Denoël, M., & Joly, P. (2000). Neoteny and progenesis as two heterochronic processes involved in paedomorphosis in *Triturus alpestris* (Amphibia: Caudata). *Proceedings of the Royal Society of London. Series B: Biological Sciences*, *267*, 1481–1485.

Dillman, C. B., & Hilton, E. J. (2015). Anatomy and early development of the pectoral girdle, fin, and fin spine of sturgeons (Actinopterygii: Acipenseridae). *Journal of Morphology*, *276*, 241–260.

Diogo, R., Oliveira, C., & Chardon, M. (2001). On the osteology and myology of catfish pectoral girdle, with a reflection on catfish (Teleostei: Siluriformes) plesiomorphies. *Journal of Morphology*, *249*, 100–125.

Egge, J.J.D., (2007). The osteology of the stonecat, *Noturus flavus* (Siluriformes: Ictaluridae), with comparisons to other siluriforms. *Alabama Museum of Natural History Bulletin*, *25*,71–89.

Egge, J. J., & Simons, A. M. (2010). Evolution of venom delivery structures in madtom catfishes (Siluriformes: Ictaluridae). *Biological Journal of the Linnean Society*, *102*, 115–129.

Esquerré, D., Sherratt, E., & Keogh, J. S. (2017). Evolution of extreme ontogenetic allometric diversity and heterochrony in pythons, a clade of giant and dwarf snakes. *Evolution*, *71*, 2829–2844.

Fine, M. L., Friel, J. P., McElroy, D., King, C. B., Loesser, K. E., & Newton, S. (1997). Pectoral spine locking and sound production in the channel catfish *Ictalurus punctatus*. *Copeia* (1997), 777–790.

Fine, M. L., McElroy, D., Rafi, J., King, C. B., Loesser, K. E., & Newton, S. (1996). Lateralization of pectoral stridulation sound production in the channel catfish. *Physiology & behavior*, *60*, 753.

Fink, S.V., & Fink, W.L. (1981). Interrelationships of the ostariophysan fishes (Teleostei). *Zoological Journal of the Linnean Society*, *72*, 297–353.

Fricke, Eschmeyer, W.N., & Fong, J.D. (2020). Species by Family/Subfamily. (http://research.calacademy.org/research/ichthyology/catalog/SpeciesByFamily.asp). Electronic version accessed 28 September 2020

Friel, J. P., & Lundberg, J. G. (1996). *Micromyzon akamai*, gen. et sp. nov., a small and eyeless banjo catfish (Siluriformes: Aspredinidae) from the river channels of the lower Amazon basin. *Copeia* (1996), 641–648.

Geerinckx, T., Brunain, M., & Adriaens, D. (2007). Development of the osteocranium in the suckermouth armored catfish *Ancistrus* cf. *triradiatus* (Loricariidae, Siluriformes). *Journal of Morphology*, *268*, 254–274.

Goswami, A., Weisbecker, V., & Sánchez-Villagra, M. R. (2009). Developmental modularity and the marsupial–placental dichotomy. *Journal of Experimental Zoology Part B: Molecular and Developmental Evolution*, *312*, 186–195.

Gould, S. J. (1977). *Ontogeny and phylogeny*. Harvard University Press, Cambridge, MA.

Grande, T., & de Pinna, M. (2004). The evolution of the Weberian apparatus: a phylogenetic perspective. *Mesozoic Fishes*, *3*, 429–448.

Grande, L., & Eastman, J. T. (1986). A review of Antarctic ichthyofaunas in the light of new fossil discoveries. *Palaeontology*, *29*, 113–137.

Grande, L., & Lundberg, J. G. (1988). Revision and redescription of the genus *Astephus* (Siluriformes: Ictaluridae) with a discussion of its phylogenetic relationships. *Journal of Vertebrate Paleontology*, *8*, 139–171.

Grande, T., & Shardo, J. D. (2002). Morphology and development of the postcranial skeleton in the channel catfish *Ictalurus punctatus* (Ostariophysi: Siluriformes) *Field Museum of Natural History 1518*, 1–30.

Haeckel, E. (1874). Die Gastraea-Theorie, die phylogenetische Classification des Thierreichs und die Homologie der Keimblätter. *enaische Zeitschrift für Naturwissenschaft*, *9*, 402–508.

Hall, B. K. (1986). The role of movement and tissue interactions in the development and growth of bone and secondary cartilage in the clavicle of the embryonic chick. *Development*, *93*, 133–152.

Hardman, M. (2002). The phylogenetic relationships among extant catfishes, with special reference to Ictaluridae (Otophysi: Siluriformes). Unpublished Ph.D. Dissertation, University of Illinois at Urbana-Champaign. Urbana, Illinois.

Hardman, M. (2005). The phylogenetic relationships among non-diplomystid catfishes as inferred from mitochondrial cytochrome b sequences; the search for the ictalurid sister taxon (Otophysi: Siluriformes). *Molecular Phylogenetics and Evolution*, *37*, 700–720.

Harrington, S. M., Harrison, L. B., & Sheil, C. A. (2013). Ossification sequence heterochrony among amphibians. *Evolution & Development*, *15*, 344–364.

Harrison, L. B., & Larsson, H. C. (2008). Estimating evolution of temporal sequence changes: a practical approach to inferring ancestral developmental sequences and sequence heterochrony. *Systematic Biology*, *57*, 378–387.

Hautier, L., Bennett, N. C., Viljoen, H., Howard, L., Milinkovitch, M. C., Tzika, A. C., Goswami, A., & Asher, R. J. (2013). Patterns of ossification in southern versus northern placental mammals. *Evolution*, *67*, 1994–2010.

Hautier, L., Weisbecker, V., Goswami, A., Knight, F., Kardjilov, N., & Asher, R. J. (2011). Skeletal ossification and sequence heterochrony in xenarthran evolution. *Evolution & Development*, *13*(5), 460-476.

Hertwig, O. (1876). Ueber das Hautskelet der Fische. *Morphologisches Jahrbuch, 2*, 328–395.

Hilton, E. J., Grande, L., & Bemis, W. E. (2011). Skeletal anatomy of the shortnose sturgeon, *Acipenser brevirostrum* Lesueur, 1818, and the systematics of sturgeons (Acipenseriformes, Acipenseridae). *Fieldiana Life and Earth Sciences*, *3*, 1–168.

Hilton, E. J., & Johnson, G. D. (2007). When two equals three: developmental osteology and homology of the caudal skeleton in carangid fishes (Perciformes: Carangidae). *Evolution & Development*, *9*, 178–189.

Hoffmann, M., & Britz, R. (2006). Ontogeny and homology of the neural complex of otophysan Ostariophysi. *Zoological Journal of the Linnean Society*, *147*, 301–330.

Hora, S. 1922. Structural modifications in the fishes of mountain torrents. *Records of the Indian Museum*, *24*, 31–61.

Hubbs, C. L., & Hibbard, C. W. (1951). *Ictalurus lambda*, a new catfish, based on a pectoral spine from the lower Pliocene of Kansas. *Copeia* (1951), 8–14.

Hugi, J., Hutchinson, M. N., Koyabu, D., & Sánchez-Villagra, M. R. (2012). Heterochronic shifts in the ossification sequences of surface-and subsurface-dwelling skinks are correlated with the degree of limb reduction. *Zoology*, *115*, 188–198.

Hunter, J. P. (1998). Key innovations and the ecology of macroevolution. *Trends in Ecology & Evolution*, *13*, 31–36.

Huysentruyt, F., & Adriaens, D. (2005). Descriptive osteology of *Corydoras aeneus* (Siluriformes: Callichthyidae). *Cybium*, *29*, 261–73.

Huysentruyt, F., Geerinckx, T., Brunain, M., & Adriaens, D. (2011). Development of the osteocranium in *Corydoras aeneus* (Gill, 1858) Callichthyidae, Siluriformes. *Journal of Morphology*, *272*, 573–582.

Ito, F., Matsumoto, T., & Hirata, T. (2019). Frequent nonrandom shifts in the temporal sequence of developmental landmark events during teleost evolutionary diversification. *Evolution & Development*, *21*, 120–134.

Jansen, G., Devaere, S., Weekers, P. H. H., & Adriaens, D. (2006). Phylogenetic relationships and divergence time estimate of African anguilliform catfish (Siluriformes: Clariidae) inferred from ribosomal gene and spacer sequences. *Molecular Phylogenetics and Evolution*, *38*(1), 65-78.

Jeffery, J. E., Bininda-Emonds, O. R., Coates, M. I., & Richardson, M. K. (2005). A new technique for identifying sequence heterochrony. *Systematic Biology*, *54*, 230–240.

Johnels, A. G. (1957). The mode of terrestrial locomotion in *Clarias*. *Oikos*, *8*, 122–129.

Johnson, G. D. (1983). *Niphon spinosus*: a primitive epinepheline serranid, with comments on the monophyly and intrarelationships of the Serranidae. *Copeia* (1983), 777–787.

Johnson, D. G., & Patterson, C. (1993). Percomorph phylogeny: a survey of acanthomorphs and a new proposal. *Bulletin of Marine Science*, *52*, 554–626.

Johnson, G. D., & Washington, B. B. (1987). Larvae of the Moorish idol, Zanclus cornutus, including a comparison with other larval acanthuroids. *Bulletin of Marine Science*, *40*, 494–511.

Kaatz, I. M., Stewart, D. J., Rice, A. N., & Lobel, P. S. (2010). Differences in pectoral fin spine morphology between vocal and silent clades of catfishes (order Siluriformes): ecomorphological implications. *Current Zoology*, *56*, 73–89.

Kappas, I., Vittas, S., Pantzartzi, C. N., Drosopoulou, E., & Scouras, Z. G. (2016). A time-calibrated mitogenome phylogeny of catfish (Teleostei: Siluriformes). *PLoS One*, *11*, e0166988.

Keyte, A. L., & Smith, K. K. (2010). Developmental origins of precocial forelimbs in marsupial neonates. *Development*, *137*, 4283-4294.

Kindred, J., (1919). The skull of *Ameiurus*. *Illinois Biological Monograph*, *5*, 1–120.

Kozarić, Z., Kužir, S., Petrinec, Z., Gjurčević, E., & Božić, M. (2008). The development of the digestive tract in larval European catfish (*Silurus glanis* L.). *Anatomia, Histologia, Embryologia*, *37*, 141–146.

Kubicek, K. M., & Conway, K. W. (2016). Developmental osteology of *Sciaenops ocellatus* and *Cynoscion nebulosus* (Teleostei: Sciaenidae), economically important sciaenids from the western Atlantic. *Acta Zoologica*, *97*, 267–301.

Kubicek, K. M., Britz, R., & Conway, K. W. (2019). Ontogeny of the catfish pectoral-fin spine (Teleostei: Siluriformes). *Journal of Morphology*, *280*, 339–359.

Larsson, H. C. E. (1998). A new method for comparing ontogenetic and phylogenetic data and its application to the evolution of the crocodilian secondary palate. *Neues Jahrbuch fur Geologie und Palaontologie-Abhandlungen*, *210*, 345–368.

Lundberg, J. G. (1975). Homologies of the upper shoulder girdle and temporal region bones in catfishes (Order Siluriformes), with comments on the skull of the Helogeneidae. *Copeia* (1975), 66–74.

Lundberg, J. G., & Case, G. R. (1970). A new catfish from the Eocene Green River formation, Wyoming. *Journal of Paleontology*, *44*, 451–457.

Lundberg, J. G., Hendrickson, D. A., Luckenbill, K. R., & Mariangeles, A. H. (2017). *Satan*'s skeleton revealed: a tomographic and comparative osteology of *Satan eurystomus*, the subterranean Widemouth Blindcat (Siluriformes, Ictaluridae). *Proceedings of the Academy of Natural Sciences of Philadelphia*, *165*, 117–173.

Lundberg, J. G., Luckenbill, K. R., Babu, K. S., & Ng, H. H. (2014). A tomographic osteology of the taxonomically puzzling catfish *Kryptoglanis shajii* (Siluriformes, Siluroidei, incertae sedis): description and a first phylogenetic interpretation. *Proceedings of the Academy of Natural Sciences of Philadelphia*, *163*, 1–41.

Lundberg, J. G., & Marsh, E. (1976). Evolution and functional anatomy of the pectoral fin rays in cyprinoid fishes, with emphasis on the suckers (family Catostomidae). *American Midland Naturalist*, 332–349.

Mabee, P. M., & Trendler, T. A. (1996). Development of the cranium and paired fins in *Betta splendens* (Teleostei: Percomorpha): intraspecific variation and interspecific comparisons. *Journal of Morphology*, *227*, 249–287.

Maehata, M. (2007). Reproductive ecology of the Far Eastern catfish, *Silurus asotus* (Siluridae), with a comparison to its two congeners in Lake Biwa, Japan. *Environmental Biology of Fishes*, *78*, 135–146.

Maxwell, E. E., Harrison, L. B., & Larsson, H. C. (2010). Assessing the phylogenetic utility of sequence heterochrony: evolution of avian ossification sequences as a case study. *Zoology*, *113*, 57-66.

Mayden, R. L., Burr, B. M., & Dewey, S. L. (1980). Aspects of the life history of the Ozark madtom, *Noturus albater*, in southeastern Missouri (Pisces: Ictaluridae). *American Midland Naturalist*, *104*, 335–340.

Mattox, G. M., Britz, R., & Toledo-Piza, M. (2014). Skeletal development and ossification sequence of the characiform *Salminus brasiliensis* (Ostariophysi: Characidae). *Ichthyological Exploration of Freshwaters*, *25*, 103–158.

Mattox, G. M., Britz, R., & Toledo-Piza, M. (2016). Osteology of *Priocharax* and remarkable developmental truncation in a miniature Amazonian fish (Teleostei: Characiformes: Characidae). *Journal of Morphology*, *277*, 65–85.

McDowell, S. B. (1973). Family Notacanthidae. *Fishes of the western North Atlantic. Memoirs of Sears Foundation for Marine Research. New Haven*, *1*, 124–207.

McMurrich, J. P., (1884). On the osteology of Amiurus catus (L.) Gill. *Zoologisches Anzeiger*, *168*, 296–299.

Miller, R. R., & Hubbs, C. L. (1960). The spiny-rayed cyprinid fishes (Plagopterini) of the Colorado River system. *Miscellaneous Publications, Museum of Zoology, University of Michigan, 115,* 1–39.

Mistri, A., Kumari, U., Mittal, S., & Mittal, A. K. (2018). Morphological specializations of the epidermis of an angler catfish *Chaca chaca* (Siluriformes, Chacidae) in relation to its ecological niche: A scanning electron microscopic investigation. *Microscopy Research and Technique*, *81*, 439–448.

Nelson, J. S., Grande, T. C., & Wilson, M. V. (2016). Fishes of the World (5th ed.). John Wiley & Sons., Hoboken, NJ.

Ng, H. H. (2015). Phylogenetic systematics of the Asian catfish family Sisoridae (Actinopterygii: Siluriformes). *Ichthyological Exploration of Freshwaters*, *26*, 97–157.

Paxton, C. G. M. (1997). Shoaling and activity levels in *Corydoras*. *Journal of Fish Biology*, *51*, 496–502.

Ng, H. H., & Kottelat, M. (1998). The catfish genus *Akysis* Bleeker (Teleostei: Akysidae) in Indochina, with descriptions of six new species. *Journal of Natural History*, *32*, 1057–1097.

Ng, H. H., & Tan, H. H. (1999). The Fishes of the Endau Drainage, Peninsular Malaysia with Descriptions of Two New Species of Catfishes (Teleostei: Akysidae, Bagridae). *Zoological Studies*, *38*, 350–366.

Nunn, C. L., & Smith, K. K. (1998). Statistical analyses of developmental sequences: the craniofacial region in marsupial and placental mammals. *The American Naturalist*, *152*, 82–101.

Ørvig T. (1967). Phylogeny of tooth tissues: evolution of some calcified tissues in early vertebrates. In: Miles AEW, editor. Structural and chemical organization of teeth, vol. 1. London: Academic Press. pp 45–110.

Peyer, B. (1922). Über die Flossenstacheln der Welse und Panzerwelse, sowie des Karpfens. *Morphologisches Jahrbücher, 51*, 493–554.

de Pinna, M. C. C. (1993). Higher-level phylogeny of Siluriformes (Teleostei, Ostariophysi), with a new classification of the order. Unpublished PhD Dissertation. *New York: City University of New York*.

de Pinna, M. C., Ferraris Jr, C. J., & Vari, R. P. (2007). A phylogenetic study of the Neotropical catfish family Cetopsidae (Osteichthyes, Ostariophysi, Siluriformes), with a new classification. *Zoological Journal of the Linnean Society*, *150*, 755–813.

de Pinna, M., Reis, V., & Britski, H. (2020). A new species of *Trichogenes* (Siluriformes, Trichomycteridae), with a discussion on the homologies of the anterior orbital bones in trichomycterids and other loricarioids. *American Museum Novitates*, *2020*(3951), 1–27.

de Pinna, M. C. C., & Winemiller, K. O. (2000). A new species of *Ammoglanis* (Siluriformes: Trichomycteridae) from Venezuela. *Ichthyological Exploration of Freshwaters*, *11*, 255–264.

Pinton, A., Fara, E., & Otero, O. (2006). Spine anatomy reveals the diversity of catfish through time: a case study of *Synodontis* (Siluriformes). *Naturwissenschaften*, *93*, 22–26.

Pruzsinszky, I., & Ladich, F. (1998). Sound production and reproductive behaviour of the armoured catfish *Corydoras paleatus* (Callichthyidae). *Environmental Biology of Fishes*, *53*, 183-191.

R Core Team (2020). R: A language and environment for statistical computing. R Foundation for Statistical Computing, Vienna, Austria. URL https://www.R-project.org/.

Rao, K. S., & Lakshmi, K. (1984). Head skeleton of the marine catfish *Arius tenuispinis* Day (Osteichthyes: Siluriformes, Ariidae). *Journal of Morphology*, *181*, 221–238.

Reed, H. D. (1924). The morphology and growth of the spines of siluroid fishes. *Journal of Morphology*, *38*, 431–451.

Reiss, J. O. (1989). The meaning of developmental time: a metric for comparative embryology. *The American Naturalist*, *134*, 170–189.

Reynolds, J. D. (1971). Biology of the small pelagic fishes in the New Volta Lake in Ghana: I. schooling and migrations. *Hydrobiologia*, *38*, 79–91.

Rocha, M. S., Oliveira, R. R. D., & Py-Daniel, L. H. R. (2008). *Scoloplax baskini*: a new spiny dwarf catfish from Rio Aripuanã, Amazonas, Brazil (Loricarioidei: Scoloplacidae). *Neotropical Ichthyology*, *6*, 323–328.

Rodiles-Hernández, R., Hendrickson, D. A., Lundberg, J. G., & Humphries, J. M. (2005). *Lacantunia enigmatica* (Teleostei: Siluriformes) a new and phylogenetically puzzling freshwater fish from Mesoamerica. *Zootaxa*, *1000*, 1–24.

Rodiles-Hernández, R., Lundberg, J. G., & Sullivan, J. P. (2010). Taxonomic discrimination and identification of extant blue catfishes (Siluriformes: Ictaluridae: *Ictalurus furcatus* Group). *Proceedings of the Academy of Natural Sciences of Philadelphia*, *159*, 67–82.

Sánchez-Villagra, M. R., Goswami, A., Weisbecker, V., Mock, O., & Kuratani, S. (2008). Conserved relative timing of cranial ossification patterns in early mammalian evolution. *Evolution & Development*, *10*(5), 519-530.

Sánchez-Villagra, M. R., Müller, H., Sheil, C. A., Scheyer, T. M., Nagashima, H., & Kuratani, S. (2009). Skeletal development in the Chinese soft-shelled turtle *Pelodiscus sinensis* (Testudines: Trionychidae). *Journal of Morphology*, *270*, 1381–1399.

Schaefer, S. A. (1991). Phylogenetic analysis of the loricariid subfamily Hypoptopomatinae (Pisces: Siluroidei: Loricariidae), with comments on generic diagnoses and geographic distribution. *Zoological Journal of the Linnean Society*, *102*, 1–41.

Schaefer, S. A., Provenzano, F., Pinna, M. D., & Baskin, J. N. (2005). New and noteworthy Venezuelan glanapterygine catfishes (Siluriformes, Trichomycteridae), with discussion of their biogeography and psammophily. *American Museum Novitates*, *3496*, 1–27.

Schulte, C. J., Allen, C., England, S. J., Juárez-Morales, J. L., & Lewis, K. E. (2011). Evx1 is required for joint formation in zebrafish fin dermoskeleton. *Developmental Dynamics*, *240*, 1240–1248.

Scott, J. E., & Dorling, J. (1965). Differential staining of acid glycosaminoglycans (mucopolysaccharides) by alcian blue in salt solutions. *Histochemie*, *5*, 221–233.

Sears, K. E. (2009). Differences in the timing of prechondrogenic limb development in mammals: the marsupial–placental dichotomy resolved. *Evolution: International Journal of Organic Evolution*, *63*, 2193-2200.

Sewertzoff, A. N. (1924). The development of the dorsal fin of *Polypterus delhesi*. *Journal of Morphology*, *38*, 551–580.

Sire, J. Y., & Huysseune, A. (1996). Structure and development of the odontodes in an armoured catfish, *Corydoras aeneus* (Siluriformes, Callichthyidae). *Acta Zoologica*, *77*, 51–72.

Slobodian, V., & Pastana, M. N. (2018). Description of a new *Pimelodella* (Siluriformes: Heptapteridae) species with a discussion on the upper pectoral girdle homology of Siluriformes. *Journal of Fish Biology*, *93*, 901–916.

Smith, K. K. (2001). Heterochrony revisited: the evolution of developmental sequences. *Biological Journal of the Linnean Society*, *73*, 169–186.

Srinivasachar, H.R. (1958) Development of the skull in catfishes. V. Development of skull in *Heteropneustes fossilis* (Bloch). *Proceedings of the National Institute of Sciences India*, *24B*, 165–190.

Starks, E. C. (1930). The primary shoulder girdle of the bony fishes. *Stanford University Publications, University Series, Biological Sciences*, 6, 147–239

Sullivan, J. P., Lundberg, J. G., & Hardman, M. (2006). A phylogenetic analysis of the major groups of catfishes (Teleostei: Siluriformes) using rag1 and rag2 nuclear gene sequences. *Molecular Phylogenetics and Evolution*, *41*, 636–662.

Taylor, W. R. (1967). An enzyme method of clearing and staining small vertebrates. *Proceedings of the United States National Museum*, *122*,1 –17.

Taylor, W. R. (1969). A revision of the catfish genus *Noturus* Rafinesque with an analysis of higher groups in the Ictaluridae. *Bulletin of the United States National Museum*, *282*, 1–315.

Taylor, W. R., & Van Dyke, G. C. (1985). Revised procedures for staining and clearing small fishes and other vertebrates for bone and cartilage study. *Cybium*, *9*, 107–119.

Tencatt, L. F. C., & Ohara, W. M. (2016). Two new species of Corydoras Lacépède, 1803 (Siluriformes: Callichthyidae) from the rio Madeira basin, Brazil. *Neotropical Ichthyology*, *14*(1).

Thomas, M. R., & Burr, B. M. (2004). *Noturus gladiator*, a new species of madtom (Siluriformes: Ictaluridae) from Coastal Plain streams of Tennessee and Mississippi. *Ichthyological Exploration of Freshwaters*, *15*, 351–368.

Vanscoy, T., Lundberg, J. G., & Luckenbill, K. R. (2015). Bony ornamentation of the catfish pectoral-fin spine: comparative and developmental anatomy, with an example of fin-spine diversity using the Tribe Brachyplatystomini (Siluriformes, Pimelodidae). *Proceedings of the Academy of Natural Sciences of Philadelphia*, *164*, 177–212.

Vigliotta, T. R. (2008). A phylogenetic study of the African catfish family Mochokidae (Osteichthyes, Ostariophysi, Siluriformes), with a key to genera. *Proceedings of the Academy of Natural Sciences of Philadelphia*, *157*(1), 73-136.

Walker, M. B., & Kimmel, C. B. (2007). A two-color acid-free cartilage and bone stain for zebrafish larvae. *Biotechnic & Histochemistry*, *82*, 23–28.

Weisbecker, V., Goswami, A., Wroe, S., & Sánchez-Villagra, M. R. (2008). Ossification heterochrony in the therian postcranial skeleton and the marsupial–placental dichotomy. *Evolution: International Journal of Organic Evolution*, *62*, 2027–2041.

Weisbecker, V., & Mitgutsch, C. (2010). A large-scale survey of heterochrony in anuran cranial ossification patterns. *Journal of Zoological Systematics and Evolutionary Research*, *48*, 332–347.

Werneburg, I., Hugi, J., Müller, J., & Sánchez-Villagra, M. R. (2009). Embryogenesis and ossification of *Emydura subglobosa* (Testudines, Pleurodira, Chelidae) and patterns of turtle development. *Developmental Dynamics*, *238*, 2770–2786.

Werneburg, I., & Sánchez-Villagra, M. R. (2015). Skeletal heterochrony is associated with the anatomical specializations of snakes among squamate reptiles. *Evolution*, *69*, 254–263.

Winemiller, K. O. (1987). Feeding and reproductive biology of the currito, *Hoplosternum littorale*, in the Venezuelan llanos with comments on the possible function of the enlarged male pectoral spines. *Environmental Biology of Fishes*, *20*, 219–227.

Wright, J. J. (2009). Diversity, phylogenetic distribution, and origins of venomous catfishes. *BMC Evolutionary Biology*, *9*, 282.

Ziermann, J. M., Mitgutsch, C., & Olsson, L. (2014). Analyzing developmental sequences with Parsimov—a case study of cranial muscle development in anuran larvae.

Journal of Experimental Zoology Part B: Molecular and Developmental Evolution, *322*, 586–606.

APPENDIX

RAW DATA FOR SEQUENCE HETEROCHRONY ANALYSES

Table A-1. Rank ordered datase of 93 skeletal elements used for sequence-ANOVA analysis of the whole skeleton.

Bone	*Danio*	*Enteromius*	*Salminus*	*Ictalurus*	*Noturus*	*Corydoras*	*Ancistrus*
Cleithrum	1	7	1	1	2	1	1
Basioccipital	3	15.5	9.5	10	6	7.5	13
Ceratobranchial 5	3	7	20.5	40	53	42.5	79
Opercle	3	7	3	2.5	2	4	7
Parasphenoid	5	7	7.5	10	19.5	14.5	36.5
Exoccipital	6	7	18	26	8	14.5	18
Hyomandibular	7	7	11.5	50	30	48.5	35
Centrum 4	8	22.5	30	10	11.5	4	13
Branchiostegal Rays	9.5	7	6	6	7	14.5	5.5
Dentary	9.5	7	3	5	4.5	14.5	17
Anterior Ceratohyal	12	7	7.5	20	24	14.5	31
Centrum 3	12	22.5	32.5	12	11.5	4	13
Centrum 5	12	22.5	30	7.5	11.5	4	13
Maxilla	14	7	5	2.5	2	7.5	3
Post-Weberian Centra	15	22.5	30	7.5	11.5	4	22
Retroarticular	16	15.5	13	60	22.5	35	64
Quadrate	17	7	9.5	30	29	28	60
Principle Caudal-Fin Rays	18	14	15.5	4	4.5	14.5	3
Premaxilla	19	7	3	13	15	24	3
Anguloarticular	20	7	25	67.5	50.5	55.5	82
Ceratobranchial 1	21.5	33	14	52.5	63.5	55.5	67.5
Ceratobranchial 2	21.5	33	15.5	40	63.5	55.5	58
Neural Arch 5	24	26.5	38.5	18	15	14.5	13
Post-Weberian Neural Arches	24	26.5	38.5	15	25	22	22
Prootic	24	42	54.5	34	65	42.5	39
Hypural 2	26.5	33	27	45.5	19.5	28	19.5
Hypural 3	26.5	33	40	45.5	37.5	28	19.5
Ventral Hypohyal	28	17	18	36	41	35	51.5
Neural Arch 4	29	26.5	42	19	17	14.5	13
Ceratobranchial 3	31	29.5	18	40	62	42.5	58
Ceratobranchial 4	31	29.5	27	38	48	42.5	58
Supracleithrum	31	20	24	26	19.5	22	8.5
Ural Centrum 1	33	62	58	31	19.5	14.5	26.5
Preopercle	34	18.5	22	29	48	81.5	72
Parhypural	35	33	27	45.5	27	55.5	26.5
Scaphium	36	37	54.5	63.5	48	28	51.5
Lateral Ethmoid	37.5	73.5	76.5	71.5	76	73.5	81
Uroneural 1	37.5	26.5	42	36	54	67	66
Hemal Arch PU2	39	47	42	45.5	42.5	35	26.5
Urohyal	40	37	11.5	36	39	59	43
Inner Arm Of Os Suspensorium	41.5	40.5	69.5	63.5	75	28	45
Tripus	41.5	40.5	72	57.5	37.5	28	38
Post-Weberian Hemal Arches	43.5	47	49	22	31	22	22
Preural Centrum 3	43.5	64	60.5	32.5	40	14.5	41
Hemal Arch PU3	46	47	52	45.5	42.5	35	26.5
Hemal Spine PU2	46	52.5	45	60	45	66	51.5
Preural Centrum 2	46	67	60.5	32.5	56	14.5	41

Table A-1. Continued

Bone	*Danio*	*Enteromius*	*Salminus*	*Ictalurus*	*Noturus*	*Corydoras*	*Ancistrus*
Epibranchial 4	50	47	37	52.5	67	48.5	67.5
Gillrakers	50	70	20.5	77	55	87	85
Hemal Spine PU3	50	57	50	60	45	61	41
Metapterygoid	50	37	47	70	58.5	68.5	51.5
Post-Weberian Neural Spines	50	39	72	51	70	42.5	62
Epibranchial 2	53.5	66	35	55	67	55.5	70
Epibranchial 3	53.5	43	35	55	67	48.5	70
Dorsal-Fin Rays	55.5	64	35	26	34	70.5	33.5
Epibranchial 1	55.5	68	45	55	78	62.5	74.5
Anal-Fin Rays	57	76	32.5	26	34	83	33.5
Post-Weberian Ribs	58	47	69.5	69	74	28	8.5
Autosphenotic	64	79	63	82	77	78	63
Post-Weberian Hemal Spines	64	64	66	45.5	69	42.5	47
Neural Arch PU2	64	47	54.5	45.5	45	35	26.5
Neural Arch PU3	64	47	51	45.5	34	35	26.5
Neural Spine PU2	64	57	60.5	67.5	71	64	51.5
Outer Arm Of Os Suspensorium	64	51	72	57.5	34	39	51.5
Parapophyses	64	57	78	23	34	14.5	13
Posterior Ceratohyal	64	18.5	23	75	50.5	35	56
Procurrent Caudal-Fin Rays	64	69	54.5	16.5	27	76	30
Pterosphenoid	64	78	74	78	81.5	73.5	80
Supraoccipital	64	80	68	73.5	72	60	45
Autopterotic	70	71	82	79.5	60.5	48.5	32
Anal-Fin Proximal Radials	71	83	60.5	81	79	86	74.5
Frontal	72	77	48	21	15	46	36.5
Infraorbital 1	74	57	89	14	22.5	92	90
Orbitosphenoid	74	88.5	81	79.5	81.5	73.5	77.5
Pectoral-Fin Rays	74	87	84	16.5	9	55.5	5.5
Epural	76	75	80	83	85	77	70
Basibranchial 2	77	60.5	64.5	89	86	84	89
Dorsal-Fin Proximal Radials	78	72	67	71.5	80	73.5	74.5
Pharyngobranchial 3	79	73.5	45	86	83	62.5	87
Mesethmoid	80	54	57	63.5	58.5	52	51.5
Autopalatine	81	57	90	73.5	73	51	45
Basibranchial 3	82	60.5	64.5	90	84	81.5	91.5
Epioccipital	83	84	85	87	88	90	65
Vomer	84	52.5	79	85	89	65	74.5
Coracoid	85	88.5	88	76	57	80	61
Pelvic-Fin Rays	86	81	86	66	60.5	79	51.5
Nasal	87	90	76.5	26	27	91	85
Basipterygia	88	85	87	88	87	85	85
Pectoral Radial 3	89	92	91.5	84	90	89	83
Dermopterotic	90	91	91.5	63.5	52	88	77.5
Hypobranchial 1	91	86	83	91	91	68.5	88
Hypobranchial 2	92	82	75	92	92	70.5	91.5

Table A-2. Rank ordered dataset of 48 skeletal elements used for sequence-ANOVA analysis of the cranial skeleton.

Bone	*Danio*	*Enteromius*	*Salminus*	*Ictalurus*	*Noturus*	*Corydoras*	*Ancistrus*
Basioccipital	2	13.5	8.5	5.5	4	2.5	5
Ceratobranchial 5	2	6.5	18.5	20	23	15.5	37
Opercle	2	6.5	2	1.5	1.5	1	4
Parasphenoid	4	6.5	6.5	5.5	9	6	11.5
Exoccipital	5	6.5	16	11.5	6	6	7
Hyomandibula	6	6.5	10.5	22	15	20.5	10
Branchiostegal Rays	7.5	6.5	5	4	5	6	3
Dentary	7.5	6.5	2	3	3	6	6
Anterior Ceratohyal	9	6.5	6.5	9	12	6	8
Maxilla	10	6.5	4	1.5	1.5	2.5	1.5
Retroarticular	11	13.5	12	28	10.5	12	26
Quadrate	12	6.5	8.5	14	14	10	24
Premaxilla	13	6.5	2	7	7.5	9	1.5
Anguloarticular	14	6.5	22	31	20.5	26.5	40
Ceratobranchial 1	15.5	20.5	13	23.5	29.5	26.5	28.5
Ceratobranchial 2	15.5	20.5	14	20	29.5	26.5	22
Prootic	17	24	31	15	31	15.5	13
Ventral Hypohyal	18	15	16	16.5	17	12	18
Ceratobranchial 3	19.5	18.5	16	20	28	15.5	22
Ceratobranchial 4	19.5	18.5	23	18	18.5	15.5	22
Preopercle	21	16.5	20	13	18.5	41.5	32
Lateral Ethmoid	22	37.5	39.5	33	37	38	39
Urohyal	23	22.5	10.5	16.5	16	29	14
Epibranchial 4	25	26	26	23.5	33	20.5	28.5
Gillrakers	25	35	18.5	37	24	44	41.5
Metapterygoid	25	22.5	29	32	25.5	34.5	18
Epibranchial 2	27.5	33	24.5	26	33	26.5	30.5
Epibranchial 3	27.5	25	24.5	26	33	20.5	30.5
Epibranchial 1	29	34	27.5	26	39	31.5	33.5
Autosphenotic	31.5	41	33	41	38	40	25
Posterior Ceratohyal	31.5	16.5	21	36	20.5	12	20
Pterosphenoid	31.5	40	37	38	40.5	38	38
Supraoccipital	31.5	42	36	34.5	35	30	15.5
Autopterotic	34	36	43	39.5	27	20.5	9
Frontal	35	39	30	10	7.5	18	11.5
Infraorbital 1	36.5	29.5	46	8	10.5	48	46
Orbitosphenoid	36.5	46	42	39.5	40.5	38	35.5
Basibranchial 2	38	31.5	34.5	45	44	43	45
Pharyngobranchial 3	39	37.5	27.5	43	42	31.5	43
Mesethmoid	40	28	32	29.5	25.5	24	18
Autopalatine	41	29.5	47	34.5	36	23	15.5
Basibranchial 3	42	31.5	34.5	46	43	41.5	47.5
Epioccipital	43	44	45	44	45	46	27
Vomer	44	27	41	42	46	33	33.5
Nasal	45	47	39.5	11.5	13	47	41.5
Dermopterotic	46	48	48	29.5	22	45	35.5
Hypobranchial 1	47	45	44	47	47	34.5	44
Hypobranchial 2	48	43	38	48	48	36	47.5

Table A-3. Rank ordered dataset of 45 skeletal elements used for sequence-ANOVA analysis of the postcranial skeleton.

Bone	*Danio*	*Enteromius*	*Salminus*	*Ictalurus*	*Noturus*	*Corydoras*	*Ancistrus*
Cleithrum	1	1	1	1	1	1	1
Centrum 4	2	5.5	7	5	5.5	3.5	8.5
Centrum 3	3.5	5.5	9.5	6	5.5	3.5	8.5
Centrum 5	3.5	5.5	7	3.5	5.5	3.5	8.5
Post-Weberian Centra	5	5.5	7	3.5	5.5	3.5	15
Principle Caudal-Fin Rays	6	2	2	2	2	9	2
Neural Arch 5	7.5	9.5	12.5	10	8	9	8.5
Post-Weberian Neural Arches	7.5	9.5	12.5	7	13	14	15
Hypural 2	9.5	13	4.5	24.5	11	18.5	12.5
Hypural 3	9.5	13	14	24.5	22.5	18.5	12.5
Neural Arch 4	11	9.5	16	11	9	9	8.5
Supracleithrum	12	3	3	15	11	14	4.5
Ural Centrum 1	13	30	26	17	11	9	19.5
Parhypural	14	13	4.5	24.5	14.5	29.5	19.5
Scaphium	15	15	24	34.5	30	18.5	34
Uroneural 1	16	9.5	16	20	31	34	39
Hemal Arch Pu2	17	21.5	16	24.5	25.5	23.5	19.5
Inner Arm Os Suspensorium	18.5	17.5	33.5	34.5	39	18.5	30
Tripus	18.5	17.5	36	30.5	22.5	18.5	26
Post-Weberain Hemal Arches	20.5	21.5	19	12	16	14	15
Preural Centrum 3	20.5	32	28.5	18.5	24	9	28
Hemal Arch PU3	23	21.5	22	24.5	25.5	23.5	19.5
Hemal Spine PU2	23	26	18	32.5	28	33	34
Preural Centrum 2	23	34	28.5	18.5	32	9	28
Hemal Spine PU3	25.5	28	20	32.5	28	31	28
Post-Weberian Neural Spines	25.5	16	36	29	36	27.5	38
Dorsal-Fin Rays	27	32	11	15	19	35	24.5
Anal-Fin Rays	28	38	9.5	15	19	41	24.5
Post-Weberian Ribs	29	21.5	33.5	38	38	18.5	4.5
Hemal Spines	33	32	31	24.5	35	27.5	31
Neural Arch PU2	33	21.5	24	24.5	28	23.5	19.5
Neural Arch PU3	33	21.5	21	24.5	19	23.5	19.5
Neural Spine PU2	33	28	28.5	37	37	32	34
Outer Arm Os Suspensorium	33	25	36	30.5	19	26	34
Parapophyses	33	28	38	13	19	9	8.5
Procurrent Caudal-Fin Rays	33	35	24	8.5	14.5	37	23
Anal-Fin Proximal Radials	37	40	28.5	41	40	43	41.5
Pectoral-Fin Rays	38	42	40	8.5	3	29.5	3
Epural	39	37	39	42	42	38	40
Dorsal-Fin Proximal Radials	40	36	32	39	41	36	41.5
Coracoid	41	43	43	40	33	40	37
Pelvic-Fin Rays	42	39	41	36	34	39	34
Basipterygia	43	41	42	44	43	42	44
Pectoral-Fin Radial 3	44	44	44	43	44	44	43

Table A-4. Rank ordered dataset of 17 skeletal elements used for sequence-ANOVA analysis of the neurocranium.

Bone	*Danio*	*Enteromius*	*Salminus*	*Ictalurus*	*Noturus*	*Corydoras*	*Ancistrus*
Basioccipital	1	3	2	1.5	1	1	1
Parasphenoid	2	1.5	1	1.5	4	2.5	4.5
Exoccipital	3	1.5	3	5.5	2	2.5	2
Prootic	4	4	5	7	10	4	6
Lateral Ethmoid	5	9	10.5	10	12	11	15
Autosphenotic	7	12	7	15	13	13	9
Pterosphenoid	7	11	9	12	14.5	11	14
Supraoccipital	7	13	8	11	11	8	7
Autopterotic	9	8	14	13.5	9	6	3
Frontal	10	10	4	4	3	5	4.5
Infraorbital 1	11.5	7	16	3	5	17	17
Orbitosphenoid	11.5	15	13	13.5	14.5	11	12.5
Mesethmoid	13	6	6	8.5	8	7	8
Epioccipital	14	14	15	17	16	15	10
Vomer	15	5	12	16	17	9	11
Nasal	16	16	10.5	5.5	6	16	16
Dermopterotic	17	17	17	8.5	7	14	12.5

Table A-5. Rank ordered dataset of 31 skeletal elements used for sequence-ANOVA analysis of the splanchnocranium and associated dermal bones.

Bone	*Danio*	*Enteromius*	*Salminus*	*Ictalurus*	*Noturus*	*Corydoras*	*Ancistrus*
Ceratobranchial 5	1.5	5.5	15.5	13	16	12	24
Opercle	1.5	5.5	2	1.5	1.5	1	4
Hyomandibula	3	5.5	8.5	15	9	15	7
Branchiostegal Rays	4.5	5.5	5	4	4	4	3
Dentary	4.5	5.5	2	3	3	4	5
Anterior Ceratohyal	6	5.5	6	6	7	4	6
Maxilla	7	5.5	4	1.5	1.5	2	1.5
Retroarticular	8	11	10	21	6	9	17
Quadrate	9	5.5	7	8	8	7	16
Premaxilla	10	5.5	2	5	5	6	1.5
Anguloarticular	11	5.5	19	22	14.5	19.5	25
Ceratobranchial 1	12.5	17.5	11	16.5	20.5	19.5	18.5
Ceratobranchial 2	12.5	17.5	12	13	20.5	19.5	14
Ventral Hypohyal	14	12	13.5	9.5	11	9	10.5
Ceratobranchial 3	15.5	15.5	13.5	13	19	12	14
Ceratobranchial 4	15.5	15.5	20	11	12.5	12	14
Preopercle	17	13.5	17	7	12.5	28.5	22
Urohyal	18	19.5	8.5	9.5	10	22	8
Epibranchial 4	20	22	23	16.5	23	15	18.5
Gillrakers	20	28	15.5	26	17	31	26
Metapterygoid	20	19.5	26	23	18	25.5	10.5
Epibranchial 2	22.5	26	21.5	19	23	19.5	20.5
Epibranchial 3	22.5	21	21.5	19	23	15	20.5
Epibranchial 1	24	27	24.5	19	26	23.5	23
Posterior Ceratohyal	25	13.5	18	25	14.5	9	12
Basibranchial 2	26	24.5	27.5	28	29	30	29
Pharyngobranchial 3	27	29	24.5	27	27	23.5	27
Autopalatine	28	23	31	24	25	17	9
Basibranchial 3	29	24.5	27.5	29	28	28.5	30.5
Hypobranchial 1	30	31	30	30	30	25.5	28
Hypobranchial 2	31	30	29	31	31	27	30.5

Table A-6. Rank ordered dataset of 31 skeletal elements used for sequence-ANOVA analysis of the vertebral column.

Bone	*Danio*	*Enteromius*	*Salminus*	*Ictalurus*	*Noturus*	*Corydoras*	*Ancistrus*
Centrum 4	1	2.5	4	3	2.5	2.5	4.5
Centrum 3	2.5	2.5	6	4	2.5	2.5	4.5
Centrum 5	2.5	2.5	4	1.5	2.5	2.5	4.5
Post-Weberian Centra	4	2.5	4	1.5	2.5	2.5	11
Neural Arch 5	5.5	6.5	7.5	6	5	7.5	4.5
Post-Weberian Neural Arches	5.5	6.5	7.5	5	9	11.5	11
Hypural 2	7.5	10	1.5	17.5	7.5	15.5	8.5
Hypural 3	7.5	10	9	17.5	15.5	15.5	8.5
Neural Arch 4	9	6.5	11	7	6	7.5	4.5
Ural Centrum 1	10	27	20	10	7.5	7.5	15.5
Parhypural	11	10	1.5	17.5	10	26	15.5
Scaphium	12	12	18.5	27.5	23	15.5	26.5
Uroneural 1	13	6.5	11	13	24	30	30
Hemal Arch PU2	14	18.5	11	17.5	18.5	20.5	15.5
Inner Arm Os Suspensorium	15.5	14.5	25.5	27.5	30	15.5	23
Tripus	15.5	14.5	28	23.5	15.5	15.5	19
Post-Weberian Hemal Arches	17.5	18.5	14	8	11	11.5	11
Preural Centrum 3	17.5	28.5	22	11.5	17	7.5	21
Hemal Arch PU3	20	18.5	17	17.5	18.5	20.5	15.5
Hemal Spine PU2	20	23	13	25.5	21	29	26.5
Preural Centrum 2	20	30	22	11.5	25	7.5	21
Hemal Spine PU3	22.5	25	15	25.5	21	27	21
Post-Weberian Neural Spines	22.5	13	28	22	27	24.5	29
Post-Weberian Ribs	24	18.5	25.5	30	29	15.5	1
Post-Weberian Hemal Spines	27.5	28.5	24	17.5	26	24.5	24
Neural Arch PU2	27.5	18.5	18.5	17.5	21	20.5	15.5
Neural Arch PU3	27.5	18.5	16	17.5	13	20.5	15.5
Neural Spine PU2	27.5	25	22	29	28	28	26.5
Outer Arm Os Suspensorium	27.5	22	28	23.5	13	23	26.5
Parapophyses	27.5	25	30	9	13	7.5	4.5
Epural	31	31	31	31	31	31	31

Table A-7. Rank ordered dataset of 29 skeletal elements used for sequence-ANOVA analysis of the median and paired fins.

Bone	*Danio*	*Enteromius*	*Salminus*	*Ictalurus*	*Noturus*	*Corydoras*	*Ancistrus*
Cleithrum	1	1	1	1	1	1	1
Principle Caudal-Fin Rays	2	2	2	2	2	3.5	2
Hypural 2	3.5	6	4.5	15	5	7.5	5.5
Hypural 3	3.5	6	8	15	12	7.5	5.5
Supracleithrum	5	3	3	6	5	6	4
Ural Centrum 1	6	15	17	8	5	3.5	9.5
Parhypural	7	6	4.5	15	7.5	13.5	9.5
Uroneural 1	8	4	9.5	11	19	18	23
Hemal Arch PU2	9	9.5	9.5	15	14.5	10.5	9.5
Preural Centrum 3	10	16.5	19.5	9.5	13	3.5	17
Hemal Arch PU3	12	9.5	14	15	14.5	10.5	9.5
Hemal Spine PU2	12	12	11	19.5	17	17	20
Preural Centrum 2	12	18	19.5	9.5	20	3.5	17
Hemal Spine PU3	14	13.5	12	19.5	17	15	17
Dorsal-Fin Rays	15	16.5	7	6	10	19	14.5
Anal-Fin Rays	16	22	6	6	10	25	14.5
Neural Arch PU2	18.5	9.5	15.5	15	17	10.5	9.5
Neural Arch PU3	18.5	9.5	13	15	10	10.5	9.5
Neural Spine PU2	18.5	13.5	19.5	22	23	16	20
Procurrent Caudal-Fin Rays	18.5	19	15.5	3.5	7.5	21	13
Anal-Fin Proximal Radials	21	24	19.5	25	24	27	25.5
Pectoral-Fin Rays	22	26	24	3.5	3	13.5	3
Epural	23	21	23	26	26	22	24
Dorsal-Fin Proximal Radials	24	20	22	23	25	20	25.5
Coracoid	25	27	27	24	21	24	22
Pelvic-Fin Rays	26	23	25	21	22	23	20
Basipterygium	27	25	26	28	27	26	28
Pectoral-Fin Radial 3	28	28	28	27	28	28	27

Table A-8. Rank ordered dataset of 93 skeletal elements, sorted by event number, used for PGi analysis of the whole skeleton.

Bone	Event #	*Danio*	*Enteromius*	*Salminus*	*Ictalurus*	*Noturus*	*Corydoras*	*Ancistrus*
Cleithrum	1	1	1	1	1	1	1	1
Opercle	2	2	1	2	2	1	2	4
Basioccipital	3	2	3	6	7	3	3	6
Ceratobranchial 5	4	2	1	12	27	28	10	39
Parasphenoid	5	3	1	5	7	10	4	17
Exoccipital	6	4	1	11	19	5	4	8
Hyomandibula	7	5	1	7	29	16	12	16
Centrum 4	8	6	7	18	7	7	2	6
Branchiostegal Rays	9	7	1	2	4	2	4	7
Dentary	10	7	1	4	5	4	4	3
Centrum 5	11	8	7	18	6	7	2	6
Centrum 3	12	8	7	19	8	7	2	6
Anterior Ceratohyal	13	8	1	5	15	12	4	13
Maxilla	14	9	1	3	2	1	3	2
Centra	15	10	7	18	6	7	2	10
Retroarticular	16	11	3	8	34	11	8	31
Quadrate	17	12	1	6	21	15	7	27
Principle Caudal-fin Rays	18	13	2	10	3	2	4	2
Premaxilla	19	14	1	2	9	8	6	2
Angulararticular	20	15	1	16	37	26	15	42
Ceratobranchial 2	21	16	10	10	27	36	15	26
Ceratobranchial 1	22	16	10	9	31	36	15	34
Neural Arch 5	23	17	8	22	13	8	4	6
Post-Weberian Neural Arches	24	17	8	22	11	13	5	10
Prootic	25	17	14	32	24	37	10	19
Hypural 2	26	18	10	17	28	10	7	9
Hypural 3	27	18	10	23	28	19	7	9
Ventral Hypohyal	28	19	4	11	25	22	8	24
Neural Arch 4	29	20	8	24	14	9	4	6
Supracleithrum	30	21	6	15	19	10	5	5
Ceratobranchial 4	31	21	9	17	26	25	10	26
Ceratobranchial 3	32	21	9	11	27	35	10	26
Ural Centrum	33	22	22	34	22	10	4	11
Preopercle	34	23	5	13	20	25	32	36
Parhypural	35	24	10	17	28	14	15	11
Scaphium	36	25	11	32	35	25	7	24
Uroneural 1	37	26	8	24	25	29	23	33
Lateral Eethmoid	38	26	31	45	40	46	26	41
Hemal Arch of Preural Centrum 2	39	27	16	24	28	23	8	11
Urohyal	40	28	11	7	25	20	16	21
Tripus	41	29	13	42	33	19	7	18
Inner Arm of Os Suspensorium	42	29	13	41	35	45	7	22
Hemal Arches	43	30	16	28	17	17	5	10
Preural Centrum 3	44	30	23	35	23	21	4	20
Hemal Arch of Preural Centrum 3	45	31	16	31	28	23	8	11
Preural Centrum 2	46	31	18	25	34	24	22	24
Hemal Spine of Preural Centrum 2	47	31	25	35	23	31	4	20
Hemal Spine of Preural Centrum 3	48	32	20	29	34	24	18	20
Metapterygoid	49	32	28	12	44	30	38	44

Table A-8. Continued

Bone	Event #	*Danio*	*Enteromius*	*Salminus*	*Ictalurus*	*Noturus*	*Corydoras*	*Ancistrus*
Post-Weberian Neural Spines	50	32	11	26	39	33	24	24
Epibranchial 4	51	32	16	21	31	38	12	34
Gillrakers	52	32	12	42	30	40	10	29
Epibranchial 3	53	33	15	20	32	38	12	35
Epibranchial 2	54	33	24	20	32	38	15	35
Dorsal-fin Rays	55	34	23	20	19	18	25	15
Epibranchial 1	56	34	26	25	32	48	19	37
Anal-fin Rays	57	35	33	19	19	18	33	15
Post-Weberian Ribs	58	36	16	41	38	44	7	5
Parapophyses	59	37	27	32	12	14	27	12
Neural Arch of Preural Centrum 3	60	37	20	46	18	18	4	6
Neural Arch of Preural Centrum 2	61	37	16	30	28	18	8	11
Procurrent Caudal-fin Rays	62	37	17	42	33	18	9	24
Supraoccipital	63	37	16	32	28	24	8	11
Hemal Spines	64	37	5	14	42	26	8	25
Outer Arm Os Suspensorium	65	37	23	38	28	39	10	23
Neural Spine of Preural Centrum 2	66	37	20	35	37	41	20	24
Posterior Ceratohyal	67	37	37	40	41	42	17	22
Autosphenotic	68	37	36	36	48	47	29	30
Pterosphenoid	69	37	35	43	45	51	26	40
Autopterotic	70	38	29	50	46	34	12	14
Anal-fin Proximal Radials	71	39	40	35	47	49	37	37
Frontal	72	40	34	27	16	8	11	17
Pectoral-fin Rays	73	41	44	52	12	6	15	3
Orbitosphenoid	74	41	20	58	10	11	43	48
Infraorbital 1	75	41	45	49	46	51	26	38
Epural	76	42	32	48	49	54	28	35
Basibranchial 2	77	43	21	37	55	55	35	47
Dorsal-fin Proximal Radials	78	44	30	39	40	50	26	37
Pharyngobranchial 3	79	45	31	25	52	52	19	45
Mesethmoid	80	46	19	33	35	33	14	24
Autopalatine	81	47	20	59	41	43	13	22
Basibranchial 3	82	48	21	37	56	53	32	49
Epioccipital	83	49	41	53	53	57	41	32
Vomer	84	50	18	47	51	58	21	37
Coracoid	85	51	45	57	43	32	31	28
Scapula	86	51	45	55	44	40	34	28
Pelvic-fin Rays	87	52	38	54	36	34	30	24
Nasal	88	53	46	45	19	14	42	44
Basypterygia	89	54	42	56	54	56	36	44
Pectoral Radial 3	90	55	48	60	50	59	40	43
Dermopterotic	91	56	47	60	35	27	39	38
Hypobranchial 1	92	57	43	51	57	60	24	46
Hypobranchial 2	93	58	39	44	58	61	25	49

Table A-9. Rank ordered dataset of 48 skeletal elements, sorted by event number, used for PGi analysis of the cranial skeleton.

Bone	Event #	*Danio*	*Enteromius*	*Salminus*	*Ictalurus*	*Noturus*	*Corydoras*	*Ancistrus*
Basioccipital	1	1	2	5	4	3	2	4
Ceratobranchial 5	2	1	1	11	15	18	7	26
Opercle	3	1	1	1	1	1	1	3
Parasphenoid	4	2	1	4	4	7	3	10
Exoccipital	5	3	1	10	9	5	3	6
Hyomandibular	6	4	1	6	16	12	9	9
Branchiostegal Rays	7	5	1	3	3	4	3	2
Dentary	8	5	1	1	2	2	3	5
Anterior Ceratohyal	9	6	1	4	7	9	3	7
Maxilla	10	7	1	2	1	1	2	1
Retroarticular	11	8	2	7	19	8	6	19
Quadrate	12	9	1	5	11	11	5	17
Premaxilla	13	10	1	1	5	6	4	1
Anguloarticular	14	11	1	14	21	16	12	29
Ceratobranchial 1	15	12	6	8	17	23	12	21
Ceratobranchial 2	16	12	6	9	15	23	12	16
Prootic	17	13	8	21	12	24	7	11
Ventral Hypohyal	18	14	3	10	13	14	6	14
Ceratobranchial 3	19	15	5	10	15	22	7	16
Ceratobranchial 4	20	15	5	15	14	15	7	16
Preopercle	21	16	4	12	10	15	21	23
Lateral Ethmoid	22	17	19	28	23	28	19	28
Urohyal	23	18	7	6	13	13	13	12
Epibranchial 4	24	19	10	17	17	25	9	21
Gillrakers	25	19	17	11	26	19	23	30
Metapterygoid	26	19	7	19	22	20	17	14
Epibranchial 2	27	20	15	16	18	25	12	22
Epibranchial 3	28	20	9	16	18	25	9	22
Epibranchial 1	29	21	16	18	18	30	15	24
Autosphenotic	30	22	22	23	29	29	20	18
Posterior Ceratohyal	31	22	4	13	25	16	6	15
Pterosphenoid	32	22	21	26	27	31	19	27
Supraoccipital	33	22	23	25	24	26	14	13
Autopterotic	34	23	18	31	28	21	9	8
Frontal	35	24	20	20	8	6	8	10
Infraorbital 1	36	25	13	34	6	8	27	34
Orbitosphenoid	37	25	27	30	28	31	19	25
Basibranchial 2	38	26	14	24	33	34	22	33
Pharyngobranchial 3	39	27	19	18	31	32	15	31
Mesethmoid	40	28	12	22	20	20	11	14
Autopalatine	41	29	13	35	24	27	10	13
Basibranchial 3	42	30	14	24	34	33	21	35
Epioccipital	43	31	25	33	32	35	25	20
Vomer	44	32	11	29	30	36	16	24
Nasal	45	33	28	28	9	10	26	30
Dermopterotic	46	34	29	36	20	17	24	25
Hypobranchial 1	47	35	26	32	35	37	17	32
Hypobranchial 2	48	36	24	27	36	38	18	35

Table A-10. Rank ordered dataset of 45 skeletal elements, sorted by event number, used for PGi analysis of the postcranial skeleton.

Bone	Event #	*Danio*	*Enteromius*	*Salminus*	*Ictalurus*	*Noturus*	*Corydoras*	*Ancistrus*
Cleithrum	1	1	1	1	1	1	1	1
Centrum 4	2	2	4	5	4	4	2	5
Centrum 3	3	3	4	6	5	4	2	5
Centrum 5	4	3	4	5	3	4	2	5
Post-Weberian Centra	5	4	4	5	3	4	2	7
Primary Caudal-Fin Rays	6	5	2	2	2	2	3	2
Neural Arch 5	7	6	5	8	8	5	3	5
Post-Weberian Neural Arches	8	6	5	8	6	8	4	7
Hypural 2	9	7	6	4	16	7	5	6
Hypural 3	10	7	6	9	16	12	5	6
Neural Arch 4	11	8	5	10	9	6	3	5
Supracleithrum	12	9	3	3	12	7	4	4
Ural Centrum 1	13	10	14	17	13	7	3	8
Parhypural	14	11	6	4	16	9	9	8
Scaphium	15	12	7	16	20	16	5	15
Uroneural 1	16	13	5	10	15	17	13	18
Hemal Arch PU2	17	14	10	10	16	14	6	8
Inner Arm Os Suspensorium	18	15	9	21	20	25	5	13
Tripus	19	15	9	22	18	12	5	11
Post-Weberian Hemal Arches	20	16	10	12	10	10	4	7
Preural Centrum 3	21	16	15	18	14	13	3	12
Hemal Arch PU3	22	17	10	15	16	14	6	8
Hemal Spine PU2	23	17	12	11	19	15	12	15
Preural Centrum 2	24	17	16	18	14	18	3	12
Hemal Spine PU3	25	18	13	13	19	15	10	12
Post-Weberian Neural Spines	26	18	8	22	17	22	8	17
Dorsal-Fin Rays	27	19	15	7	12	11	14	10
Anal-Fin Rays	28	20	20	6	12	11	20	10
Post-Weberian Ribs	29	21	10	21	23	24	5	4
Post-Weberian Hemal Spines	30	22	15	19	16	21	8	14
Neural Arch PU2	31	22	10	16	16	15	6	8
Neural Arch PU3	32	22	10	14	16	11	6	8
Neural Spine PU2	33	22	13	18	22	23	11	15
Outer Arm Os Suspensorium	34	22	11	22	18	11	7	15
Parapophyses	35	22	13	23	11	11	3	5
Procurrent Caudal-Fin Rays	36	22	17	16	7	9	16	9
Anal-Fin Proximal Radials	37	23	22	18	27	26	23	20
Pectoral-Fin Rays	38	24	24	25	7	3	9	3
Epural	39	25	19	24	28	28	17	19
Dorsal-Fin Proximal Radials	40	26	18	20	24	27	15	20
Coracoid	41	27	25	29	25	19	19	16
Scapula	42	27	25	27	26	22	21	16
Pelvic-Fin Rays	43	28	21	26	21	20	18	15
Basipterygium	44	29	23	28	30	29	22	22
Pectoral-Fin Radial 3	45	30	26	30	29	30	24	21

Table A-11. Rank ordered dataset of 17 skeletal elements, sorted by event number, used for PGi analysis of the neurocranium.

Bone	Event #	*Danio*	*Enteromius*	*Salminus*	*Ictalurus*	*Noturus*	*Corydoras*	*Ancistrus*
Basioccipital	1	1	2	2	1	1	1	1
Parasphenoid	2	2	1	1	1	4	2	4
Exoccipital	3	3	1	3	4	2	2	2
Prootic	4	4	3	5	5	10	3	5
Lateral Ethmoid	5	5	8	10	7	12	9	13
Supraoccipital	8	6	12	8	8	11	7	6
Autosphenotic	6	6	11	7	11	13	10	8
Pterosphenoid	7	6	10	9	9	14	9	12
Autopterotic	9	7	7	13	10	9	5	3
Frontal	10	8	9	4	3	3	4	4
Orbitosphenoid	12	9	14	12	10	15	9	11
Infraorbital 1	11	9	6	15	2	5	14	15
Mesethmoid	13	10	5	6	6	8	6	7
Epioccipital	14	11	13	14	13	16	12	9
Vomer	15	12	4	11	12	17	8	10
Nasal	16	13	15	10	4	6	13	14
Dermopterotic	17	14	16	16	6	7	11	11

Table A-12. Rank ordered dataset of 31 skeletal elements, sorted by event number, used for PGi analysis of the splanchnocranium and associated dermal bones.

Bone	Event #	*Danio*	*Enteromius*	*Salminus*	*Ictalurus*	*Noturus*	*Corydoras*	*Ancistrus*
Opercle	1	1	1	1	1	1	1	3
Ceratobranchial 5	2	1	1	11	10	13	7	18
Hyomandibular	3	2	1	6	11	8	8	6
Dentary	4	3	1	1	2	2	3	4
Branchiostegal Rays	5	3	1	3	3	3	3	2
Anterior Ceratohyal	6	4	1	4	5	6	3	5
Maxilla	7	5	1	2	1	1	2	1
Retroarticular	8	6	2	7	14	5	6	13
Quadrate	9	7	1	5	7	7	5	12
Premaxilla	10	8	1	1	4	4	4	1
Anguloarticular	11	9	1	14	15	12	10	19
Ceratobranchial 2	12	10	6	9	10	17	10	11
Ceratobranchial 1	13	10	6	8	12	17	10	14
Ventral Hypohyal	14	11	3	10	8	10	6	9
Ceratobranchial 4	15	12	5	15	9	11	7	11
Ceratobranchial 3	16	12	5	10	10	16	7	11
Preopercle	17	13	4	12	6	11	15	16
Urohyal	18	14	7	6	8	9	11	7
Epibranchial 4	19	15	9	17	12	18	8	14
Metapterygoid	20	15	7	19	16	15	13	9
Gillrakers	21	15	14	11	19	14	17	20
Epibranchial 3	22	16	8	16	13	18	8	15
Epibranchial 2	23	16	12	16	13	18	10	15
Epibranchial 1	24	17	13	18	13	20	12	17
Posterior Ceratohyal	25	18	4	13	18	12	6	10
Basibranchial 2	26	19	11	20	21	23	16	23
Pharyngobranchial 3	27	20	15	18	20	21	12	21
Autopalatine	28	21	10	23	17	19	9	8
Basibranchial 3	29	22	11	20	22	22	15	24
Hypobranchial 1	30	23	17	22	23	24	13	22
Hypobranchial 2	31	24	16	21	24	25	14	24

Table A-13. Rank ordered dataset of 31 skeletal elements, sorted by event number, used for PGi analysis of the vertebral column.

Bone	Event #	*Danio*	*Enteromius*	*Salminus*	*Ictalurus*	*Noturus*	*Corydoras*	*Ancistrus*
Centrum 4	1	1	1	2	2	1	1	2
Centrum 5	2	2	1	2	1	1	1	2
Centrum 3	3	2	1	3	3	1	1	2
Post-Weberian Centra	4	3	1	2	1	1	1	4
Neural Arch 5	5	4	2	4	5	2	2	2
Post-Weberian Neural Arches	6	4	2	4	4	5	3	4
Hypural 2	7	5	3	1	12	4	4	3
Hypural 3	8	5	3	5	12	9	4	3
Neural Arch 4	9	6	2	6	6	3	2	2
Ural Centrum 1	10	7	11	13	9	4	2	5
Parhypural	11	8	3	1	12	6	8	5
Scaphium	12	9	4	12	16	13	4	10
Uroneural 1	13	10	2	6	11	14	12	12
Hemal Arch Pu2	14	11	7	6	12	11	5	5
Tripus	15	12	6	17	14	9	4	6
Inner Arm Os Suspensorium	16	12	6	16	16	20	4	8
Post-Weberian Hemal Arches	17	13	7	8	7	7	3	4
Preural Centrum 3	18	13	12	14	10	10	2	7
Hemal Arch Pu3	19	14	7	11	12	11	5	5
Preural Centrum 2	20	14	13	14	10	15	2	7
Hemal Spine Pu2	21	14	9	7	15	12	11	10
Hemal Spine Pu3	22	15	10	9	15	12	9	7
Post-Weberian Neural Spines	23	15	5	17	13	17	7	11
Post-Weberian Ribs	24	16	7	16	18	19	4	1
Parapophyses	25	17	10	18	8	8	2	2
Neural Arch Pu3	26	17	7	10	12	8	5	5
Neural Arch Pu2	27	17	7	12	12	12	5	5
Post-Weberian Hemal Spines	28	17	12	15	12	16	7	9
Outer Arm Os Suspensorium	29	17	8	17	14	8	6	10
Neural Spine Pu2	30	17	10	14	17	18	10	10
Epural	31	18	14	19	19	21	13	13

Table A-14. Rank ordered dataset of 29 skeletal elements, sorted by event number, used for PGi analysis of the median and paired fins.

Bone	Event #	*Danio*	*Enteromius*	*Salminus*	*Ictalurus*	*Noturus*	*Corydoras*	*Ancistrus*
Cleithrum	1	1	1	1	1	1	1	1
Primary Caudal-Fin Rays	2	2	2	2	2	2	2	2
Pectoral-Fin Rays	3	16	19	18	3	3	6	3
Supracleithrum	4	4	3	3	4	4	3	4
Hypural 2	5	3	5	4	8	4	4	5
Hypural 3	6	3	5	7	8	7	4	5
Ural Centrum 1	7	5	9	14	5	4	2	6
Neural Arch PU3	8	14	6	11	8	6	5	6
Hemal Arch PU2	9	8	6	8	8	9	5	6
Hemal Arch PU3	10	10	6	12	8	9	5	6
Neural Arch PU2	11	14	6	13	8	10	5	6
Parhypural	12	6	5	4	8	5	6	6
Procurrent Caudal-Fin Rays	13	14	12	13	3	5	13	7
Dorsal-Fin Rays	14	12	10	6	4	6	11	8
Anal-Fin Rays	15	13	15	5	4	6	17	8
Preural Centrum 3	16	9	10	15	6	8	2	9
Preural Centrum 2	17	10	11	15	6	12	2	9
Hemal Spine PU3	18	11	8	10	9	10	7	9
Neural Spine PU2	19	14	8	15	11	16	8	10
Hemal Spine PU2	20	10	7	9	9	10	9	10
Pelvic-Fin Rays	21	20	16	19	10	14	15	10
Coracoid	22	19	20	22	13	13	16	11
Scapula	23	19	20	20	14	15	18	11
Uroneural 1	24	7	4	8	7	11	10	12
Epural	25	17	14	17	16	19	14	13
Dorsal-Fin Proximal Radials	26	18	13	16	12	18	12	14
Anal-Fin Proximal Radials	27	15	17	15	15	17	20	14
Pectoral-Fin Radial 3	28	22	21	23	17	21	21	15
Basipterygium	29	21	18	21	18	20	19	16